Experimental Investigations of EMG-Torque Modeling for the Human Upper Limb

by

Pu Liu

A Dissertation

Submitted to the Faculty

of the

WORCESTER POLYTECHNIC INSTITUTE

in partial fulfillment of the requirements for the

Degree of Doctor of Philosophy

in

Electrical and Computer Engineering

by

_____

May 2014

APPROVED:

_____

Dr. Edward A. Clancy, Major Advisor

_____

Dr. D. Richard Brown III, Committee Member

_____

Dr. Denis Rancourt, Committee Member
Sherbrooke University, Mechanical Engineering Department

Abstract

The electrical activity of skeletal muscle—the electromyogram (EMG)—is of value to many different application areas, including ergonomics, clinical biomechanics and prosthesis control. For many applications, the EMG is related to muscular tension, joint torque and/or applied forces. In these cases, a goal is for an EMG-torque model to emulate the natural relationship between the central nervous system (as evidenced in the surface EMG) and peripheral joints and muscles. This thesis work concentrated on experimental investigations of EMG-torque modeling. My contributions include: 1) continuing to evaluate the advantage of advanced EMG amplitude estimators, 2) studying system identification techniques (regularizing the least squares fit and increasing training data duration) to improve EMG-torque model performance, and 3) investigating the influence of joint angle on EMG-torque modeling. Results show that the advanced EMG amplitude estimator reduced the model error by 21%–71% compared to conventional estimators. Use of the regularized least squares fit with 52 seconds of training data reduced the model error by 20% compared to the least squares fit without regulation when using 26 seconds of training data. It is also demonstrated that the influence of joint angle can be modeled as a multiplicative factor in slowly force-varying and force-varying contractions at various, fixed angles. The performance of the models that account for the joint angle are not statistically different from a model that was trained at each angle separately and thus does not interpolate across angles. The EMG-torque models that account for joint angle and utilize advanced EMG amplitude estimation and system identification techniques achieved an error of $4.06 \pm 1.2\%$ MVC_{F90} (i.e., error referenced to maximum voluntary contraction at 90 °flexion), while models without using these advanced techniques and only accounting for a joint angle of 90 ºgenerated an error of $19.15 \pm 11.2\%$ MVC_{F90}.

This thesis also summarizes other collaborative research contributions performed as part of this thesis. (1) EMG-force modeling at the finger tips was studied with the purpose of assessing the ability to determine two or more independent, continuous degrees of freedom of control from the muscles of the forearm [with WPI and Sherbrooke University]. (2) Investigation of EMG bandwidth requirements for whitening for real-time applications of EMG whitening techniques [with WPI colleagues]. (3) Investigation of the ability of surface EMG to estimate joint torque at future times [with WPI colleagues]. (4) Decomposition of needle EMG data was performed as part of a study to characterize motor unit behavior in patients with amyotrophic lateral sclerosis (ALS) [with Spaulding Rehabilitation Hospital, Boston, MA].

Acknowledgements

Foremost, I am greatly thankful to my research advisor, Dr. Edward A. Clancy, not only for his guidance, support in academics and research, but also enlightening me with the general philosophy of life. His insight, knowledge and experience helped me attain the objectives of this research.

I am extremely grateful to members of the thesis committee, Dr. D. Richard Brown III and Dr. Denis Rancourt. I appreciate their advice and feedback in spite of tight schedules.

Many thanks go to Lukai Liu for his help with the experiment, discussion and comments through this research.

I would also like to thank Dr. Yehia Massoud and Dr. Fred Looft as the department head of the Electrical and Computer Engineering Department in WPI who gave me the opportunity to continue my studies here in WPI as a TA.

Simply, I could not have reached where I am today without my father, Mr. Yuanqiu Liu, my mother, Ms. Jianhua Pan and my husband, Jingkai Su. Without their unconditional love and support, this work wouldn’t have been possible.

TABLE OF CONTENTS

CHAPTER 1—INTRODUCTION

During my Ph.D. degree studies, I worked on electromyogram (EMG) signal processing and modeling. Most of my work concentrated on investigating the relationship between surface EMG and the torque/force produced by the associated muscles. I was also involved in a project that studied indwelling EMG decomposition. This chapter will first introduce the background and motivation of my work, and then highlight my contributions to the EMG-torque area. The details of the work are provided in the subsequent chapters, in the form of published and submitted manuscripts.

When skeletal muscle fibers contract, they conduct electrical activity that can be measured and recorded by electrodes inserted into the muscle through skin or secured to the surface of the skin above the muscle. This electrical activity is referred to as the electromyogram (EMG). EMG signals can be divided into two types — indwelling EMG and surface EMG— according to what kind of electrodes are used to record signals. Indwelling needle/wire electrodes are inserted into the muscles to be located close to motor units (small functional groups of muscle fibers, described in the next paragraph) and typically can view only a few motor units. Surface EMG electrodes have a relatively large pick-up area and typically can view many motor units. They usually cannot distinguish the electrical activity of individual motor units.

A motor unit contains a motor nerve and all its innervated muscle fibers, shown in Fig. 1. When a motor unit is stimulated, its pulse can be recorded by electrodes and displayed as an electrical action potential, known as a motor unit action potential. An engineering model of the surface EMG signal models the EMG signal as the superposition (sum) of many individual motor unit action potentials DeLuca [1979]. Fig. 2 shows the schematic representation of this model for generation of the surface EMG signal.

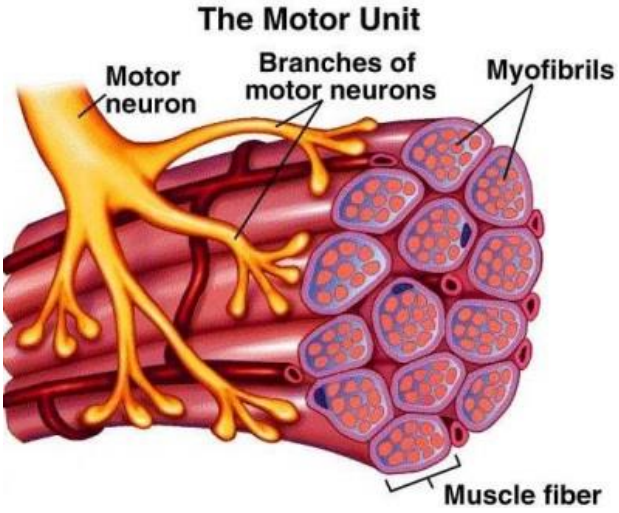

Fig. 1: A motor unit [http://academic.wsc.edu/faculty/jatodd1/351/ch6outline.html]

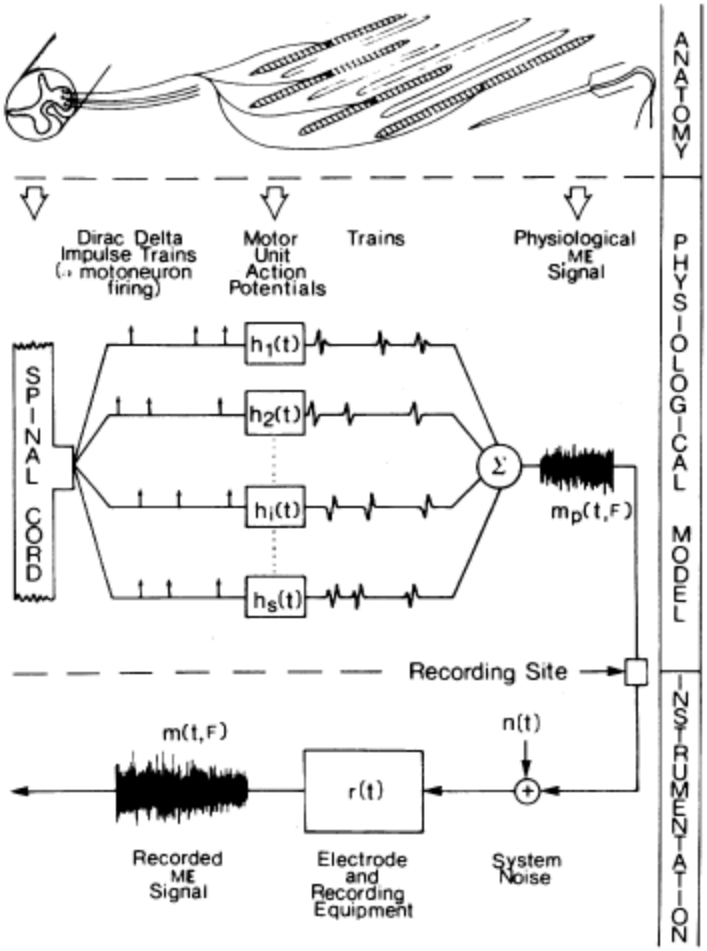

Fig. 2: Schematic representation of a model for generation of the surface EMG signal [DeLuca, 1979]

Surface EMG provides a non-invasive measure of muscle activation and therefore it has been used to relate EMG to muscle tension and joint torque for a long time [An et al., 1983; Clancy and Hogan, 1997; Clancy et al., 2012; Doheny et al., 2008; Hasan and Enoka, 1985; Heckathorne and Childress, 1981; Hof and Van den Berg, 1981; Hogan and Mann, 1980b; Inman et al., 1952; Lawrence and DeLuca, 1983; Sanger, 2007; Shin et al., 2009; Solomonow et al., 1986; Staudenmann et al., 2009; Thelen et al., 1994; Vredenbregt and Rau, 1973; (see Staudenmann et al. (2010) for a recent review)]. This relation provides a non-invasive tool for applications in many different fields, such as myoelectric control of prosthesis [Parker et al., 2006], clinical biomechanics [Disselhorst-Klug et al., 2009; Doorenbosch and Harlaar, 2003], EMG biofeedback for rehabilitation [Armagan et al., 2003; Holtermann et al., 2010], ergonomic analysis/ task analysis [Hagg et al., 2004; Kumar and Mital, 1996; Mathissen et al., 1995], biomechanical modeling [Karlsson et al., 1992], measurement in motion control studies [Fukuda et al., 2003], and so on. Surface EMG generally does not resolve the electrical activity of individual motor units, is dominated by the activity of superficial muscle fibers and recordings from one muscle can easily be contaminated by crosstalk arising from the adjacent muscles. Nonetheless, total joint torque estimation based on surface EMG can more than offset these drawbacks and be very useful for the applications mentioned above. First, being non-invasive makes surface EMG more widely accepted than indwelling EMG, as it is less painful to people, the procedure is much simpler and less expensive, and surface electrodes can be applied for a longer period. Second, the individual contributions of underlying muscles may not necessary for the estimation of total torque about a joint as the superficial muscle activity can be sufficient to identify total joint torque, due to the synergistic activation of relatively large muscle groups. Third, the surface EMG to total joint torque relation can automatically account for certain crosstalk contributions, even if crosstalk is hard to attribute to individual muscle activities [Clancy, 1991].

The aim of EMG-torque models is to emulate the natural relationship between the central nervous system (as evidenced in the surface EMG) and peripheral joints/muscles. A classic paradigm to relate the surface EMG signal to total torque about a joint is shown in Fig. 3. There are two main steps in this paradigm – EMG amplitude estimation ($\hat{s}_E$ and $\hat{s}_F$) and total joint torque estimation (T_{Ext}). The goal is to optimize each of the two steps to achieve non-invasive advanced, high-fidelity EMG amplitude and torque estimation. My thesis work concentrated on optimization of the second step, relating EMG amplitude estimates to joint torque.

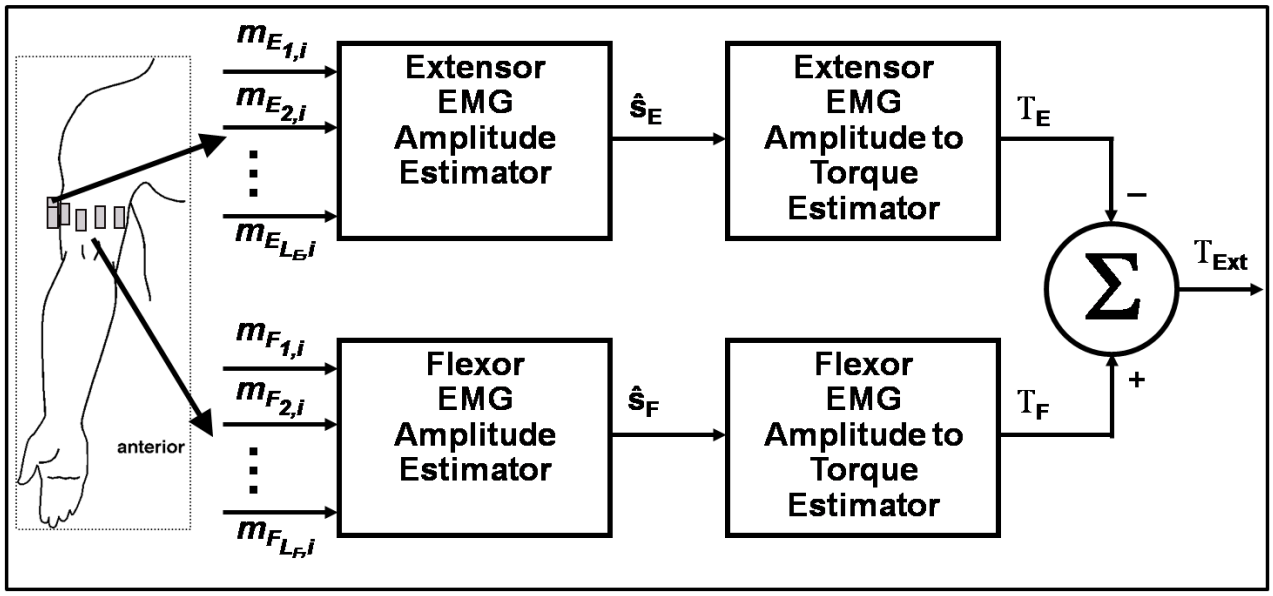

Fig. 3: A classic EMG-torque model

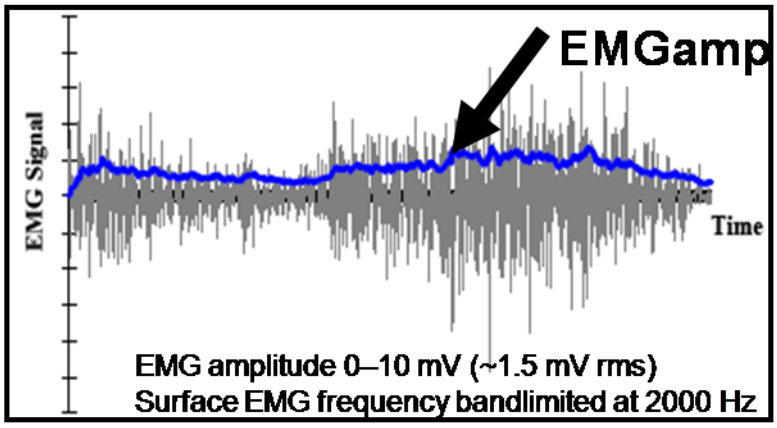

Fig. 4: Raw EMG signal (in grey) and its EMG amplitude (in blue)

The standard deviation of the electrical activity generated by a muscle is commonly referred to as the amplitude of the EMG, which measures the intensity of muscular activation level. Fig. 4 shows an example of raw EMG signal (in grey) and its EMG amplitude (in blue). The earliest continuous EMG amplitude estimator was established by Inman et al. [1952] as an analog full-wave rectifier followed by a simple RC low-pass filter. Although the earliest EMG amplitude estimator was not sophisticated, it led to the routine use of a non-linear detector (analog rectifier) and smoothing (lowpass filtering) of the raw EMG signal to form EMG amplitude estimates. In the following decades, significant contributors began to apply engineering and mathematic models to the EMG signal. Basmajian and DeLuca [1985] and Parker and Scott [1986] established models based on motor unit firings. Hogan and Mann [1980a and 1980b] established a phenomenological model, which models the EMG signal as an amplitude-modulated,

Gaussian random process. With this model, EMG amplitude is defined as the time-varying standard deviation of the noise-free EMG signal. Then, stochastic estimation techniques can be used to improve EMG amplitude estimation from a sample of EMG. This EMG modeling method has led to progressive iterative improvement in EMG amplitude estimations over the past few decades. Here I will focus on presenting the "state of the art" in EMG amplitude estimation. Given the phenomenological model, EMG amplitude estimation becomes the problem of estimating the time-varying standard deviation of a modulated random process in the presence of additive noise. Hogan and Clancy derived an optimal closed-form analytic solution for achieving this goal [Hogan and Mann, 1980a, 1980b; Clancy, 1991]. They pointed out that techniques of whitening and multiple-channel combination can effectively improve EMG amplitude estimation. Fig. 5 shows the effect of whitening on the EMG amplitude estimation. The upper left plot shows a one second of raw EMG signal (total trial length is five seconds) during a constant-posture, constant-force contraction of elbow flexors at 75% MVC (maximum voluntary contraction). The upper right plot is the EMG amplitude estimate from the raw EMG. The lower left plot is the corresponding measured torque. The lower right plot is the EMG amplitude estimate from the whitened EMG. In this example, whitening improved the SNR by 71% [Clancy and Hogan, 1994]. Fig. 6 shows the effect of whitening and multiple-channel combination on the EMG amplitude estimation. The upper left is the measured torque for constant-posture, constant-force contraction of elbow flexors at 25% MVC. The upper right is the EMG amplitude estimate from a single channel EMG without whitening. The lower left is the EMG amplitude estimate from a single channel whitened EMG. The lower right is the EMG amplitude estimate from eight channels, whitened EMG. In this example, whitening and multiple-channel combination improved the SNR by 170% [Clancy and Hogan, 1995].

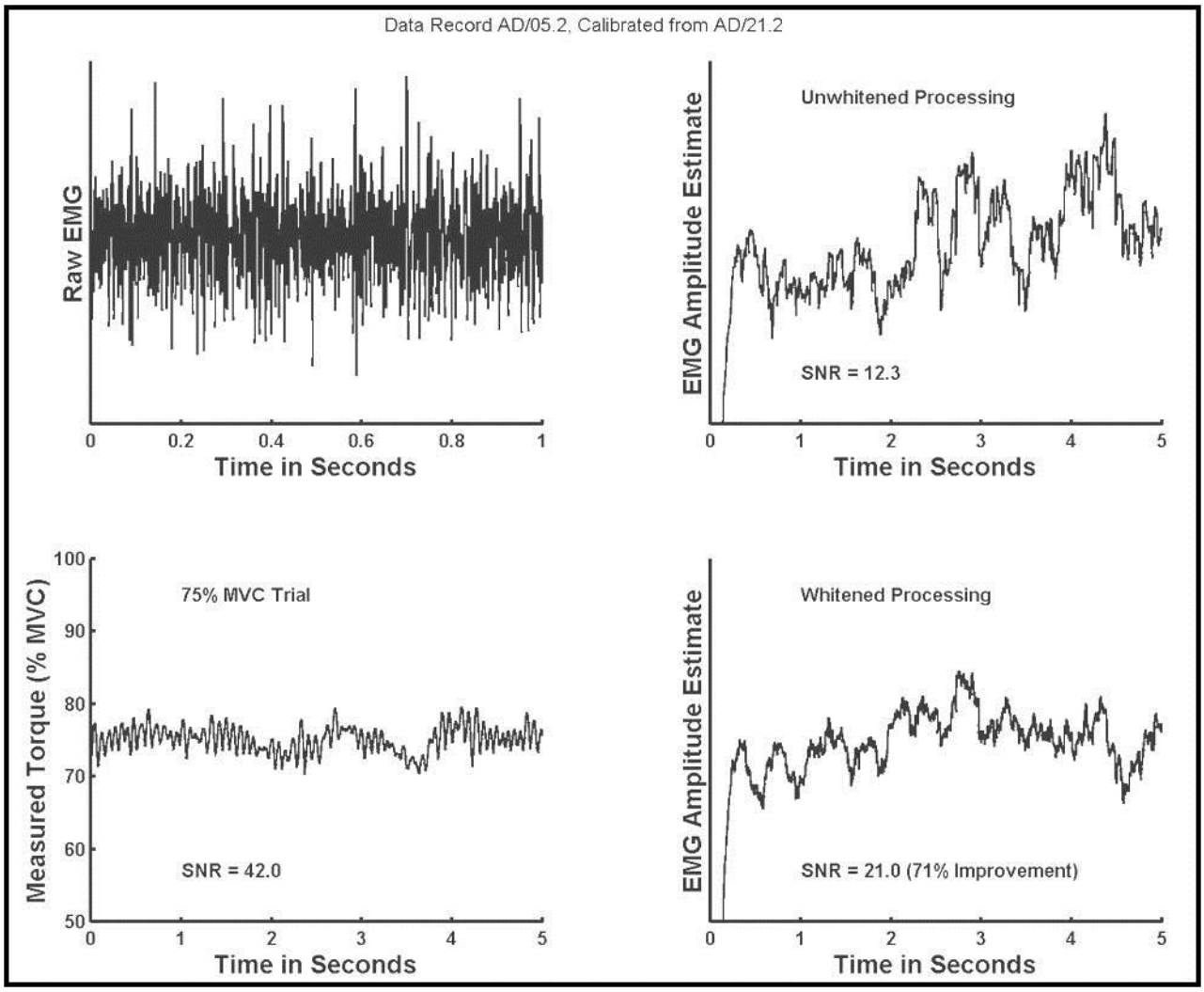

Fig. 5: Effect of whitening on EMG amplitude estimation. [Clancy and Hogan, 1994]

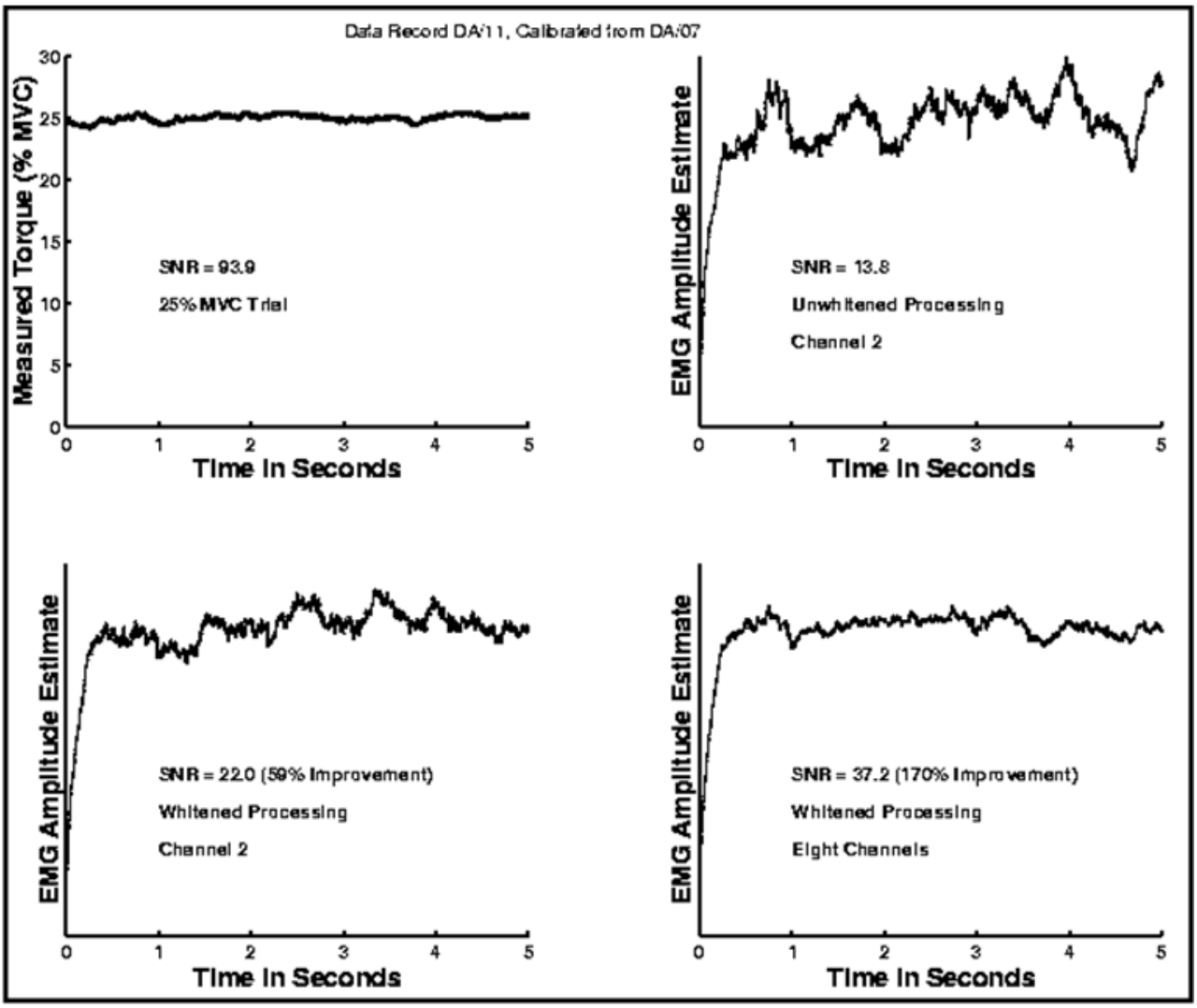

Fig. 6: Effect of whitening and multiple-channel combination on EMG amplitude estimation. [Clancy and Hogan, 1995]

The second step to achieve a non-invasive advanced, high-fidelity EMG-torque model is to optimize torque estimation from EMG amplitude. Lots of research has been done to relate EMG to torque/force, most having ignored the effects of agonist muscle activity in their models to simplify the problem. This simplification is not accurate since antagonist muscle activity accompanies agonist contraction and actually generates considerable effort during the contraction [An et al., 1983; Solomonow et al., 1986]. Many of the earlier researchers used relatively simple linear models [Gottlieb and Agarwal, 1971; Thelen et al., 1994] to study the EMG-torque/force relationship. In recent decades, researchers have begun to use various more complex system identification models to better estimate movement from surface EMG signals. Mountjoy et al. used Hill-based models to predict translational force at the wrist from flexion and extension torque at the elbow [2010]. Cheron et al. [1995] used artificial neural networks to relate EMG to arm trajectory during complex movement. Au and Kirsch predicted shoulder

and elbow kinematics (angles, angular velocities, angular accelerations) from EMG via a time-delayed artificial neural network [Au and Kirsch, 2000]. Therefore, more robust system identification that could apply to this field becomes more and more important because it can improve the performance of these models and lead to low-error EMG-torque estimation for use in various applications. In prosthesis control, it would provide more accurate emulation of the natural command relationship between the central nervous system and peripheral muscles/joints [Parker et al., 2006]. In clinical biomechanics and ergonomics, it would lead to better estimates of joint loading and muscle tension in studies of worker tasks and biomechanical evaluations [Kumar and Mital, 1996; Mathiassen et al., 1995; Hagg et al., 2004; Disselhorst-Klug et al., 2009; Doorenbosch and Harlaar, 2003]. It would also favor the investigation of motor control and control of powered exoskeletons [Kiguchi et al., 2004; Dollar and Herr, 2008; Lenzi et al., 2012].

Previous studies show that muscle fiber length and the associated joint angle have a significant impact on the maximum tension that a muscle can generate [Rack and Westbury, 1969; Zajac, 1989]. It has been found that altering joint angle affects neuromuscular activity during isometric contractions, such as the contractile response to motoneuron stimulation rate [Rack and Westbury, 1969] and motor unit recruitment thresholds [Miles et al., 1986]. Also, a study of biceps and triceps muscles [Solomonow et al., 1986] indicated that the contributions of antagonist muscles vary considerably across angle. All these results suggest that the influence of joint angle is important to establish EMG-torque/force models that are more representative of human movement. However, limited investigations have been done to fully understand the role of joint angle in EMG-torque models.

My research contributions are focused on experimental investigations of estimating torque/force from EMG amplitude for the human upper limb. My study conditions ranged from constant-posture, slowly force-varying ("static") to constant-posture, force-varying ("dynamic") contractions. The former condition is relatively simple and thus is good for initial methodological investigation. The latter one is more representative of the range of application tasks, so I used this condition to further investigate the methodologies I proposed. The posture-varying, force-varying condition would be the most complete case and represents unconstrained movement. Models incorporating this condition represent extensions of my own work and should benefit from the results of my work. Based on past research results, I studied various linear/non-linear polynomial models which account for the co-contraction of agonist and antagonist muscle pairs and also incorporated the advanced techniques of EMG amplitude whitening and multi-channel combinations into the EMG-torque modeling. Also, I evaluated the effects of regularization

of singular-value-decomposition-based least squares pseudo-inverse method and increasing the training data duration on the EMG-torque modeling. Especially, I emphasized the investigation of the influence of joint angle on EMG-torque modeling and established models that facilitate interpolation across angles with promising performance. An overview of each of these contributions, which has resulted in archival publications/submissions, is provided below. The introduction chapter overviews each of them, with relevant details provided in the publications/submissions which form the remaining chapters of this dissertation.

Incorporation of Advanced EMG Amplitude Processing Techniques: EMG amplitude estimation is the first step of EMG-torque modeling and previous researchers showed that improved EMG amplitude estimates produce decreased EMG-torque error [Clancy et al., 2002; Clancy et al., 2006; Clancy and Farry, 2000; Clancy and Hogan, 1994; Clancy and Hogan, 1995; Clancy and Hogan, 1997; Hogan and Mann, 1980a; Hogan and Mann, 1980b; Potvin and Brown, 2004; Staudenmann et al., 2010]. Therefore, advanced EMG amplitude processing techniques can improve the EMG amplitude estimates and thus improve the performance of EMG-torque modeling. Based on the previous work of Clancy et al. [1997, 2002 and 2006], I continued to study the advantage of advanced EMG amplitude processing techniques to a broader range of conditions. I compared standard EMG amplitude processing to advanced processors that include signal whitening and multiple channel combination on EMG-torque models during constant-posture, force-varying toque contractions at joint angle of 90 °(Chapters 4 and 12). Then I extended this investigation to various joint angles during constant-posture, both slowly force-varying (Chapters 5 and 13) and force-varying torque contractions (Chapter 17). The results clearly demonstrated that multi-channel whitened EMG amplitude processing improved EMG-torque estimation. It is well established that these methods decrease the variability of the EMG amplitude estimation [Hogan and Mann, 1980b; Liu, Liu et al., 2013], hence increasing the SNR in the training and testing sets.

System Identification: This topic is related to the second step of EMG-torque modeling. Based on past research results [An et al., 1983; Brown and McGill, 2008; Mathiassen et al., 1995; Solomonow et al., 1986], we hypothesized that incorporating non-linear model structures into the EMG-torque problem would further reduce joint torque error. However, non-linear models typically require additional parameters, which can lead to over-fitting [Ljung, 1999]. There exists a complex interplay between the number of fit parameters in the model, training data duration, the SNR of the training data, and the system identification method [Ljung, 1999]. This section will first briefly introduce my investigation of linear vs.

non-linear EMG-torque models. Then, it will overview my contributions on providing more robust system identification to EMG-torque modeling, explicitly addressing model over-fitting problem.

A collaborative work (Chapters 4 and 12) in which I participated, compares linear and non-linear polynomial EMG-torque models on constant posture, force-varying contractions at an elbow angle of 90 °. Previously collected data were used for this study. The results showed that a linear model was statistically different (poorer) than non-linear models (polynomial degree D=2, 3, 4) when 52-second training durations were used. In the project investigating the influence of joint angle during constant-posture, slowly force-varying (Chapters 5 and 13), I modeled both the angle influence and the EMG-torque relation at one angle using linear/non-linear models. The best non-linear model (EMG polynomial degree D=2, angle polynomial degree A=2) was statistically different (better) than the linear model (D=1, A=1). For non-linear models, when both A and D were high (≥4), the error became extremely large, likely due to over-fitting. Some over-fitting also may have occurred when only one of the two polynomial degrees was high (e.g., D=5, A=3). Then I extended the investigation to constant-posture, force-varying contractions at multiple joint angles (Chapter 17). Again, the best non-linear models were statistically different (better) than the linear model. Based on these studies, we found that non-linear models provide better performance than the linear model, as long as the least squares (a common method used to solve the model parameters) is appropriately regularized (regularization of least squares will be discussed in the following paragraph).

As the models become more complex and the model parameters increased, over-fitting become a bigger obstacle preventing the performance of the models from improving or even making it worse. Therefore, I investigated different methods to address this problem. I started from regularizing the singular-value-decomposition-based least squares pseudo-inverse method that is commonly used to solve the model parameters [Press et al., 1994] (Chapter 12). In this method, small singular values likely provide little information but contain considerable noise. The reciprocals of these small singular values need to be computed to obtain the least squares estimate of the fit parameters, which allows the noise to affect the training of the model parameters. In order to reduce this effect, I replaced the reciprocals of these small singular values with the value zero when training the model parameters. The tolerance for replacement was based on the ratio of each singular value in the "design matrix" [Press et al., 1994] to the maximum singular value, ranging over 40 values spanning 10^{-16} to 0.5 in logarithmic increments. This method is evaluated on linear (D=1) and non-linear (D=2-4) EMG-torque models during constant-posture, force-varying contractions at 90 °. Results showed that tuning the tolerance value improved the model

performance (please refer to Chapter 12 for detailed results). Results also indicate that tolerance value tuning is more critical when the data are more susceptible to over-fitting, i.e., for short duration training sets, poorer EMG amplitude processing, high non-linear degree (i.e., more parameters), and high dynamic model order (i.e., more parameters).

Increased training data duration is another possible way to address over-fitting, however it has seen limited evaluation. I evaluated the effect of training data duration on non-linear EMG-torque models during constant-posture, force-varying contractions at 90 °(Chapters 4 and 12). The models were trained on 26 and 52 seconds of data. Results demonstrated that increasing the training data duration provided a clear improvement, with considerably lower test errors and reduced sensitivity to the number of model parameters. I then extended this method to EMG-torque models at various angles during constant-posture, force-varying contractions, which required even more model parameters (Chapter 17). The models were trained on 26, 52 and 78 seconds of data. Results again showed that increasing the training data duration improved the model performance and supported higher non-linear model degree (i.e., more parameters).

Therefore, in order to overcome the over-fitting problem and provide more robust system identification, one can regularize the singular-value-decomposition-based least squares pseudo-inverse method and increase training data duration.

Influence of Joint Angle on EMG-Torque Model: This topic covers the most substantial independent contributions of my Ph.D. work and it is a topic with more limited prior study. The EMG-torque relationship changes with angle, at least due to the length-tension relationship [Rack and Westbury, 1969; Zajac, 1989], changes in muscle moment arms [Messier et al., 1971] and the movement of electrodes with respect to underlying muscle tissue and the innervation zone [Martin and MacIsaac, 2006; Rainoldi et al., 2000]. Vredenbregt and Rau [1973] found evidence of a multiplicative influence of angle on EMG-torque, at least during constant-force contractions at various torque levels (more recently supported by the work of Doheny et al., [2008]). That is, the EMG-torque curve has the same shape at each angle, but is scaled by a gain factor that is distinct for each angle.

Motivated by the above observation, I hypothesized that we can model the relationship between EMG and torque at various joint angles by modeling the joint angle influence as a multiplicative factor (which is a function of angle) to the EMG-torque model at one particular angle (90 °for example). I decided to model the joint angle influence itself using polynomials first not only because it is simple to investigate but also due to the quadratic shape of the classic length-tension curve. I designed and

conducted an experiment of 12 healthy subjects and collected surface EMG from their biceps/triceps muscle groups along with the elbow torque at seven joint angles (spanning 45 °to 135 °) during constant-posture, slowly force-varying contractions. I proposed three non-linear EMG-torque model structures (all accounted for muscle co-contractions and utilized the advanced EMG amplitude techniques) and evaluated their performance on these experimental data (Chapters 5 and 13). One model structure (angle-specific model) which was formed separately for each of the seven distinct joint angles and thus did not directly facilitate interpolation across angles, was used to generate the minimum "gold standard" error result, since it optimized the model coefficients at each particular joint angle. Both of the other two model structures captured the multiplicative angle factor. A "flex-extend multiplicative model" modeled the angle influences for flexion electrodes and extension electrodes with two respective polynomials, while the "single multiplicative model" used one overall polynomial. Each of the three model structures modeled the EMG-torque relationship at one angle using two polynomials of equal degree *D* (one for flexion EMG amplitude and one for extension EMG amplitude, respectively). The best overall performance of the angle-specific model (polynomial degree *D*=3) gave an error of 4.23 ±2.2% MVC_{F90} (i.e., error relative to maximum voluntary contraction at 90 °flexion), which was used as the "gold standard" to evaluate the other two multiplicative models. The best flex-extend model (EMG polynomial degree *D*=2, angle polynomial degree *A*=2) had an error of 4.17 ±1.7% MVC_{F90} and did not differ statistically from the best angle-specific model. The best performance of the single multiplicative model (*D*=2, *A*=2) was 5.65 ±1.9% MVCF90, which was statistically different (poorer) than the best angle-specific model and the best (*D*=2, *A*=2) flex-extend model. The results showed that the joint angle influence can be model as a multiplicative factor, at least during slowly force-varying contractions at various torque levels, and the performance of the flex-extend multiplicative model was quite promising.

Next, I conducted another experimental study in order to extend the experimental conditions to constant-posture, *force-varying* contractions conducted over a range of fixed joint angles (Chapter 17). This experiment was done on 25 healthy subjects (23 of them had usable data) at six joint angles spanning from 60 °to 135 °. (The joint angle of 45 °was eliminated from this experiment because many subjects from the prior experimental trial found it awkward to orient their elbow to this joint angle and subjects related difficulty in producing torque at this angle with all 12 electrodes mounted on their biceps/triceps.) I specifically investigated the appropriateness of the multiplicative model vs. joint angle. Three dynamic non-linear polynomial model structures were proposed and evaluated on the experimental data. As with the constant posture, slowly force-varying project, the angle-specific model was used to generate the "gold standard" error result. The polynomial-gain model (denoted the flex-extend multiplicative model in

the last project) was also evaluated on the force-varying (dynamic) data. Since we hypothesized that the joint angle influence can be modeled as a multiplicative factor to the EMG-torque model at one particular angle, why not simplify this multiplicative factor (which is a function of angle) by utilizing distinct flexion and extension gains at each angle? Therefore, a new model, the piece-wise-gain model was proposed to do so. Note that the EMG dynamic model coefficients were fixed across angle. This model did not facilitate immediate gain interpolation across angle; however, gain vs. angle functions which preserve the exact gain values at the measured angles (e.g., spline functions) can be fit post hoc to provide interpolation across angle. Also, longer training data duration was used in this study (training data duration =26s, 52s or 78s) to further improve the model performance and support higher non-linear model degrees. The best performance of various models all happened when training data duration is 78s. The best overall performance of the angle-specific model (polynomial degree D=3) gave an error of 4.01 ±1.15% MVC_{F90}, which was used as the "gold standard" to evaluate the other two models. The best polynomial-gain model (EMG polynomial degree D=4, angle polynomial degree A=2) had an error of 4.16 ±1.18% MVC_{F90} and the best piece-wise-gain model (EMG polynomial degree D=3) had an error of 4.06 ±1.19% MVC_{F90}. Both of these two models did not differ statistically from the best angle-specific model. The results demonstrated that the joint angle influence can be modeled as a multiplicative factor during force-varying contractions with quite promising performance.

The Influence of Co-Contraction on EMG-Torque Model: In EMG-torque models at various angles during constant-posture, slowly force-varying contractions, I also compared the EMG–torque relationship with and without consideration of muscle co-contraction (Chapter 13). As expected, models that do not account for co-contraction generate lower individual flexion and extension muscle tension estimates, likely underestimating true muscle tension. This error is substantial: for flexion, the models with co-contraction estimated ~29% more tension; for extension, the models with co-contraction estimated ~68% more tension. If joint impedance were to be volitionally increased by subjects, one would expect even larger errors. Purposeful co-contraction to increase impedance is common in many tasks wherein the endpoint limb segment must be stabilized [Rancourt and Hogan, 2001].

Various Applications: A primary application of EMG-torque/force modeling is for EMG control of powered upper-limb prostheses. Existing commercial EMG-controlled powered hand prostheses are limited to rudimentary control capabilities of either three discrete states (open, close, off) or one degree of freedom of proportional control [Parker et al., 2006]. In order to assess the ability to determine two or more degrees of freedom of control from the agonist-antagonist muscles of the forearm, we did a pilot

laboratory study that related forearm flexor and extensor EMG to flexion-extension force generated at the tips of the four fingers (index, middle, ring, pinky) during constant-posture, slowly force-varying contractions (Chapter 6, 10 and 11). Although the sample size was small (N=3), the results showed evidence that surface EMG activity from the forearm encodes multiple degrees of freedom of proportional control information that may be sufficient for use in controlling prosthetic wrists, hands and/or fingers – at least when tested on intact subjects.

I was involved in a study that investigated the surface EMG bandwidth requirement for whitening (Chapter 15). Previous studies utilizing contraction levels up to maximum voluntary contraction (MVC) show that whitening is useful over a frequency band extending to 1000–2000 Hz [Clancy and Farry, 2000; Prakash et al., 2005], however, EMG electrode systems, particularly in real-time applications, do not have such wide bandwidth. Also, MVC contraction levels are not common. In order to apply our whitening technique to real-time applications, we studied the relationship between the frequency band over which whitening was performed vs. the resulting performance. The low-level contractions (average torque level of 18.5% flexion MVC) which represent most daily tasks showed that performance utilizing frequencies out to 400–500 Hz was not statistically different than results out to the full available frequency (2000 Hz). For the medium-level (50% MVC) contractions, frequencies out to 800–900 Hz were statistically equivalent to the full bandwidth. These results suggest that conventional electrodes with a typical passband of ~500 Hz are appropriate for whitening data from contraction levels typically experienced in many applications. For strenuous activities, wider whitening bandwidths may be helpful.

I was also involved in a study that investigated the ability of surface EMG to estimate joint torque at future times, up to 750ms (Chapter 16). It has been known that EMG activity from muscles precedes the associated mechanical activity by approximately 50–100 ms [Inman et al, 1952; Li and Baum, 2004; Howatson, 2010]. This property can be exploited to anticipate muscle mechanical activity and has various applications: optimizing controller delay in myoelectric prostheses, user control of exoskeleton suits and the actuation of rehabilitation devices from impaired limbs. “Anticipatory” EMG-torque estimation can benefit from the advanced EMG-torque modeling techniques mentioned in previous sections of this chapter. These techniques have been shown to reduce EMG-torque errors and influenced the realization of electromechanical delay within EMG-torque models.

Decomposition of Needle EMG: My earliest work (Chapter 2) was collaborative with Spaulding Rehabilitation Hospital in Boston, MA and the Department of Physical Medicine and Rehabilitation, Harvard Medical School in Boston. The study aimed to characterize motor unit behavior in patients with

amyotrophic lateral sclerosis (ALS). ALS, also known as Lou Gehrig's disease, is a neurodegenerative disease that affects both the lower (LMN) and upper (UMN) motor neurons. It is a progressive, fatal, neurodegenerative disease with most affected patients dying of respiratory compromise and pneumonia after two to three years [Kasi et al., 2009]. To date, the cause of ALS has not been determined thus making the search for a cure very difficult. In this study, needle EMG signals were collected from control subjects and patients with both LMN and UMN dominant forms of ALS. Needle EMG decomposition, the process of breaking down the complex EMG signal into individual motor unit trains that comprise the signal, was performed on the collected data. Mean motor unit firing rate differences, motor unit substitution, and increasing complexity in motor unit action potential (MUAP) waveforms were observed from ALS patients, compared with control subjects. My contribution to the work was decomposing parts of the needle EMG signal collected both from healthy control subjects and ALS patients. The decomposition was challenging in patient recordings because MUAP waveforms in patients were typically more complex than in healthy control subjects. In addition, changes over time in MUAP waveform shape in patient recordings were more dramatic than in control recordings, which made the data difficult to decompose. Therefore, I had to combine the use of automated decomposition software [Florestal et al., 2009] with editing tools [McGill et al., 2005], and also visually inspect/edit each recording to assure reliability of the results. The complexity of the EMG decomposition further increased when waveform superimpositions occurred. Data were analyzed using an algorithm designed to automatically resolve superimpositions [McGill, 2002]. Instances that were not resolved by the automated algorithm were resolved manually.

To sum up, I focused on EMG-torque modeling during my Ph.D. studies. EMG-torque modeling is typically divided into two steps: EMG amplitude estimation from raw EMG signals and torque estimation from EMG amplitude estimates. My contributions are mostly related to the second step and are listed as follows:

- Continued to evaluate the advantage of advanced EMG amplitude estimators, using a wider range of conditions because better EMG amplitude estimation improves the performance of the EMG-torque models. (Related to the first step of EMG-torque modeling.)
- Continued to study the advantage of non-linear model structures, using a wider range of conditions. (Related to the second step of EMG-torque modeling.)

- Studied the system identification technique of regularizing the least squares fit (pseudo-inverse approach) to improve the performance of EMG-torque modeling. (Related to the second step of EMG-torque modeling.)
- Studied the system identification technique of increasing training data duration to improve the performance of EMG-torque modeling. (Related to the second step of EMG-torque modeling.)
- Investigated the influence of joint angle on EMG-torque modeling and studied applicability of multiplicative factor models in slowly force-varying and force-varying contractions at various, fixed angles. (Related to the second step of EMG-torque modeling.)
- Assessed the ability to determine two or more degrees of freedom of control from the agonist-antagonist muscles of the forearm through a pilot laboratory study (EMG-torque modeling applications).
- Contributed to the investigation of EMG bandwidth requirement for whitening which showed that commercial electrode systems generally have adequate bandwidth for common motion activities. Higher bandwidths are useful when higher contraction levels are utilized. (Related to the application of the first step of EMG-torque modeling.)
- Contributed to the investigation of the ability of surface EMG to estimate joint torque at future times. (EMG-torque modeling applications.)

Published Conference Manuscripts:

- Patrick K. Kasi, Lisa S. Krivickas, Melvin Meister, Effie Chew, Paolo Bonato, Maurizio Schmid, Gary Kamen, Pu Liu and Edward A. Clancy. "Characterization of motor unit behavior in patients with amyotrophic lateral sclerosis." *2009 IEEE/EMBS 4th International Conference on Neural Engineering (NER '09)*, pp. 10–13, 29 April–2 May, 2009.
- Pu Liu, Lukai Liu, Francois Martel, Denis Rancourt and Edward A. Clancy. "EMG-Torque Estimation of Constant-Posture, Quasi-Constant-Torque Contractions at Varied Joint Angles." *2011 IEEE 37th Annual Northeast Bioengineering Conference*, 1–3 April, 2011.
- Pu Liu, Donald R. Brown, Francois Martel, Denis Rancourt and Edward A. Clancy. "EMG-to-Force Modeling for Multiple Fingers." *2011 IEEE 37th Annual Northeast Bioengineering Conference*, 1–3April, 2011.
- Lukai Liu, Pu Liu, Edward A. Clancy, Erik Scheme and Kevin B. Englehart. "Signal Whitening Preprocessing for Improved Classification Accuracies in Myoelectric Control." *2011 IEEE 37th Annual Northeast Bioengineering Conference*, 1–3 April, 2011.
- Lukai Liu, Pu Liu, Daniel V. Moyer and Edward A. Clancy. "System Identification of Non-Linear, Dynamic EMG-Torque Relationship About the Elbow." *2011 IEEE 37th Annual Northeast Bioengineering Conference*,1–3 April, 2011.
- Lukai Liu, Pu Liu, Edward A. Clancy, Erik Scheme and Kevin B. Englehart. "Whitening of the Electromyogram for Improved Classification Accuracy in Prosthesis Control," *Annual International Conference of the IEEE Engineering in Medicine and Biology Society*, Vol. 34, pp. 2627–2630, 2012.
- Kishor Koirala, Meera Dasog, Pu Liu and Edward A. Clancy. "EMG-Torque Estimation at Future Times," *2013 IEEE 39th Annual Northeast Bioengineering Conference*, Syracuse University, pp. 59–60, 5–7 April, 2013.
- Meera Dasog, Kishor Koirala, Pu Liu and Edward A. Clancy. "EMG Bandwidth Used in Signal Whitening," *2013 IEEE 39th Annual Northeast Bioengineering Conference*, Syracuse University, 189–190, 5–7 April, 2013.
- Pu Liu, Donald R. Brown, Edward A. Clancy, Francois Martel and Denis Rancourt. "EMG-Force Estimation for Multiple Fingers," *2013 IEEE Signal Processing in Medicine and Biology Symposium (SPMB)*, Polytechnic Institute of New York University, New York, NY, 7 December 2013.

- Pu Liu, Francois Martel, Denis Rancourt, Edward A. Clancy, and D. Richard Brown III, “Fingertip Force Estimation from Forearm Muscle Electrical Activity,” IEEE International Conference on Acoustics, Speech and Signal Processing (ECASSP 2014), in press.

Published Journal Manuscripts:

- Edward A. Clancy, Lukai Liu, Pu Liu and Daniel V. Moyer, "Identification of Constant-Posture EMG-Torque Relationship About the Elbow Using Nonlinear Dynamic Models," *IEEE Transactions on Biomedical Engineering*, Vol. 59, No. 1, pp. 205-212, 2012.
- Pu Liu, Lukai Liu, Francois Martel, Denis Rancourt and Edward A. Clancy, "Influence of Joint Angle on EMG-Torque Model During Constant-Posture Quasi-Constant-Torque Contractions," *Journal of Electromyography and Kinesiology*, Vol. 23, No. 5, pp. 1020–1028, 2013.
- Lukai Liu, Pu Liu, Edward A. Clancy, Erik Scheme and Kevin B. Englehart, "Electromyogram Whitening for Improved Classification Accuracy in Upper Limb Prosthesis Control," *IEEE Transactions on Neural Systems and Rehabilitation Engineering*, Vol. 21, No. 5, pp. 767–774, 2013.
- Meera Dasog, Kishor Koirala, Pu Liu and Edward A. Clancy, "Electromyogram Bandwidth Requirements When the Signal is Whitened," *IEEE Transactions on Neural Systems and Rehabilitation Engineering*, in press.

Journal Manuscripts In Review or In Preparation:

- Kishor Koirala, Meera Dasog, Pu Liu, and Edward A. Clancy, “Using the Electromyogram to Anticipate Torques About the Elbow.” In review.
- Pu Liu, Lukai Liu and Edward A. Clancy, “Influence of Joint Angle on EMG-Torque Model During Constant-Posture, Torque-Varying Contractions.” In preparation.

References:

An KN, Cooney WP, Chao EY, Askew LJ, Daube JR. Determination of forces in extensor pollicislongus and flexor pollicislongus of the thumb. J Applied Physiol: Resp Env Exer Physiol 1983; 54: 714–719.

Armagan O, Tascioglu F, Oner C. Electromyographic biofeedback in the treatment of the hemiplegic hand: aplacebo-controlled study. Am J Phys Med Rehabil 2003; 82: 856–861.

Au TC, Kirsch RF. EMG-based prediction of shoulder and elbow kinematics in able-bodied and spinal cord injured individuals. IEEE Trans Rehab Eng 2000; 8: 471–480.

Basmajian JV, DeLuca CJ. Muscles alive: Their functions revealed by electromyography. Williams & Wilkins, 1985.

Brown SHM, McGill SM. Co-activation alters the linear versus non-linear impression of the EMG-torque relationship of trunk muscles. J Biomech, 2008; 41: 491–497.

Cheron G, Draye JP, Brougeios M, Libert G. A dynamic neural network identification of electromyography and arm trajectory relationship during complex movements. IEEE Trans Biomed Eng 1995;43: 552–558.

Clancy EA. Stochastic modeling of the relationship between the surface electromyogram and muscle torque. Massachusetts Institute of Technology; Cambridge, MA, USA 1991:343–345. Ph.D. thesis.

Clancy EA, Bida O, Rancourt D. Influence of advanced electromyogram (EMG) amplitude processors on EMG-to-torque estimation during constant-posture, force-varying contractions. J Biomech.2006; 39: 2690– 2698.

Clancy EA, Farry KA. Adaptive whitening of the electromyogram to improve amplitude estimation. IEEE Trans Biomed Eng 2000; 47: 709–719.

Clancy EA, Hogan N. Single site electromyograph amplitude estimation. IEEE Trans Biomed Eng 1994; 41: 159–167.

Clancy EA, Hogan N. Multiple site electromyograph amplitude estimation. IEEE Trans Biomed Eng 1995; 42: 203–211.

Clancy EA, Hogan N. Relating agonist-antagonist electromyograms to joint torque during isometric, quasi-isotonic, non-fatiguing contractions. IEEE Trans Biomed Eng 1997; 44: 1024–1028.

Clancy EA, Liu L, Liu P, Moyer DV, Identification of constant-posture EMG-torque relationships about the elbow using nonlinear dynamic models. IEEE Trans Biomed Eng 2012; 59: 205–212.

Clancy EA, Morin EL, Merletti R. Sampling, noise-reduction and amplitude estimation issues in surface electromyography. J Electromyo Kinesiol 2002; 12: 1–16.

DeLuca CJ. Physiology and Mathematics of Myoelectric Signals. IEEE Trans Biomed Eng 1979; 26:313–325.

Disselhorst-Klug C, Schmitz-Rode T, Rau G. Surface electromyography and muscle force: Limits in sEMG-force relationship and new approaches for applications. Clin Biomech 2009; 24: 225-235.

Doheny EP, Lowery MM, FitzPatrick DP, O'Malley MJ. Effect of elbow joint angle on force-EMG relationships in human elbow flexor and extensor muscles. J Electromyogr Kinesiol 2008; 18: 760–770.

Dollar AM, Herr H. Lower extremity exoskeletons and active orthoses: challenges and state-of-the-art. IEEE Trans Robot 2008; 24: 144–158.

Doorenbosch CMA, Harlaar J. A clinically applicable EMG-force model to quantify active stabilization of the knee after a lesion of the anterior cruciate ligament. Clin Biomech 2003; 18: 142–149.

Florestal JR, Mathieu PA, McGill KC. Automatic decomposition of multichannel intramuscular EMG signals. J Electromyogr Kinesiol 2009; 19: 1-9.

Fukuda O, Tsuji T, Kaneko M, Otsuka A. A human-assisting manipulator teleoperated by EMG signals and arm motions. IEEE Trans Robot Autom 2003; 19: 210–222.

Gottlieb GL, Agarwal GC. Dynamic relationship between isometric muscle tension and the electromyogram in man. J Appl Physiol 1971;30:345–351.

Hagg GM, Melin B, Kadefors R. Applications in Ergonomics. In: Merletti R, Parker PA, editors. Electromyography: Physiology, Engineering, and Noninvasive Applications. Hoboken, NJ: John Wiley & Sons, Inc., 2004: 343–363.

Hasan Z, Enoka RM. Isometric torque-angle relationship and movement-related activity of human elbow flexors: Implications for the equilibrium-point hypothesis. Exp Brain Res 1985; 59: 441–450.

Heckathorne CW, Childress DS. Relationships of the surface electromyogram to the force, length, velocity, and contraction rate of the cineplastic human biceps. Am J Phys Med 1981; 60: 1–19.

Hof AL, Van den Berg J. EMG to force processing I: An electrical analogue of the hill muscle model. J Biomech 1981; 14: 747–758.

Hogan N, Mann RW. Myoelectric signal processing: Optimal estimation applied to electromyography—Part 1. Derivation of the optimal myoprocessor. IEEE Trans Biomed Eng 1980a; 27: 382–395.

Hogan N, Mann RW. Myoelectric signal processing: Optimal estimation applied to electromyography—Part 11. Experimental demonstration of optimal myoprocessor performance. IEEE Trans Biomed Eng 1980b; 27: 396–410.

Holtermann A, Mork PJ, Andersen LL, Olsen HB, Sogaard K. The use of EMG biofeedback for learning of selective activation of intra-muscular parts within the serratus anterior muscle: A novel approach for rehabilitation of scapular muscle imbalance. J Electromyogr Kinesiol 2010; 20:359–365.

Howatson G. The impact of damaging exercise on electromechanical delay in biceps brachii. J Electromyo Kinesiol 2010: 20:477–481.

Inman VT, Ralston HJ, Saunders JBCM, Feinstein B, Wright EW. Relation of human electromyogram to muscular tension. Electroencephalogr and ClinNeurophysiol.1952;4:187–194.

Karlsson J, Peterson L, Andreasson G, Hogfors C. The unstable ankle: a combined EMG and biomechanical modeling study. Int J Sport Biomech 1992; 8: 129–144.

Kasi PK, Krivickas LS, Meister M, Chew E, Bonato P, Schmid M, Kamen G, Liu P, Clancy EA. Characterization of motor unit behavior in patients with amyotrophic lateral sclerosis. IEEE/EMBS 4th Int Conf on Neura Eng (NER '09) 2009; 10–13.

Kiguchi K, Tanaka T, Fukuda T. Neuro-fuzzy control of a robotic exoskeleton with EMG signals. IEEE Trans Fuzzy Sys 2004; 12: 481–490.

Kumar S, Mital A, editors. Electromyography in Ergonomics. Briston, PA: Taylor & Francis, 1996.

Lawrence JH, DeLuca CJ. Myoelectric signal versus force relationship in different human muscles. J Appl Physiol 1983; 54: 1653–1659.

Lenzi T, DeRossi SMM, Vitiello N, Carrozza MC. Intention-based EMG control for powered exoskeletons. IEEE Trans Biomed Eng 2012; 59: 2180–2190.

Li L, Baum BS. Electromechanical delay estimated by using electromyography during cycling at different pedaling frequencies. J Electromyo Kinesiol 2004; 14: 647–652.

Ljung L. System Identification: Theory for the User. Upper Saddle River, NJ: Prentice-Hall, 1999: 491–519.

Martin S, Maclsaac D. Innervation zone shift with changes in joint angle in the brachial biceps. J Electromyogr Kinesiol 2006; 16: 144–148.

Mathiassen SE, Winkel J, Hagg GM. Normalization of surface EMG amplitude from the upper trapezius muscle in ergonomic studies—A review. J Electromyogr Kinesiol 1995; 5: 197–226.

McGill KC. Optimal resolution of superimposed action potentials. IEEE Trans Biomed Eng 2002; 49: 640-650.

McGill KC, Lateva ZC, Marateb HR. EMGLAB: An interactive EMG decomposition program. J Neuroscience Methods 2005; 149: 121-133.

Messier RH, Duffy J, Litchman HM, Paslay PR, Soechting JF, Stewart PA. The electromyogram as a measure of tension in the human biceps and triceps muscles. Int J Mech Sci 1971; 13: 585–598.

Miles TS, Nordstrom MA, Turker KS. Length-related changes inactivation threshold and wave form of motor units in human masseter muscle. J Physiol 1986; 370: 457–465.

Mountjoy K, Morin E, Hashtrudi-Zaad K. Use of the Fast Orthogonal Search Method to Estimate Optimal Joint Angle For Upper Limb Hill-Muscle Models. IEEE Trans Biomed Eng 2010; 57: 790–798.

Parker P, Englehart K, Hudgins B. Myoelectric signal processing for control of powered limb prostheses. J Electromyogr Kinesiol 2006; 16: 541–548.

Parker PA, Scott RN. Myoelectric control of prostheses. Crit Rev Biomed Eng, 1986; 13: 283–310.

Potvin JR, Brown SHM. Less is more: High pass filtering, to remove up to 99% of the surface EMG signal power, improves EMG-based biceps brachii muscle force estimates. J Electromyogr Kinesiol 2004; 14: 389–399.

Prakash P, Salini CA, Tranquilli JA, Brown DR, Clancy EA. Adaptive whitening in electromyogram amplitude estimation for epoch-based applications. IEEE Trans Biomed Eng 2005; 52: 331–334.

Press WH, Teukolsky SA, Vetterling WT, Flannery BP. Numerical Recipes in C, 2nd ed. New York: Cambridge Univ Press 1994; 671–681.

Rack PMH, Westbury DR. The effects of length and stimulus rate on tension in the isometric cat soleus muscle. J Physiol 1969; 204: 443–460.

Rancourt D, Hogan N. Stability in force-production tasks. J Motor Behav 2001; 33(2): 193–204.

Rainoldi A, Nazzaro M, Merletti R, Farina D, Caruso I, Gaudenti S. Geometrical factors in surface EMG of the vastusmedialis and lateralis muscles. J Electromyo Kinesiol 2000;10: 327–336.

Sanger TD. Bayesian filtering of myoelectric signals. J Neurophysiol 2007; 97: 1839–1845.

Shin D, Kim J, Koike Y. A Myokinetic Arm Model for Estimating Joint Torque and Stiffness from EMG Signals during Maintained Posture. J Neurophysiol 2009; 101: 387–401.

Solomonow M, Guzzi A, Baratta R, Shoji H, D'Ambrosia R. EMG-force model of the elbow's antagonistic muscle pair: the effect of joint position, gravity and recruitment. Am J Phys Med 1986; 65: 223–244.

Staudenmann D, Kingma I, Daffertshofer A, Stegeman DF, van Dieen JH. Heterogeneity of muscle activation in relation to force direction: A multi-channel surface electromyography study on the triceps surae muscle. J Electromyogr Knnesiol 2009; 19: 882-895.

Staudenmann D, Roeleveld K, Stegeman DF, van Dieen J. Methodological aspects of SEMG recordings for force estimation—A tutorial and review. J Electromyogr Kinesiol 2010; 20: 375–387.

Thelen DG, Schultz AB, Fassois SD, Ashton-Miller JA. Identification of dynamic myoelectric signal-to-force models during isometric lumbar muscle contractions. J Biomech 1994; 27: 907–919.

Vredenbregt J, Rau G. Surface electromyography in relation to force, muscle length and endurance. New Developments in Electromyogr Clin Neurophysiol 1973; 1: 607–622.

Zajac FE. Muscle and tendon: properties, models, scaling, and application to biomechanics and motor control. Crit Rev Biomed Eng 1989; 17: 359–411.

CHAPTER 2

Copy of published conference paper:

Patrick K. Kasi, Lisa S. Krivickas, Melvin Meister, Effie Chew, Paolo Bonato, Maurizio Schmid, Gary Kamen, Pu Liu and Edward A. Clancy. “Characterization of motor unit behavior in patients with amyotrophic lateral sclerosis.” *2009 IEEE/EMBS 4th International Conference on Neural Engineering (NER '09)*, pp. 10–13, 29 April–2 May, 2009.

Proceedings of the 4th International
IEEE EMBS Conference on Neural Engineering
Antalya, Turkey, April 29 - May 2, 2009

Characterization of Motor Unit Behavior in Patients with Amyotrophic Lateral Sclerosis

Patrick K. Kasi
Lisa S. Krivickas
Melvin Meister
Effie Chew
Paolo Bonato
Dept. of PM&R
Harvard Medical School
Boston MA, USA

Maurizio Schmid
Dept. of Applied Electronics
Università degli Study
Roma Tre
Rome, Italy

Gary Kamen
Dept. of Kinesiology
University of Massachusetts
Amherst MA, USA

Pu Liu,
Edward A. Clancy,
Dept. of Electrical and Computer Engineering,
Worcester Polytechnic Institute,
Worcester MA, USA

***Abstract*— In this study, we investigated the behavior of active motor units identified via analysis of electromyographic (EMG) signals recorded from the first dorsal interosseous (FDI) muscle using a quadrifilar needle electrode. Data was collected from control subjects and patients with both lower (LMN) and upper (UMN) motor neuron dominant forms of amyotrophic lateral sclerosis (ALS). EMG recordings were gathered during isometric contractions reaching 20 or 50 % of the force output produced during a maximum voluntary contraction (MVC). Recordings were analyzed using available EMG decomposition software (EMGLAB). Results showed differences in mean motor unit firing rates between patients with ALS and control subjects. Differences were also observed between patients with LMN- and UMN-dominant forms of ALS. Motor unit substitution was observed in patients despite the contractions lasting just a few seconds. Finally, we observed that motor unit action potential (MUAP) waveforms recorded from patients were more complex than those recorded from control subjects as often observed in motor neuron diseases.**

Keywords: Amyotrophic lateral sclerosis; motor units; motor unit firing rate; motor unit decomposition

I. Introduction

Amyotrophic lateral sclerosis (ALS), also known as Lou Gehrig's disease, is a neurodegenerative disease that affects both the lower (LMN) and upper (UMN) motor neurons. ALS is typically seen in individuals 40 to 70 years old, with a slight male predominance. It is estimated that in the US alone, about 30,000 people are affected by ALS and more than 5,000 people are newly diagnosed each year. It can be difficult to diagnose ALS in the early stages of the disease because its symptoms may mimic other disorders. To date, the cause of ALS has not been determined thus making the search for a cure very difficult.

In order to detect small changes in the rate of disease progression, multiple outcome measures are normally used [1]. The neurophysiologic measures that have been utilized to date are: (1) the compound motor action potential (CMAP) amplitude, (2) the motor unit number estimate (MUNE), and (3) the neurophysiologic index derived from motor nerve conduction study parameters [2]. Both the CMAP amplitude and the MUNE decline over time in ALS [1]. All of the measures mentioned above are sensitive to changes in the number of motor units, which decreases as the disease progresses. However, these measures do not allow one to assess the firing characteristics of the motor units. Since functional impairment in ALS is caused by muscle weakness (i.e. the inability to generate force), and given that in addition to motor unit number, the motor unit firing rate characteristics influence the generation of muscle force, it is important to study the firing rate characteristics of the remaining motor units (in addition to their number) in order to fully understand the etiology of muscle weakness in ALS.

II. Methods

A. Subject Recruitments

Eight control subjects, 56.6 ± 7.7 years of age (mean ± SD) were enrolled in the study. Each control subject was examined by a practicing physiatrist for exclusion criteria including neuromuscular disorders and the use of medications that could affect muscle activity. Six subjects 52 ± 5.3 years of age (mean ± SD) with ALS were also recruited in the study. Individuals with ALS were recruited among patients routinely examined at the EMG clinic, Massachusetts General Hospital. Patients met clinical and electro-diagnostic criteria for definite ALS. Four patients had dominant LMN dysfunction and two had dominant UMN dysfunction. The Revised ALS Functional Rating scale (ALSFRS-R), a standard clinical assessment tool based on interviewing and clinically observing patients, was administered. Also, a muscle stretch reflex assessment was performed. Biceps, triceps, brachioradialis, knee and ankle reflexes were tested using standard physical examination techniques and graded using a scale ranging from 0 to 4. The modified Ashworth scale, a standard clinical assessment tool for assessing spasticity, was used to evaluate elbow flexor spasticity. Finally, a nerve conduction test was performed on all subjects (including both control subjects and ALS patients.).

This work was supported by the Harvard NeuroDiscovery Center under the project entitled "Motor Unit Behavior in Amyotrophic Lateral Sclerosis". The authors would like to thank Rita Brugarolas for her help in performing some of the data analysis utilized in this study.

978-1-4244-2073-5/09/$25.00 ©2009 IEEE

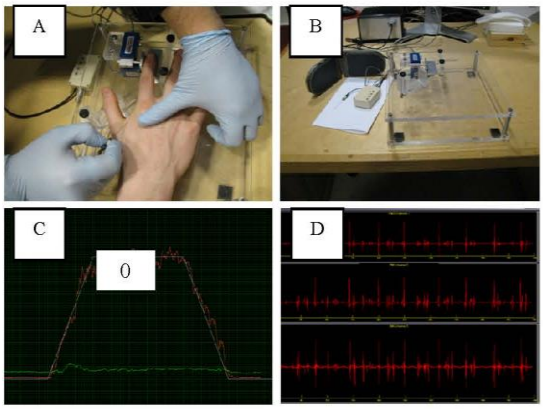

Figure 1. Motor unit data collection. A) Needle insertion. B) Equipment used during the EMG data collection. C) The trapezoidal trajectory that subjects traced during an isometric muscle contraction. D) Raw EMG data for three of the channels recorded using the quadrifilar needle.

B. *Experimental Setup*

A device to monitor index finger abduction force was used (Figure 1). The device was adjustable and accommodated different hand sizes. Two force transducers were used to provide subjects with feedback concerning abduction and flexion of the index finger. The acquisition system was set up with a first screen utilized to help the researcher conducting the data collection to inspect the quality of the data and a second screen to provide subjects with a template of the force trajectory to be followed during testing. A set of speakers was used for feedback to the researcher as well. Sound generated by the EMG signal, in addition to visual feedback, was used to assess whether we were recording high quality EMG data.

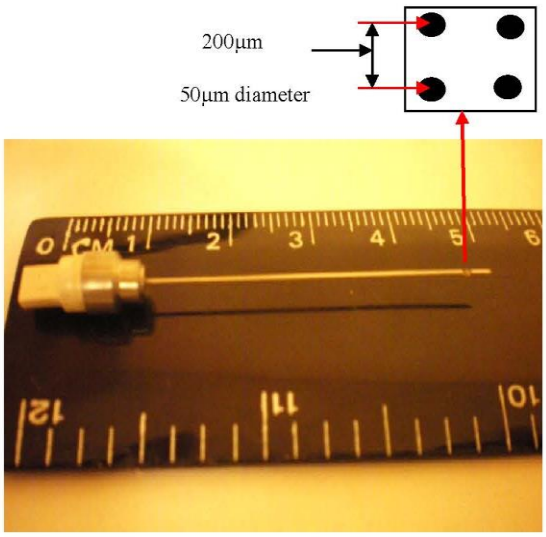

Figure 2. The quadrifilar needle electrode utilized to record motor unit action potential waveforms

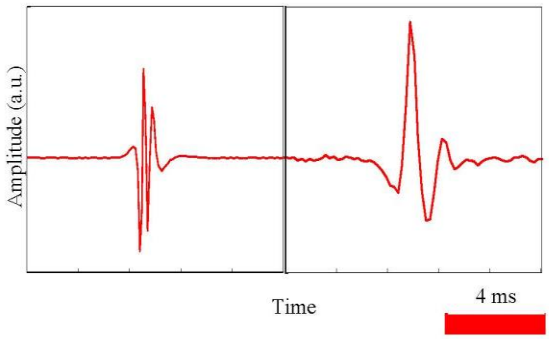

Figure 3. The left panel shows a polyphasic MUAP waveform representative of the recordings we gathered from patients with ALS. The right panel shows a MUAP waveform representative of our observations in control subjects.

A 25-gauge stainless steel quadrifilar needle electrode was used to record electromyographic (EMG) signals. The quadrifilar needle electrode was composed of four electrodes made of platinum wires with diameter of 50 µm. The wires were fed through the cannula of the needle and reached a side port where the electrodes were arranged in a 2x2 array with inter-electrode distance of 200 µm (Figure 2). Four channels (differentially amplified) of EMG data were recorded.

Data was sampled at 25 kHz using a 16-bit acquisition card (NI6035E). When active muscle fibers were within the detection volume of the quadrifilar needle electrode, motor unit action potential (MUAP) waveforms were recorded. MUAPs related to different motor units were marked by different shapes and amplitude values, due to the orientation of each recording area relative to the propagation of the electric field associated with the presence of depolarized zones traveling along the muscle fibers.

C. *Protocol*

All study procedures were approved by the local ethical committee. All subjects provided written informed consent before taking part in the study. EMG data was recorded from the first dorsal interosseous (FDI) muscle of the right hand. A quadrifilar needle electrode was inserted into the FDI muscle (approximately 0.25-0.5 cm deep) and positioned in a manner so as to obtain MUAP recordings that were assessed (via visual inspection) to be suitable for the analysis of motor unit firing rate characteristics. Based on our experience, we considered the uniqueness of the MUAP waveforms associated with each motor unit and the consistency of the MUAP shapes over time to predict the number of motor units whose firing rate characteristics could be derived. Subjects abducted their index finger in order to activate the FDI muscle while tracing a trapezoidal template (a ramp up and a ramp down were set with a slope of 10% MVC/s) displayed on a computer screen as shown in Figure 1. The plateau of the trapezoidal trajectory lasted for 15 s for the 20% MVC tests and 5 s for the 50% MVC tests. Subjects rested for at least one minute after each contraction.

D. *Data Analysis*

We analyzed the EMG signals by relying on a procedure known as "motor unit decomposition technique". The motor unit decomposition technique is a method designed to identify the occurrence of MUAP waveforms related to the activity of a given set of motor units. We utilized a software tool (EMGLAB) developed by McGill et al [3].

During the decomposition process, visual inspection of the recordings and results of the automated analysis was performed to assure reliability of the results. Estimation of the firing rate of a specific motor unit was based on associating a specific MUAP waveform shape with a given motor unit.

The analysis of the EMG data was challenging in recordings from patients because MUAP waveforms in patients were typically more complex than in healthy control subjects. In addition, changes over time in MUAP waveform shape in recordings from patients were more dramatic than in recordings from control subjects. Figure 3 shows two examples of MUAP waveforms recorded from a control subject and a patient with ALS. The complexity of the polyphasic waveform recorded from the patient compared to the relatively simple waveform recorded from the control subject is apparent. The complexity of the MUAP waveform made the data difficult to decompose because the shape of the waveform changed over time. Therefore, we had to combine the use of automated decomposition software [4] with editing tools [3]. The complexity of the EMG decomposition further increased when waveform superpositions occurred. Data were analyzed using an algorithm designed to automatically resolve superpositions [5]. Instances that were not resolved by the automated algorithm were resolved manually.

After the decomposition process, we derived the instantaneous motor unit firing rate time series from occurrences of MUAP waveforms that belonged to a given motor unit. Firing rate time series were defined taking the inverse of the inter-pulse intervals of MUAP waveform occurrences.

III. RESULTS

Examples of motor unit firing rate time series are shown in Figures 4 and 5. These examples demonstrate one of the main observations we performed in this study, namely the fact that motor unit substitution occurred in individuals with ALS despite the short duration of the contractions performed in the study. This observation was made in patients with dominant UMN dysfunction. Motor unit substitution has been observed before in healthy subjects, but only when contractions of long duration (i.e. minutes) were performed [6]. The observation of motor unit substitution during contractions of short duration suggests an early onset of fatigue in individuals with ALS with dominant UMN dysfunction. Comparison of the results we obtained from control subjects and individuals with ALS and comparison of the results we obtained from subjects with dominant LMN dysfunction and subjects with dominant UMN dysfunction revealed other interesting characteristics of motor unit behavior (Figures 6 and 7). Mean firing rate values in control subjects were generally in the range between 15 and 20 Hz with slightly lower values for motor unit recordings performed at 20 % MVC compared to motor unit recordings performed at 50 % MVC. Larger variability was observed in motor unit recordings from individuals with dominant LMN dysfunction. Besides, a difference in mean firing rate was observed in patients with ALS compared to controls. We observed a higher mean firing rate value in patients with dominant LMN dysfunction likely due to a compensatory mechanism aimed at producing the desired force output despite the loss of motor units. We observed a lower mean firing rate value in patients with dominant UMN dysfunction likely due to a lack of "central drive". Finally, we observed a decrease in variability of the motor unit firing rate time series in patients with dominant LMN dysfunction compared to both control subjects and patients with dominant UMN dysfunction. This observation is likely due to spasticity in patients that have dominant LMN dysfunction.

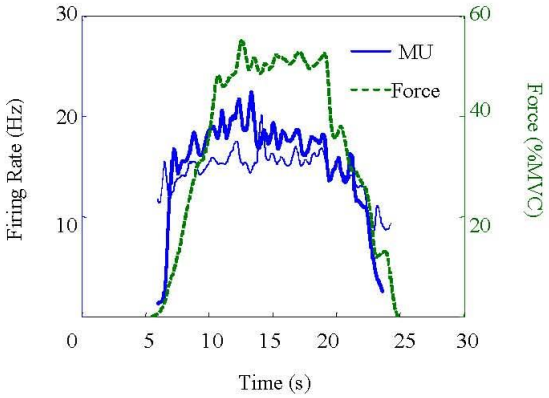

Figure 4. Firing rate time series from a 50% MVC contraction (control subject). The green trajectory is the index abduction force measured by a force transducer, and the blue trajectories are the motor unit firing rate time series of two of the detected motor units.

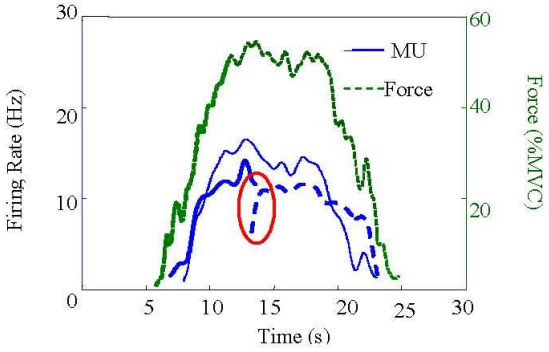

Figure 5. Firing rate time series from a 50% MVC contraction (patients with ALS). The green trajectory is the index abduction force measured by a force transducer, and the blue trajectories are the motor unit firing rate time series of two of the detected motor units. This figure shows a motor unit substitution. Thin dashed line is force trajectory and the others represent motor units.

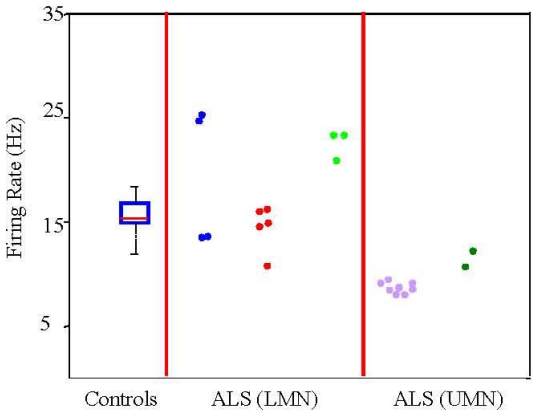

Figure 6. Motor unit firing rate characteristics in control subjects and individuals with dominant LMN and dominant UMN dysfunction for recordings performed at 20% MVC. Data is shown as a box plot for the control subjects and as collection of mean values for individual motor units for patients with ALS.

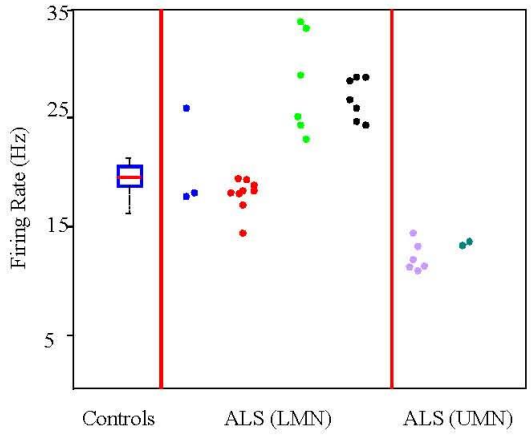

Figure 7. Motor unit firing rate characteristics in control subjects and individuals with dominant LMN and dominant UMN dysfunction for recordings performed at 50% MVC. Data is shown as a box plot for the control subjects and as collection of mean values for individual motor units for patients with ALS.

IV. Conclusions

To our knowledge, this is the first report concerning the characteristics of motor unit behavior in individuals with ALS. Our study identified several unique features of motor unit behavior in individuals with ALS compared to control subjects. Besides, we identified differences between recordings performed in patients with dominant LMN dysfunction and recordings performed in patients with dominant UMN dysfunction. MUAP waveforms recorded form patients were generally more complex then MUAP waveforms recorded from control subjects. The firing rate time series recorded in patients with dominant UMN dysfunction showed motor unit substitution despite the short duration of the contractions. Greater variability in the mean motor unit firing rate was observed in patients with dominant LMN dysfunction compared to control subjects. Decreased variability in motor unit firing was observed in patients with dominant UMN dysfunction. Elevated motor unit firing rate values were observed in patients with dominant LMN dysfunction likely due to a compensatory mechanism to cope with the loss of motor units. Decreased motor unit firing rate was observed in patients with dominant UMN dysfunction likely because of lack of "central drive". Decreased variability in the firing rate time series was observed in recordings from patients with dominant UMN dysfunction likely because of spasticity.

References

[1] J.M. Shefner, M.E. Cudkowicz, H. Zhang, D. Schoenfeld, D. Jillapalli, "The use of statistical MUNE in a multicenter clinical trial", *Muscle Nerve*, vol. 30, n. 4, p. 463-469, 2004.

[2] M. deCarvalho, J. Costa, M. Swash, "Clinical trials in ALS: A review of the role of clinical and neurophysiological measurements", *Amyotroph Lateral Scler Other Motor Neuron Disord*, vol. 6, n. 4, p. 202-212, Dec. 2005.

[3] K.C. McGill, Z.C. Lateva, H.R. Marateb, "EMGLAB: An interactive EMG decomposition program", *Journal of Neuroscience Methods*, vol. 149, n. 2, p. 121-133, Dec. 2005.

[4] J.R. Florestal, P.A. Mathieu, KC McGill, "Automatic decomposition of multichannel intramuscular EMG signals", *J Electromyogr Kinesiol*, vol. 19, n. 1, p. 1-9, Febr. 2009.

[5] K.C. McGill, "Optimal resolution of superimposed action potentials", *IEEE Trans Biomed Eng*, vol. 49, n. 7, p. 640-650, 2002.

[6] R.H. Westgaard, C.J. De Luca, "Motor unit substitution in long-duration contractions of the human trapezius muscle", *J Neurophysiol*, vol. 82, n. 1, p. 501-504, 1999.

CHAPTER 3

Copy of published conference paper:

Lukai Liu, Pu Liu, Edward A. Clancy, Erik Scheme and Kevin B. Englehart. "Signal Whitening Preprocessing for Improved Classification Accuracies in Myoelectric Control." *2011 IEEE 37th Annual Northeast Bioengineering Conference*, 1–3 April, 2011.

Signal Whitening Preprocessing for Improved Classification Accuracies in Myoelectric Control

Lukai Liu[1], Pu Liu[1], Edward A. Clancy[1], Erik Scheme[2] and Kevin B. Englehart[2]
[1]Worcester Polytechnic Institute, 100 Institute Road, Worcester, MA 01609 U.S.A.
[2]Institute of Biomedical Engineering, University of New Brunswick, Fredericton, NB E3B 5A3, Canada.

Abstract— **The surface electromyogram (EMG) signal collected from multiple channels has frequently been investigated for use in controlling upper-limb prostheses. One common control method is EMG-based motion classification. Time and frequency features derived from the EMG have been investigated. We propose the use of EMG signal whitening as a preprocessing step in EMG-based motion classification. Whitening decorrelates the EMG signal, and has been shown to be advantageous in other EMG applications. In a ten-subject study of up to 11 motion classes and ten electrode channels, we found that whitening improved classification accuracy by approximately 5% when small window length durations (<100ms) were considered.**

I. Introduction

The surface EMG has often been used in prosthesis control, ergonomics analysis and clinical biomechanics. Whitening has been used as a preprocessor to decorrelate the EMG signal. In the context of EMG-based motion selection for prosthetic control, we hypothesized that whitening would provide a decrease in the in-class variation of features leading to improved classification accuracy. The present study examined the influence of whitening on classification using time and frequency features of the EMG, in particular at shorter time durations. Three time domain features: mean absolute value (MAV), signal waveform length and zero-crossing rate; and 7th order autoregressive (AR) coefficients as frequency features, were used in our study. We observed an accuracy improvement of about 5% at smaller window lengths (less than 100 ms) with diminishing returns at longer window durations.

II. Methods

A. Experimental Data and Methods

Data from a prior study [1] were reanalyzed. The WPI IRB approved and supervised this reanalysis. Briefly, ten electrodes were applied transversely about the entire circumference of the proximal forearm. A custom electrode amplifier system provided a frequency response spanning approximately 30–450 Hz. Ten subjects with intact upper limbs began and ended each trial at "rest" with their elbow supported on an armrest. Each trial consisted of two repetitions of 11 sequential motion classes: 1, 2) wrist pronation/supination; 3, 4) wrist flexion/extension; 5) hand open; 6) key grip; 7) chuck grip; 8) power grip; 9) fine pinch grip; 10) tool grip; and 11) no motion. Each motion within a trial was maintained for 4 s, after which the subject returned to no motion for a specified inter-motion delay period. Trials 1–4 used an inter-motion delay of 3, 2, 1 and 0 s, respectively, and trials 5–8 used an inter-motion delay of 2 s. A minimum 2-min rest was given between trials. EMG data were sampled at 1000 Hz with a 16-bit ADC. Notch filters were used to attenuate power-line interference at the fundamental frequency and its harmonics.

B. Methods of Analysis

The inter-trial delay segments were removed from the data recordings, resulting in 22, four-second epochs per electrode, per trial (two repetitions of 11 motion classes). For all features, 0.5 seconds of data were truncated from the beginning and end of each epoch. Contiguous, non-overlapping windows were formed from the remaining 3-second epoch segments.

Feature sets were computed for each window within an epoch. A time-domain feature set consisting of three features per window—MAV, signal length and zero-crossing [2] rate—was evaluated. A frequency domain feature set consisted of seven features per window, comprised of the coefficients of a seventh order autoregressive (AR) power spectral density estimate [3]. A third feature set concatenating the seven frequency domain features and the MAV was also evaluated.

Trials 1–4 were used to train the coefficients of the classifier, and trials 5–8 were used to test classifier performance. Initially, all channels and all motions were included in the classifier. The models were trained and tested for each individual subject. Only the test results are reported.

Ten window durations were used: 25, 50, 75, 100, 150, 200, 250, 300, 400 and 500 ms. The analysis was then repeated after the data had been whitened. When doing so, each epoch was high-pass filtered at 15Hz, then adaptively whitened using an algorithm that is tuned to the power spectrum of each EMG channel [4]. Two global variants were also considered. First, the entire analysis was repeated using only nine pre-selected motion classes (the classes denoted above as numbers 1–8 and 11), and again using only seven pre-selected motion classes (1–5, 8 and 11). Second, the entire analysis was repeated using a preselected set of six of the electrode channels. A linear discriminant classifier was used for the recognition task.

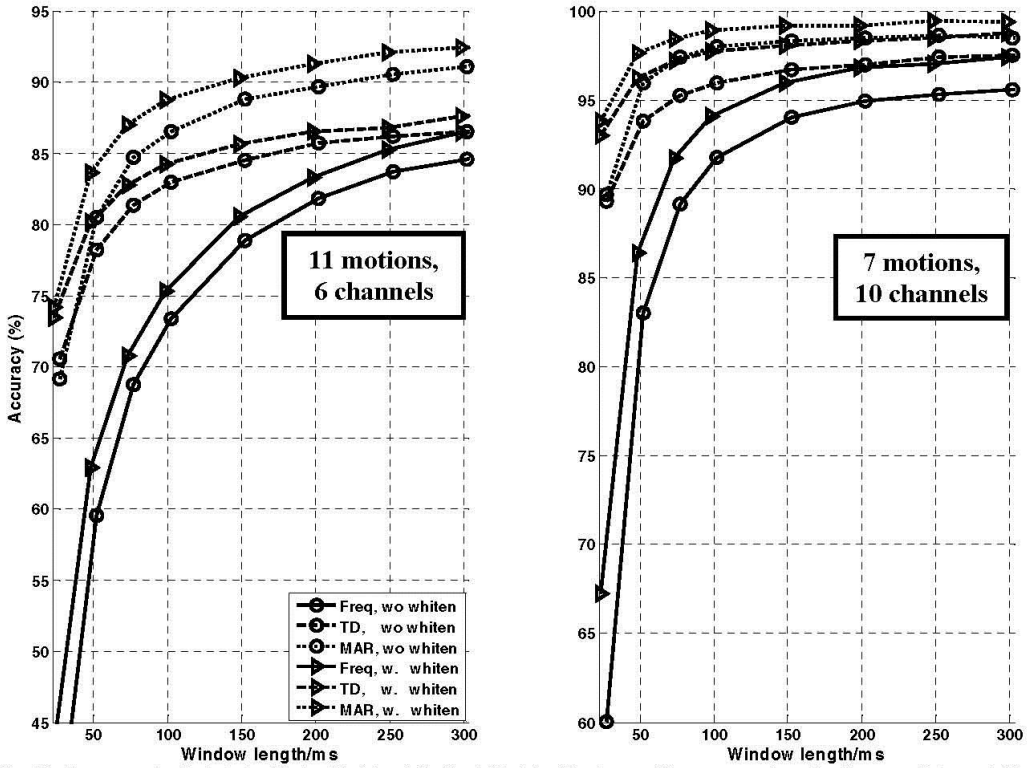

Fig. 1. Classification accuracies for intact subjects with (triangle)/without (circle) whitening used for pre-processing. The frequency feature set (Freq) is comprised of the seven AR coefficients. The time domain feature set (TD) is comprised of three features, and the concatenated feature set (MAR) uses the AR coefficients and MAV. Window durations up to 300 ms are shown. Note the different y-axis scale for each plot.

III. Results

Fig. 1 shows the averaged test accuracies for the motion–channel combinations with lowest (left) and highest (right) overall performance. Classifying with more channels and fewer motion types (right) produced better overall performance. The concatenated (AR-MAV) feature set gave the highest overall classification accuracy, and the frequency domain feature set the lowest. A consistent 4–5% classification performance increase can be seen at shorter window durations for all three feature sets due to whitening, although the improvement decreases with longer window duration. Paired t-tests ($p<0.05$) at all window lengths suggest that use of whitening as a preprocessing stage provides a statistically significant performance improvement.

IV. Discussion

We have shown that the use of signal whitening prior to classification analysis of the EMG system consistently improves the recognition accuracy, especially at shorter time durations. This improvement is modest (~5% for window durations less than 100 ms), but may help improve the accuracy of EMG-based artificial limb controllers. The fact that the most substantial improvement is seen with small window lengths is important, as it may allow a control system to use less data, and therefore improve response time.

Further work may apply to other EMG processing techniques, such as universal principal components analysis [1] and more sophisticated classifiers to further improve classification performance.

References

[1] L. J. Hargrove, G. Li, K. B. Englehart, B. S. Hudgins, "Principal Components Analysis for Improved Classification Accuracies in Pattern-Recognition-Based Myoelectric Control," *IEEE Trans. Biomed. Eng.*, Vol 56, pp. 1407–1414, 2009.

[2] B. Hudgins, P. Parker, R. N. Scott, "A New Strategy for Multifunction Myoelectric Control," *IEEE Trans. Biomed. Eng.*, Vol 40, pp 82–94, 1993.

[3] A. Neumaier, T. Schneider, "Estimation of Parameters and Eigenmodes of Multivariate Autoregressive Models," *ACM Trans. Math. Software*, vol. 27, pp. 27–57, 2001.

[4] E. A. Clancy, K. A. Farry, "Adaptive whitening of the electromyogram to improve amplitude estimation," *IEEE Trans. Biomed. Eng.*, vol. 47, pp. 709–719, 2000.

CHAPTER 4

Copy of published conference paper:

Lukai Liu, Pu Liu, Daniel V. Moyer and Edward A. Clancy. "System Identification of Non-Linear, Dynamic EMG-Torque Relationship About the Elbow." *2011 IEEE 37th Annual Northeast Bioengineering Conference*, 1–3 April, 2011.

System Identification of Non-Linear, Dynamic EMG-Torque Relationship About the Elbow

Lukai Liu, Pu Liu, Daniel V. Moyer and Edward A. Clancy
Worcester Polytechnic Institute, 100 Institute Road, Worcester, MA 01609 U.S.A.

Abstract— **The surface electromyogram (EMG) from biceps/triceps muscles of 33 subjects was related to elbow torque, contrasting EMG amplitude (EMGσ) estimation processors, linear/non-linear model structures and system identification techniques. EMG-torque performance was improved by: advanced (i.e., whitened, multiple-channel) EMGσ processors; longer duration training sets (52 s vs. 26 s); and determination of model parameters via the use of the pseudo-inverse and ridge regression methods. Best performance provided an error of 4.65% maximum voluntary contraction (MVC) flexion.**

I. Introduction

The surface EMG has often been used in prosthesis control, ergonomics analysis and clinical biomechanics. We applied advanced EMGσ estimates (whitening, multiple-channel combination) and different parametric model structures to the EMG-torque problem to reduce torque estimation error. The present study examined system identification methods for non-linear, dynamic EMG-torque models which utilized advanced EMGσ processors and explicitly addressed model over-fitting. Four system identification concepts were compared. First, Hammerstein and Weiner model structures were specifically selected to have a small number of parameters [1]. Second, we investigated the fitting of model parameters via least squares, utilizing the singular value decomposition-based pseudo-inverse approach [2]. Third, we evaluated least squares estimation using ridge regression [3]. Fourth, we increased the duration of the training data.

II. Methods

A. Experimental Data and Methods

Experimental data from 33 subjects from two prior studies ([4] and [5]) were reanalyzed. The WPI IRB stipulated that supervision was not required. A subject was secured into the seat of a Biodex exercise machine with their right shoulder abducted 90°, their forearm oriented in a parasaggital plane, the wrist fully supinated and the elbow flexed 90°. The subject was rigidly attached to the Biodex dynamometer with a cuff at the styloid process. An array of four EMG electrode-amplifiers was placed transversely across each of the biceps and triceps muscles. Signals were sampled at 4096 Hz at 16-bit resolution. Twelve force-varying contraction trials of 30 s duration were recorded during which the subjects used a feedback signal to track a computer-generated target that moved on a screen as a band-limited (1 Hz) uniform random process, spanning 50% MVC extension to 50% MVC flexion. Eight trials per subject were used to fit model coefficients and four distinct trials were used for testing. Only test trial results are presented.

B. Methods of Analysis

Two distinct EMGσ processors were created from each of the extension and flexion muscle groups for each 30 s trial—single-channel unwhitened and four-channel whitened [5]. EMGσ and torque signals were decimated by a factor of 100 to a sampling rate of 40.96 Hz.

Extension and flexion EMGσs were related to joint torque using four parametric, dynamic model structures. For each structure, m was the decimated discrete-time sample index; $T[m]$ was the measured torque; a_0 was an offset parameter; e_q and f_q were the extension and flexion fit parameters, respectively; and $\sigma_E[m]$ and $\sigma_F[m]$ were the extension and flexion EMGσ estimates, respectively. The model structures were:

1) Linear time invariant (LTI) FIR system of order Q.
2) Polynomial non-linear model of degree D, order Q:

$$T[m] = a_0 + \sum_{d=1}^{D}\sum_{q=0}^{Q} e_{q,d}\sigma_E^d[m-q] + \sum_{d=1}^{D}\sum_{q=0}^{Q} f_{q,d}\sigma_F^d[m-q]. \quad (1)$$

3) Hammerstein model (D^{th}-order polynomial static non-linearity cascaded with a Q^{th}-order, LTI, FIR system).
4) Weiner model (Q^{th}-order, LTI, FIR system cascaded with a D^{th}-degree polynomial static non-linearity).

The LTI system order ranged from $1 \le Q \le 30$ and the polynomial degree ranged from $1 \le D \le 4$. Two seconds of data were excluded from the beginning and end of each 30 s trial.

Three approaches were evaluated to reduce least squares over-fitting. First, the singular value decomposition-based pseudo-inverse was used, in which the reciprocals of small singular values were replaced with zero. Forty tolerance values ranged logarithmically from 10^{-16} to 0.5. The offset term a_0 was not used. Second, ridge regression [3] was used and the offset term a_0 was included in the model. Ridge parameter k ranged logarithmically from 10^{-7} to 10^{4} in 112 values. Third, the duration of data available to the least squares fit was altered between 26 s or 52 s.

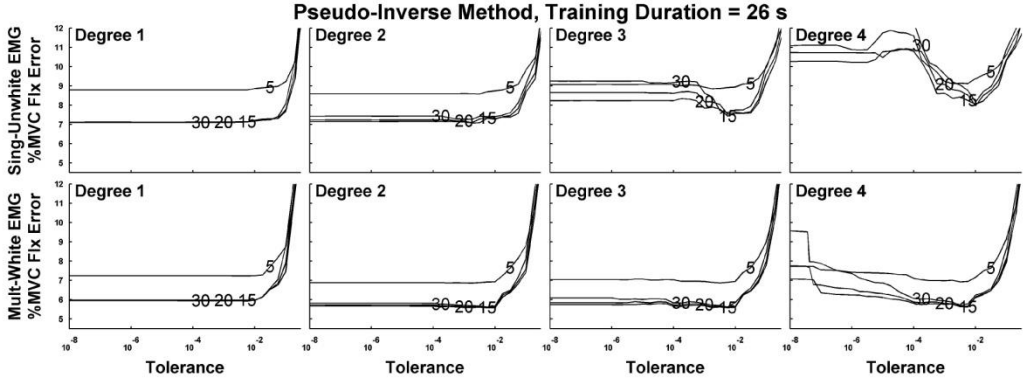

Fig. 1. EMG-torque errors vs. tolerance value for **pseudo-inverse** system identification method, **26 s of training data**. Results for tolerance values below 10^{-8} not shown, but follow similar trend. Rows plot results from the two different EMGσ processors; columns distinguish polynomial model degrees (*D*). Each plot shows the results for representative model orders (*Q*) 5, 15, 20 and 30, as labeled. Each result is average of 132 test trials (33 subjects x 4 test trials/subject).

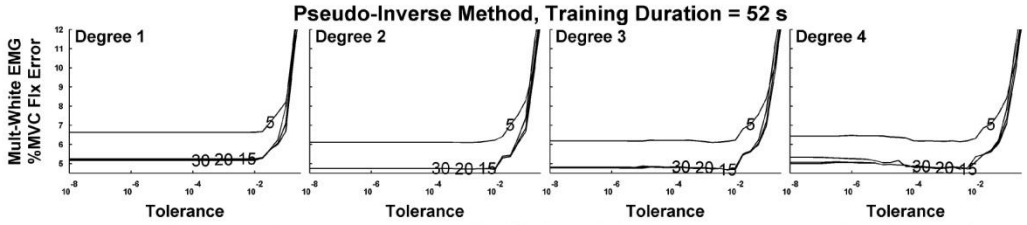

Fig.2. EMG-torque errors vs. tolerance value for **pseudo-inverse** system identification method, **52 s of training data**. Plot details similar to Fig. 1, except only results from the multiple-channel, whitened EMGσ processor are shown.

III. Results

Figs. 1–2 show representative aspects of the overall results. Models which utilized a low linear model order (e.g., $Q \leq 5$) exhibited high error. High model order often also led to higher error, particularly for high polynomial model degrees and with single-channel unwhitened EMGσ processors (or their combination). Excessively large pseudo-inverse tolerance values and ridge *k* values exhibited poor performance.

Although results are not shown here, the Weiner models were clearly inferior to the polynomial non-linear model. Hammerstein model results were also inferior to the pseudo-inverse and ridge regression results, but only mildly so. The best pseudo-inverse results (4.65% MVC flexion; $D=3$, $Q=28$, $Tol=5.6\text{x}10^{-3}$, 52 s training set, multiple whitened EMGσ) were not statistically different ($p=0.5$; paired sign test) than the best ridge regression results. Error was consistently reduced by fitting with a longer duration training set (52 s).

IV. Discussion

The multiple-channel whitened EMGσ processor was again demonstrated to improve EMG-torque estimation. Increasing training set duration from 26 s to 52 s provided a clear improvement, with less sensitivity to the number of model parameters. Surprisingly, this improvement occurred even if the corresponding 26 s duration error did not vary much as a function of model order. Even though Weiner models contained the same number of coefficients as equivalent Hammerstein models, their results were consistently poorer. Hammerstein models exhibited performance close to that of the non-linear polynomial models. With the non-linear polynomial model, the best pseudo-inverse tolerance gave performance similar to that of the best ridge method. However, the range of pseudo-inverse tolerances over which a nearly optimal fit occurred ($\sim 10^{-16} < Tol < 10^{-2}$) was wider than the range of ridge values for its near optimal fit ($1 < k < 10^{3}$).

The merging of advanced EMGσ processors (whitening, multiple-channel combination), more complex EMG-torque models (e.g., non-linear polynomial model) and robust system identification techniques (pseudo-inverse/ ridge regression, longer duration training sets) has reduced the EMG-torque error to 4.65% of MVC flexion—a substantial improvement over previous EMG-torque models.

References

[1] Ljung, *System Identification: Theory for the User*. Upper Saddle River, NJ: Prentice-Hall, 1999: 143–146, 444–452, 491–519.

[2] Press, Teukolsky, Vetterling, Flannery, *Numerical Recipes in C (second edition)*, Cambridge University Press, New York, 1994: 671–681.

[3] Jones, "Multiple regression with correlated independent variables," *Math Geol* **4**:203–218, 1972.

[4] Clancy, "Electromyogram amplitude estimation with adaptive smoothing window length," *IEEE Trans Biomed Eng* **46**:717–729, 1999.

[5] Clancy, Farry, "Adaptive whitening of the electromyogram to improve amplitude estimation," *IEEE Trans Biomed Eng* **47**:709–719, 2000.

CHAPTER 5

Copy of published conference paper:

Pu Liu, Lukai Liu, Francois Martel, Denis Rancourt and Edward A. Clancy. "EMG-Torque Estimation of Constant-Posture, Quasi-Constant-Torque Contractions at Varied Joint Angles." *2011 IEEE 37th Annual Northeast Bioengineering Conference*, 1–3 April, 2011.

EMG-Torque Estimation of Constant-Posture, Quasi-Constant-Torque Contractions at Varied Joint Angles

Pu Liu[1], Lukai Liu[1], Francois Martel[2], Denis Rancourt[2] and Edward A. Clancy[1]
[1]Worcester Polytechnic Institute, 100 Institute Road, Worcester, MA 01609 U.S.A.
[2]University of Sherbrooke, Mechanical Engineering, Sherbrooke, PQ, J1K2R1, Canada

Abstract— **This paper describes an experimental study which relates the simultaneous biceps/triceps surface electromyogram (EMG) of 12 subjects to elbow torque at seven joint angles during constant-posture, quasi-constant-torque contractions. Advanced EMG amplitude (EMGσ) estimation processors were investigated, and an EMG-torque model considering agonist and antagonist co-contractions was evaluated at each joint angle. Preliminary results show that advanced (i.e., whitened, multiple-channel) EMGσ processors lead to improved joint torque estimation and that the EMGσ torque relationship may only change by a scaling factor as a function of joint angle.**

I. Introduction

A significant literature has developed around the problem of relating the surface EMG to muscle tensions and joint torque. However, most investigators have not accounted for muscle co-contractions by assuming that an agonist muscle can be contracted while the antagonist muscle is inhibited [1], [2]. Also, there are clear advances in EMGσ processing techniques over the last few years [3], yet little have been incorporated into EMG-torque estimation. The present study investigated the EMG-torque problem by modeling agonist-antagonist co-contractions over a wide range of joint torques at seven different angles, and also applied advanced EMGσ processing techniques (whitening, multiple-channel combination).

II. Methods

A. Experimental Data and Methods

Similar experimental apparatus and methods are described in detail elsewhere [3], [4]. Briefly, experimental data from 12 healthy subjects (9 male, 3 female; aged 18–52 years) were analyzed. A subject was secured into a custom-built straight-back chair with their right shoulder abducted 90°, their forearm oriented in a parasaggital plane, the wrist fully supinated (palm perpendicular to the floor) and the wrist tightly cuffed to a load cell (Vishay Tedea-Huntleigh Model 1042). The angle between the upper arm and the forearm was selectable, but fixed. An array of six EMG electrode-amplifiers was placed transversely across each of the biceps and triceps muscle groups to record EMG signals. Signals were sampled at 4096 Hz at 16-bit resolution. A sequence of constant-posture, quasi-constant-torque contractions was conducted at elbow angles of 45°, 60°, 75°, 90°, 105°, 120° and 135°. The order of the angles was randomized. At each angle, three tracking trials of forty-five second duration were recorded during which the subjects used a feedback signal to track a computer-generated target linearly ramping slowly in time between 50% MVC flexion and 50% MVC extension. Additionally, subjects performed ten second duration 50% MVC and rest trials (0% MVC), used to calibrate the advanced EMGσ processors.

B. Methods of Analysis

The sampled EMG data were notch filtered at the power line frequency and all harmonics, and then two different EMGσ processors were contrasted. Processor 1 was the "conventional" single-channel, unwhitened processor which used EMG recordings from a centrally located electrode. The EMG signal was high-pass filtered at 15 Hz and then rectified. Processor 2 was a four-channel, whitened processor. Each channel was similarly high-pass filtered, adaptively whitened prior to rectification [3], and then normalized and ensemble averaged. Prior to use in model fits, EMGσ and torque signals were effectively low-pass filtered at 3.3 Hz and decimated by a factor of 1000 (resulting sampling rate of 4.096 Hz).

The decimated extension and flexion EMGσs (inputs) were related to joint torque (output) using a degree D polynomial non-linear model:

$$T[m] = \sum_{d=1}^{D} e_{d,\theta}\sigma_E^d[m] + \sum_{d=1}^{D} f_{d,\theta}\sigma_F^d[m]. \quad (1)$$

where m was the decimated discrete-time sample index; $T[m]$ was the measured torque; $e_{d,\theta}$ and $f_{d,\theta}$ were the extension and flexion fit parameters at joint angle θ, respectively; and $\sigma_E[m]$ and $\sigma_F[m]$ were the extension and flexion EMGσ estimates, respectively. The polynomial degree ranged from $1 \le D \le 5$ and 7.5 seconds of data were excluded from the beginning and end of each 45 s trial to account for filter transients.

A train-test paradigm was utilized in which the model coefficients were determined using linear least squares from a training trial and then used to "predict" the torque from a distinct test trial [5]. An error signal was obtained from the difference between the predicted and actual test trial torque. All errors were normalized to twice the torque at 50% flexion MVC at joint angle 90°. To quantify these errors, we used the mean absolute error (MAE) computed for each testing trial,

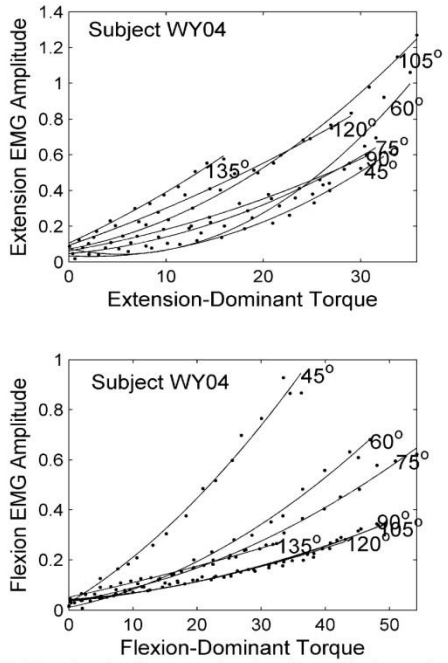

Fig. 1: EMGσ estimation shown as a function of normalized extension (top) and flexion (bottom) dominant joint torque at seven joint angles for subject WY04. The dots are real data and the solid lines are the second-degree polynomial fits, using multiple-channel, whitened EMGσ processor.

TABLE 1: EMG-TORQUE ERROR (PERCENT OF MEAN ABSOLUTE MVC FLEXION AT 90°). EACH RESULT IS THE MEDIAN OF 24 TEST TRIALS (12 SUBJECTS X 2 TRIALS/SUBJECT).

Joint Angle/ EMGσ Processor	Polynomial Degree (*D*) $D=1$	$D=2$	$D=3$	$D=4$	$D=5$
45°					
Single, Unwhite	6.79%	5.27%	4.87%	4.71%	4.70%
Multiple, White	5.35%	4.65%	4.22%	4.32%	4.33%
60°					
Single, Unwhite	6.53%	5.14%	5.09%	4.96%	4.73%
Multiple, White	5.69%	4.23%	3.96%	4.08%	3.88%
75°					
Single, Unwhite	5.76%	4.39%	4.19%	4.21%	4.10%
Multiple, White	4.80%	3.36%	3.07%	2.88%	2.88%
90°					
Single, Unwhite	5.06%	4.60%	4.18%	3.98%	3.91%
Multiple, White	4.59%	3.38%	3.15%	3.30%	3.29%
105°					
Single, Unwhite	4.78%	4.21%	4.23%	4.12%	4.02%
Multiple, White	4.18%	3.22%	3.16%	3.21%	3.26%
120°					
Single, Unwhite	4.86%	4.22%	4.19%	4.17%	4.17%
Multiple, White	3.33%	2.90%	2.86%	2.79%	2.69%
135°					
Single, Unwhite	4.13%	3.75%	3.73%	3.68%	3.66%
Multiple, White	2.46%	2.26%	2.24%	2.23%	2.26%

and took the median of 24 MAEs (12 subjects x 2 test trials per angle) at each joint angle.

III. PRELIMINARY RESULTS

Fig. 1 shows the normalized joint torque vs. EMGσ during extension-dominant (top) and flexion-dominant (bottom) portions of the tracking task at seven different joint angles for subject WY04. The EMGσ-torque curves at different joint angles exhibit a similar shape but different gains. The EMGσ-torque curves were also generated for the other 11 subjects, and this observation was consistent across the subjects.

Table 1 provides the summary results of analysis of median errors between the predicted and actual torques from all subjects, at seven different joint angles, when the polynomial degree ranged from $1 \le D \le 5$, and using two distinct EMGσ processors. For each joint angle and polynomial degree, the four-channel whitened processor produced a lower median error than the signal-channel unwhitened processor.

IV. DISCUSSION

First, advanced EMGσ estimation was applied to the EMG-torque problem at multiple joint angles for constant-posture, quasi-constant-torque contractions about the elbow. Results from 12 subjects showed that the multiple-channel whitened EMGσ processor consistently produced improved EMG-torque estimation. Depending on the joint angle, use of the multiple-channel whitened EMGσ processor with higher polynomial degrees produced a median error that was 50%-66% that found when using the single-channel, unwhitened EMGσ processor with a polynomial degree of $D=1$. Second, the EMGσ-torque curves of individual subjects, viewed across multiple joint angles, indicated that the relationship between EMGσ and joint torque might be multiplicative as a function of angle [1]. Therefore, EMG-torque models might be calibrated at certain joint angles and then applied to other angles via only a change in model gain.

REFERENCES

[1] J. Vredenbregt and G. Rau, "Surface electromyography in relation to force, muscle length and endurance," *New Developments in Electromyogr., Clin. Neurophysiol.*, vol. 1, pp. 607–622, 1973.

[2] J. J. Woods and B. Bigland-Ritchie, "Linear and non-linear surface EMG/force relationships in human muscles," *Amer. J. Phys. Med.*, vol. 62, pp. 287–299, 1983.

[3] Edward A. Clancy and Kristin A. Farry, "Adaptive Whitening of the Electromyogram to Improve Amplitude Estimation," *IEEE Transactions on Biomedical Engineering*, vol. 47, No. 6, pp. 709–719, 2000.

[4] Edward A. Clancy and Neville Hogan, "Relating Agonist-Antagonist Electromyograms to Joint Torque During Isometric, Quasi-Isotonic, Non-Fatiguing Contractions," *IEEE Transactions on Biomedical Engineering*, vol. 44, No. 10, pp. 1024–1028, 1997.

[5] L. Ljung, *System Identification: Theory for the User.* Upper Saddle River, NJ: Prentice-Hall, 1999, pp. 143–146, 444–452, 491–519.

CHAPTER 6

Copy of published conference paper:

Pu Liu, Donald R. Brown, Francois Martel, Denis Rancourt and Edward A. Clancy. “EMG-to-Force Modeling for Multiple Fingers.” *2011 IEEE 37th Annual Northeast Bioengineering Conference*, 1–3April, 2011.

EMG-to-Force Modeling for Multiple Fingers

Pu Liu[1], Donald R. Brown[1], Francois Martel[2], Denis Rancourt[2] and Edward A. Clancy[1]
[1]Worcester Polytechnic Institute, 100 Institute Road, Worcester, MA 01609 U.S.A.
[2]Université de Sherbrooke, 2500, boul. de l'Université Sherbrooke (Québec) CANADA J1K 2R1

***Abstract*—We provide a preliminary report on work to relate the EMG activity from forearm flexors and extensors to the flexion-extension forces generated at the finger tips during constant-posture, slowly force-varying contractions. EMG electrode arrays (up to 64 channels) were applied over the flexor and, separately, extensor musculature of the forearm. Spatial filters were used to create derived EMG channels that were then related to finger tip force (via least squares models). Preliminary results identify the "pinky" finger as having the most independent EMG-force control, with moderate control available from some combinations of the other fingers.**

I. Introduction

Existing commercial EMG-controlled powered hand prostheses are limited to rudimentary control capabilities of either three discrete states (open, close, off) or one degree of freedom of proportional control [1]. Some studies of finger movement have considered multi-finger proportional control via EMG-based estimation of finger tip forces or finger joint angles [2], [3]. In this report, we describe *preliminary* findings of an exploratory study to relate forearm flexor and extensor EMG to flexion-extension force generated at the tips of the four fingers during constant-posture, slowly force-varying contractions. A high resolution EMG array was utilized over the flexion and extension muscles of the forearm, and spatial filters were formed to enhance signal separation. The project goal was to assess the ability to determine two or more independent, continuous degrees of freedom of control from the antagonist muscles of the forearm.

II. Methods

A. Experimental Apparatus and Methods

Experimental procedures were approved by the New England IRB. Subjects provided written informed consent. A custom-built restraint, shown in Fig. 1, was rigidly clamped to a table. The palm of the seated subject's hand was secured to the restraint with the thumb directed upwards, the four remaining digits were passively extended beyond the restraint and the elbow angle was 90°. The distal phalange of any one digit was secured to a load cell.

Two, 64-channel monopolar electrode arrays acquired the EMG (ELSCH064R3S Adhesive Electrode Arrays, EMG-USB Amplifier; OT Bioeletronica, Torino, Italy). Each array was a 13x5 matrix of electrodes (one corner electrode omitted), utilizing 2 mm diameter electrodes (gel-filled) separated by 8 mm. The "flexion" array was oriented along the medial aspect of the forearm, the "extension" array along the lateral aspect. Eight extension electrodes were unused. Each electrode channel had a bandwidth from 10–750 Hz. EMG data were sampled at 2048 Hz (12-bits). A PC sampled the finger tip flexion-extension load cell data (128 Hz sampling rate, 16 bits) and served as a subject display.

Four subjects completed one experiment. Each subject performed separate maximum voluntary contraction (MVC) flexion, then extension trials for each of the four digits. Thereafter, subjects performed a series of slowly force-varying tracking trials, with their force ranging between 30% MVC extension and 30% MVC flexion. Four tracking trials of 30 s duration were completed per digit.

B. Methods of Analysis

Data Preprocessing: Each monopolar EMG signal from the electrode arrays was band-pass filtered (15–700 Hz) and notch filtered at the power line frequency and all harmonics. Then, each trial was manually reviewed. EMG signals with anomalous data (e.g., obviously corrupted by excessive power line noise or motion artifact) were removed.

Formation of Classic Spatial Filters: Classic spatially filtered channels, using known (pre-selected) spatial filter weights [4], were formed. A spatial filter is a memory-less weighted sum of the monopolar signals. First, L (preprocessed) monopolar signals were extracted for each of

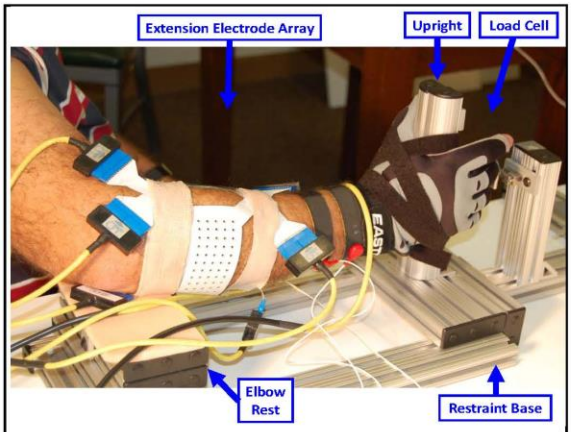

Fig. 1. Photograph of hand/arm secured into finger restraint. Velcro strap is wrapped around one finger (not visible) to secure it to the load cell. Gloved hand is held to the restraint upright using Velcro. Electrode arrays are mounted over the medial (flexion array—not visible) and lateral (extension array) aspects of forearm.

Supported by U.S. Army under USAMRAA Grant W81XWH-08-1-0422.

the extensor and flexor muscle groups. These extracted channels served as a baseline set of spatially filtered channels. Separate such channel sets were formed for L=13, 7, 5, 4, 3 and 2 signals (spread transversely about the muscles). Second, bipolar channels and, third, linear double difference (LDD) channels were formed. Separate channel sets were again formed for L=13, 7, 5, 4, 3 and 2 signals. Lastly, normal double difference (NDD) filters were formed for L=11, 6, 4, 3 and 2. In total, 23 distinct spatially filtered channels were created for each of the flexor and extensor muscle groups.

EMG-Force Estimation: A separate EMG-force analysis was conducted for each of the 23 distinct spatially filtered channel sets. The EMG standard deviation (EMGσ; a.k.a. EMG amplitude estimate) of each spatially filtered channel was computed and then decimated to 20.48 Hz. The first and last five seconds of each 30 s tracking trial were discarded, to eliminate filter startup transients. Four trials, representing data from each of the four digits, were combined to form an analysis record. When one finger tip was active in the load cell, the finger tip force of the three remaining unmeasured finger tips was set to zero. Linear least squares was used to simultaneously relate the L extension EMGσ's and L flexion EMGσ's to the four finger tip forces. Separate training and testing records were used.

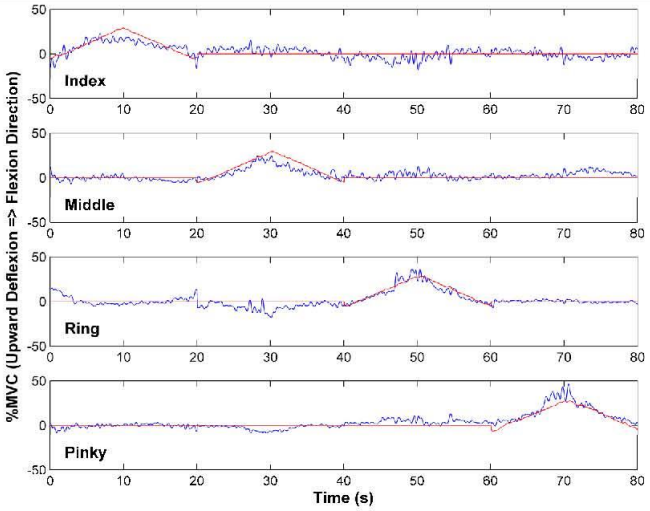

Fig. 2. Constant-Posture, Slowly Force-Varying Record: EMG-force test results of estimated (jagged blue line) and actual force (red line) vs. time for four combined ramp trials to 30% flexion-30% extension MVC using L=13 bipolar spatial filters. Upward force is in the flexion direction. Each finger is active for 20 s. For example, the index finger is active during the first 20 s of this record. Thereafter, other fingers are secured to the load cell and, thus, the index finger tip force is set to zero. Subject WY04; trials 22, 23, 32, 33.

III. Preliminary Results

Only preliminary results are available at this time. Fig. 2 shows results using a bipolar montage of 13 derived electrode channels from each of the flexion and extension arrays. In these results, the "pinky" finger seems to exhibit excellent independent control and the "index" finger the least independent control. Some amount of EMG cross talk/muscle co-activation is visible in the EMG-force estimates for the index, middle and ring fingers.

Although statistical comparisons are not yet available, there did not seem to be an obvious advantage to use of the more complex spatial filter montages (LDD, NDD). One concern is that formation of these montages in software from monopolar electrodes is technically more challenging than doing so in hardware, and may lead to inferior comparisons.

IV. Discussion

In this study, we are concentrating on determining available degrees of freedom of independent, proportional control, expecting that future research would determine how those signals might be fully utilized to control a hand prosthesis. This study was intended as an initial assessment of EMG-force estimation in the finger tips. As such, several study limitations should be noted. First, data were only successfully collected from four subjects. Additional subjects would improve generalizability of the results. Second, subjects only produced constant-posture, slowly force-varying contractions. Third, the performance of EMG-force models has seen little testing relative to the influences of localized muscle fatigue, electrode movement and day-to-day variations.

The electrode arrays used in this project are not appropriate for use in reusable systems (such as prosthetics) that are routinely donned and doffed by their user. The system was selected for its large number of active electrodes, with the understanding that knowledge learned in this study might direct research towards a more deployable electrode solution in the future. Future EMG-based prosthesis control systems might achieve high selectivity and better noise/interference performance via indwelling electrodes.

References

[1] P. A. Parker, K. Englehart and B. Hudgins, "Myoelectric signal processing for control of powered limb prostheses," *J. Electromyo. Kinesiol.*, vol. 16, pp.541–548, 2006.

[2] C. Castellini and P. van der Smagt, "Surface EMG in Advanced Hand Prosthetics," *Bio. Cyber.*, vol. 100, pp. 35–47, 2009.

[3] R. J. Smith, D. Huberdeau, F. Tenore and N. V. Thakor, "Real-Time Myoelectric Decoding of Individual Finger Movements For a Virtual Target Task," *Proc. 31st Ann. Int. Conf. IEE EMBS*, 2009, pp. 2376–2379.

[4] C. Disselhorst-Klug, J. Bahm, V. Ramaekers, A. Trachterna and G. Rau, "Non-invasive approach of motor unit recording during muscle contractions in humans," *Eur. J. Appl. Physiol.*, vol. 83, pp. 144–150, 2000.

CHAPTER 7

Copy of published conference paper:

Lukai Liu, Pu Liu, Edward A. Clancy**,** Erik Scheme and Kevin B. Englehart. "Whitening of the Electromyogram for Improved Classification Accuracy in Prosthesis Control." *Annual International Conference of the IEEE Engineering in Medicine and Biology Society*, Vol. 34, pp. 2627–2630, 2012.

34th Annual International Conference of the IEEE EMBS
San Diego, California USA, 28 August - 1 September, 2012

Whitening of the Electromyogram for Improved Classification Accuracy in Prosthesis Control

Lukai Liu, Pu Liu, Edward A. Clancy, *Senior Member, IEEE*, Erik Scheme, *Student Member, IEEE* and Kevin B. Englehart, *Senior Member, IEEE*

Abstract— **The electromyogram (EMG) signal has been used as the command input to myoelectric prostheses. A common control scheme is based on classifying the EMG signals from multiple electrodes into one of several distinct classes of user intent/function. In this work, we investigated the use of EMG whitening as a preprocessing step to EMG pattern recognition. Whitening is known to decorrelate the EMG signal, with improved performance shown in the related applications of EMG amplitude estimation and EMG-torque processing. We reanalyzed the EMG signals recorded from 10 electrodes placed circumferentially around the forearm of 10 intact subjects and 5 amputees. The coefficient of variation of two time-domain features—mean absolute value and signal length—was significantly reduced after whitening. Pre-whitened classification models using these features, along with autoregressive power spectrum coefficients, added approximately five percentage points to their classification accuracy. Improvement was best using smaller window durations (<100 ms).**

I. Introduction

Traditional myoelectric-controlled upper limb prostheses provide one degree of freedom of proportional control, often by subtracting the EMG amplitudes of an antagonist pair of muscles. The amputee uses manual mode switches to cycle between distinct functions (e.g., hand-wrist-elbow) in order to sequentially control different devices [1], [2]. More natural control of multiple degrees of freedom is greatly desired by below-elbow amputees [3]. One emerging method for such advanced control is based on EMG pattern recognition [1], [4]–[9]. A window ("epoch") of data from multiple electrodes is used to discriminate between a set of distinct hand/wrist/elbow actions. For continuous control, classification can be performed on the EMG signal stream at a periodic rate.

Pattern recognition consists of the sequential steps of EMG signal conditioning/ preprocessing, feature extraction, dimension reduction and pattern classification. Classification errors are due both to a systematic component (e.g., inability of the available features to distinguish all investigated motions) and a random component. In the related areas of EMG amplitude estimation and EMG-torque modeling, whitening has been shown to reduce the variation (i.e., random component) in the EMG signal and improve performance [10], [11]. Physiologically, whitening may counteract, in part, the lowpass filter effect imposed on the signal as it propagates from its origin along the muscle fiber membranes; through intervening muscle, fat and skin; before being recorded at the electrodes. From a stochastic processing standpoint, whitening temporally decorrelates the EMG signal, increasing the effective number of signal samples (a.k.a., statistical degrees of freedom), which reduces the variance in the amplitude estimate. Thus, we hypothesized that pre-whitening of the EMG signal would reduce the random variation of the EMG features used in classification, resulting in improved classification performance. This effect should be more evident at small window durations, since classification accuracy already approaches 100% when long epoch lengths are used. A preliminary report of this work appeared in [12].

L. Liu (e-mail: lliu35@wpi.edu), P. Liu (e-mail: puliu@wpi.edu) and E. A. Clancy (e-mail: ted@wpi.edu) are with the Electrical and Computer Engineering Department, Worcester Polytechnic Institute, 100 Institute Rd, Worcester, MA 01609.

E. Scheme (e-mail: escheme@unb.ca) and K. B. Englehart (e-mail: kengleha@unb.ca) are with the Institute of Biomedical Engineering, University of New Brunswick, Fredericton, NB E3B 5A3, Canada.

978-1-4577-1787-1/12/$26.00 ©2012 IEEE

II. Methods

A. Experimental Methods

Data from two prior experiments with similar protocols were available for reanalysis. The reanalysis was approved and supervised by the WPI IRB. The original data collection was approved by the human studies boards of the respective institutions and written informed consent was received from each subject. Data from ten intact-limbed subjects were collected at the University of New Brunswick [5]. Data from five unilateral transradial amputees were collected at the Rehabilitation Institute of Chicago [6]. Distinct EMG acquisition systems were available at each site. In each case, ten disposable bipolar electrodes (3M Duotrode for intacts; Noraxon 1.25cm diameter Ag/AgCl for amputees) were secured about the circumference of the proximal forearm, oriented along the presumed direction of action potential conduction. EMG data were bandpass filtered (30–350 Hz for intacts; 5–400 Hz for amputees) and sampled at 1000 Hz.

Subjects completed two repetitions of eight trials. Each trial was initiated and terminated at rest with the subject's elbow supported on an armrest. Each trial was comprised of the sequential performance (or, for amputees, *attempted* performance) of 11 motion classes: 1, 2) wrist pronation/supination; 3, 4) wrist flexion/extension; 5) hand open; 6) key grip; 7) chuck grip; 8) power grip; 9) fine pinch grip; 10) tool grip; and 11) no motion. Each motion within a trial was maintained for 4 s, and the subject returned to the rest posture for a specified inter-motion delay period. Trials 1–4 used an inter-motion delay of 3, 2, 1 and 0 s respectively, and trials 5–8 used an inter-motion delay of 2 s. A minimum of two minutes rest was given between trials.

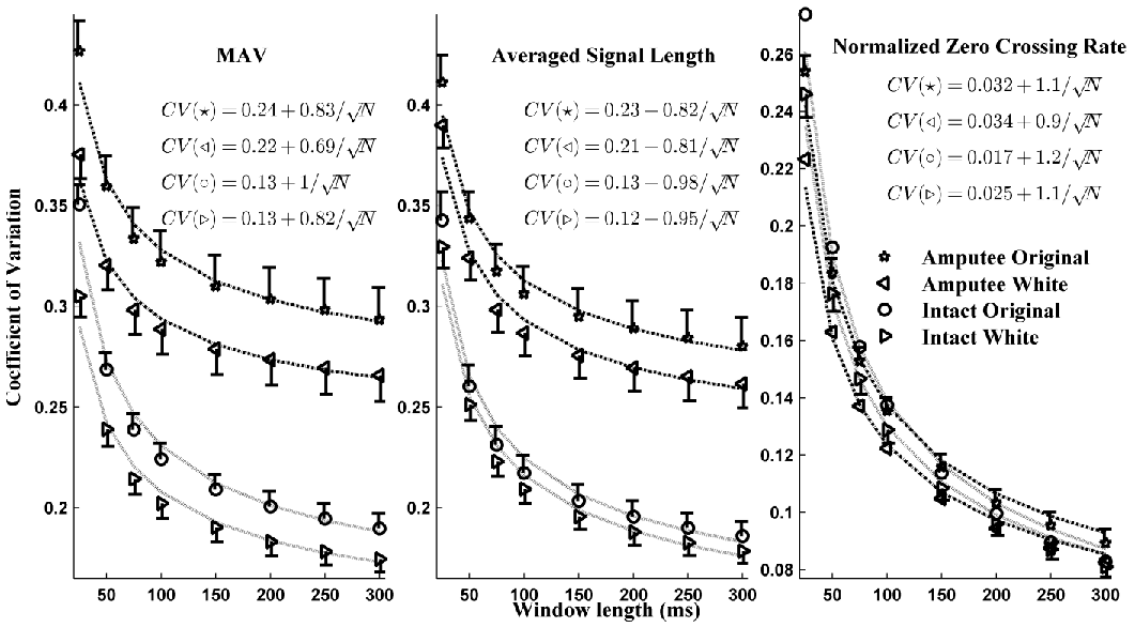

Fig. 1. Average coefficient of variation (plus or minus one standard error) for the time-domain features from ten intact and (separately) five amputee subjects, with and without whitening. Lines show fit to the model: $\mathrm{CoV}[N] = a + b/\sqrt{N}$. Scale of y-axis differs for normalized zero crossing rate. Sample size is 100 for intact subjects, 50 for amputee subjects.

B. Computation of EMG Features

The inter-motion delay portions of the data were removed, leaving epochs 4 s in duration. Each epoch was notch filtered at the power line frequency and each of its harmonics. When whitening was desired, each epoch was highpass filtered at 15 Hz, then adaptively whitened using the algorithm of [10], [13]. This algorithm initially whitens the complete signal (EMG signal plus noise) based on an estimate of the noise-free spectrum of the EMG signal. Unfortunately, this fixed filter also accentuates the high-frequency portion of the noise spectrum. Hence, an adaptive Weiner filter (optimal linear filter to attenuate additive noise) is cascaded after the fixed whitening filter. This filter adapts its shape based on the spectra of the background noise and the EMG signal. The EMG signal spectrum is amplitude modulated with muscle effort, while the background noise spectrum is fixed. In practice, the Weiner filter is lowpass in shape, with a higher cutoff location occurring when muscle effort is high. Adaptive whitening requires calibration to a rest and an active contraction, for each electrode. The "no motion" class was used as the rest contraction. One active class was manually selected per electrode per subject, corresponding to the class with the largest EMG amplitude. After this filtering, the first and last 0.5 seconds of the epoch were discarded, to account for filter start-up transients.

Features were then extracted from each trimmed (3 s) epoch by segregating the epoch into contiguous windows. The following window durations were investigated: N = 25, 50, 75, 100, 150, 200, 250 and 300 ms. The time-domain feature set consisted of the three features: mean absolute value (MAV), average signal length (SL) and normalized zero crossing rate (ZC) (see [4] for definitions). Our ZC feature used a noise threshold of approximately 1/6$^{\text{th}}$ the average RMS value of the "no motion" class. The frequency-domain feature set consisted of the coefficients of a seventh-order autoregressive (AR) model [8], [14]. The "combined" feature set used the AR coefficients along with MAV.

C. Analysis of Coefficient of Variation of EMG Features

Since the mechanism of improvement due to signal whitening is hypothesized to be a reduction in the variation of feature values, we computed the coefficient of variation (CoV) of the features. We limited this analysis to the three time-domain features. For each electrode for each subject, we identified two classes with the largest EMG amplitudes. The CoV was computed for each epoch as the standard deviation of the features divided by their mean. Low amplitude recordings were avoided, since the CoV calculation is erratic when the mean feature value and its standard deviation are both small numbers. These CoV values were averaged across the two selected trials and across all subjects. Results were computed both with and without whitening, separately for intact-limbed subjects and amputees, and for each window duration N. Thereafter, a modified power decay model was fit to the mean values, using the model: $\mathrm{CoV}[N] = a + b/\sqrt{N}$. Lower CoV values denote less variability in the features.

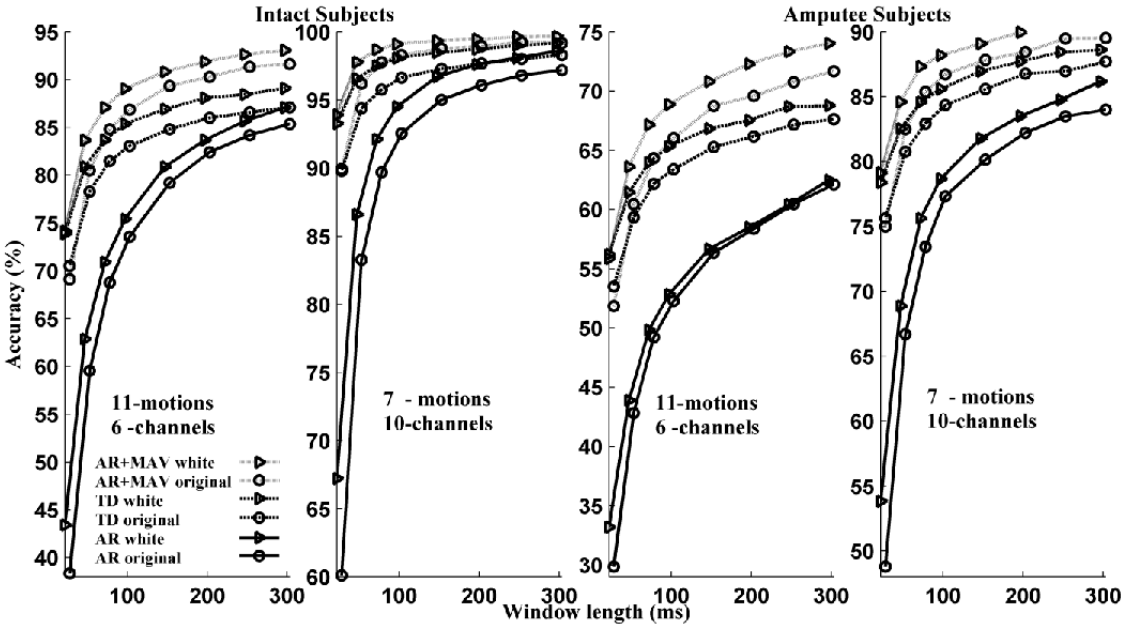

Fig. 2. Exhaustive selection average classification accuracies from ten intact (left) and five amputee (right) subjects for each of the three feature sets, with and without whitening. The motion-channel combinations shown represent the lowest accuracies (fewest channels and most motion classes) and highest (most channels and fewest classes). Window durations vary from 25 to 300 ms. Note the different y-axis scale for each plot.

D. Analysis of Classification Performance

Linear discriminant classification was used with an exhaustive search over all possible electrode combinations. For ten electrode channels, there were 1023 possible electrode combinations evaluated. Both repetitions of data trials 1–4 were used for training and both repetitions of data trials 5–8 were used for testing. The results from the best test result per subject are reported. The entire analysis was repeated using a preselected set of six electrodes spread evenly about the circumference of the forearm. For six electrode channels, there were 63 possible electrode combinations evaluated. The analysis was repeated again using only a preselected set of nine motion classes (classes 1–8 and 11); and again using a preselected set of seven motion classes (classes 1–5, 8 and 11). Results for intact-limbed subjects and amputees are reported separately for each of the window durations.

III. Results

Fig. 1 shows the average plus/minus standard error CoV results for the three time-domain features, with and without whitening, plotted separately for intact-limbed and amputee subjects. Whitening substantially reduced feature variation at all window durations for the MAV and SL features. There was rather limited affect due to whitening for the ZC feature. The CoV values were lower in the intact-limbed subjects. All plots fit well to the offset power law model.

Classification accuracy results were higher when the number of EMG channels was larger and when the number of motion classes was lower. Thus, results will only be presented for the best (10-channel, 7-motion) and worst (6-channel, 11-motion) combination. Fig. 2 shows the across-subject average classification accuracy for these channel-motion combinations, with and without whitening, for each of the three feature sets (time-domain, frequency-domain and combined), plotted separately for intact-limbed and amputee subjects. Whitening provided a consistent increase in performance. At low window durations, the performance increase is as much as five percent. The "combined" feature set (AR coefficients along with MAV) consistently provided the highest average classification accuracy. Accuracy was higher in the intact-limbed subjects than in the amputees.

IV. Discussion

Although signal whitening methods have been available for several years, they do not seem to have been applied to the EMG pattern recognition problem. When computing EMG MAV, the signal to noise ratio (SNR) of the amplitude estimate has been shown to increase with window duration in a square root fashion [15], with whitening improving the SNR. Since CoV is defined as the reciprocal of the SNR, it follows that the CoV of the MAV feature should decrease with window length as the reciprocal of a square root; thus our use of the power law model for fitting to the CoV values. Further, whitened MAV features should have lower CoV values than unwhitened MAV features. We found, however, that an offset term was needed in the power law model in

order to achieve an acceptable fit (Fig. 1). Manual inspection of the epochs used to calculate the CoV showed that many subjects did not maintain a constant effort level across the 3 s used to form features. If the feature values are changing *within* a 3 s epoch, then a larger sample standard deviation will be found for that mean feature value. A larger CoV estimate will result. The inflated MAV CoV values fit better to a power law model that included an offset term than to the theoretically expected model that is absent an offset.

Although not described here, analytic and simulation analysis also predicted an inverse square root relationship with window duration for the SL and ZC features. Fig.1 shows that the SL feature also required substantial offset values in the power law fit, but the ZC feature did not. As effort varied *within* an epoch, the CoV of the SL feature would be expected to inflate, again due to the increased within-epoch variance. But, zero crossings are not substantially influenced by modulations in EMG amplitude within an epoch—so long as the EMG amplitude remains above the noise floor. Hence, the ZC features exhibited the lowest overall CoV values (and the lowest standard errors).

One would expect much lower CoV values for the MAV and SL features if the subject contractions were held more constant. However, acquisition of such data is only relevant to this intermediate evaluation of CoV. For training classifiers, it is better to collect data with the full range of within-epoch modulation that is representative of actual prosthesis control use. The classifier will then optimize for that realistic condition.

Regardless of this inter-epoch modulation concern, whitening decreased the CoV, making the features more repeatable. As shown in Fig. 2, an improvement in classification accuracy resulted. The improvement was most prominent at the shorter window durations. This result was expected, since classification performance increases towards 100% at the longer window durations. No further increase is possible.

V. Conclusion

We investigated whitening as a preprocessing step to EMG pattern recognition in intact-limb and amputee subjects. Whitening was shown to decrease the average CoV for MAV and SL features, with less influence on the ZC feature. Whitening was shown to consistently improve the average classification accuracy when distinguishing up to 11 distinct motion classes using up to 10 different electrodes. Improvement due to whitening was also found using fewer motion classes and fewer electrode channels.

Acknowledgment

The authors thank Guanglin Li and the Neural Engineering Center for Artificial Limbs, Rehabilitation Institute of Chicago, Chicago, IL 60611 USA, for providing the amputee data for this study.

References

[1] P. Parker, K. Englehart and B. Hudgins, "Myoelectric Signal Processing for Control of Powered Limb Prostheses," *J. Electromyogr. Kinsesiol.*, vol. 16, pp. 541–548, 2006.

[2] H. A. Varol, F. Sup and M. Goldfarb, "Multiclass Real-Time Intent Recognition of a Powered Lower Limb Prosthesis," *IEEE Trans. Biomed. Eng.*, vol. 57, pp. 542–551, 2010.

[3] D. Atkins, D. C. Y. Heard and W. H. Donovan, "Epidemiologic Overview of Individuals with upper-limb loss and their Reported Research Priorities," *J. Prosthet. Orthot.*, vol. 8, pp. 2–11, 1996.

[4] B. Hudgins, P. Parker, R. N. Scott, "A New Strategy for Multifunction Myoelectric Control," *IEEE Trans. Biomed Eng.*, vol. 40, pp. 82–94, 1993.

[5] L. J. Hargrove, G. Li, K. B. Englehart, and B. S. Hudgins, "Principle Component Analysis for Improved Classification Accuracies in Pattern-Recognition-Based Myoelectric Control," *IEEE Trans. Biomed. Eng.*, vol. 56, pp. 1407–1414, 2009.

[6] G. Li, A. E. Schultz, and T. A. Kuiken "Quantifying Pattern Recognition–Based Myoelectric Control of Multifunctional Transradial Prosthesis," *IEEE Trans. Neural Sys. Rehab. Eng.*, vol. 18, pp. 185–192, 2010.

[7] M. R. Ahsan, M. I. Ibrahimy and O. O. Khalifa, "Advances in Electromyogram Signal Classification to Improve the Quality of Life for the Disabled and Aged People," *J. Comp. Science*, vol. 6, pp. 706-715, 2010.

[8] D. Graupe and W. K. Cline, "Functional separation of EMG signals via ARMA identification methods for prosthesis control purposes," *IEEE Trans. Sys. Man Cyber.*, vol. 5, pp. 252–259, 1975.

[9] R. Boostani and M. H. Moradi, "Evaluation of Forearm EMG Signal Features for the Control of a Prosthetic Hand," *Physio. Meas.*, vol. 24, pp. 309–319, 2003.

[10] E. A. Clancy and K. A. Farry, "Adaptive Whitening of the Electromyogram to Improve Amplitude Estimation," *IEEE Trans. Biomed. Eng.*, vol. 47, pp. 709–719, 2000.

[11] N. Hogan, R. W. Mann, "Myoelectric Signal Processing: Optimal Estimation Applied to Electromyography–Part II: Experimental Demonstration of Optimal Myoprocessor Performance," *IEEE Trans. Biomed. Eng.*, vol. BME-27, pp. 396–410, 1980.

[12] L. Liu, P. Liu, E. A. Clancy, E. Scheme and K. B. Englehart, "Signal Whitening Preprocessing for Improved Classification Accuracies in Myoelectric Control," *IEEE 37th Northeast Bioeng. Conf.*, 2011.

[13] P. Prakash, C. A. Salini, J. A. Tranquilli, D. R. Brown and E. A. Clancy, "Adaptive whitening in electromyogram amplitude estimation for epoch-based applications," *IEEE Trans. Biomed. Eng.*, vol. 52, pp. 331-334, 2005.

[14] A. Neumaier and T. Schneider, "Estimation of Parameters and Eigenmodes of Multivariate Autoregressive Models," *ACM Trans. Math. Software*, vol. 27, pp. 27–57, 2001.

[15] E. A. Clancy and N. Hogan, "Probability Density of the Surface Electromyogram and its Relationship to Amplitude Detectors," *IEEE Trans. Biomed. Eng.*, vol. 46, pp. 730–739, 1999.

CHAPTER 8

Copy of published conference paper:

Kishor Koirala, Meera Dasog, Pu Liu and Edward A. Clancy. "EMG-Torque Estimation at Future Times." *2013 IEEE 39th Annual Northeast Bioengineering Conference*, Syracuse University, pp. 59–60, 5–7 April, 2013.

EMG-Torque Estimation at Future Times

Kishor Koirala, Meera Dasog, Pu Liu and Edward A. Clancy
Worcester Polytechnic Institute, USA [kkoirala, mgdasog, puliu, ted]@wpi.edu

***Abstract*— This paper investigates the ability of surface electromyogram (EMG) to estimate joint torque at future times, up to 1 s. EMG was recorded from the biceps and triceps muscles of 54 subjects during constant-posture, force-varying contractions and related to the torque produced about the elbow. EMG to joint torque was predicted up to 80 ms into the future without any changes in the minimum least square error of 5.48% of maximum voluntary contraction for the best estimation model investigated: whitened, multiple-channel EMG used with a non-linear model. Error progressively increased for prediction times above 80 ms.**

I. Introduction

Real-time applications such as myoelectric prosthesis control [7], teleoperations and control of exoskeletons require minimization of time delays introduced between intention sensing and actuator activation. Similarly, virtual environment applications [8] employing head mounted displays need to reduce the latency between movement and scene generation. These applications motivate the need to anticipate torque ahead of time. In this regard, EMG is an attractive control source, since peak electrical activation of a muscle precedes peak twitch force by 40–100 ms. It has previously been shown that EMGσ-torque performance is improved by advanced (i.e., whitened, multiple-channel) EMGσ processing [4]. Thus, this processor was used to estimate torque at future times up to 1 second and the change in maximum voluntary contraction (MVC) flexion error was observed. Linear and non-linear models were investigated using the pseudo-inverse to regularized the least squares model fit.

II. Methods

A. Experimental Data and Methods

Experimental data from 54 subjects (30 male, 24 female; aged 37.6±16.5 years) from three prior studies were utilized. The study was approved by the WPI IRB. Subjects had previously provided written informed consent. The three studies had nearly identical apparatus and protocols with respect to the data reanalyzed [1], [3]. Subjects were seated and secured with their shoulder abducted 90°, forearm oriented in a parasagittal plane, wrist fully supinated and elbow flexed 90°. Their right wrist was rigidly cuffed to a load cell (Biodex dynamometer; or Vishay Tedea-Huntleigh Model 1042, 75 kg capacity). Skin above the muscles under investigation was scrubbed with an alcohol wipe. In one study, a small bead of electrode gel was massaged into the skin. Four bipolar electrode-amplifiers were placed transversely across each of the biceps and triceps muscles, midway between the elbow and the midpoint of the upper arm, centered on the muscle midline. Custom electronics amplified each EMG signal (CMRR of ~90 dB at 60 Hz) followed by bandpass filtering (either a 2nd-order, 10–2000 Hz bandpass filter; or 8th-order highpass at 15 Hz followed by a 4th-order lowpass at 1800 Hz). All signals were sampled at 4096 Hz with 16-bit resolution.

After a warm-up period, MVC torque was measured in both elbow extension and flexion. Five-second, constant-posture constant-force contractions at 50% MVC extension, 50% MVC flexion and rest were recorded for calibration of advanced EMGσ estimation [3], [6]. Then, a real-time feedback signal consisting of either the load cell voltage or a four-channel whitened EMGσ processor (formed by subtracting the extensor EMGσ from the flexor EMGσ) was provided on a computer screen. Thirty-second duration, constant-posture force-varying contraction trials were then recorded. The subjects used the feedback signal to track a computer-generated target that moved on the screen in the pattern of a band-limited (1 Hz) uniform random process, spanning 50% MVC extension to 50% MVC flexion. Three trials were collected.

B. Methods of Analysis

All analysis was performed offline in MATLAB. Two distinct EMGσ processors were used: single-channel unwhitened (using a centrally located electrode) and four-channel whitened [2], [3]. Each processor used a 15 Hz highpass filter (causal, 5th-order, Butterworth) and first-order (i.e., absolute value) demodulation. The four-channel processor whitened each channel prior to demodulation [6] and then averaged the four channels after demodulation. Finally, the EMGσ signal was formed by decimated this signal by a factor of 100 to a sampling rate of 40.96. To do so, the signal was decimated twice by a factor of ten (effective lowpass filter prior to downsampling of 16.4 Hz, causal, 9th-order, Chebychev Type 1). The torque signal was similarly decimated, yielding a bandwidth approximately one tenth that of the input EMGσ signals [5]. Extension and flexion EMGσs were related to joint torque via the parametric model [4]:

$$T[m] = \sum_{d=1}^{D}\sum_{q=0}^{Q} e_{q,d}\,\sigma_E^d[m-q] + \sum_{d=1}^{D}\sum_{q=0}^{Q} f_{q,d}\,\sigma_F^d[m-q]$$

where $T[m]$ is the decimated torque signal, σ_E is the extension EMGσ, σ_F is the flexion EMGσ, $e_{q,d}$ are extension fit coefficients and $f_{q,d}$ are flexion fit coefficients. Integer Q sets the number of signal lags. When integer $D=1$, the model is linear. When integer $D=2$, a nonlinear dynamic model is facilitated. Parameter Q was set to 30 for our linear model and 15 for our non-linear model. The pseudo-inverse tolerance values for varied combinations of EMG estimates were chosen based on performance results of torque estimates using the singular value decomposition pseudo-inverse technique [4]. A 5 ms time resolution was used to advance the EMG. Two seconds of data were excluded from the beginning of each 30s trial to account for filter start-up transients.

978-0-7695-4964-4/13 $26.00 © 2013 IEEE
DOI 10.1109/NEBEC.2013.88

III. RESULTS

Fig. 1 shows the average error for four processing combinations: single-channel unwhitened vs. multiple-channel whitened EMGσ estimates; cascaded with a linear vs. non-linear model structure. The lowest error is 5.48% (referenced to MVC flexion), achieved using the multiple-channel whitened EMGσ estimator and the non-linear model structure. The error does not vary for prediction times up to approximately 80 ms. This result suggests that EMG-based torque prediction at 80 ms into the future has an error that is no different than estimating torque at the current time. Table 1 shows the lowest average MVC error of the predicted torque for each of the four processing combinations.

TABLE 1 : LOWEST AVERAGE ERROR FOR FOUR EMGσ PROCESSORS

System Identification Model/EMGσ Technique	*Lowest Average Error (% MVC Flexion)*
Linear/Single Channel, Unwhitened	8.62 %
Non-linear/Single Channel, Unwhitened	7.65 %
Linear/Multiple Channel, White	6.24 %
Non-Linear/Multiple Channel, White	5.48 %

IV. DISCUSSION

EMG to torque prediction was performed to investigate error as a function of future time. Error varied with processing technique. Multiple-channel whitened EMGσ estimators provided lower errors than single-channel unwhitened. A second-degree non-linear model provided lower error than a linear model. These results are consistent with past observation in EMG-torque models [4].We observed no differences in torque estimation errors for the range of prediction times between 0–80 ms. This result is unexpected, as most researchers explicitly model delays of 40–100 ms to improve EMG-torque performance. However, these other models tend to apply fixed dynamics (e.g., first- or second-order Butterworth lowpass filter with cut-off frequency between 1–3 Hz). Our models adapt their dynamics to each subject. After prediction times of 80 ms, error grew with the amount of time into the future, until error leveled-off at approximately 600 ms with a worst-case value of approximately 18% MVC flexion. At this error, EMG is no longer indicative of the torques being produced in this experiment. The lowest errors occurred at any future time between 0–80 ms using the multiple-channel whitened EMGσ estimator and a non-linear model structure. The error corresponding to these conditions was 5.48% MVC flexion.

REFERENCES

[1] E.A. Clancy, "Electromyogram amplitude estimation with adaptive smoothing window length," IEEE Trans. Biomed. Eng., vol. 46, pp. 717–729, 1999.

[2] E.A. Clancy. EMG Amplitude Estimation Toolbox:User's Guide. Alpha version 0.07, 2010 [Online]. Available: http://www.wpi.edu/~ted/emg_tool.htm.

[3] E.A. Clancy and K.A. Farry, "Adaptive whitening of the electromyogram to improve amplitude estimation," IEEE Trans. Biomed. Eng., vol. 47, pp. 709–719, 2000.

[4] E.A. Clancy, L. Liu, P. Liu and D.V.Z. Moyer, "Identification of constant-posture EMG-torque relationship about the elbow using nonlinear dynamic models," IEEE Trans. Biomed. Eng., vol. 59, pp. 205-212, 2012.

[5] L. Ljung, System Identification: Theory for the User.. Upper Saddle River, NJ: Prentice-Hall, 1999, pp. 491–519.

[6] P. Prakash, C.A. Salini, J.A. Tranquilli, D.R. Brown and E.A. Clancy, "Adaptive whitening in electromyogram amplitude estimation for epoch-based applications," IEEE Trans. Biomed. Eng., vol. 52, pp. 331–334, 2005.

[7] T.R. Farrell and R.F. Weir, "The Optimal Controller Delay for Myoelectric Prostheses," IEEE Trans. Neural Sys. Rehab. Eng., vol. 15, pp. 111–115, 2007.

[8] Y. Barniv, M. Aguilar and E. Hasanbelliu, "Using EMG to Anticipate Head Motion for Virtual-Environment Applications, IEEE Trans. Biomed. Eng., vol. 52, pp. 1078–1093, 2005.

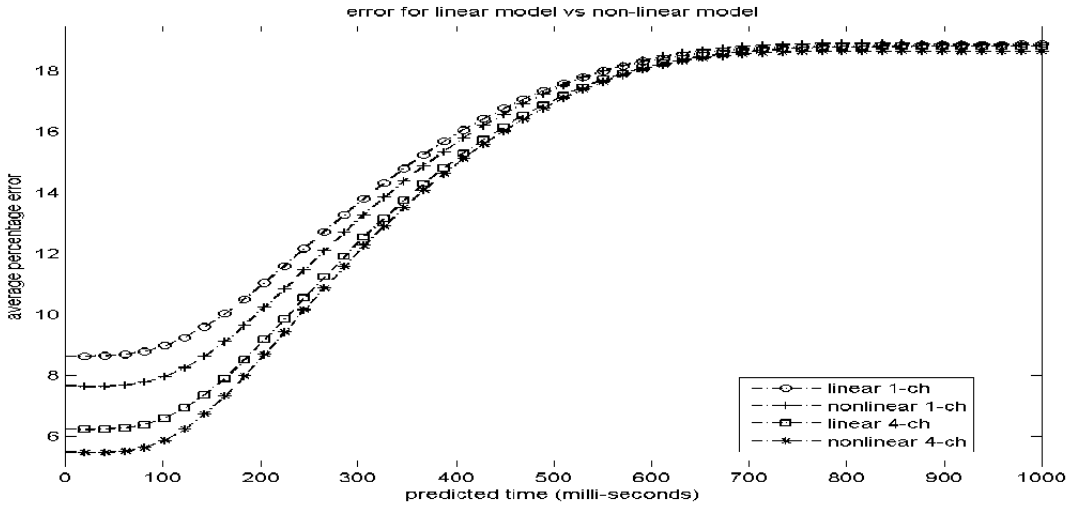

Fig. 1. Error (percent maximum voluntary flexion contraction) vs. time predicted into the future for EMG-torque processing. Error is shown for the four combinations of EMGσ estimators (single-channel unwhitened and multiple-channel whitened) and model structures (linear and non-linear). Torque estimates were computed every 5 ms. Each estimate is the average result from 54 subjects.

CHAPTER 9

Copy of published conference paper:

Meera Dasog, Kishor Koirala, Pu Liu and Edward A. Clancy. "EMG Bandwidth Used in Signal Whitening." *2013 IEEE 39th Annual Northeast Bioengineering Conference*, Syracuse University, 189–190, 5–7 April, 2013.

EMG Bandwidth Used in Signal Whitening

Meera Dasog, Kishor Koirala, Pu Liu and Edward A. Clancy
Worcester Polytechnic Institute, USA [mgdasog, kkoirala, puliu, ted]@wpi.edu

***Abstract*—It has been demonstrated that whitening the surface electromyogram (EMG) improves EMG amplitude (EMGσ) estimation. But, due to the wide bandwidth ranges often used when whitening, custom high-cost electrodes (bandwidth of ~2000 Hz) have been used. This paper investigates the effect of limiting the bandwidth for the whitened EMG data. The change in the average error of EMG to torque estimation was observed for 54 subjects over different whitening bandwidths ranging from 20–2000 Hz. We found that the average error remained the same for bandwidth limits between 600 Hz to 2000 Hz, suggesting that wider EMG electrodes were not helpful with this data set.**

I. INTRODUCTION

Whitening of the surface electromyogram (EMG) has been shown to improve EMG amplitude estimation and to lower EMG-torque errors [1], [2]. The current adaptive whitening approach used in our laboratory [3] utilizes more signal bandwidth when EMGσ is large (SNR is high) but less signal bandwidth when EMGσ is low (more noise than signal only exists at the lower frequencies). This strategy has been shown advantageous when contraction levels extent to 50–75% of maximum voluntary contraction (MVC) [1], [3]. To take advantage of the broader bandwidth during higher contraction levels, our work has utilized custom-designed electrodes with a passband to nearly 2,000 Hz. As a result, we typically sample the incoming EMG signal at 4096 Hz and implement adaptive signal whitening over the entire Nyquist bandwidth (2048 Hz). However, most day-to-day contractions occur at average levels below 25% MVC. At these contraction levels, the adaptive whitening may be discarding much of the higher frequencies in the signal. Given the cost and effort required for custom electrodes, we wanted to rigorously investigate the role of bandwidth on EMGσ processing at more modest contraction levels. In this work, the maximum frequency out to which whitening was applied was limited using digital lowpass filtering. We examined bandwidth limiting for frequencies ranging from 20 Hz to the full whitening bandwidth of 2048 Hz. For each of these bandwidths, EMG to torque estimation was performed for 54 subjects and the average error in percent MVC flexion was computed.

II. METHODS

A. Experimental Data and Methods

Experimental data from 54 subjects (30 male, 24 female; aged 37.6±16.5 years) from three prior experimental studies were analyzed. This study was approved and supervised by the WPI IRB. All subjects had previously provided written informed consent. The three studies had nearly identical experimental apparatus and protocols (fully described in [3] and [4]). Subjects were seated and secured with their shoulder abducted 90°, forearm oriented in a parasagittal plane, wrist fully supinated and elbow flexed 90°. Their right wrist was tightly cuffed to a load cell (Biodex dynamometer; or Vishay Tedea-Huntleigh Model 1042, 75 kg capacity) at the styloid process. Skin above the muscles under investigation was scrubbed with an alcohol wipe. In one study, a small bead of electrode gel was massaged into the skin. Four bipolar electrode-amplifiers were placed transversely across each of the biceps and triceps muscles, midway between the elbow and the midpoint of the upper arm, centered on the muscle midline. Each electrode-amplifier had a pair of 4-mm (or 8mm) diameter, stainless steel, hemispherical contacts separated by 10 mm edge-to-edge, oriented along the muscle's long axis. The distance between adjacent electrode-amplifiers was ~1.75 cm. A single ground electrode was gelled and secured above the acromion process or on the upper arm. Custom electronics amplified each EMG signal (CMRR of approximately 90 dB at 60 Hz) followed by bandpass filtering (either a second-order, 10–2000 Hz bandpass filter; or 8th-order highpass at 15 Hz followed by a 4th-order lowpass at 1800 Hz). All signals were sampled at 4096 Hz with 16-bit resolution.

After a warm-up period, MVC torque was measured in both elbow extension and flexion. Two repetitions of five-second duration, constant-posture constant-force contractions at 50% MVC extension, 50% MVC flexion and rest were recorded. A real-time feedback signal consisting of either the load cell voltage or a four-channel whitened EMGσ processor (formed by subtracting the extensor EMGσ from the flexor EMGσ) was provided on a computer screen. Thirty-second duration, constant-posture force-varying contraction trials were then recorded. The subjects used the feedback signal to track a computer-generated target that moved on the screen as a band-limited (1 Hz) uniform random process, spanning 50% MVC extension to 50% MVC flexion. Three trials were collected. At least three minutes of rest was provided between contractions to prevent cumulative fatigue. Additional sensors were applied and tracking trials collected, but not used in this study.

B. Methods of Analysis

All analysis was performed offline in MATLAB. A four-channel whitened (but bandwidth restricted) EMGσ processor was used. Each processor used a 15 Hz highpass filter (causal, 5th-order, Butterworth) and first-order (i.e., absolute value) demodulation. The four-channel processor whitened each channel (causal algorithm of Clancy and colleagues [3], [5], [6]). Whitening filters were calibrated from one of the constant-force contraction sets, comprised of a 50% MVC extension, 50% MVC flexion and a rest recording. To restrict bandwidth, the whitened signal was lowpass filtered using a causal, 9th-order, Chebychev Type I whose cutoff frequency was selectable. Cutoff frequencies incremented by 10 Hz between 20 and 200 Hz, and then incremented by 100 Hz up to 2000 Hz. After bandwidth restriction, each signal was demodulated and then the four EMG channels were averaged.

978-0-7695-4964-4/13 $26.00 © 2013 IEEE
DOI 10.1109/NEBEC.2013.87

Finally, the EMGσ signal was formed by decimating this signal by a factor of 100 to a sampling rate of 40.96. To do so, the signal was decimated twice by a factor of ten (effective lowpass filter prior to downsampling of 16.4 Hz, causal, 9th-order, Chebychev Type I). The torque signal was similarly decimated, yielding a bandwidth approximately one tenth that of the input EMGσ signals [7]. Extension and flexion EMGσs were related to joint torque via the parametric model [2]:

$$T[m] = \sum_{d=1}^{D}\sum_{q=0}^{Q} e_{q,d}\sigma_E^d[m-q] + \sum_{d=1}^{D}\sum_{q=0}^{Q} f_{q,d}\sigma_F^d[m-q]$$

where $T[m]$ is the decimated torque signal, σ_E is the extension EMGσ, σ_F is the flexion EMGσ, $e_{q,d}$ are extension fit coefficients and $f_{q,d}$ are flexion fit coefficients. Integer Q sets the number of signal lags. When integer D=1, the model is linear. When integer D=2, a nonlinear dynamic model is facilitated. Parameter Q was set to 30 for our linear model and 15 for our non-linear model. Fit parameters were found via least squares, regularized via the pseudo-inverse approach [2].

III. Results

Fig. 1 shows the average error (difference in the estimated vs. actual torque) from all 54 subjects for whitened multiple channel EMG, using the linear and non-linear models, as a function of maximum frequency used for whitening. The average error remains at almost constant value of 5.48% (non-linear) and 6.24% (linear) for maximum frequencies between ~600 Hz and 2000 Hz. Below maximum frequencies of ~600 Hz, the error increases. A steep error increase occurs for maximum whitening frequencies below 200 Hz.

IV. Discussion

EMG estimation was performed using different bandwidths of the whitened EMG in order to observe the change in error. It was observed that the error both for linear and non-linear models remained relatively constant over a wide range of maximum frequencies, i.e. 600 Hz up to 2000 Hz. This result questions the need for adaptive whitening over such a wide frequency range as 2048 Hz, at least for contractions at these levels. These data ranged in contraction from 50% MVC flexion to 50% MVC flexion, with an average contraction level below 25%. This result also supports eliminating the requirement to use custom high bandwidth electrodes when acquiring data with these contraction characteristics, as most off-the-shelf EMG hardware has a bandwidth up to ~500 Hz.

References

[1] E. A. Clancy and N. Hogan, "Single Site Electromyograph Amplitude Estimation," IEEE Trans. Biomed. Eng., vol. 41, pp. 159–167, 1994.

[2] E. A. Clancy, L. Liu, P. Liu and D.V.Z. Moyer, "Identification of constant-posture EMG-torque relationship about the elbow using nonlinear dynamic models," IEEE Trans. Biomed. Eng., vol. 59, pp. 205-212, 2012.

[3] E. A. Clancy and K. A. Farry, "Adaptive whitening of the electromyogram to improve amplitude estimation," IEEE Trans. Biomed. Eng., vol. 47, pp. 709–719, 2000.

[4] E. A. Clancy, "Electromyogram amplitude estimation with adaptive smoothing window length," IEEE Trans. Biomed. Eng., vol. 46, pp. 717–729, 1999.

[5] E. A. Clancy. (2010 Aug.). EMG Amplitude Estimation Toolbox:User's Guide. Alpha version 0.07, 2010 [Online]. Available: http://www.wpi.edu/~ted/emg_tool.htm.

[6] P. Prakash, C. A. Salini, J. A. Tranquilli, D. R. Brown and E. A. Clancy, "Adaptive whitening in electromyogram amplitude estimation for epoch-based applications," IEEE Trans. Biomed. Eng., vol. 52, pp. 331–334, 2005.

[7] L. Ljung, System Identification: Theory for the User.. Upper Saddle River, NJ: Prentice-Hall, 1999, pp. 491–519.

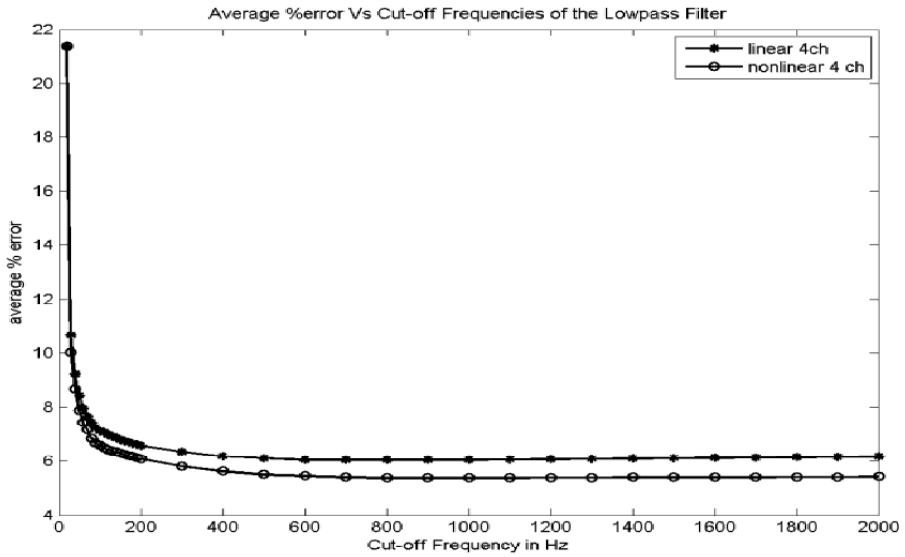

Fig. 1. Plot of average error (percent maximum voluntary flexion contraction) vs. maximum whitening frequency (a.k.a. cut-off frequency) for the linear and non-linear models.

CHAPTER 10

Copy of published conference paper:

Pu Liu, Donald R. Brown, Edward A. Clancy, Francois Martel and Denis Rancourt. "EMG-Force Estimation for Multiple Fingers." *2013 IEEE Signal Processing in Medicine and Biology Symposium (SPMB)*, Polytechnic Institute of New York University, New York, NY, 7 December 2013.

2013 IEEE Signal Processing in Medicine and Biology Symposium (SPMB),
Polytechnic Institute of New York University, New York, NY, 7 December, 2013.

EMG-Force Estimation for Multiple Fingers

Pu Liu, Donald R. Brown and *Edward A. Clancy
Department of Electrical and Computer Engineering
Worcester Polytechnic Institute, Worcester, MA, U.S.A
{puliu, drb, ted}@wpi.edu

Francois Martel and Denis Rancourt
Department of Mechanical Engineering
University of Sherbrooke, Sherbrooke, Quebec, Canada
{Francois.Martel2, Denis.Rancourt}@USherbrooke.ca

***Abstract*—Electromyogram (EMG) activity from the extensor and flexor muscles of the forearm was sensed with high-density surface electrode arrays and related to the force produced at the four fingertips during constant-posture, slowly force-varying contractions from three healthy subjects. Various electrode montages (spatial filters) and number of electrodes used in the system identification were studied. Average errors were small, ranging from 4.21 to 8.10 %MVC$_F$ (flexion maximum voluntary contraction), with errors trending lower when more EMG channels were used and when a monopolar electrode montage was selected. Results are supportive that multiple degrees of freedom of proportional control information are available from the surface EMG of the forearm, at least in intact subjects. Applications for future study include the control of prosthetic upper limb devices in amputees.**

Keywords—Biological system modeling; electromyography; EMG signal processing; biomedical signal processing.

I. Introduction

Numerous research studies have attempted to relate the electromyogram (EMG) activity of the forearm muscles to the mechanical activity of the wrist, hand and/or fingers. A primary interest is for EMG control of powered upper-limb prostheses, with additional interests including ergonomic analysis of manual tasks and clinical neuromuscular evaluation. The long-term goal for prosthetic control is to provide a replacement limb with functionality and control similar to that of an intact limb, i.e. "… simultaneous, independent, and proportional control of multiple degrees of freedom …" [1]. Existing commercial EMG-controlled powered hand prostheses are limited to rudimentary control capabilities of either three discrete states (open, close, off) or one degree of freedom of proportional control [1]. To extend control capabilities, several classification schemes using inputs from conventional surface EMG electrodes have been demonstrated in various laboratory conditions for discriminating between 5–10 hand/wrist functions [2]–[8] or for classification of individual finger movements [9]–[13]. Classification accuracy above 95% has been reported in some conditions, with accuracy decreasing as the number of classes increases, the number of EMG electrodes decreases and the window length of the EMG processor decreases. These methods may provide for increased amputee function, even though continuous proportional control of movement is generally not achieved. Some studies of finger movement have considered proportional control via EMG-based estimation of finger forces or finger joint angles [13]–[15].

Supported by U.S. Army under USAMRAA Grant W81XWH-08-1-0422.

Many studies have approached this problem while limiting the number of EMG electrodes and the amount of computer computation, since prosthesis-based solutions must fit into low power, low weight, portable systems. However, advances in EMG electrode technology and low power microprocessors are rapidly making these concerns moot, and such concerns are not as pressing in ergonomic and medical applications. In recent years, high resolution spatial filtering of surface EMG has been used to localize electrical potentials to small volumes of muscle tissue [16]–[18]. These systems are attractive for the small muscles of the forearm, in order to reduce EMG cross-talk that might hinder signal separation from functionally distinct muscles that lie in close proximity.

In this report, we describe a laboratory study that relates forearm flexor and extensor EMG to flexion-extension force generated at the tips of the four fingers (index, middle, ring, pinky) during constant-posture, slowly force-varying contractions. A high resolution EMG array was applied over the flexion and extension muscles of the forearm, and various spatial filters were utilized to enhance signal separation. The project goal was to assess the ability to determine two or more degrees of freedom of control from the agonist-antagonist muscles of the forearm.

II. Methods

A. Experimental Apparatus

The experimental apparatus consisted of a restraint device for constant-posture finger flexion-extension, a custom LabView interface for acquisition and real-time display of finger forces, and a commercial EMG amplifier array and acquisition system. The finger restraint and an EMG electrode array are shown in Fig. 1. The experimental apparatus and procedures were approved by the New England Institutional Review Board, an IRB of record for Worcester Polytechnic Institute.

The finger restraint was custom built using modular framing (10 Series Profiles, 80/20 Inc., Columbia City, IN, U.S.A.). As shown in Fig. 1, the restraint contained a rectangular base with outer dimensions of 20 by 45 cm, with extensions that were rigidly clamped to a heavy table. The subject sat along the table edge with their elbow forming a 90^o angle. A cushioned elbow rest plate was mounted at the rear of the base. The location of this plate (distance from the restraint upright) was adjusted for each subject such that the forearm was only supported by the olecranon process. The EMG electrodes, once mounted on the forearm, were never in contact

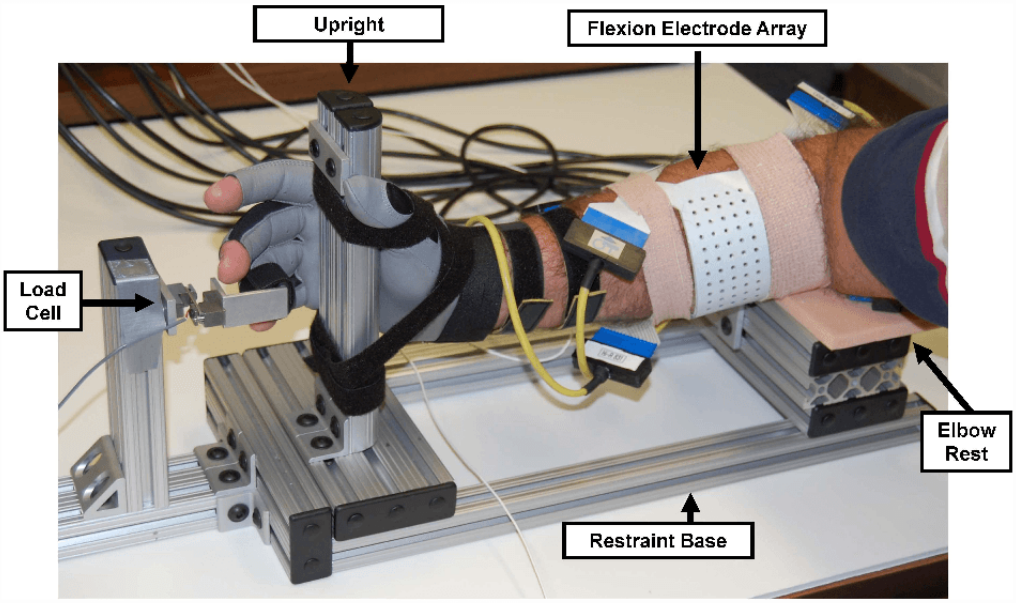

Fig. 1. Photograph of hand/arm secured into the finger restraint. A Velcro strap is wrapped around one finger (the fourth digit is used in this photo) to secure it to the load cell, which measures finger flexion-extension. The gloved hand is held to the restraint upright using Velcro. Electrode arrays are mounted over the medial (flexion array) and lateral (extension array—not visible) aspects of the forearm.

with the finger restraint. The height of the elbow rest plate was also adjusted for each finger to keep the long axis of the forearm parallel to the table. After donning a glove, the palm of the hand was secured to the front of the restraint to an upright, using Velcro. The glove adhered to the Velcro better than the bare hand and prevented the need to actively stabilize the hand during contractions of a finger. The hand was oriented with the thumb directed upwards and the four remaining digits passively curled and extending beyond the upright. The height of the hand above the base could be adjusted so that the distal phalange of any one of the four remaining digits was aligned with the load beam. A phalange was secured to the load beam by wrapping a thin Velcro strip around the beam and distal phalange. The load on this beam was measured with a one degree of freedom load cell and amplifier (Load Cell Model LCL-040, Amplifier Model DMD-465WB; Omega Engineering, Inc., Stamford, CT, U.S.A.). The cut-off frequency of the amplifier lowpass filter was set at 9.4 Hz (second-order, Bessel). A constant-posture flexion force was directed towards the restraint upright and an extension force was directed away. Measurement was only made on one digit at a time. The load cell amplifier was re-zeroed before each contraction to prevent drift during the experiment. Between trials, subjects were released from the Velcro restraints, as needed, so as to maintain normal circulation to the hand.

For EMG recordings, the skin over the circumference of the proximal right forearm was scrubbed with an alcohol wipe. Two, 64-channel monopolar electrode arrays and their associated commercial amplification-acquisition system recorded the EMG (ELSCH064R3S Adhesive Electrode Arrays, EMG-USB Amplifier; OT Bioeletronica, Torino, Italy). Each array was a rectangular, 13x5 matrix of electrodes (with one corner electrode omitted), utilizing 2 mm diameter electrodes (gel-filled) separated by 8 mm (center-to-center). The long axis of the "flexion" array was oriented and secured along the circumference of the right forearm, centered on the mid-line of the medial aspect of the forearm. The omitted corner electrode was closest to the base of the finger restraint, in the most proximal electrode column. The second "extension" array was secured with the long axis oriented along the right forearm circumference, centered on the mid-line of the lateral aspect of the forearm. The omitted corner electrode was closest to the base of the finger restraint, in the most distal electrode column. The eight extension electrodes located furthest from the base of the finger restraint along the most proximal electrode column were not recorded, leaving 56 electrodes. A gap of 3.5–7 cm existed between the two electrode arrays, both at the restraint base and 180° along the forearm circumference. The proximal edge of each EMG array was located three fingers width from the olecranon process [19]. A wrist-band reference electrode was applied to the left wrist. Two wrist-band electrodes were also used to operate a "driven-right-leg" interference attenuation circuit. Both of these electrodes were applied to the right arm, typically distal to the recording electrodes. Each electrode channel had a gain of 20,000, a bandwidth extending from 10–750 Hz, a CMRR greater than 104 dB at the power line frequency, an input impedance greater than 10^{14} Ω, and an input referred noise of less than 1 μV RMS. EMG data were sampled within the commercial amplifier system at 2048 Hz using a 12-bit ADC, and then transferred to a dedicated PC that controlled operation of the EMG system. As a measure of total EMG system noise, data from the three electrode rows closest to the muscle mid-line were analyzed while subjects relaxed their arm completely.

The recorded signal's MAV level, containing equipment noise as well as ambient physiological activity, averaged 9.44 ± 5.48% of the MAV EMG at 30% maximum voluntary contraction (MVC).

A second PC was used to collect the finger flexion-extension load cell data (after amplification) and as a subject display. The 18 inch monitor of this PC was placed approximately 1 m in front of the subject. A custom LabView interface displayed a vertical line on the screen that moved horizontally with the subject's extension-flexion force. A fixed or dynamic target could also be displayed on the screen as well as a text box indicating the voltage level corresponding to the instantaneous force exerted by the subject. The flexion-extension load cell data were acquired at 128 Hz using a 16-bit ADC (model PCI6229, National Instruments, Austin, TX, U.S.A.). In addition, a signal generator was used to produce a 1 V, 0.5 Hz sine wave. This sine wave was simultaneously acquired by the LabView PC and EMG array hardware, and utilized off-line to time synchronize the data recordings from these two devices.

B. *Experimental Methods*

Three subjects successfully completed one experiment each. Subjects had no known neuromuscular deficits of their right hand, arm or shoulder. Each subject was instructed to relax all muscles not directly involved in the task, and to maintain consistent postures and contraction techniques for each finger throughout all trials. After signing written informed consent, subjects were fitted into the hand restraint device. Subjects warmed up and accommodated to the contraction task by producing force against the load cell separately with each digit, followed by a three minute rest period to avoid fatigue. Thereafter, each subject performed separate maximum flexion, then extension trials for each of the four digits, repeated twice. For each contraction, subjects began at rest and then took 2–4 s to ramp force up to their maximum. The plateau maximum that was maintained for approximately 1 s was recorded. Consistent verbal encouragement was provided for each trial. The average flexion plateau for each digit and the average extension plateau for each digit were used as the respective MVC values. Subsequent contractions were scaled to the MVC of the respective digit.

The EMG electrode arrays were then secured to the forearm, as detailed above. Subjects then performed a series of slowly force-varying tracking tasks. The LabView display of extension-flexion force was scaled over the range from 30% MVC extension to 30% MVC flexion. A target signal on the screen began at the force level half-way between these two extremes (this level was not equivalent to zero force, since extension and flexion MVCs are not equal in magnitude), advanced to 30% extension, continued to 30% flexion, returned to 30% extension, and ended back at the half-way force. This tracking lasted 30 s, with all target movement at a constant speed equal to 6% MVC_{Ave} per second, where MVC_{Ave} is the average of the flexion and extension MVCs. Four tracking tasks were completed per digit. A typical experiment lasted approximately three hours. Explicit rest was not provided between exertion trials, since adequate rest to prevent localized fatigue was provided by only utilizing one digit per trial and rotating through the digits.

C. *Methods of Analysis*

Data Preprocessing: All data analysis was performed off-line using MATLAB (The MathWorks, Natick, MA). The sampled EMG data were bandpass filtered (15–700 Hz) using a fourth-order Butterworth filter, and second-order notch filters at the power line frequency and all harmonics (due to the presence of significant power line interference). Filtering was applied in the forward, then reverse time directions to achieve zero phase. Each data recording was plotted and reviewed. Channels with anomalous data (e.g., obviously corrupted by excessive power line noise or motion artifact) were marked and avoided from further use. Nonetheless, all desired electrode configurations were achieved. The finger force data were upsampled to the same rate as the EMG data (2048 Hz), time-aligned to the EMG data and scaled to its respective flexion MVC value (MVC_F). The fingertip force for inactive fingers was set to zero.

EMG-Force Using Classic Spatial Filters: The EMG-force model is shown in Fig. 2. Numerous classic spatial filters with known (pre-selected) spatial filter coefficients were investigated. The preprocessed extensor/flexor signal sets ($e_{E,i}[n]$, $e_{F,i}[n]$, where i indexes the spatial channels and n indexes time) were spatially filtered to produce L extensor/flexor channels ($m_{E,i}[n]$, $m_{F,i}[n]$). A spatial filter is a memory-less weighted sum of the monopolar potentials. The EMG standard deviation (EMG amplitude estimate) of each channel was computed by rectifying each channel and then decimating to 10.24 Hz. After decimating, the signal was further lowpass filtered (cut-off frequency of 1 Hz, fourth-order Butterworth filter applied in the forward, then reverse time directions), producing signals $EMG\sigma_{E,i}[m]$ and $EMG\sigma_{F,i}[m]$, where m indexes time at the reduced rate. The first and last five seconds of each 30 s tracking trial were discarded, to eliminate filter startup transients, leaving one complete contraction cycle of duration 20 s per digit. Four sequential tracking recordings, representing data from each of the four digits, were concatenated to form an 80 s data set. A fit coefficient was multiplied by each of the L extension EMGσ's to estimate each of the four digit extension force contributions (total of $4L$ coefficients). Another $4L$ coefficients were similarly required to estimate flexion force contributions. Their difference was the estimate of total force for each finger. Linear least squares was used to estimate the fit coefficients from an 80 s tracking set. Four tracking data sets were available per subject. Three data sets were used for coefficient training and the fourth for performance testing, with full leave-one-out cross-validation. The average error from the four cross-validations was expressed in percent MVC flexion (%MVC_F), relative to each respective digit.

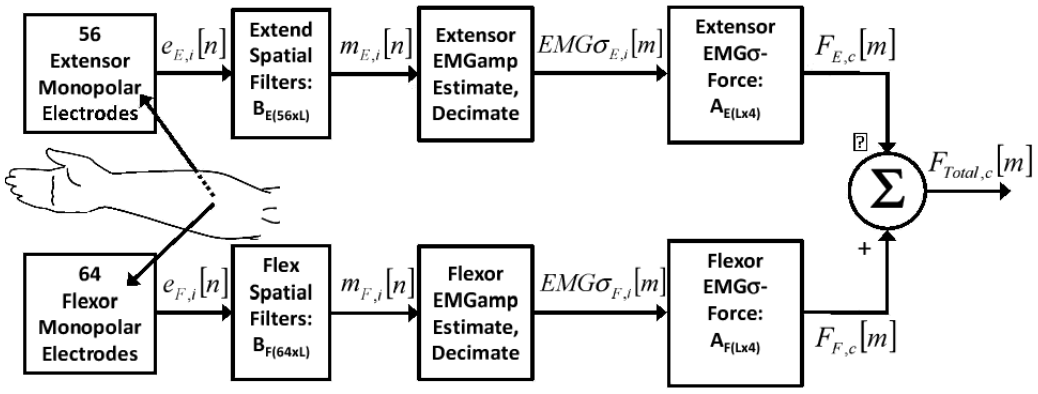

Fig. 2. EMG-force model. Each of the 56 extension and 64 flexion monopolar arrays are spatially filtered into L signals, each signal being used to produce one EMG standard deviation (EMGσ) estimate at the reduced sampling rate. Least squares estimation is then used to simultaneously relate the EMGσ's to force of the four (or selections of two) fingertips (indexed by c). Sample index n denotes signals at the rate of 2048 Hz, while sample index m denotes signals at the rate of 20.48 Hz. The "B" matrices hold the coefficients of the spatial filters, while the "A" matrices hold the coefficients relating EMGσ to torque.

Each extension/flexion EMG array contained 13 rows of electrodes. An L=13 channel monopolar spatial filter (montage) was formed by choosing one of the central electrodes in each row. Then, alternate rows were selected to form an L=7 channel monopolar spatial filter. By skipping increasingly more rows, filters were formed for L=5 and 4 channels. Next, these four row selections were repeated, utilizing additional adjacent columns to form bipolar and linear double difference (LDD) filters [16]. Note that these filters were formed along the presumed direction of action potential propagation. Lastly, normal double difference (NDD) filters were formed. Because of the additional rows required to form NDD filters, the selected channel sizes were L=11, 6 and 4. Thus a total of 15 classic spatial filters were investigated.

Models were initially formed relating the EMG channels simultaneously to forces in all four fingers. Modeling was then repeated to relate the EMG channels to force in each pair of fingers, of which there were six combinations (index-middle, index-ring, index-pinky, middle-ring, middle-pinky, ring-pinky).

III. Results

Fig. 3 shows sample results using a monopolar montage of 13 electrode channels per extension and flexion array. The pinky finger seems to exhibit the most independent control and the index finger the least. Table I shows RMS error results for the various electrode montages and number of channels, when force was simultaneously estimated in *all four* fingertips. The trend was for lower error when more EMG channels were used and when the monopolar montage was selected. In many applications, as few as two degrees of freedom of proportional control would represent a significant control advantage. Thus, Table II shows RMS error results for each *pair* of fingers for various electrode montages, using the maximum number of channels. The trend was for lower errors when using the monopolar montage and when one of the fingers in a pair was the pinky finger. All of these errors are similar in general magnitude to EMG-force errors found in studies of other joints (c.f., [20]). Given the small number of subjects (three), statistical comparisons were not pursued.

IV. Discussion

Although the sample size was small, the results showed relatively small EMG-force errors, averaging 4.21–8.10 $\%MVC_F$, depending on the number of electrode channels and the montage used. The evidence from this research work, as well as prior research (see the Introduction section) suggests that surface EMG activity from the forearm encodes multiple degrees of freedom of proportional control information that may be sufficient for use in controlling prosthetic wrists, hands and/or fingers—*at least when tested on intact subjects*. It would, therefore, seem appropriate to encourage investigation of the use of these EMG-force algorithms in amputees. It seems important to determine if the extent of information and control available in the intact forearm is also available in the remnant forearm muscles of amputees. In an off-line, four-class study, Hudgins *et al.* [5] found an average ± standard deviation classification accuracy of 91.2% ± 5.6% for able-bodied subjects and 85.5 ± 9.8% for amputees. In an off-line, 11-class study of amputees, Li *et al.* [6] found a classification accuracy of 94% ± 3% with the intact arm vs. 79% ± 11% with the amputated arm. Real-time evaluation using a virtual prosthesis showed additional performance deficits comparing the amputated side to the intact side. The reason(s) for the lower performance in these studies from the amputated side is unclear. Perhaps damage to the remnant muscle tissue has adversely altered the anatomy through reduced muscle mass, altered muscle locations, scar tissue (which insulates the EMG signal from the surface electrodes), or other affects. Alternatively, perhaps the loss of afferent receptors in the amputated arm hinders calibration of the EMG-based controllers (e.g., it is difficult for subjects to repeat a task with precision when joint torques cannot be measured)—an issue that might be alleviated through repetitive training.

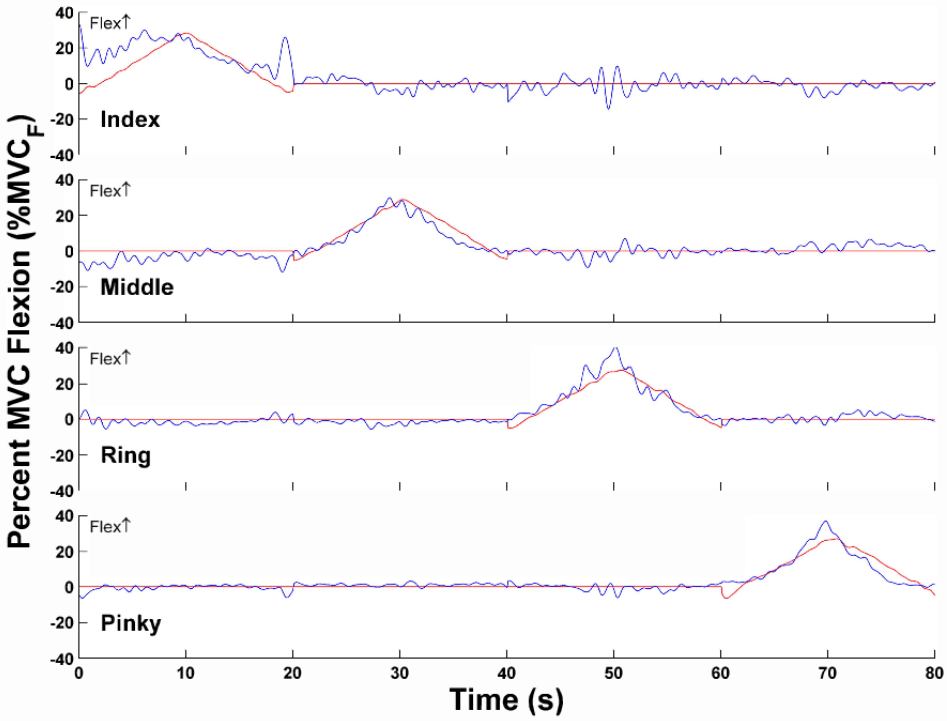

Fig. 3. Sample EMG-force test results of estimated (jagged blue line) and actual (solid red line) force vs. time using L=13 monopolar montage. Four, 20 s ramp trials are combined to form each plot. Each finger is only active for one 20-s portion and resting otherwise. Subject WY04, trials 22, 23, 32, 33.

TABLE I
AVERAGE RMS TEST ERROR RESULTS (%MVC$_F$) FROM THREE SUBJECTS FOR FINGERTIP TRACKING TRIALS WHEN ESTIMATING FORCES IN **FOUR** FINGERS SIMULTANEOUSLY

EMG Channels (L)	Spatial Filter			
	Mono	Bipolar	LDD	NDD
13 (11 for NDD)	4.41	5.49	5.97	5.51
7 (6 for NDD)	4.51	5.68	5.73	5.58
5	4.69	5.37	5.91	—
4	4.84	5.45	5.99	5.51

TABLE II
AVERAGE RMS TEST ERROR RESULTS (%MVC$_F$) FROM THREE SUBJECTS FOR FINGERTIP TRACKING TRIALS WHEN ESTIMATING FORCES IN **TWO** FINGERS SIMULTANEOUSLY, 13 EMG CHANNELS (11 FOR NDD)

Finger Pair	Spatial Filter			
	Mono	Bipolar	LDD	NDD
Index-Middle	5.82	8.10	7.72	7.60
Index-Ring	5.59	6.30	**6.14**	**5.51**
Index-Pinky	5.41	6.34	7.01	5.91
Middle-Ring	5.03	5.93	6.16	6.80
Middle-Pinky	**4.21**	5.85	6.79	6.46
Ring-Pinky	4.81	**5.81**	7.28	7.71

This study was intended as an initial assessment of EMG-force estimation in the fingers. As such, several study limitations should be noted. First, data were only analyzed from three subjects. Additional subjects would improve generalizability of the results. Second, subjects only produced constant-posture, slowly force-varying contractions. It is well known that the EMG-force relationship varies with posture [21], [22] and with force dynamics [23], [24]. Third, the performance of EMG-force models has seen little testing relative to the influences of localized muscle fatigue, electrode movement and day-to-day variations (when applicable). Fourth, the electrode arrays used in this project are not appropriate for use in reusable systems (such as prosthetics) that are routinely donned and doffed by their user. The system was selected for its large number of active electrodes, with the understanding that knowledge learned in this study might direct research towards a more deployable electrode solution in the future. Fifth, the spatial filters derived in software from the acquired monopolar EMG channels do not have characteristics identical to hardware-based spatial filters. In particular, software-derived EMG signals tend to contain higher common-mode interference (thus, our need to notch filter the power-line and its harmonics—losing a portion of the usable EMG spectrum in the process) and the smaller surface area of the array electrodes tend to exhibit more random (background) measurement noise [25]. Nonetheless, we selected a high resolution surface array to take advantage of its small inter-electrode distance (to improve selectivity), which is generally not available with conventional bipolar surface EMG systems (due to the risk of electrode shorting, among other concerns). Future EMG-based prosthesis control systems might achieve high selectivity and better noise/interference performance via indwelling electrodes [26], [27]. Lastly, our modeled relationship between forearm EMG and finger forces does not include thumb movement, thus leaving ambiguity as to how

several common hand motions (e.g., key grip, pinch grip), or even concomitant wrist activation, might be controlled. In this study, we have concentrated on determining available degrees of freedom of independent, proportional control, expecting that future research would determine how those signals might be fully utilized to control a prosthesis (or be utilized in other applications).

V. Conclusion

EMG signals were acquired from the extensor and flexor muscles of the forearm during constant-posture, slowly force-varying contractions and related to the force produced in the four fingers (index, middle, ring and pinky). Various conventional electrode montages and number of EMG channels were considered. Over a range of contraction forces spanning 30% MVC extension to 30% MVC flexion, RMS EMG-force error ranged from 4.21–8.10 $\%MVC_F$, depending on the montage and number of channels. Errors tended to be lower when more channels were used and when the monopolar montage was selected. Results were encouraging for forearm EMG-force applications in areas such as prosthesis control and ergonomic analysis.

References

[1] P. A. Parker, K. Englehart and B. Hudgins, "Myoelectric signal processing for control of powered limb prostheses," *J. Electromyo. Kinesiol.*, vol. 16, pp.541–548, 2006.

[2] K. Englehart, B. Hudgins and P. A. Parker, "A Wavelet-Based Continuous Classification Scheme for Multifunction Myoelectric Control," *IEEE Trans. Biomed. Eng.*, vol. 48, pp.302–311, 2001.

[3] K. A. Farry, I. D. Walker and R. G. Baraniuk, "Myoelectric Teleoperation of a Complex Robotic Hand," *IEEE Trans. Robot. Automat.*, vol. 12, pp. 775–788, 1996.

[4] B. Karlik, M. O. Tokhi and M. Alci, "A Fuzzy Clustering Neural Network Architecture for Multifunction Upper-Limb Prosthesis," *IEEE Trans. Biomed. Eng.*, vol. 50, pp.1255–1261, 2003.

[5] B. Hudgins, P. A. Parker, R. N. Scott, "A New Strategy for Multifunction Myoelectric Control," *IEEE Trans. Biomed. Eng.*, vol. 40, pp.82–94, 1993.

[6] G. Li, A. E. Schultz and T A. Kuiken, "Quantifying Patter Recognition-Based Myoelectric Control of Multifuntional Transradial Prostheses," *IEEE Trans. Biomed. Eng.*, vol. 18, pp. 185–192, 2010.

[7] P. Shenoy, K. J. Miller, B. Crawford and R. P. Rao, "Online Electromyographic Control of a Robotic Prosthesis," *IEEE Trans. Biomed. Eng.*, vol. 55, pp. 1128–1135, 2008.

[8] M. Zecca, S. Micera, M. C. Carrozza and P. Dario, "Control of Multifunctional Prosthetic Hands by Processing the Electromyographic Signal," *Crit. Rev. Biomed. Eng.*, vol. 30, pp. 459–485, 2002.

[9] A. Andrews, E. Morin and L. McLean, "Optimal Electrode Configurations for Finger Movement Classification using EMG," *Proc. 31st Ann. Int. Conf. IEEE EMBS*, 2009, pp. 2987–2990.

[10] J. Z. Wang, R. C. Wang, F. Li, W. Jiang and D. W. Jin, "EMG Signal Classification for Myoelectric Teloperating a Dexterous Robot Hand," *Proc. 27th Ann. Int. Conf. IEEE EMBS*, 2005, pp. 5931–5933.

[11] D. Peleg, E. Braiman, E. Yom-Tov and G. F. Inbar, "Classification of Finger Activation for Use in a Robotic Prosthesis Arm," *IEEE Trans. Neural Sys. Rehab. Eng.*, vol. 10. pp. 290–293, 2002.

[12] F. V. G. Tenore, A. Ramos, A. Fahmy, S. Acharya, R. Etienne-Cummings and N.V. Thakor, "Decoding of Individuated Finger Movements Using Surface Electromyography," *IEEE Trans. Biomed. Eng.*, vol. 56, pp. 1427–1434, 2009.

[13] C. Castellini and P. van der Smagt, "Surface EMG in Advanced Hand Prosthetics," *Bio. Cyber.*, vol. 100, pp. 35–47, 2009.

[14] R. J. Smith, D. Huberdeau, F. Tenore and N. V. Thakor, "Real-Time Myoelectric Decoding of Individual Finger Movements For a Virtual Target Task," *Proc. 31st Ann. Int. Conf. IEEE EMBS*, 2009, pp. 2376–2379.

[15] R. J. Smith, F. Tenore, D. Huberdeau, R. Etienne-Cummings and N. V. Thakor, "Continuous Decoding of Finger Position from Surface EMG Signals for the Control of Powered Prostheses," *Proc 30th Ann. Int. Conf. IEEE EMBS*, 2008, pp. 197–200.

[16] C. Disselhorst-Klug, J. Bahm, V. Ramaekers, A. Trachterna and G. Rau, "Non-invasive approach of motor unit recording during muscle contractions in humans," *Eur. J. Appl. Physiol.*, vol. 83, pp. 144–150, 2000.

[17] H. Reucher, G. Rau and J. Silny, "Spatial Filtering of Noninvasive Multielectrode EMG. I: Introduction to Measuring Technique and Implications," *IEEE Trans. Biomed. Eng.*, vol. 34, pp. 98–105, 1987.

[18] H. Reucher, J. Silny and G. Rau, "Spatial Filtering of Noninvasive Multielectrode EMG. II: Filter performance in theory and modeling," *IEEE Trans. Biomed. Eng.*, vol. 34, pp. 106–113, 1987.

[19] A. O. Perotto, *Anatomical Guide for the Electromyographer.* Third edition, Springfield, IL: Charles C Thomas, 1994, pp. 30–73.

[20] E. A. Clancy, L. Liu, P. Liu and D. V. Z. Moyer, "Identification of Constant-Posture EMG-Torque Relationship About the Elbow Using Nonlinear Dynamic Models," *IEEE Trans. Biomed. Eng.*, vol. 59, pp. 205–212, 2012.

[21] Z. Hasan and R. M. Enoka, "Isometric torque-angle relationship and movement-related activity of human elbow flexors: Implications for the equilibrium-point hypothesis," *Exp. Brain Res.*, vol. 59, pp. 441–450, 1985.

[22] J. Vredenbregt and G. Rau, "Surface electromyography in relation to force, muscle length and endurance," *New Developments in Electromyogr., Clin. Neurophysiol.*, vol. 1, pp. 607–622, 1973.

[23] G. L. Gottlieb and G. C. Agarwal, "Dynamic relationship between isometric muscle tension and the electromyogram in man," J. App. Physiol., vol. 30, pp 345–351, 1971.

[24] E. A. Clancy, O. Bida and Denis Rancourt, "Influence of advanced electromyogram (EMG) amplitude processors on EMG-to-torque estimation during constant-posture, force-varying contractions," *J. Biomech.*, vol. 39, pp. 2690-2698, 2006.

[25] R. Merletti and H. Hermens, "Detection and Conditioning of the Surface EMG Signal," in *Electromyography: Physiology, Engineering, and Noninvasive Applications.* Hoboken, NJ: R. Merletti and P. A. Parker (eds.), John Wiley & Sons, Inc., 2004, pp. 107–131.

[26] J. J. Baker, E. Scheme, K. Englehart, D. T. Hitchinson and B. Greger, "Continuous Detection and Decoding of Dexterous Finger Flexions with Implantable MyoElectric Sensors," *IEEE Trans. Rehab. Eng. Neural Sys.*, vol. 18, pp. 424–432, 2010.

[27] M. Lowery, R. F. Weir and T. A. Kuiken, "Simulation of Intramuscular EMG Signals Detected Using Implantable Myoelectric Sensors (IMES)," *IEEE Trans. Biomed. Eng.*, vol. 53, pp. 1926–1933, 2006.

CHAPTER 11

Copy of published conference paper:

Pu Liu, Francois Martel, Denis Rancourt, Edward A. Clancy, and D. Richard Brown III. “Fingertip Force Estimation from Forearm Muscle Electrical Activity.” *IEEE International Conference on Acoustics, Speech and Signal Processing (ECASSP 2014)*, in press.

FINGERTIP FORCE ESTIMATION FROM FOREARM MUSCLE ELECTRICAL ACTIVITY

Pu Liu[*], *Francois Martel*[†], *Denis Rancourt*[†], *Edward A. Clancy*[*] *and D. Richard Brown III*[*]

[*] Worcester Polytechnic Institute, Worcester, MA, USA, {puliu, ted, drb}@wpi.edu
[†] University of Sherbrooke, Sherbrooke, QC, Canada, {Francois.Martel2, Denis.Rancourt}@USherbrooke.ca

ABSTRACT

Existing commercial hand prostheses can be controlled from the electrical activity (electromyogram or EMG) of remnant muscle tissue within the forearm, but are limited in function to one degree of freedom of proportional control. In a pilot study (N=3 subjects), we used least squares estimation to identify a model between forearm electrical activity recorded by high-resolution (64 channel) electrode arrays (applied over the flexor and, separately, extensor muscles of the forearm) to force in the four fingertips. Average errors ranged from 4.21 to 10.20 $\%MVC_F$ (flexion maximum voluntary contraction), depending on the muscle contraction task performed, number of EMG electrodes in the model and the electrode montage selected. Results suggest that, at least for intact subjects, 2–4 degrees of freedom of proportional control are available from the EMG signals of the forearm.

Index Terms— EMG signal processing, biomedical signal processing, EMG-force, electromyography

1. INTRODUCTION

Classic myoelectric control of a hand prosthesis provides, at most, one degree of freedom of proportional control from the electromyogram (EMG) of one extension electrode and one flexion electrode, each placed on the skin over the remnant muscle tissue of the forearm [1, 2]. Amputees desire improved control capabilities, particularly an increase in the number of degrees of freedom [1, 2]. One approach to increased control is multifunction selection in which classification analysis is used to relate features derived from forearm EMG to various hand/wrist functions [3–9]. Classification accuracies above 95% have been achieved, with higher accuracies found when more electrodes are used, fewer functions are selected and/or longer EMG signal durations are observed. Some studies have concentrated on classification of individual finger movements [10–14]. This approach can increase amputee function, but does not provide the desired proportional control.

Supported by U.S. Army under USAMRAA grant W81XWH-08-1-0422.

Some recent effort [14–17] has concentrated on the goal of providing proportional finger control via EMG-based estimation of finger joint angles or forces. Force estimation may be preferable, as it is likely to be less influenced by external forces that interact with the hand. However, many questions remain, particularly with respect to the number of electrodes required and how their signal should be acquired and processed. In particular, the muscles of the forearm are small in cross section and packed tightly beside each other, making it difficult to sense their activities independently. Over the past few years, high resolution spatial filtering of EMG array signals has been used to localize the electrical potentials of small muscle tissue volumes [18–20]. We hypothesized that such systems would be useful in separating the source electrical activity of distinct hand muscles within the forearm, facilitating more accurate EMG-force identification.

This paper presents the methods and results of a pilot study (N=3 subjects) in which commercial high-resolution (64 channel) electrode arrays were used to measure EMG signals from the extensor and flexor muscles of the forearm while recording fingertip flexion-extension forces during constant-posture contractions. The goal of the study was to investigate and compare the performance of various EMG spatial filters ("montages") in terms of their ability to identify an EMG-force relationship for the fingertips. Our results showed average errors ranged from 4.21 to 10.20 $\%MVC_F$, depending on the muscle contraction task performed, number of EMG electrodes in the model and the electrode montage selected. Our results also suggest that, at least for intact subjects, 2–4 degrees of freedom of proportional control are available from the forearm EMG.

2. METHODS

2.1. Experimental Apparatus

The arm restraint device, shown in Fig. 1, was used to record constant-posture finger flexion-extension. The subject sat along the table edge with their elbow forming a 90° angle. The height of the elbow rest plate was adjusted for each finger to keep the long axis of the forearm parallel to the table. After donning a glove, the palm of the hand

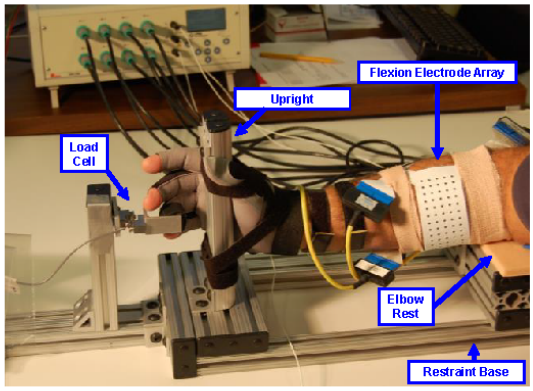

Fig. 1. Photograph of hand/arm secured into the finger restraint. Electrode arrays are mounted over the medial (flexion array) and lateral (extension array—not visible) aspects of the forearm.

was secured at the front of the restraint to an upright via Velcro. The hand was oriented with the thumb directed upwards and the four remaining digits passively curled beyond the upright. The height of the hand was adjusted to align the distal phalange of any one digits with the load beam. A phalange was secured to the load beam by a tightly-wrapped Velcro strip. Load on this beam was measured with a one degree of freedom load cell and amplifier (models LCL-040 and DMD-465WB, respectively; Omega Engineering, Inc., Stamford, CT, USA). The cut-off frequency of the amplifier lowpass filter was 9.4 Hz (second-order, Bessel). Measurement was only made on one digit at a time.

The skin over the circumference of the proximal right forearm was scrubbed with an alcohol wipe. Two, commercial 64-channel monopolar electrode arrays were applied (ELSCH064R3S Adhesive Electrode Arrays, EMG-USB Amplifier; OT Bioeletronica, Torino, Italy). Each array was a rectangular, 13x5 matrix of electrodes (with one corner electrode omitted), utilizing 2 mm diameter gel-filled electrodes separated by 8 mm center-to-center. The long axis of the "flexion" array was oriented along the circumference of the right forearm, centered on the mid-line of the medial aspect of the forearm. The second "extension" array was secured with the long axis oriented along the right forearm circumference, centered on the mid-line of the lateral aspect of the forearm. The eight extension electrodes located furthest from the base of the finger restraint along the most proximal electrode column were not used, leaving 56 electrodes. A gap of 3.5–7 cm existed between the superior and inferior edges of the two electrode arrays. The proximal edge of each EMG array was located three fingers width from the olecranon process [21]. A reference electrode was applied to the left wrist and a power-line attenuation circuit ("driven-right-leg") was applied to the right arm. Each electrode channel had a passband from 10–750 Hz, CMRR greater than 104 dB at the power line frequency, input impedance greater than 10^{14} Ω, and input referred noise <1 μV RMS. EMG data were sampled at 2048 Hz with 12-bit resolution.

A PC was used to collect the finger flexion-extension load cell data (128 Hz, 16 bits; synchronized offline with the EMG data) and as a subject display. Its 18 inch monitor was placed approximately one meter in front of the subject. A custom LabView interface displayed a vertical line on the screen that moved horizontally with the subject's extension-flexion force. A fixed or dynamic target could also be displayed on the screen.

2.2. Experimental Methods

The New England IRB approved and supervised the human studies. Three subjects each completed one experiment. Subjects had no known neuromuscular deficits of their right hand, arm or shoulder. After signing written informed consent, subjects were fitted into the hand restraint device. Each subject performed separate maximum flexion, then extension trials for each of the four digits, repeated twice. The average flexion plateau for each digit and the average extension plateau for each digit were used as the respective maximum voluntary contraction (MVC) values. Subsequent contractions were scaled to the MVC of the respective digit. The EMG electrode arrays were then secured (see above).

Subjects next performed five-second *constant-force* contractions. Two such recordings were made for 30% MVC flexion and, separately, 30% MVC extension, for each digit. Subjects lastly performed a series of *slowly force-varying (ramp)* tracking tasks. The LabView display of extension-flexion force was scaled over the range from 30% MVC extension to 30% MVC flexion. A target signal began at the force level half-way between these two extremes (this level was not equivalent to zero force, since extension and flexion MVCs are not equal), advanced to 30% extension, continued to 30% flexion, returned to 30% extension, and ended back at the half-way force. Tracking lasted for 30 seconds, with all target movement at a constant speed. Four tracking tasks were completed per digit.

2.3. Methods of Analysis

Data Preprocessing: Data analysis was performed off-line using MATLAB. The sampled EMG data were bandpass filtered (15–700 Hz) using a fourth-order Butterworth filter, and second-order notch filters at the power line frequency and all harmonics. Filtering was applied in the forward, then reverse time directions to achieve zero phase. Each data recording was plotted and reviewed. Channels with anomalous data (e.g., obviously corrupted by excessive power line noise or motion artifact) were avoided from further use. Regardless, all desired electrode configurations were achieved. The finger force data were upsampled to the same rate as the EMG data (2048 Hz), time-aligned to the

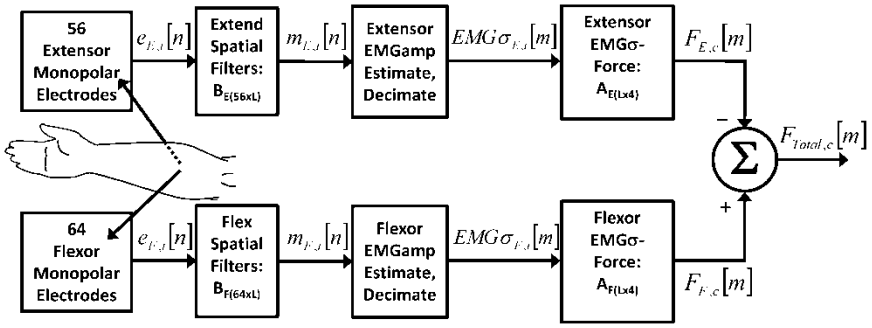

Fig. 2. EMG-force model. Extension and flexion monopolar arrays are spatially filtered into L signals, each signal being used to produce one EMG standard deviation (EMGσ) estimate. Least squares estimation then relates the EMGσ's to force of the four fingertips (indexed by c). The "B" matrices hold the coefficients of the spatial filters; the "A" matrices hold the coefficients relating EMGσ to force.

EMG data and scaled to its respective flexion MVC value. The fingertip force for inactive fingers was set to zero.

EMG-Force Processing: The EMG-force model is shown in Fig. 2. Numerous classic spatial filters with known (pre-selected) spatial filter coefficients were investigated. The preprocessed extensor/flexor signal sets ($e_{E,i}[n]$, $e_{F,i}[n]$, where i indexes the spatial channels and n indexes time) were spatially filtered to produce L extensor/flexor channels ($m_{E,i}[n]$, $m_{F,i}[n]$). A spatial filter is a memory-less weighted sum of the monopolar potentials. The EMG standard deviation (EMG amplitude estimate) of each channel was computed by rectifying each channel and then decimating to 10.24 Hz. After decimating, the signal was further lowpass filtered (cut-off frequency of 1 Hz, fourth-order Butterworth filter applied in the forward, then reverse time directions), producing signals $EMG\sigma_{E,i}[m]$ and $EMG\sigma_{F,i}[m]$, where m indexes time at the reduced rate. This reduced rate is appropriate as it is approximately ten times that of the force signal being estimated [22, 23].

For the *constant-force* recordings, distinct five second flexion and extension recordings from each finger were concatenated, forming a 40 second data set (4 fingers x 10 seconds per finger). A fit coefficient was multiplied by each of the L extension EMGσ's to estimate each of the four digit extension force contributions (total of $4L$ coefficients). Another $4L$ coefficients were similarly required to estimate flexion force contributions. Their difference was the estimate of total force for each finger. Linear least squares was used to estimate the fit coefficients from a 40 second data set. Since there were two constant-force recordings per finger per flexion/extension contraction, two such sets were available per subject. One set was used for coefficient training and the second for performance testing, with full leave-one-out cross-validation. The average error from the two test cross-validations was expressed in percent MVC flexion (%MVC$_F$), relative to each respective digit.

For the *slowly force-varying (ramp)* contractions, the first and last five seconds of each 30 second tracking trial were discarded, leaving one complete contraction cycle of duration 20 seconds per digit. Four sequential tracking recordings, representing data from each of the four digits, were concatenated to form an 80 second data set. Linear least squares was again used to estimate fit coefficients (same method as described above) from an 80 second tracking set. Four tracking data sets were available per subject. Three data sets were used for coefficient training and the fourth for performance testing, with full leave-one-out cross-validation. The average error from the four cross-validations was expressed in %MVC$_F$, relative to each respective digit.

For each of the constant-force and ramp contraction data sets, each extension/flexion EMG array contained 13 rows of electrodes. An L=13 channel monopolar spatial filter (montage) was formed by choosing one of the central electrodes in each row. Then, alternate rows were selected to form an L=7 channel monopolar spatial filter. By skipping increasingly more rows, filters were formed for L=5 and 4 channels. Next, these four row selections were repeated, utilizing additional adjacent columns to form bipolar and linear double difference (LDD) filters [20]. Note that these filters were formed along the presumed direction of action potential propagation. Lastly, normal double difference (NDD) filters were formed. Because of the additional rows required to form NDD filters, the selected channel sizes were L=11, 6 and 4. Thus, a total of 15 classic spatial filters were investigated.

3. RESULTS

Fig. 3 shows sample results from the *constant-force trials* using a 5-channel, bipolar electrode montage. Table I shows the complete summary results for all montages and number of EMG channels studied. Fig. 4 shows sample results from the *slowly force-varying (ramp) trials* using a 13-channel monopolar montage. Table II shows the complete summary results. Taken together, the results suggest that the montages known to be more spatially selective (LDD and

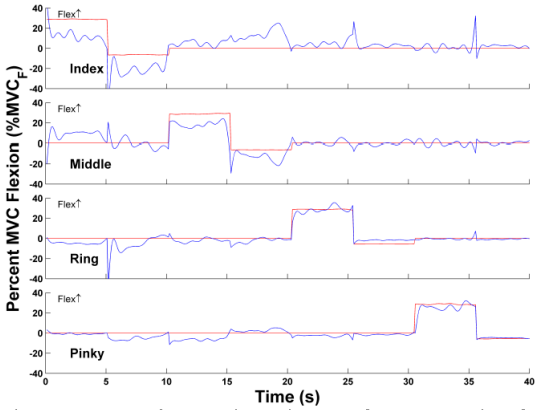

Fig. 3. *Constant-force trial* sample EMG-force test results of estimated (jagged blue line) and actual (solid red line) force vs. time using L=5 bipolar montage. Subject WZ04, trials 01–08.

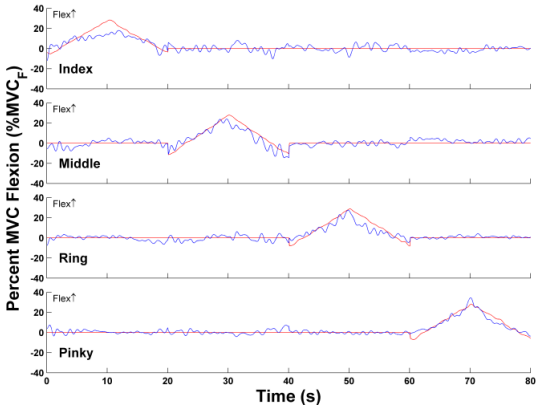

Fig. 4. *Slowly force-varying (ramp) force trial* sample EMG-force test results of estimated (jagged blue line) and actual (solid red line) force vs. time using L=13 monopolar montage. Subject WZ09, trials 26, 27, 36, 37.

TABLE I
CONSTANT-FORCE TRIAL AVERAGE RMS TEST ERROR RESULTS (%MVC$_F$)

EMG Channels (L)	Spatial Filter			
	Mono	Bipolar	LDD	NDD
13 (11 for NDD)	9.25	8.03	10.02	10.03
7 (6 for NDD)	8.95	8.99	8.64	10.20
5	8.34	7.22	10.31	—
4	7.82	8.43	8.17	8.82

TABLE II
SLOWLY FORCE-VARYING (RAMP) TRIAL AVERAGE RMS TEST ERROR RESULTS (%MVC$_F$)

EMG Channels (L)	Spatial Filter			
	Mono	Bipolar	LDD	NDD
13 (11 for NDD)	4.41	5.49	5.97	5.51
7 (6 for NDD)	4.51	5.68	5.73	5.58
5	4.69	5.37	5.91	—
4	4.84	5.45	5.99	5.51

NDD) did ***not*** produce lower EMG-force estimation errors; in fact, their errors were generally higher. There was also not a strong trend for lower errors as the number of EMG channels was increased. The constant-force results seem to show higher average errors overall, perhaps due to the small duration of signal (5 seconds) available for training [24]. Given the small number of subjects, statistical comparisons were not pursued.

4. DISCUSSION AND CONCLUSIONS

The EMG-force errors found in this study (ranging from 4.21 to 10.20 %MVC$_F$) are similar to errors found in studies of other joints (c.f., [24]). This outcome is significant, since there is currently no consensus within the literature that multiple degrees of freedom of proportional control are available—*at least in intact subjects*—to relate forearm electrical activity to fingertip forces. Further, these results suggest that there may be no obvious advantage to high-resolution (and high channel count) electrode arrays and spatial montages. Such arrays are thought to reduce EMG crosstalk (undesired recording of more distant muscles away from the recording site). Crosstalk is thought to confound EMG-force identification, although blind source separation techniques have been attempted to resolve this problem [25]. If high resolution arrays provide little or no advantage, then standard electrode hardware might be used instead. Such hardware is simpler, less expensive and more readily available. In fact, existing commercial high resolution arrays are not suitable (or designed) for use in commercial prostheses.

The sample size used in this study was small and primarily intended as part of a pilot study. While the results are encouraging, a number of limitations exist, including: the lack of dynamics in the contraction forces, the limitation of constant-posture contractions, the omission of models that incorporate the thumb (necessary for many hand actions/grips) and the limited model forms studied.

In summary, EMG signals were acquired from the extensor and flexor muscles of the forearm during constant-posture contractions and related to the force produced in the four fingers (index, middle, ring and pinky). Various conventional electrode montages and number of EMG channels were considered. Over a range of contraction forces spanning 30% MVC extension to 30% MVC flexion, RMS EMG-force error ranged from 4.21–10.20 %MVC$_F$, depending on the montage and number of channels. Results were encouraging for finger EMG-force applications in prosthesis control.

5. REFERENCES

[1] P. A. Parker, K. Englehart and B. Hudgins, "Myoelectric signal processing for control of powered limb prostheses," *J. Electromyo. Kinesiol.*, vol. 16, pp.541–548, 2006.

[2] D. Atkins, D. C. Y. Heard and W. H. Donovan, "Epidemiologic overview of individuals with upper-limb loss and their reported research priorities," *J. Prosthet. Orthot.*, vol. 8, pp. 2-11, 1996.

[3] B. Hudgins, P. A. Parker, R. N. Scott, "A New Strategy for Multifunction Myoelectric Control," *IEEE Trans. Biomed. Eng.*, vol. 40, pp.82–94, 1993.

[4] K. A. Farry, I. D. Walker and R. G. Baraniuk, "Myoelectric Teleoperation of a Complex Robotic Hand," *IEEE Trans. Robot. Automat.*, vol. 12, pp. 775–788, 1996.

[5] K. Englehart, B. Hudgins and P. A. Parker, "A Wavelet-Based Continuous Classification Scheme for Multifunction Myoelectric Control," *IEEE Trans. Biomed. Eng.*, vol. 48, pp.302–311, 2001.

[6] M. Zecca, S. Micera, M. C. Carrozza and P. Dario, "Control of Multifunctional Prosthetic Hands by Processing the Electromyographic Signal," *Crit. Rev. Biomed. Eng.*, vol. 30, pp. 459–485, 2002.

[7] B. Karlik, M. O. Tokhi and M. Alci, "A Fuzzy Clustering Neural Network Architecture for Multifunction Upper-Limb Prosthesis," *IEEE Trans. Biomed. Eng.*, vol. 50, pp.1255–1261, 2003.

[8] P. Shenoy, K. J. Miller, B. Crawford and R. P. Rao, "Online Electromyographic Control of a Robotic Prosthesis," *IEEE Trans. Biomed. Eng.*, vol. 55, pp. 1128–1135, 2008.

[9] G. Li, A. E. Schultz and T A. Kuiken, "Quantifying Patter Recognition-Based Myoelectric Control of Multifuntional Transradial Prostheses," *IEEE Trans. Biomed. Eng.*, vol. 18, pp. 185–192, 2010.

[10] A. Andrews, E. Morin and L. McLean, "Optimal Electrode Configurations for Finger Movement Classification using EMG," *Proc. 31st Ann. Int. Conf. IEEE EMBS*, 2009, pp. 2987–2990.

[11] D. Peleg, E. Braiman, E. Yom-Tov and G. F. Inbar, "Classification of Finger Activation for Use in a Robotic Prosthesis Arm," *IEEE Trans. Neural Sys. Rehab. Eng.*, vol. 10. pp. 290–293, 2002.

[12] J. Z. Wang, R. C. Wang, F. Li, W. Jiang and D. W. Jin, "EMG Signal Classification for Myoelectric Teloperating a Dexterous Robot Hand," *Proc. 27th Ann. Int. Conf. IEEE EMBS*, 2005, pp. 5931–5933.

[13] F. V. G. Tenore, A. Ramos, A. Fahmy, S. Acharya, R. Etienne-Cummings and N.V. Thakor, "Decoding of Individuated Finger Movements Using Surface Electromyography," *IEEE Trans. Biomed. Eng.*, vol. 56, pp. 1427–1434, 2009.

[14] C. Castellini and P. van der Smagt, "Surface EMG in Advanced Hand Prosthetics," *Bio. Cyber.*, vol. 100, pp. 35–47, 2009.

[15] R. J. Smith, F. Tenore, D. Huberdeau, R. Etienne-Cummings and N. V. Thakor, "Continuous Decoding of Finger Position from Surface EMG Signals for the Control of Powered Prostheses," *Proc 30th Ann. Int. Conf. IEEE EMBS*, 2008, pp. 197–200.

[16] R. J. Smith, D. Huberdeau, F. Tenore and N. V. Thakor, "Real-Time Myoelectric Decoding of Individual Finger Movements For a Virtual Target Task," *Proc. 31st Ann. Int. Conf. IEEE EMBS*, 2009, pp. 2376–2379.

[17] S. Muceli and D. Farina, "Simultaneous and proportional estimation of hand kinematics from EMG during mirrored movements at multiple degrees-of-freedom, "IEEE Trans. Neural Sys. Rehabil. Eng., vol. 20, pp. 371–378, 2012.

[18] H. Reucher, G. Rau and J. Silny, "Spatial Filtering of Noninvasive Multielectrode EMG. I: Introduction to Measuring Technique and Implications," *IEEE Trans. Biomed. Eng.*, vol. 34, pp. 98–105, 1987.

[19] H. Reucher, J. Silny and G. Rau, "Spatial Filtering of Noninvasive Multielectrode EMG. II: Filter performance in theory and modeling," *IEEE Trans. Biomed. Eng.*, vol. 34, pp. 106–113, 1987.

[20] C. Disselhorst-Klug, J. Bahm, V. Ramackers, A. Trachterna and G. Rau, "Non-invasive approach of motor unit recording during muscle contractions in humans," *Eur. J. Appl. Physiol.*, vol. 83, pp. 144–150, 2000.

[21] A. O. Perotto, *Anatomical Guide for the Electromyographer*. Third edition, Springfield, IL: Charles C Thomas, 1994, pp. 30–73.

[22] L. Ljung, *System Identification: Theory for the User*. Upper Saddle River, NJ: Prentice-Hall, 1999, pp. 491–519.

[23] E. A. Clancy, O. Bida, and D. Rancourt, "Influence of advanced electromyogram (EMG) amplitude processors on EMG-to-torque estimation during constant-posture, force-varying contractions," *J. Biomech.*, vol. 39, pp. 2690–2698, 2006.

[24] E. A. Clancy, L. Liu, P. Liu and D. V. Z. Moyer, "Identification of constant-posture EMG-torque relationship about the elbow using nonlinear dynamic models," *IEEE Trans. Biomed. Eng.*, vol. 59, pp. 205–212, 2012.

[25] D. Farina, C. Fevotte, C. Doncarli and R. Merletti, "Blind separation of linear instantaneous mixtures of nonstationary surface myoelectric signals," *IEEE Trans. Biomed. Eng.*, vol. 51, pp. 1555–1567, 2004.

CHAPTER 12

Copy of published journal paper:

Edward A. Clancy, Lukai Liu, Pu Liu and Daniel V. Moyer. "Identification of Nonlinear, Dynamic EMG-Torque Relationship About the Elbow." *IEEE Transactions on Biomedical Engineering*, Vol. 59, No. 1, pp. 205-212, 2012.

Identification of Constant-Posture EMG–Torque Relationship About the Elbow Using Nonlinear Dynamic Models

Edward A. Clancy*, *Senior Member, IEEE*, Lukai Liu, Pu Liu, and Daniel V. Zandt Moyer

***Abstract*—The surface electromyogram (EMG) from biceps and triceps muscles of 33 subjects was related to elbow torque, contrasting EMG amplitude (EMGσ) estimation processors, linear/nonlinear model structures, and system identification techniques. Torque estimation was improved by 1) advanced EMGσ processors (i.e., whitened, multiple-channel signals); 2) longer duration training sets (52 s versus 26 s); and 3) determination of model parameters via pseudoinverse and ridge regression methods. Dynamic, nonlinear parametric models that included second- or third-degree polynomial functions of EMGσ outperformed linear models and Hammerstein/Weiner models. A minimum error of 4.65 $\pm$ 3.6% maximum voluntary contraction (MVC) flexion was attained using a third-degree polynomial, 28th-order dynamic model, with model parameters determined using the pseudoinverse method with tolerance 5.6×10^{-3} on 52 s of four-channel whitened EMG data. Similar performance (4.67 $\pm$ 3.7% MVC flexion error) was realized using a second-degree, 18th-order ridge regression model with ridge parameter 50.1.**

***Index Terms*—Biological system modeling, biomedical signal processing, electromyography, EMG amplitude estimation, EMG signal processing.**

I. Introduction

THE SURFACE electromyogram (EMG) reflects the neural activity of the underlying musculature, and has often been used to estimate torque produced about joints. Typically, EMG amplitude (EMGσ)—the time-varying standard deviation of the EMG waveform—is estimated and then related to joint torque through parametric models determined via system identification techniques. Both agonist and antagonist muscles are included in these models to account for cocontraction (particularly at higher contraction levels) [1]–[3]. Low-error EMG–torque estimation has several applications. In prosthesis control [4], it would be expected to provide more accurate emulation of the natural command relationship between the central nervous system and peripheral joints/muscles. In ergonomics [5]–[7] and clinical biomechanics [8], [9], it should lead to better estimates of joint loading and muscle tension in studies of worker tasks and biomechanical evaluations. Other applications include investigation of motor control [10] and control of powered exoskeletons [11]–[13].

Numerous studies, concentrating on various aspects of the EMG-torque problem, have been conducted over the years (see [14] for a recent review). Study conditions have ranged from constant-posture, constant-torque (the simplest) to posture-varying, torque-varying (the most complete case, representing unconstrained movement). The latter condition is most representative of the full range of application tasks, but can be too complex when studying methodological improvements (such as those presented herein). To reduce EMG–torque estimation error, some research has applied advanced EMGσ estimation methods [15]–[25] or advanced/nonlinear system identification methods relating EMGσ to torque [1]–[3], [6], [26]–[29].

Based on past research results, we hypothesized that incorporating nonlinear model structures into the EMG-torque problem—along with advanced EMGσ processors—would further reduce joint torque error. However, nonlinear models typically require additional parameters, which can lead to overfitting [30]. There exists a complex interplay between the number of fit parameters in the model, training data duration, the SNR of the training data, and the system identification method [30].

Accordingly, this study compares system identification methods for nonlinear EMG–torque models using advanced EMGσ processors (whitening and multiple-channel combination), explicitly addressing model overfitting. Hammerstein and Weiner models were specifically examined because their smaller number of model parameters is expected to alleviate overfitting [30]. We investigated the fitting of model parameters through the singular-value-decomposition-based least squares pseudoinverse approach, in which certain linear combinations of the training data—those that likely provide little information but contain considerable noise—are omitted from the training solution [31]. We evaluated least squares estimation of the training parameters using ridge regression [32]–[34]. Additionally, we studied the effect of training data duration, as longer training datasets support models with more parameters.

II. Methods

A. Experimental Data and Methods

A subset of experimental data from 33 subjects (18 male and 15 female, ranging in age from 18 to 65 years) from two

Manuscript received February 21, 2011; revised July 15, 2011; accepted September 20, 2011. Date of publication October 3, 2011; date of current version December 21, 2011. *Asterisk indicates corresponding author.*

*E. A. Clancy is with the Department of Electrical and Computer Engineering, Worcester Polytechnic Institute (WPI), Worcester, MA 01609 USA, and also with the Department of Biomedical Engineering, WPI, Worcester, MA 01609 USA (e-mail: ted@wpi.edu).

L. Liu and P. Liu are with the Department of Electrical and Computer Engineering, Worcester Polytechnic Institute, Worcester, MA 01609 USA (e-mail: lliu35@wpi.edu; puliu@wpi.edu).

D. V. Z. Moyer is with Genapsys, Inc., Menlo Park, CA 94025-1438 USA (e-mail: korthog@gmail.com).

Digital Object Identifier 10.1109/TBME.2011.2170423

prior studies of the upper arm (fully described in [35] and [36]) were reanalyzed. Because these data had been de-identified and unlinked, the WPI Institutional Review Board stipulated that supervision of this reanalysis was not required. In these studies, each subject was secured into the seat of a Biodex exercise machine with his/her shoulder abducted 90°, forearm oriented in a parasaggital plane, wrist fully supinated, and elbow flexed 90°. The subject was rigidly attached to the Biodex dynamometer with a cuff at the styloid process. The skin above the muscles under investigation was cleaned with an alcohol wipe. An array of four Liberty Technology, Hopkinton, MA, MYO115 EMG electrode-amplifiers were placed transversely across each of the biceps and triceps muscles, midway between the elbow and the midpoint of the upper arm, centered on the muscle midline. Each electrode-amplifier had a pair of 4-mm diameter, stainless steel, hemispherical contacts separated by 15 mm (center to center), oriented along the muscle's long axis. The distance between adjacent electrode-amplifiers was approximately 1.75 cm. A single ground electrode was gelled and secured above the acromion process. Custom electronics amplified and filtered each EMG signal (common mode rejection ratio of approximately 90 dB at 60 Hz; second-order, 10–2000 Hz bandpass filter) before being sampled at 4096 Hz with 16-bit resolution.

Each subject was provided a warm-up period, after which MVC torque was measured in both elbow extension and flexion. 5-s duration, constant-posture constant-force contractions at 50% MVC extension, 50% MVC flexion and rest were recorded. These contractions were used to calibrate the advanced EMGσ estimation algorithms [36], [37]. Then, a real-time feedback signal consisting of one of four EMGσ processors (formed by subtracting the extensor EMGσ from the flexor EMGσ) was provided on a computer screen. The processors were single-channel unwhitened, single-channel whitened, multiple-channel unwhitened, and multiple-channel whitened. 30-s duration, constant-posture force-varying contraction trials were then recorded. The subjects used the feedback signal to track a computer-generated target that moved on the screen in the pattern of a bandlimited (1 Hz) uniform random process, spanning 50% MVC extension to 50% MVC flexion. Twelve trials (three per feedback signal) were collected in a randomized order. Additional tracking trials not used in this study were also collected. Rest was provided between trials to prevent cumulative fatigue.

B. Methods of Analysis

All analysis was performed offline in MATLAB. Two distinct EMGσ processors were created from each of the extension and flexion muscle groups for each 30 s trial using our open-source MATLAB toolbox [38]. The estimates were either single-channel unwhitened (using an electrode located centrally on the muscle) or four-channel whitened [19]. Each estimator utilized a 15-Hz high-pass filter (fifth-order Butterworth applied in the forward and reverse time directions to achieve zero phase) and a first-order demodulator (rectifier). Whitened channels used the noncausal adaptive whitening algorithm of Clancy and colleagues [36], [37]. After demodulation, signals were decimated by a factor of 100 to a sampling rate of 40.96 Hz, using a low-pass filter with cutoff frequency of 16.4 Hz (that also served as the smoothing stage of the amplitude estimate). The torque signal was similarly decimated, producing a dataset with a bandwidth approximately ten times that of the torque signal being estimated [22], [30].

Extension and flexion EMGσs were related to joint torque using four parametric, dynamic model structures. For each structure $T[m]$ was the measured torque at the mth decimated sample; a_0 was an offset parameter (not used in all system identification techniques); e_q and f_q were the extension and flexion fit parameters, respectively, and $\sigma_E[m]$ and $\sigma_F[m]$ were the extension and flexion EMGσ estimates, respectively. The model structures were the following.

1) Linear, time invariant (LTI) system of dynamic order Q

$$T[m] = a_0 + \sum_{q=0}^{Q} e_q \sigma_E[m-q] + \sum_{q=0}^{Q} f_q \sigma_F[m-q]. \tag{1}$$

2) Polynomial nonlinear model of degree D, dynamic order Q

$$T[m] = a_0 + \sum_{d=1}^{D}\sum_{q=0}^{Q} e_{q,d}\sigma_E^d[m-q] + \sum_{d=1}^{D}\sum_{q=0}^{Q} f_{q,d}\sigma_F^d[m-q]. \tag{2}$$

3) Hammerstein model: This model was comprised of a Dth-degree polynomial static nonlinearity cascaded with a Qth-order, LTI, finite impulse response (FIR) system, for each of the extension and flexion EMGσ inputs. The sum of the extension and flexion outputs was related to joint torque.
4) Weiner model: This model was comprised of a Qth-order, LTI, FIR system cascaded with a Dth-degree polynomial static nonlinearity, for each of the extension and flexion EMGσ inputs. The sum of the extension and flexion outputs was related to joint torque.

In these four model structures, the LTI system order ranged from $1 \leq Q \leq 30$ and the polynomial degree ranged from $1 \leq D \leq 4$. 2 s of data were excluded from the beginning and end of each 30 s signal to mitigate filter start-up transients.

The parameters of the LTI and polynomial models were estimated using linear least squares. Three approaches were evaluated to reduce overfitting during parameter estimation. First, the singular value decomposition-based pseudoinverse was used, in which the reciprocals of small singular values were replaced with the value zero [31]. The tolerance for replacement was based on the ratio of each singular value to the maximum singular value, ranging over 40 values spanning 10^{-16} to 0.5 in logarithmic increments. The pseudoinverse model did not include an offset term a_0. Second, ridge regression [32]–[34] was investigated, including an offset term a_0 in the model. The ridge parameter k ranged from 10^{-7} to 10^4 in 112 logarithmic increments. Third, we examined the effect of increasing the duration of data available to train the least squares, as described in detail in the following. Parameters of the Hammerstein and Weiner

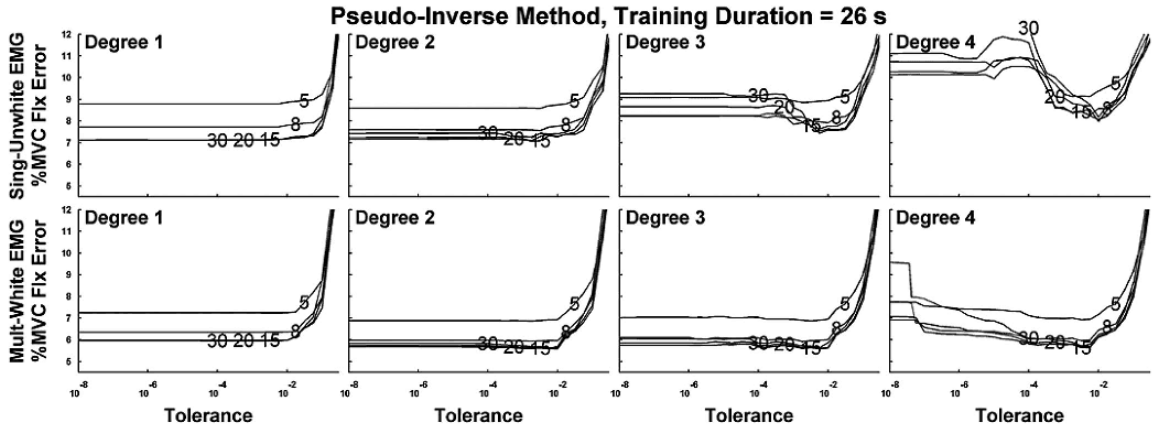

Fig. 1. EMG–torque error as a function of tolerance value, using the *pseudoinverse* system identification method, with 26 s of *training data*. Results for tolerance values below 10^{-8} not shown, but follow similar trend. Each row shows results from the two EMGσ processors; columns distinguish the different polynomial model degrees D. Each plot shows the results for representative dynamic model orders (Q) 5, 8, 15, 20, and 30, as labeled. Each result is the average from 33 subjects.

models were determined via nonlinear least squares using the MATLAB system identification toolbox.

As noted previously, each subject completed 12 tracking trials, consisting of three repetitions each of four different feedback options. Each set of three repetitions (representing one feedback style) was used to produce one test result. In the single-trial calibration method, the first trial was used as training data and the second as a test set. Then, the third trial was used as training data and the second was again used as the test set. The average mean absolute value error (between the actual torque and that predicted by the EMG–torque model) of these two test results is reported as the test error value. In the dual-trial calibration method, the first and third trials were simultaneously used to train one set of parameters (effective sequence duration of 52 s), and then tested on the second trial. Since all of this analysis was performed postexperiment, tracking performance during data collection was not directly relevant. Rather, the recorded EMG was related to the recorded joint torque from the load cell—the real-time feedback signal was not considered. In general, each of the feedback options produced torque with a similar characteristic (uniform random signal bandlimited to 1 Hz). Nonetheless, all training and testing remained within a feedback style. In all cases, error is reported as a percent of the MVC flexion torque. Only test trial results are presented. For statistical analysis, the four test trial results from each subject were averaged, and these average values subjected to a paired sign test [39].

Finally, it was desired to compare the results using these advanced EMGσ processors and models to a "conventional" EMG-torque estimator. A conventional estimator was formed by filtering the single-channel unwhitened EMGσs from each of the biceps and triceps muscles through a second-order, Butterworth, low-pass filter, gain scaling these outputs based on their respective 50% MVC contractions (achieved by using the 50% MVC contractions to calibrate a zero-order linear model using the pseudoinverse approach with the default tolerance in MATLAB), and then subtracting them to form the torque estimate. Typically, the cutoff frequency of the low-pass filter in conventional estimators is set at a few Hertz [29], [40], [41]. In our case, selection of the appropriate cutoff frequency was unclear. Thus, we repeated conventional torque estimation 40 times with cutoff frequencies ranging from 0.1 to 4.0 Hz, in increments of 0.1 Hz. The best of these 40 results is reported. Note that the cutoff frequency was not adapted to individual subjects; only one flexion and one extension gain was subject-specific (based on the 50% MVC contractions). Training and testing proceeded as described previously.

III. Results

EMG-torque performance was studied as a function of two EMGσ processors, four model structures, and three system identification techniques. Figs. 1–4 graphically depict the representative aspects of the overall test results. Fig. 1 concentrates on results from the pseudoinverse approach, Fig. 2 on ridge regression results, Fig. 3 on Hammerstein/Weiner model results, and Fig. 4 on results using the longer duration training data (52 s). Figs. 1, 2, and 4 show results only from dynamic model orders $Q = 5$, 8, 15, 20, and 30, which form a representative subset of the 30 model orders evaluated. Table I lists the lowest test error, along with the corresponding model parameters, for the pseudoinverse approach results. Overall, models that utilized a low model order (e.g., $Q \leq 5$) exhibited high error, presumably because this low model order did not sufficiently capture the system's true dynamic behavior. Exceptionally high dynamic model order often also led to higher error, particularly for high polynomial model degrees and with single-channel unwhitened EMGσ processors (or their combination), presumably due to overfitting. Excessively large pseudoinverse tolerance values or ridge k values exhibited poor performance, and should be avoided.

Figs. 1 and 2 each provide direct comparison between the EMGσ processors. Excluding tolerance values above $\sim 10^{-2}$ (see Fig. 1) and ridge k values below ~ 1 (see Fig. 2)—regions

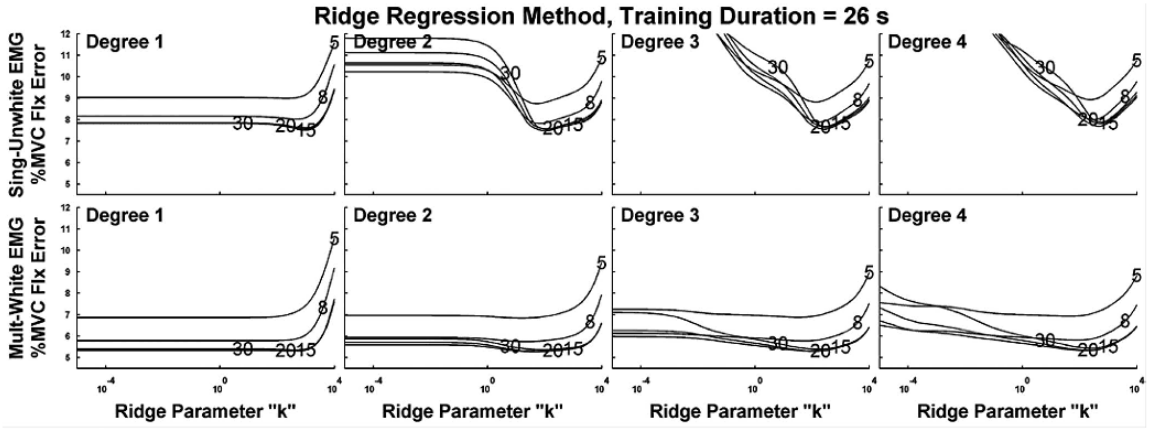

Fig. 2. EMG–torque error as a function of ridge "k" value, using the *ridge regression* system identification method, with 26 s of *training data*. Results for "k" values below 10^{-5} not shown, but follow similar trend. Each row shows results from the two EMGσ processors; columns distinguish the different polynomial model degrees D. Each plot shows the results for representative dynamic model orders (Q) 5, 8, 15, 20, and 30, as labeled. Each result is the average from 33 subjects.

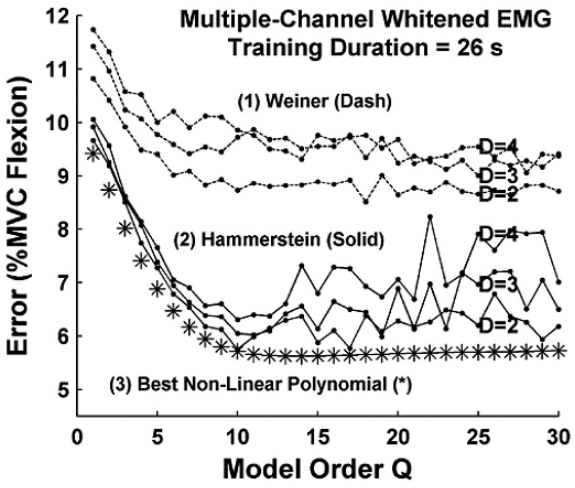

Fig. 3. EMG–torque error as a function of dynamic model order Q, using the *Hammerstein and Weiner* system identification methods, with 26 s of *training data* and multiple-channel whitened EMGσ processor. Polynomial degree D is labeled on each plot. (Degree one not shown, since it is equivalent to the linear model, shown elsewhere.) For comparison, asterisks show the best results using the pseudoinverse method (polynomial degree $D = 2$, tolerance $= 5.6 \times 10^{-4}$). Each result is the average from 33 subjects.

that users would avoid due to very high error—multiple-channel whitened processors consistently performed better than single-channel unwhitened. Statistically, the results for parameters of best performance (see Table I) for the pseudoinverse method, 26 s training duration, were compared between the two EMGσ methods for each polynomial degree. This comparison was repeated for the ridge regression results and for the 52-s training duration. Each comparison was significant ($p \leq 6.8 \times 10^{-3}$).

Fig. 3 shows that the Weiner models were clearly inferior to the best polynomial nonlinear model. The results for parameters of best performance for the Weiner model ($D = 2$, $Q = 18$, multiple whitened EMGσ) were statistically different from those of the best pseudoinverse-based polynomial nonlinear model ($p < 10^{-8}$). The Hammerstein model's performance was closer to that of the pseudoinverse and ridge regression methods. Comparing the results for parameters of best performance for the Hammerstein model ($D = 2$, $Q = 10$, multiple whitened EMGσ) to results from the best pseudoinverse-based polynomial nonlinear model was marginally significant ($p = 0.0175$). With the available MATLAB toolbox, it was not possible to produce results that combined two training trials into a 52-s training duration for the Hammerstein and Weiner models.

The best pseudoinverse results ($4.65 \pm 3.6\%$ MVC flexion; $D = 3$, $Q = 28$, Tol $= 5.6 \times 10^{-3}$, 52-s training set, multiple whitened EMGσ) were not statistically different ($p = 0.5$) from the best ridge regression results ($4.67 \pm 3.7\%$ MVC flexion; $D = 2$, $Q = 18$, $k = 50.1$, 52-s training set, multiple whitened EMGσ). Differences between results were most consistent when using multiple-channel whitened EMGσ processing. The pseudoinverse results for a linear model ($D = 1$) differed from each of the three nonlinear degrees ($D = 2$, 3, 4) when using either single unwhite or multiple white EMGσ processors ($p \leq 1.8 \times 10^{-3}$). Results were less consistent with the 26-s training duration.

Comparison of the results shown in Fig. 4 to those in Fig. 1 clearly demonstrates that the error is reduced by a longer duration training set (52 s). Statistically, the results for parameters of best performance for the pseudoinverse method, single-channel unwhitened EMGσ were compared between the two training durations for each polynomial degree. This comparison was repeated for the ridge regression results and for the multiple-channel whitened EMGσ method. All differences were significant ($p < 1.6 \times 10^{-4}$).

Finally, results for the "conventional" processor varied as a function of the low-pass filter cutoff frequency of the Butterworth filter. The best cutoff frequency was 1.3 Hz, with considerably poorer performance at both lower and higher frequencies.

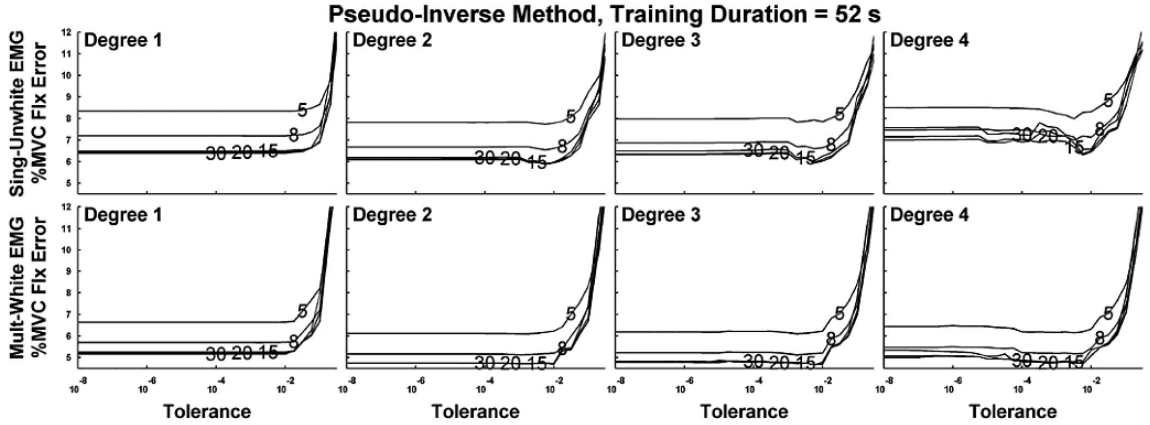

Fig. 4. EMG–torque error as a function of tolerance value, using the *pseudoinverse* system identification method, with 52 s *of training data*. Results for tolerance values below 10^{-8} not shown, but follow similar trend. Each row shows results from the two EMGσ processors; columns distinguish the different polynomial model degrees D. Each plot shows the results for representative dynamic model orders (Q) 5, 8, 15, 20, and 30, as labeled. Each result is the average from 33 subjects.

TABLE I
LOWEST EMG–TORQUE ERROR (MEAN ± STANDARD DEVIATION ABSOLUTE%MVC FLEXION) WITH CORRESPONDING TOLERANCE (TOL) AND DYNAMIC MODEL ORDER (Q) FOR PSEUDOINVERSE METHOD

EMGσ	Polynomial Degree (D)			
	$D=1$ (Tol, Q)	$D=2$ (Tol, Q)	$D=3$ (Tol, Q)	$D=4$ (Tol, Q)
26 s Training				
Single Channel, Unwhitened	7.10±5.9% (5.6e-4, 25)	7.06±5.7% (1.8e-3, 15)	7.43±6.2% (5.6e-3, 14)	7.97±7.0% (1.0e-2, 20)
Multiple Channel, Whitened	5.93±4.5% (5.6e-3, 30)	5.55±4.5% (1.0e-2, 16)	5.56±4.6% (5.6e-3, 16)	5.62±4.6% (5.6e-3, 14)
52 s Training				
Single Channel, Unwhitened	6.38±5.4% (3.2e-4, 30)	5.86±4.0% (5.6e-3, 18)	5.92±4.0% (5.6e-3, 16)	6.29±5.1% (5.6e-3, 14)
Multiple Channel, Whitened	5.15±3.8% (5.6e-3, 30)	4.69±3.6% (1.0e-2, 15)	4.65±3.6% (5.6e-3, 28)	4.70±3.6% (5.6e-3, 16)

Each result from 33 subjects.

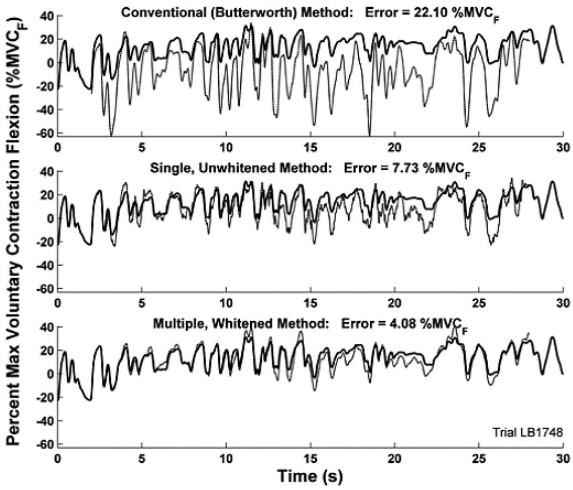

Fig. 5. Representative sample of actual and estimated elbow torque as a function of time. Solid line in each graph is the actual torque, scaled to percent maximum voluntary contraction flexion (%MVC$_F$), for the same 30-s contraction trial. Positive values denote flexion torque. Dotted line in each plot shows torque estimated by training a model to distinct trials, then using EMG to estimate torque from this trial. (Top) Estimate from the best "conventional" method (1.3-Hz cutoff frequency). (Middle) Best single-channel unwhitened method (second-degree polynomial, 18th-order dynamic model, pseudoinverse tolerance of 5.6×10^{-3}, 52-s training). (Bottom) Best multiple-channel whitened method (third-degree polynomial, 28th-order dynamic model, pseudoinverse tolerance of 5.6×10^{-3}, 52-s training). Estimated torques omit approximately 2 s from the beginning and end of trial to account for filter start-up transients.

At this cutoff frequency, the error was $19.15 \pm 11.15\%$ MVC flexion. Statistically, the best "conventional" torque estimator was compared to the single-channel unwhitened results using a 26-s training duration ($D = 2$, $Q = 15$, Tol $= 1.8 \times 10^{-3}$). This comparison was significant ($p < 10^{-5}$), showing that "conventional" modeling performed poorer than our more advanced single-channel models (and, by statistical inference, also poorer than our multiple-channel models and models that utilized 52-s training durations). Fig. 5 displays a representative elbow torque profile, along with the torque predicted using the best "conventional" method, best single-channel unwhitened method, and best multiple-channel whitened method.

IV. DISCUSSION

Though models with a small number of parameters risk missing significant relationships in the data, overfitting poses an obstacle to parameter identification in models with a large number of parameters. Factors known to decrease the severity of overfitting include training sets with higher SNR, larger training sets, model structures with fewer parameters, and system identification techniques that are robust with respect to training set noise and correlated features. In this study, several clear trends emerged from the methodological comparisons performed.

First, the multiple-channel whitened EMGσ processor was again demonstrated to improve EMG–torque estimation. It is

well established that these methods decrease the variability of the EMGσ estimate [15]–[19], [25], hence increasing the SNR in the training and testing sets. Anecdotally, whitening seemed to provide the clearest performance improvement in this study. While multiple-channel EMGσ processors offer improved performance in many situations, problems can arise if even one of the raw EMG signals contains a large amount of noise [18]. In addition, in less constrained contractions, multiple electrodes placed longitudinally across a muscle group might need to be modeled as separate electrical sources (rather than being combined into one EMGσ) [42], [43].

Second, increasing the training set duration from 26 to 52 s provided a clear improvement, with considerably lower test errors and reduced sensitivity to the number of model parameters. A larger dataset helps to reduce the influence of training set noise, because parameter estimates are averaged over more training samples. Training from multiple trials can also help average trial-to-trial variations in posture, since joint angle affects the EMG–torque relation [44]–[46]. For example, the single-channel unwhitened results based on a 26-s training duration (see Fig. 1) show that test set error grows as dynamic model order is increased above approximately 15th-order, for nonlinear polynomial degrees of $D = 3$ and 4. However, when a 52-s training duration was used with the single-channel unwhitened data (see Fig. 4), the error was lower and remained so at higher model orders. Interestingly, the multiple-channel whitened results for first- and second-degree polynomial models with 26-s training duration (see Fig. 1) do not exhibit the upward trend in error at high model orders. Thus, one might be convinced that adequate training had occurred without overfitting. However, the corresponding 52-s training set results shown in Fig. 4 still exhibit substantially lower errors. Thus, the fact that error ceases to vary as model order increases does not necessarily indicate that an optimal model has been found. Further reduction in the EMG–torque error might be realized using even longer training sets or more training trials.

Third, the Weiner model results were consistently poorer than those of the nonlinear polynomial models. The Hammerstein models exhibited performance close to, but not as good as, the best nonlinear polynomial models. Because the Hammerstein and Weiner models contain fewer coefficients, it is possible that they simply did not capture the full complexity of the true EMG–torque relationship. These reduced parameter models might be advantageous in situations where only short durations of training data (i.e., less than 26 s) are available.

Fourth, with the nonlinear polynomial model ($D = 2$ or 3), system identification using the best pseudoinverse tolerance gave performance similar to that of the best ridge method. However, the range of pseudoinverse tolerances over which a nearly optimal fit occurred ($10^{-16} < \text{Tol} < 10^{-2}$) was much wider than the range of ridge k values for its near-optimal fit ($1 < k < 10^3$). Hence, the pseudoinverse method may be less sensitive and easier to tune. Results also indicate that tolerance/ridge k value tuning is more critical when the data are more susceptible to overfitting, i.e., for short duration training sets, single-channel unwhitened EMGσ processing, high nonlinear degree, and high dynamic model order. Note that the tolerance value and ridge k value were fixed in this analysis, and then studied as a function of the fixed value. It is possible that better performance is available by adapting the tolerance/ridge k value based on information within each training set. Anecdotal analysis suggests that the optimal ridge k value for individual subjects ranged across five orders of magnitude. Indeed, selection of a ridge k value is often performed based on case-by-case (graphical) evaluation of a "ridge trace" [32]–[34]. Herein, manual evaluation of the ridge trace was not compatible with automated calibration of the EMG–torque relationship. But, automated algorithms for ridge trace evaluation might be considered in the future.

Note that our experimental situation is limited (constant-posture) and does not mimic fully dynamic, unconstrained motion. In addition, most daily movement activities of the upper limb encompass a smaller range of effort levels [47] and may not mimic the bandwidth investigated herein. However, improvement due to advanced EMGσ processing should apply to the more complex movement cases since a lower variance signal is produced. In addition, there is considerable evidence of intersubject variability in EMG–torque/force relationships as, for example, a function of joint angle [44]–[46]. Hence, attention to system identification methods for calibrating to these differences should also be useful. Nonetheless, most EMG–torque applications will require that the results of this study be appropriately translated to, and verified with, more dynamic and unconstrained motions. The relative impact of reducing EMG amplitude variance and improving model accuracy can vary between applications.

Taken together, the several techniques utilized in this study provide a substantial improvement over typical EMG–torque performance. The best "conventional" estimator provided an error of $19.15 \pm 11.15\%$ MVC flexion. The merging of advanced EMGσ processors (whitening and multiple-channel combination), more complex EMG-torque models (e.g., nonlinear polynomial model), and robust system identification techniques (pseudoinverse/ridge regression, and longer duration training sets) reduced the EMG–torque error in these constant-posture, torque-varying contractions to $4.65 \pm 3.6\%$ of MVC flexion, a substantial performance improvement. These results should be informative to applications such as clinical biomechanics, EMG/neural control of powered prostheses, ergonomic analyses, motor control, and powered exoskeletons.

REFERENCES

[1] K. N. An, W. P. Cooney, E. Y. Chao, L. J. Askew, and J. R. Daube, "Determination of forces in extensor pollicis longus and flexor pollicis longus of the thumb," *J. Appl. Physiol.*, vol. 54, pp. 714–719, 1983.

[2] M. Solomonow, A. Guzzi, R. Baratta, H. Shoji, and R. D'Ambrosia, "EMG-force model of the elbow's antagonistic muscle pair: The effect of joint position, gravity and recruitment," *Amer. J. Phys. Med.*, vol. 65, pp. 223–244, 1986.

[3] S. H. M. Brown and S. M. McGill, "Co-activation alters the linear versus non-linear impression of the EMG-torque relationship of trunk muscles," *J. Biomech.*, vol. 41, pp. 491–497, 2008.

[4] P. Parker, K. Englehart, and B. Hudgins, "Myoelectric signal processing for control of powered limb prostheses," *J. Electromyogr. Kinesiol.*, vol. 16, pp. 541–548, 2006.

[5] S. Kumar and A. Mital, Eds., *Electromyography in Ergonomics*. Briston, PA: Taylor & Francis, 1996.

[6] S. E. Mathiassen, J. Winkel, and G. M. Hagg, "Normalization of surface EMG amplitude from the upper trapezius muscle in ergonomic studies—A review," *J. Electromyogr. Kinesiol.*, vol. 5, pp. 197–226, 1995.
[7] G. M. Hagg, B. Melin, and R. Kadefors, "Applications in Ergonomics," in *Electromyography: Physiology, Engineering, and Noninvasive Applications*, R. Meletti and P. A. Parker, Eds. Hoboken, NJ: Wiley, 2004, pp. 343–363.
[8] C. Disselhorst-Klug, T. Schmitz-Rode, and G. Rau, "Surface electromyography and muscle force: Limits in sEMG-force relationship and new approaches for applications," *Clin. Biomech.*, vol. 24, pp. 225–235, 2009.
[9] C. A. M. Doorenbosch and J. Harlaar, "A clinically applicable EMG-force model to quantify active stabilization of the knee after a lesion of the anterior cruciate ligament," *Clin. Biomech.*, vol. 18, pp. 142–149, 2003.
[10] D. J. Ostry and A. G. Feldman, "A critical evaluation of the force control hypothesis in motor control," *Exp. Brain Res.*, vol. 153, pp. 275–288, 2003.
[11] C. Fleischer and G. Hommel, "A human-exoskeleton interface utilizing electromyography," *IEEE Trans. Robot.*, vol. 24, no. 4, pp. 872–882, Aug. 2008.
[12] J. Rosen, M. Brand, M. B. Fuchs, and M. Arcan, "A myosignal-based powered exoskeleton system," *IEEE Trans. Syst., Man, Cybern. A, Syst. Humans*, vol. 31, no. 3, pp. 210–222, May 2001.
[13] Z. O. Khokhar, Z. G. Xiao, and C. Menon, "Surface EMG pattern recognition for real-time control of a wrist exoskeleton," *Biomed. Eng. OnLine*, vol. 9, p. 41, 2010.
[14] D. Staudenmann, K. Roeleveld, D. F. Stegeman, and J. van Dieen, "Methodological aspects of SEMG recordings for force estimation—A tutorial and review," *J. Electromyogr. Kinesiol.*, vol. 20, pp. 375–387, 2010.
[15] N. Hogan and R. W. Mann, "Myoelectric signal processing: Optimal estimation applied to electromyography—Part I: Derivation of the optimal myoprocessor," *IEEE Trans. Biomed. Eng.*, vol. BME-27, no. 7, pp. 382–395, Jul. 1980.
[16] N. Hogan and R. W. Mann, "Myoelectric signal processing: Optimal estimation applied to electromyography—Part II: Experimental demonstration of optimal myoprocessor performance," *IEEE Trans. Biomed. Eng.*, vol. BME-27, no. 7, pp. 396–410, Jul. 1980.
[17] E. A. Clancy and N. Hogan, "Single site electromyograph amplitude estimation," *IEEE Trans. Biomed. Eng.*, vol. 41, no. 2, pp. 159–167, Feb. 1994.
[18] E. A. Clancy and N. Hogan, "Multiple site electromyograph amplitude estimation," *IEEE Trans. Biomed. Eng.*, vol. 42, no. 2, pp. 203–211, 1995.
[19] E. A. Clancy, E. L. Morin, and R. Merletti, "Sampling, noise-reduction and amplitude estimation issues in surface electromyography," *J. Electromyogr. Kinesiol.*, vol. 12, pp. 1–16, 2002.
[20] E. A. Clancy and N. Hogan, "Relating agonist-antagonist electromyograms to joint torque during isometric, quasi-isotonic, non-fatiguing contractions," *IEEE Trans. Biomed. Eng.*, vol. 44, no. 10, pp. 1024–1028, Oct. 1997.
[21] E. A. Clancy, S. Bouchard, and D. Rancourt, "Estimation and application of EMG amplitude during dynamic contractions," *IEEE Eng. Med. Biol. Soc. Mag.*, vol. 20, no. 6, pp. 47–54, Nov./Dec. 2001.
[22] E. A. Clancy, O. Bida, and D. Rancourt, "Influence of advanced electromyogram (EMG) amplitude processors on EMG-to-torque estimation during constant-posture, force-varying contractions," *J. Biomech.*, vol. 39, pp. 2690–2698, 2006.
[23] T. D. Sanger, "Bayesian filtering of myoelectric signals," *J. Neurophysiol.*, vol. 97, pp. 1839–1845, 2007.
[24] D. Staudenmann, J. R. Potvin, I. Kingma, D. F. Stegeman, and J. H. van Dieen, "Effects of EMG processing on biomechanical models of muscle joint systems: Sensitivity of trunk muscle moments, spinal forces, and stability," *J. Biomech.*, vol. 40, pp. 900–909, 2007.
[25] J. R. Potvin and S. H. M. Brown, "Less is more: High pass filtering, to remove up to 99% of the surface EMG signal power, improves EMG-based biceps brachii muscle force estimates," *J. Electromyogr. Kinesiol.*, vol. 14, pp. 389–399, 2004.
[26] G. L. Gottlieb and G. C. Agarwal, "Dynamic relationship between isometric muscle tension and the electromyogram in man," *J. Appl. Physiol.*, vol. 30, pp. 345–351, 1971.
[27] D. G. Thelen, A. B. Schultz, S. D. Fassois, and J. A. Ashton-Miller, "Identification of dynamic myoelectric signal-to-force models during isometric lumbar muscle contractions," *J. Biomech.*, vol. 27, pp. 907–919, 1994.
[28] K. Mountjoy, E. Morin, and K. Hashtrudi-Zaad, "Use of the fast orthogonal search method to estimate optimal joint angle for upper limb Hill-muscle models," *IEEE Trans. Biomed. Eng.*, vol. 57, no. 4, pp. 790–798, Apr. 2010.
[29] T. K. K. Koo and A. F. T. Mak, "Feasibility of using EMG driven neuromusculoskeletal model for prediction of dynamic movement of the elbow," *J. Electromygr. Kinesiol.*, vol. 15, pp. 12–26, 2005.
[30] L. Ljung, *System Identification: Theory for the User.*. Upper Saddle River, NJ: Prentice-Hall, 1999, pp. 491–519.
[31] W. H. Press, S. A. Teukolsky, W. T. Vetterling, and B. P. Flannery, *Numerical Recipes in C*, 2nd ed. New York: Cambridge Univ. Press, 1994, pp. 671–681.
[32] T. A. Jones, "Multiple regression with correlated independent variables," *Math. Geol.*, vol. 4, pp. 203–218, 1972.
[33] A. E. Hoerl and R. W. Kennard, "Biased estimation for nonorthogonal problems," *Technometrics*, vol. 12, pp. 55–67, 1970.
[34] D. W. Marquardt and R. D. Snee, "Ridge regression in practice," *Amer. Statistician*, vol. 29, pp. 3–20, 1975.
[35] E. A. Clancy, "Electromyogram amplitude estimation with adaptive smoothing window length," *IEEE Trans. Biomed. Eng.*, vol. 46, no. 6, pp. 717–729, Jun. 1999.
[36] E. A. Clancy and K. A. Farry, "Adaptive whitening of the electromyogram to improve amplitude estimation," *IEEE Trans. Biomed. Eng.*, vol. 47, no. 6, pp. 709–719, Jun. 2000.
[37] P. Prakash, C. A. Salini, J. A. Tranquilli, D. R. Brown, and E. A. Clancy, "Adaptive whitening in electromyogram amplitude estimation for epoch-based applications," *IEEE Trans. Biomed. Eng.*, vol. 52, no. 2, pp. 331–334, Feb. 2005.
[38] E. A. Clancy. (2010 Aug.). *EMG Amplitude Estimation Toolbox: User's Guide*. Alpha version 0.07, 2010 [Online]. Available: http://www.wpi.edu/~ted/emg_tool.htm
[39] I. Miller and J. E. Freund, *Probability and Statistics for Engineers*. Englewood Cliffs, NJ: Prentice-Hall, 1977, pp. 272–275.
[40] D. G. Lloyd and T. F. Besier, "An EMG-driven musculoskeletal model to estimate muscle forces and knee joint moments in vivo," *J. Biomech.*, vol. 36, pp. 765–776, 2003.
[41] C. A. M. Doorenbosch and J. Harlaar, "Accuracy of a practicable EMG to force model for knee muscles," *Neurosci. Lett.*, vol. 368, pp. 78–81, 2004.
[42] D. Staudenmann, I. Kingma, A. Daffertshofer, D. F. Stegeman, and J. H. van Dieen, "Heterogeneity of muscle activation in relation to force direction: A multi-channel surface electromyography study on the triceps surae muscle," *J. Electromyogr. Kinesiol.*, vol. 19, pp. 882–895, 2009.
[43] T. M. M. Vieira, R. Merletti, and L. Mesin, "Automatic segmentation of surface EMG images: Improving the estimation of neuromuscular activity," *J. Biomech.*, vol. 43, pp. 2149–2158, 2010.
[44] Z. Hassan and R. M. Enoka, "Isometric torque-angle relationship and movement-related activity of human elbow flexors: Implications for the equilibrium-point hypothesis," *Exp. Brain Res.*, vol. 59, pp. 441–450, 1985.
[45] E. P. Doheny, M. M. Lowery, D. P. FitzPatrick, and M. J. O'Malley, "Effect of elbow joint angle on force-EMG relationships in human elbow flexor and extensor muscles," *J. Electromygr. Kinesiol.*, vol. 18, pp. 760–770, 2008.
[46] J. Vredenbregt and G. Rau, "Surface electromyography in relation to force, muscle length and endurance," *New Develop. Electromyogr., Clin. Neurophysiol.*, vol. 1, pp. 607–622, 1973.
[47] D. S. Kern, J. G. Semmler, and R. M. Enoka, "Long-term activity in upper- and lower-limb muscles of humans," *J. Appl. Physiol.*, vol. 91, pp. 2224–2232, 2001.

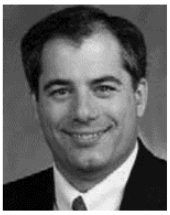

Edward A. Clancy (S'83–M'91–SM'98) received the B.S. degree from Worcester Polytechnic Institute, Worcester, MA, and the S.M. and Ph.D. degrees from the Massachusetts Institute of Technology, Cambridge, all in electrical engineering.

He has worked in industry for medical instrumentation and analysis companies interested in electromyography, EEG, ECG, and blood pressure, and the defense industry (aircraft instruments and radar). He is an Associate Professor in the Department of Electrical and Computer Engineering, and the Department of Biomedical Engineering, WPI. His research interests include signal processing, stochastic estimation and system identification, particularly as applied to problems in medical engineering and human rehabilitation.

Lukai Liu received the B.S. degree in electrical engineering from Xian Jiaotong University, Xian, China, and the M.S. degree in electrical and computer engineering from the Illinois Institute of Technology, Chicago, in 2003 and 2009, respectively. He is currently working toward the Ph.D. degree from the Department of Electrical and Computer Engineering, Worcester Polytechnic Institute, Worcester, MA.

His research interests include biomedical signal processing, biomedical imaging, and machine learning.

Pu Liu received the B.S. degree from Fudan University, Shanghai, China, and the M.S. degree from Worcester Polytechnic Institute (WPI), Worcester, MA, both in electrical engineering. She is currently working toward the Ph.D. degree from the Department of Electrical and Computer Engineering, WPI.

Her research interests include signal processing, modeling and instrumentation, principally as applied to biomedical engineering.

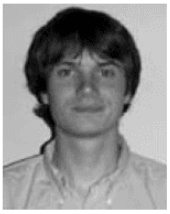

Daniel Van Zandt Moyer was born in Portola Valley, CA, in 1989. He received the B.S. and M.S. degrees in electrical engineering from Worcester Polytechnic Institute, Worcester, MA, in 2011.

Since then, he has been at Genapsys, Inc., Menlo Park, CA. His research interests include DNA sequencing and digital signal processing.

CHAPTER 13

Copy of published journal paper:

Pu Liu, Lukai Liu, Francois Martel, Denis Rancourt and Edward A. Clancy. "Influence of Joint Angle on EMG-Torque Model During Constant-Posture Quasi-Constant-Torque Contractions." *Journal of Electromyography and Kinesiology*, Vol. 23, No. 5, pp. 1020–1028, 2013.

Journal of Electromyography and Kinesiology 23 (2013) 1020–1028

Contents lists available at ScienceDirect

Journal of Electromyography and Kinesiology

journal homepage: www.elsevier.com/locate/jelekin

Influence of joint angle on EMG–torque model during constant-posture, quasi-constant-torque contractions

Pu Liu [a], Lukai Liu [a], Francois Martel [b], Denis Rancourt [b], Edward A. Clancy [a,*]

[a] Worcester Polytechnic Institute, Worcester, MA 01609, USA
[b] Sherbrooke University, Quebec J1K2R1, Canada

ARTICLE INFO

Article history:
Received 2 January 2013
Received in revised form 20 June 2013
Accepted 20 June 2013

Keywords:
Biological system modeling
Electromyography
EMG amplitude estimation
EMG signal processing
Joint angle influence

ABSTRACT

Electromyogram (EMG)–torque modeling is of value to many different application areas, including ergonomics, clinical biomechanics and prosthesis control. One important aspect of EMG–torque modeling is the ability to account for the joint angle influence. This manuscript describes an experimental study which relates the biceps/triceps surface EMG of 12 subjects to elbow torque at seven joint angles (spanning 45–135°) during constant-posture, quasi-constant-torque contractions. Advanced EMG amplitude (EMGσ) estimation processors (i.e., whitened, multiple-channel) were investigated and three non-linear EMGσ–torque models were evaluated. When EMG–torque models were formed separately for each of the seven distinct joint angles, a minimum "gold standard" error of 4.23 ± 2.2% MVC_{F90} resulted (i.e., error relative to maximum voluntary contraction at 90° flexion). This model structure, however, did not directly facilitate interpolation across angles. The best model which did so (i.e., parameterized the angle dependence), achieved an error of 4.17 ± 1.7% MVC_{F90}. Results demonstrated that advanced EMGσ processors lead to improved joint torque estimation. We also contrasted models that did vs. did not account for antagonist muscle co-contraction. Models that accounted for co-contraction estimated individual flexion muscle torques that were ~29% higher and individual extension muscle torques that were ~68% higher.

1. Introduction

The surface electromyogram (EMG) provides a non-invasive measure of muscle activation and hence has been used to estimate muscle tension and joint torque (see Staudenmann et al. (2010) for a recent review) (An et al., 1983; Clancy et al., 2006, 2012; Clancy and Hogan, 1997; Doheny et al., 2008; Gottlieb and Agarwal, 1971; Hasan and Enoka, 1985; Heckathorne and Childress, 1981; Hof and Van den Berg, 1981; Hogan and Mann, 1980b; Lawrence and DeLuca, 1983; Messier et al., 1971; Potvin and Brown, 2004; Sanger, 2007; Shin et al., 2009; Solomonow et al., 1986; Staudenmann et al., 2009; Thelen et al., 1994; Vredenbregt and Rau, 1973). EMG–torque models have application in ergonomics, clinical biomechanics and prosthesis control (Disselhorst-Klug et al., 2009; Doorenbosch and Harlaar, 2003; Hagg et al., 2004; Kumar and Mital, 1996; Mathiassen et al., 1995; Parker et al., 2006). These models aim to emulate the natural relationship between the central nervous system and peripheral joints/muscles. This relationship must account for changes in muscle length/joint angle for several reasons, including the muscle length-tension relationship, muscle moment arms and the relative positioning of recording electrodes with respect to the underlying muscle and innervation zone (Martin and MacIsaac, 2006; Messier et al., 1971; Rack and Westbury, 1969; Zajac, 1989).

Limited studies have been conducted over the years to model the influence of joint angle on the EMG–torque relationship. Vredenbregt and Rau's (1973) classic single-subject study of biceps muscles (more recently supported by the work of Doheny et al. (2008)) suggests that this EMG–torque relationship may only change by a multiplicative gain factor as a function of joint angle. That is, the *shape* of the EMG–torque relationship is the same at each joint angle, but a distinct gain scales this shape for each angle. Vredenbregt and Rau did not account for agonist-antagonist co-contraction, although Solomonow et al. (1986) have shown antagonist muscle activity to be considerable (antagonist EMG amplitude levels often 10–20% that of the agonist). An additional modeling concern is that Hasan and Enoka (1985) have shown that the EMG–torque variation across angle changes considerably person-to-person, with the angular location of the force peak varying up to 50°. Each of the above three studies utilized constant-posture, constant-torque contractions. These results suggest that

* Corresponding author. Address: Department of Electrical and Computer Engineering, Worcester Polytechnic Institute, 100 Institute Road, Worcester, MA 01609, USA. Tel.: +1 (508) 831 5778; fax: +1 (508) 831 5491.
E-mail address: ted@wpi.edu (E.A. Clancy).

1050-6411/$ - see front matter © 2013 Elsevier Ltd. All rights reserved.
http://dx.doi.org/10.1016/j.jelekin.2013.06.011

EMG–torque models should account for both individual subject differences, as well as agonist and antagonist muscles.

Advanced EMG amplitude (EMGσ—the time-varying standard deviation of the EMG waveform) processing techniques have been developed over the last few years, incorporating multiple-channel combination and whitening. Improved EMGσ estimates produce decreased EMG–torque error, as do improvements to system identification (i.e., model selection and fitting procedures) (Clancy et al., 2002, 2006, 2012; Clancy and Farry, 2000; Clancy and Hogan, 1995, 1997; Hogan and Mann, 1980a, 1980b; Potvin and Brown, 2004; Sanger, 2007; Staudenmann et al., 2010; Thelen et al., 1994). These advances have not been incorporated into EMG–torque modeling when multiple joint angles are considered. The purpose of this study was to systematically investigate the influence of elbow joint angle on EMG–torque modeling during constant-posture, quasi-constant-torque contractions, while incorporating advanced EMGσ processors and muscular co-activation.

2. Methods

2.1. Experimental data and methods

Experiments were approved and supervised by the WPI IRB. All subjects provided written informed consent. Experimental data were acquired from 12 healthy subjects (9 male, 3 female; aged 18–52 years). Subjects were strapped into a custom-built straight-back chair (shown in Fig. 1) with their right shoulder abducted 90°, their forearm oriented in a parasaggital plane, the wrist fully supinated (palm perpendicular to the floor) and the wrist tightly cuffed to a load cell (Vishay Tedea–Huntleigh Model 1042, 75 kg full scale). The angle between the upper arm and the forearm was selectable, but fixed. Skin above the muscles under investigation was cleaned with an alcohol wipe and a small bead of electrode gel was massaged into the overlying skin. Six bipolar EMG electrode-amplifiers were placed transversely across each of the biceps and triceps muscle groups, midway between the elbow and the midpoint of the upper arm, this positioning being intended to avoid the tendon distally and the innervation zone proximally. Subjects were instructed to tense their muscles at both angular extremes (45°, 135°) to aid in visualizing the distal tendon and the muscle midpoint locations. EMG recording over the tendon is discouraged as it is not electrically active tissue and because our own experience finds this location prone to motion artifacts. Recording over the innervation zone (typically located near the muscle mid-point for the biceps and triceps) can lead to large swings in EMGσ values with small changes in location (Rainoldi et al., 2000). The electrodes were also centered on the muscle midline, to best avoid crosstalk from adjacent muscles. Each electrode-amplifier had a pair of 8 mm diameter, stainless steel, hemispherical contacts separated by 1 cm edge-to-edge, oriented along the muscle's long axis. The distance between adjacent electrode-amplifiers was ~1.75 cm. A ground electrode was gelled and secured on the upper arm. Custom electronics amplified and filtered each EMG signal (CMRR greater than 90 dB at 60 Hz; 8th-order Butterworth highpass at 15 Hz; 4th-order Butterworth lowpass at 1800 Hz) before being sampled at 4096 Hz with 16-bit resolution. The RMS EMG signal level at rest (representing equipment noise plus ambient physiological activity) was on average 2.9 ± 4.3% of the RMS EMG at 50% maximum voluntary contraction (MVC) at 90°.

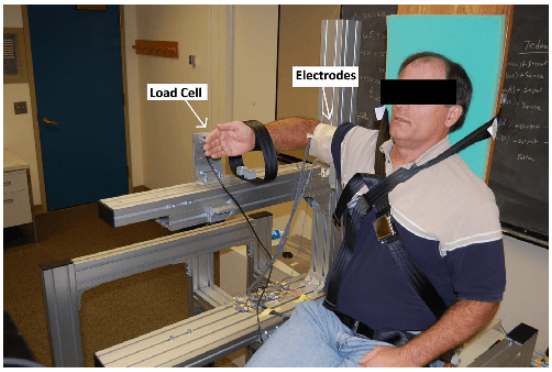

Fig. 1. Experimental apparatus. The subject's right arm is oriented in a plane parallel to the floor, the upper arm is directed laterally outward from the shoulder, and the angle between the upper arm and the forearm is selectable, but fixed (shown here at 90°). EMG electrodes are mounted over the biceps and triceps muscles. The wrist is tightly cuffed to a load cell at the level of the styloid process.

All contractions were constant-posture, with the elbow angle selectable. Subjects were provided a warm-up period, then rested four minutes. MVCs were then measured. Subjects took 2–3 s to slowly ramp up to MVC and maintained that force for two seconds. The average load cell value during the contraction plateau was taken as the MVC. Both elbow extension and flexion MVC were measured at a joint angle of 90°. Ten second duration, constant-force contractions at 50% MVC extension, 50% MVC flexion and at rest (arm removed from the wrist cuff) were next recorded at a joint angle of 90°. These contractions were used to calibrate advanced EMGσ estimation algorithms (Clancy and Farry, 2000; Prakash et al., 2005). Then, a sequence of constant-posture, quasi-constant-torque contractions was conducted at randomized elbow angles of 45°, 60°, 75°, 90°, 105°, 120° and 135°. Elbow angle was the included angle between the forearm and upper arm. At each angle, MVC torque was measured in both elbow extension and flexion. The average of these two MVC torques was denoted the torque range midpoint. Then, three tracking trials of 45 s duration were recorded during which the subjects used the load cell as a feedback signal to track a computer-generated torque target ramping at a constant absolute torque rate from the torque range midpoint, to 50% MVC flexion, to 50% MVC extension, back to 50% MVC flexion, and then back to the torque range midpoint. Two-three minutes of rest was provided between trials to avoid cumulative fatigue.

2.2. Methods of analysis

All analysis was performed offline in MATLAB. The sampled EMG data were notch filtered at the power line frequency and all harmonics (2nd-order IIR filter, notch bandwidth $\leqslant$0.5 Hz). Small amounts of power line interference, which can be larger in magnitude than the EMG signal power at high frequencies, can be inappropriately accentuated due to the high gain of whitening filters at these frequencies. The narrow bandwidth of these notch filters eliminated this interference source, with limited decrease in the overall statistical bandwidth of the signal (Bendat and Piersol, 1971). Next, two distinct EMGσ processors were created for each of the extension and flexion muscle groups for each 45 s trial. Estimators were either single-channel, unwhitened (using a centrally located electrode) or four-channel whitened (using the four centrally located electrodes). As depicted in Fig. 2, each estimator utilized a 15 Hz highpass filter (5th-order Butterworth applied in the forward and reverse time directions to achieve zero phase) and a first-order demodulator (e.g., rectifier). Whitened channels used the non-causal adaptive whitening algorithm of Clancy and Farry (2000). After demodulation, signals were lowpass filtered at 1.6 Hz while being decimated by a factor of 1000, producing a resampled frequency of 4.096 Hz. The torque signal was similarly decimated, producing an EMG data set with a bandwidth approximately 10 times that of the torque signal being estimated (Ljung,

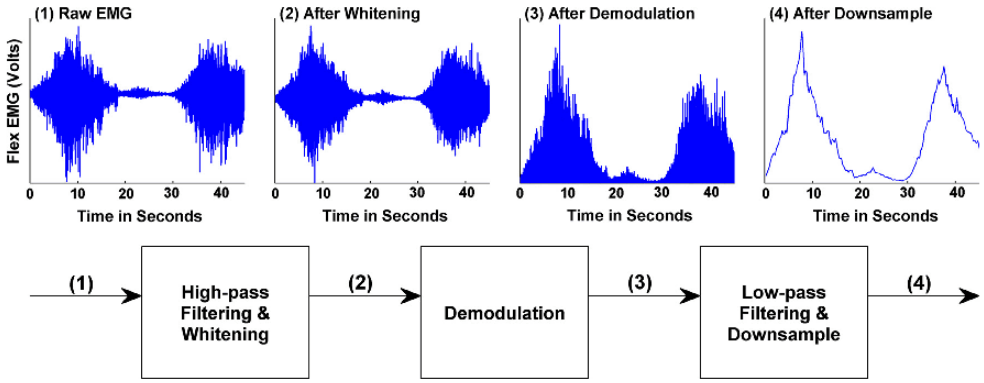

Fig. 2. A single channel EMG signal (top plots) passing through various steps of EMGσ estimation (bottom plot). Data (45 s in duration) were collected from a biceps muscle channel at a joint angle of 90° for subject WY01. For simplicity, only one whitened channel is shown however, in practice, four channels were combined after demodulation whenever whitening was applied.

1999). This decimated sampling rate is best for system identification, being large enough to capture the system dynamics (the fundamental period of force variation was 45 s) and small enough to avoid noise existing out of the signal band (Clancy et al., 2006; Ljung, 1999). The original sampling rate of 4096 Hz is necessary for acquiring the raw EMG, but is not appropriate once an EMGσ estimate has been formed. The first and last 7.5 s of data were excluded from each 45 s trial to account for filter start-up transients.

The decimated extension and flexion EMGσ inputs were related to joint torque (output) using three non-linear polynomial model structures:

(1) Angle-specific model:

$$T[m] = \sum_{d=1}^{D} f_{d,\theta}\sigma_F^d[m] - \sum_{d=1}^{D} e_{d,\theta}\sigma_E^d[m] \quad (1)$$

(2) Flex-extend multiplicative model:

$$T[m] = \left(\sum_{a=0}^{A} g_{a,F}\theta^a[m]\right)\left(\sum_{d=1}^{D} f_d\sigma_F^d[m]\right) - \left(\sum_{a=0}^{A} g_{a,E}\theta^a[m]\right)\left(\sum_{d=1}^{D} e_d\sigma_E^d[m]\right) \quad (2)$$

(3) Single multiplicative model:

$$T[m] = \left(\sum_{a=0}^{A} g_a\theta^a[m]\right)\left(\sum_{d=1}^{D} f_d\sigma_F^d[m] - \sum_{d=1}^{D} e_d\sigma_E^d[m]\right) \quad (3)$$

where m was the decimated discrete-time sample index; T[m] was the measured torque; e_d and f_d were the extension and flexion fit parameters (which specified the *shape* of the EMGσ–torque relationship), respectively; $\sigma_E[m]$ and $\sigma_F[m]$ were the extension and flexion EMGσ estimates, respectively; g_a were the angle fit parameters (which specified the multiplicative gain vs. joint angle); and θ was the elbow joint angle. The EMGσ polynomial degree was varied from $1 \leqslant D \leqslant 5$. The angle polynomial degree was varied from $1 \leqslant A \leqslant 5$. Both "$A$" and "$D$" were always the same for extension and flexion portions within any one model.

The "angle-specific" model estimated the extension and flexion fit parameters at the seven elbow joint angles separately, using linear least squares. The "flex-extend multiplicative" model contained two sets of gains (one each for extension and flexion activities) which were polynomial functions of elbow joint angle, and simultaneously estimated the extension and flexion fit parameters across the seven elbow angles. The multiplicative gain functions account for *all* factors associated with EMGσ–torque changes across angle, including muscle moment arms, muscle length–tension relationships, and movement of the electrodes with respect to the underlying muscles and innervation zones. The "single multiplicative" model was similar, except that it contained only one multiplicative gain function. Parameters of the flex-extend and single multiplicative models were estimated using non-linear least squares. For the multiplicative models, the inclusion of both EMGσ and angle polynomials resulted in one redundant overall scaling parameter. Anecdotally, this additional degree of freedom seemed to aid the least squares minimization, thus was retained. However, for consistency across angles, the angle polynomial was rescaled to a gain of one at 90° after the fit was complete, with a compensatory inverse scaling applied to the EMGσ polynomial.

Each subject completed three tracking trials at seven distinct angles. Seven trials, one per angle, were combined to form an analysis record (three per subject). The first analysis record was used as training data and the second as a test set. Then, the third record was used as training data and the second again used as the test set. The mean absolute difference between the actual torque and that predicted by the EMG–torque model was computed while the actual torque was between 40% MVC extension and 40% MVC flexion. Limiting the evaluation range reduces extrapolation errors due to trial-to-trial differences in actual torque (Clancy and Hogan, 1997). The average of these two mean absolute difference values was reported as the test error value. All error values were normalized to twice the torque at 50% flexion MVC at angle 90° (MVC_{F90}). Only test trial results are presented. For statistical analysis, test error values were subjected to a paired sign test (Miller and Freund, 1977). Eighty four values contributed to each sign test (seven angles × 12 subjects).

3. Results

Fig. 3 shows an example of the estimated torque and actual torque vs. time for seven elbow angles using the three different model structures. The angle-specific model was considered the "gold standard," since it optimized the model coefficients at each particular joint angle. It does not interpolate across angles. Table 1 gives the mean plus/minus standard deviation test error results for the angle-specific model for each combination of angle, model order and EMGσ processor. The bottom rows of the table list overall errors that collapse results across angle. Error was averaged across the

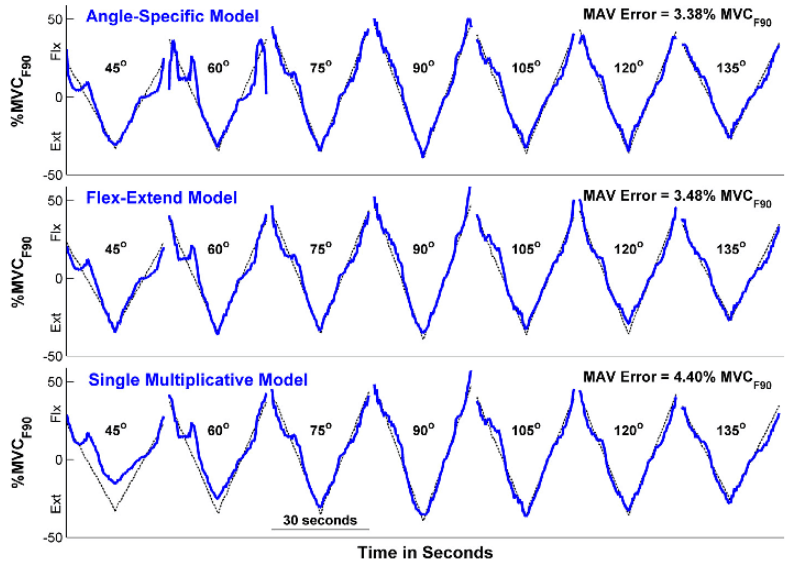

Fig. 3. EMGσ–torque test results of estimated (solid line) and actual torque (dotted line) vs. time for seven elbow angles using three model structures (subject WY01). Data for each angle (30 s in duration, after exclusion of filter transients) were collected during distinct trials, then concatenated in the figure. Results use multiple-channel whitened EMGσ processing, the best EMGσ polynomial degree ($D = 3$ for the angle-specific model and $D = 2$ for the other two models) and an angle polynomial degree of $A = 2$.

Table 1
Angle-specific model: mean ± std. dev. EMG–torque error (% mean absolute MVC flexion at 90° from 12 test trials).

Joint angle/	Polynomial degree (D)				
EMGσ	$D = 1$	$D = 2$	$D = 3$	$D = 4$	$D = 5$
45°/					
Single, unwhite	8.43 ± 6.1	7.22 ± 7.2	7.12 ± 7.5	7.88 ± 11	9.92 ± 18
Multiple, white	7.44 ± 6.2	6.76 ± 7.2	6.34 ± 6.6	6.40 ± 7.3	7.12 ± 10
60°/					
Single, unwhite	7.52 ± 2.6	6.21 ± 3.1	5.96 ± 3.3	5.80 ± 3.3	5.84 ± 3.5
Multiple, white	6.94 ± 4.1	6.33 ± 5.8	6.18 ± 5.5	13.2 ± 30	35 ± 105
75°/					
Single, unwhite	6.64 ± 2.1	5.11 ± 1.8	4.83 ± 1.9	5.77 ± 5.4	11.1 ± 23
Multiple, white	5.45 ± 2.2	4.21 ± 1.7	3.99 ± 1.9	4.07 ± 2.5	4.73 ± 4.8
90°/					
Single, unwhite	5.89 ± 2.6	4.70 ± 1.8	4.59 ± 1.8	4.55 ± 1.8	4.61 ± 1.8
Multiple, white	5.14 ± 2.5	3.90 ± 1.6	3.63 ± 1.5	3.63 ± 1.5	3.71 ± 1.5
105°/					
Single, unwhite	5.04 ± 1.4	4.26 ± 1.3	4.16 ± 1.3	4.14 ± 1.2	4.14 ± 1.2
Multiple, White	4.32 ± 1.7	3.33 ± 1.5	3.29 ± 1.4	3.34 ± 1.5	3.32 ± 1.4
120°/					
Single, unwhite	5.46 ± 2.2	4.56 ± 2.0	4.58 ± 2.0	4.58 ± 2.2	4.65 ± 2.3
Multiple, white	4.12 ± 2.0	3.37 ± 1.6	3.35 ± 1.6	3.32 ± 1.6	3.45 ± 1.8
135°/					
Single, unwhite	3.94 ± 1.2	3.80 ± 1.1	3.79 ± 1.2	3.91 ± 1.4	4.05 ± 1.7
Multiple, white	2.95 ± 1.5	2.69 ± 1.3	2.80 ± 1.6	2.94 ± 2.0	3.69 ± 4.3
Overall/					
Single, unwhite	6.13 ± 2.1	5.12 ± 2.2	5.00 ± 2.2	5.23 ± 3.1	6.32 ± 6.6
Multiple, white	5.19 ± 2.4	4.37 ± 2.3	4.23 ± 2.2	5.27 ± 5.2	8.66 ± 16

Table 2
Multiplicative models: mean ± std. dev. EMG–torque error (% mean absolute MVC flexion at 90° from 12 test trials). "A.P.D" = Angle Polynomial Degree.

A.P.D. (A)/	EMGσ polynomial degree (D)				
Model	$D = 1$	$D = 2$	$D = 3$	$D = 4$	$D = 5$
A = 1/					
Flex-extend	5.55 ± 2.0	4.66 ± 1.5	4.94 ± 2.0	4.67 ± 1.9	5.26 ± 2.9
Single	6.90 ± 1.9	6.14 ± 1.7	6.67 ± 2.5	6.00 ± 1.7	6.92 ± 3.3
A = 2/					
Flex-extend	5.15 ± 2.2	4.17 ± 1.7	4.97 ± 2.9	4.85 ± 2.3	6.52 ± 3.7
Single	6.34 ± 2.2	5.65 ± 1.9	5.78 ± 2.1	6.11 ± 2.7	6.87 ± 2.9
A = 3/					
Flex-extend	5.26 ± 2.3	4.35 ± 1.8	6.25 ± 5.2	4.79 ± 2.8	28 ± 58
Single	6.50 ± 2.7	5.73 ± 2.0	7.06 ± 5.1	7.15 ± 4.3	15.6 ± 13
A = 4/					
Flex-extend	6.27 ± 2.4	5.24 ± 2.1	7.13 ± 5.4	28 ± 44	47 ± 118
Single	7.37 ± 3.1	6.41 ± 2.1	6.55 ± 2.5	9.67 ± 6.2	38 ± 74
A = 5/					
Flex-extend	14.7 ± 9.7	12.3 ± 7.4	12.0 ± 7.1	64 ± 154	282 ± 727
Single	9.31 ± 8.3	6.81 ± 2.9	8.08 ± 3.4	28 ± 62	33 ± 46

seven angles for each subject, then the mean and standard deviation
of these 12 values reported. The best overall performance was found using the multiple white EMGσ processor and polynomial degree $D = 3$, giving an error of 4.23 ± 2.2% MVC$_{F90}$. For all angles and EMGσ polynomial degrees, multiple-channel whitened processors consistently performed better than single-channel unwhitened, except for $D \geqslant 2$ at 60°. Statistically, results between the two EMGσ processors were compared for each EMGσ polynomial degree $1 \leqslant D \leqslant 5$. The multiple whitened processor was significantly better in all cases ($p < 0.001$). Note that the "Overall" results for $D \geqslant 2$ in Table 1 obscure this difference, due to the large errors associated with one subject at 60°. However, the *nonparametric* statistical analysis (paired sign test) confirms the difference. We next statistically compared the best ($D = 3$) multiple whitened processor results to the other multiple whitened processor results. Results for polynomial orders $D = 1$ and 2 were statistically inferior ($p < 0.001$), while results for $D = 4$ and 5 did not differ ($p > 0.07$).

Table 2 gives the mean plus/minus standard deviation test error results for the two multiplicative models, for only the multiple-channel whitened EMGσ processor. For each cell, error was averaged across the seven angles for each subject, then the mean and standard deviation of these 12 values reported. For both multiplicative models, when both D and A were high ($\geqslant 4$), the error be-

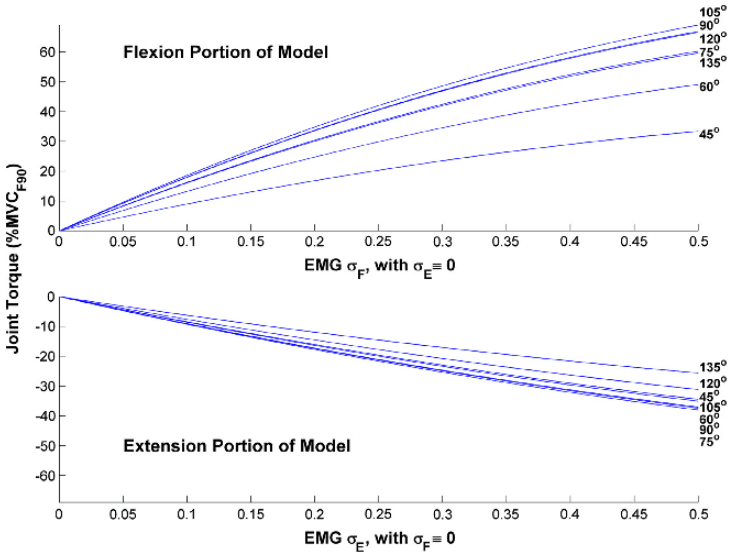

Fig. 4. Flex-extend multiplicative model fits at each angle (subject WY04), using multiple white EMGσ processing, an EMGσ polynomial degree of $D = 2$ and an angle polynomial degree of $A = 2$. Plots provided for each of the seven joint angles (as labeled). Top plots formed from Eq. (2), while setting σ_E to zero and the multiplicative gains to one. Bottom plots formed from Eq. (2) while setting σ_F to zero and the multiplicative gains to one.

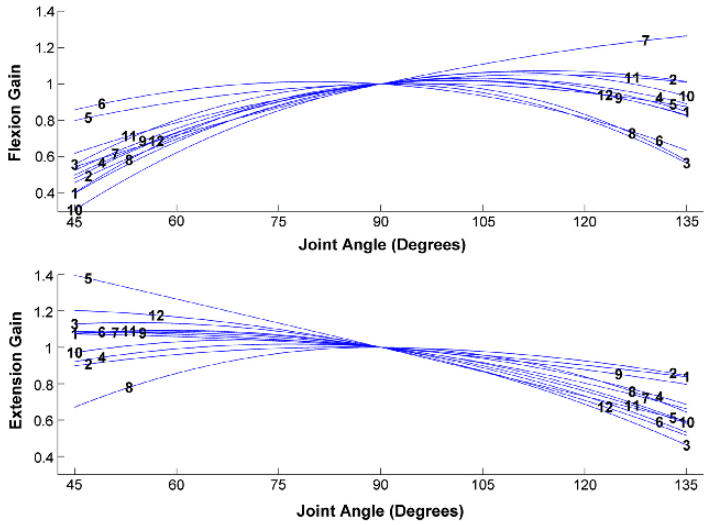

Fig. 5. Flexion (top) and extension (bottom) gain functions vs. angle for the twelve subjects (numbered 1–12) with the flex-extend multiplicative model, using multiple white EMGσ processing, an EMGσ polynomial degree of $D = 2$ and an angle polynomial degree of $A = 2$. Note that the model requires a gain of one at joint angle 90°.

came extremely large, likely due to over-fitting. Some over-fitting also may have occurred when only one of the two polynomial degrees was high (e.g., $D = 5$, $A = 3$). The best flex-extend model ($D = 2$, $A = 2$) had an error of 4.17 ± 1.7% MVC$_{F90}$ and did not differ significantly from the best angle-specific model ($p = 0.29$). Fig. 4 graphs an example set of flex-extend model fits for $D = 2$ and $A = 2$. Fig. 5 graphs the gain functions for the flex-extend model (one per subject), again for $D = 2$ and $A = 2$. Considerable gain variation (exceeding a factor of two) exists across the span of angles studied. The best performance of the single multiplicative model ($D = 2$, $A = 2$) was 5.65 ± 1.9% MVC$_{F90}$, which was statistically different (poorer) than the best angle-specific model ($p < 0.001$) and the best ($D = 2$, $A = 2$) flex-extend model ($p < 0.001$).

We also statistically compared EMGσ processors for the flex-extend model. The multiple white processor consistently produced lower errors ($p < 0.006$) when both polynomial degrees were three or less. For other polynomial degree combinations, results were either equivocal or not significant. However, these parameter combinations corresponded to higher errors and would not be utilized. Similarly, comparison between the two EMGσ processors with the single multiplicative model gave equivocal results particularly when the error was high.

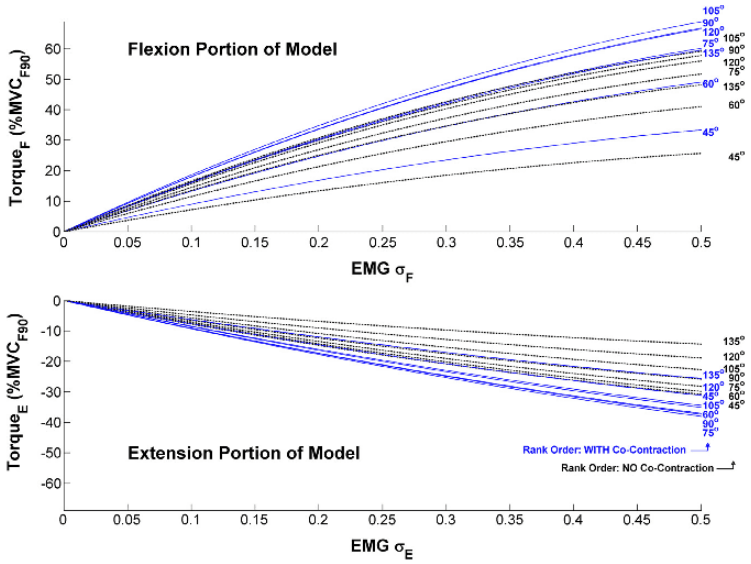

Fig. 6. EMGσ–torque relationship with (solid lines) and without (dotted lines) accounting for muscle co-contraction. An EMGσ polynomial degree of $D = 2$ and an angle polynomial degree of $A = 2$. Plots provided for each of the seven joint angles (subject WY04).

Table 3
Mean ± std. dev. EMG-estimated muscle torque using models with and without co-contraction (% mean absolute MVC flexion at 90°). Results computed over all angles for 12 subjects.

Model	EMGσ value			
	0.1	0.2	0.3	0.4
Flexion				
Co-contract	11.8 ± 2.5	22.7 ± 4.4	32.7 ± 5.8	41.8 ± 6.6
No co-contract	9.1 ± 3.0	17.6 ± 5.2	25.3 ± 6.6	32.3 ± 7.3
Extension				
Co-contract	14.2 ± 5.2	26.5 ± 9.6	37.0 ± 13.3	45.5 ± 16.5
No co-contract	8.2 ± 2.5	15.6 ± 4.3	22.2 ± 5.4	28.0 ± 6.2

Finally, we also produced flex-extend model EMGσ–torque relationships *without* accounting for muscular co-contraction by ignoring the antagonist muscle term in Eq. (2). Only parameters $D = 2$, $A = 2$ were considered. Within the flexion-dominant range of a tracking trial, we related flexion EMGσ to joint torque; and similarly for the extension-dominant portion of a tracking trial. Fig. 6 shows an example result ($D = 2$ and $A = 2$). At every angle, *each* subject's model (flexion or extension) that accounted for co-contraction estimated higher muscle torques at every EMGσ value. We then computed the model-estimated EMGσ–torque with vs. without modeling co-contraction at normalized EMGσ values of 0.1, 0.2, 0.3 and 0.4 (where 1.0 denotes the EMGσ value at MVC), separately for each of the flexion and extension portions of the models. For each subject, results were averaged across the seven angles. Table 3 gives the mean plus/minus standard deviation results, computed across the 12 subjects. For flexion, the models with co-contraction estimated ~29% more torque. For extension, the models with co-contraction estimated ~68% more torque.

4. Discussion

We examined three non-linear models for relating EMGσ to joint torque at different joint angles during constant-posture, slowly-torque-varying (quasi-constant-torque) contractions, as well as the role of advanced EMGσ processors and muscular co-activation. Rather clear distinctions emerged. The advanced EMGσ processing technique that combined whitening and multiple channels consistently provided an approximate 15–20% performance improvement, compared to unwhitened single-channel performance, for the better model structures. Although EMG performance differences were equivocal for the poorer performing model structures, these models would not be selected for use. These improvement results are consistent with past experimental evaluations (Clancy and Hogan, 1995, 1997; Clancy et al., 2012; Hogan and Mann, 1980b; Potvin and Brown, 2004; Prakash et al., 2005), reflecting that a lower variance EMGσ signal used as the input to system identification produces lower modeling errors. There are, however, some possible drawbacks to using multiple recording channels, including: increased hardware costs; the risks that artifacts on only one channel can greatly degrade the entire EMGσ estimate (Clancy and Hogan, 1995); and the possibility during less constrained contractions that the many electrodes should not be combined into one EMGσ, but should be represented as distinct electrical sources/muscle compartments (Staudenmann et al., 2009; Vieira et al., 2010).

The particular model structures chosen for evaluation in this study were strongly influenced by prior literature in this field. Vredenbregt and Rau (1973) suggested that the constant-posture EMGσ–torque relation only varies by a multiplicative gain as a function of angle. These prior experiments, however, did not account for possible muscle co-activation and could not benefit from more recent advances in EMGσ processing. Thus, we selected two models that included multiplicative gain as a function of angle. Angle-dependent gain was implemented via a polynomial, consistent with the expectation of a singly-peaked function (Hasan and Enoka, 1985). The EMGσ–torque relationship at a given angle was also implemented via a polynomial (Clancy and Hogan, 1997; Vredenbregt and Rau, 1973). These models considered muscular co-activation and were calibrated from contraction trials that included both flexion-dominant and extension-dominant contraction.

The optimal EMGσ polynomial degree for the angle-specific model was $D = 3$, consistent with prior work (Clancy and Hogan, 1997). The EMGσ–torque relationship shown in Fig. 4, however, is much closer to a straight line than that typically plotted in the

literature, at least for the biceps muscles (Lawrence and DeLuca, 1983; Vredenbregt and Rau, 1973). One reason for this difference is that we only used efforts up to 50% MVC. Past studies have shown the relationship to be mostly straight over this region, with a more curved (non-linear) shape at higher effort levels. The dependence of gain on joint angle (Fig. 5) did not consistently exhibit a singly-peaked function as might have been anticipated (Hasan and Enoka, 1985). Modeling muscle co-contraction likely influenced this shape, e.g., flexion gain was calibrated from both flexion-dominant and extension-dominant torques. In addition, subjects generally produced lower absolute torque at the extreme joint angles (see Fig. 3). Thus, the least squares parameter fit criterion would have given more influence to those joint angles closest to 90°, perhaps reducing the influence of the more extreme angles.

Fig. 6 and Table 3 show the constant-posture EMGσ–torque relationship with and without consideration of muscle co-contraction. As expected, models that do not account for co-contraction estimate lower flexion and extension muscle torque contributions, likely underestimating true muscle torque contributions. This error is substantial: for flexion, the models with co-contraction estimated ~29% more torque; for extension, the models with co-contraction estimated ~68% more torque. Unfortunately, studies that ignore co-contraction are generally blind to this error. Least squares selection of the fit coefficients will reliably match agonist EMG to agonist-direction torque (e.g., biceps EMG to flexion-direction torque). *Net* joint torque will be appropriately estimated, but internal torques (i.e., the flexion and extension muscle torque contributions) will not—in fact, no antagonist torque is even considered. Of course, such models render large errors if the antagonist muscle activity changes from that which was experienced during calibration of the model. In most EMGσ–torque studies, subjects are asked to minimize muscle co-contraction. Doing so is advantageous from a system identification perspective, so as to most independently excite all modes of a system. But, real-life contractions will not always preserve the same level of co-contraction. If joint impedance were to be volitionally increased by subjects, one would expect even larger errors. For example, purposeful co-contraction to increase impedance is common in many tasks wherein the endpoint limb segment must be stabilized (Rancourt and Hogan, 2001). Hence, modeling of muscular co-contraction is essential for generalization of an EMGσ–torque model.

It is not surprising that high degree multiplicative gain functions performed significantly poorly, particularly when the EMGσ polynomial model order was high. Data from only seven distinct angles were acquired experimentally. Hence, high angle polynomial degrees (A) would be expected to lead to over-fitting. One interesting solution to this problem would be to separately calibrate the angular dependence and the EMGσ dependence. That is, an angle-specific EMGσ–torque polynomial model might be calibrated at one reference angle (e.g., 90°) and these coefficients fixed. Thereafter, data could be collected while the joint angle was slowly varied across angle (quasi-constant-torque). The coefficients of the angle function could then be independently calibrated. In doing so, many more angle values would be available, perhaps leading support to a higher degree angle polynomial. This calibration technique would also require far less data collection. The reduced number of required contractions might further permit repeated training trials for each contraction, which might lead to even lower model error (Clancy et al., 2012). Note that many subjects found it awkward to orient their elbow to the 45° joint angle and related difficulty in producing torque at this angle. This orientation might be outside the range of angles that need be considered in future research.

The fixed posture and avoidance of dynamic force changes in these experiments simplified study of the EMGσ–torque relationship versus joint angle, but may require caution when applying the results in less constrained application areas. Our intent was to limit the number of variables studied and concentrate on the role of joint angle. It would, therefore, be appropriate to reduce these postural and force limitations in future studies, transitioning towards EMGσ–torque models in more dynamic, unconstrained contractions. For example, when joint angle is allowed to vary dynamically (not the case in this study), EMGσ–torque models will likely need to differ as a function of eccentric vs. concentric contraction (Komi et al., 2000). Also, our sample size in this study was limited (12 subjects) and predominantly male. Larger and more diverse subject pools can aid in the development of EMGσ–torque models that are representative of different body types (e.g., height, weight, arm strength) as well as differences that are more specific to EMG signal acquisition and processing (e.g., arm circumference, amount of subcutaneous fat, relative composition of fast- vs. slow-twitch fibers).

These results extend the classic results of Vredenbregt and Rau (1973) by considering muscular co-activation, applying optimized EMGσ estimates, evaluating alternative models, quantifying the angular dependence and providing rigorous statistical support of all results from multiple subjects. In practice, the results provide strong support that the constant-posture, constant-torque EMGσ–torque relationship about the elbow maintains the same *shape* across angles, differing only by a multiplicative gain factor as a function of angle. Further, a polynomial function is sufficient to model the necessary gain vs. angle. Fig. 5, for example, could be used to develop normative gain vs. angle functions, or better results would be expected if these functions are fit to each subject (as performed in this work). In prosthetics, these results suggest that more natural control of a powered elbow might be provided if the gain between EMG and motor torque were adjusted as a function of the elbow angle. In ergonomic and biomechanical analyses, these results provide a model form in order to account for the angle dependence, which should lead to better tracking of predicted joint torques.

Lastly, this work quantifies the differences in estimated internal muscle tensions with vs. without consideration of muscular co-contraction. The differences are quite large, suggesting that co-activation about the joint must be considered in musculoskeletal models. Formally, doing so is best approached by quantifying joint mechanical impedance. That is, net torque about the joint is related to the *difference* between flexion and extension torques, while impedance about the joint is related to the *sum* of the flexion and extension torques. Simultaneously quantifying both joint torque and impedance provides a more complete mechanical description of the joint. Rigorous methods for relating EMG to joint impedance are just now emerging in the literature (Pfeifer et al., 2012).

In summary, EMGσ–torque models were formed during constant-posture, slowly force-varying contractions ranging in joint angle from 45° to 135°, while modeling muscular co-activation. Advanced EMGσ processing, including signal whitening and multiple channel combination, provided consistent performance improvements for the better models. A gold standard model was calibrated at each specific angle using a polynomial EMGσ–torque relationship. A third-degree polynomial produced the lowest estimation error of 4.23 ± 2.2% MVC_{F90}. Models were also formed in which the angular dependence was parameterized via a multiplicative gain function written as a polynomial. When distinct gains were applied to each of flexion and extension, the best performance (EMGσ polynomial degree of two, angle polynomial degree of two) was 4.17 ± 1.7% MVC_{F90}. Models which did not account for co-contraction were compared to those that do so. Flexion torque was ~29% higher and extension torque was ~68% higher in the models which included co-contraction. Thus, failure to account for antagonist muscle activity can considerably underestimate individual muscle torques.

Conflict of Interest

None of the authors is aware of any conflict of interest associated with this work or its submission to the Journal of Electromyography and Kinesiology.

References

An KN, Cooney WP, Chao EY, Askew LJ, Daube JR. Determination of forces in extensor pollicis longus and flexor pollicis longus of the thumb. J Appl Physiol Resp Environ Exer Physiol 1983;54:714–9.

Bendat JS, Piersol AG. Random data: analysis and measurement procedures. New York: John Wiley and Sons Inc.; 1971.

Clancy EA, Bida O, Rancourt D. Influence of advanced electromyogram (EMG) amplitude processors on EMG-to-torque estimation during constant-posture, force-varying contractions. J Biomech 2006;39:2690–8.

Clancy EA, Farry KA. Adaptive whitening of the electromyogram to improve amplitude estimation. IEEE Trans Biomed Eng 2000;47:709–19.

Clancy EA, Hogan N. Multiple site electromyograph amplitude estimation. IEEE Trans Biomed Eng 1995;42:203–11.

Clancy EA, Hogan N. Relating agonist-antagonist electromyograms to joint torque during isometric, quasi-isotonic, non-fatiguing contractions. IEEE Trans Biomed Eng 1997;44:1024–8.

Clancy EA, Liu L, Liu P, Moyer DV. Identification of constant-posture EMG–torque relationships about the elbow using nonlinear dynamic models. IEEE Trans Biomed Eng 2012;59:205–12.

Clancy EA, Morin EL, Merletti R. Sampling, noise-reduction and amplitude estimation issues in surface electromyography. J Electromyo Kinesiol 2002;12:1–16.

Disselhorst-Klug C, Schmitz-Rode T, Rau G. Surface electromyography and muscle force: limits in sEMG–force relationship and new approaches for applications. Clin Biomech 2009;24:225–35.

Doheny EP, Lowery MM, FitzPatrick DP, O'Malley MJ. Effect of elbow joint angle on force-EMG relationships in human elbow flexor and extensor muscles. J Electromyogr Kinesiol 2008;18:760–70.

Doorenbosch CMA, Harlaar J. A clinically applicable EMG–force model to quantify active stabilization of the knee after a lesion of the anterior cruciate ligament. Clin Biomech 2003;18:142–9.

Gottlieb GL, Agarwal GC. Dynamic relationship between isometric muscle tension and the electromyogram in man. J Appl Physiol 1971;30:345–51.

Hagg GM, Melin B, Kadefors R. Applications in ergonomics. In: Merletti R, Parker PA, editors. Electromyography: physiology, engineering, and noninvasive applications. Hoboken (NJ): John Wiley & Sons, Inc.; 2004. p. 343–63.

Hasan Z, Enoka RM. Isometric torque–angle relationship and movement-related activity of human elbow flexors: implications for the equilibrium-point hypothesis. Exp Brain Res 1985;59:441–50.

Heckathorne CW, Childress DS. Relationships of the surface electromyogram to the force, length, velocity, and contraction rate of the cineplastic human biceps. Am J Phys Med 1981;60:1–19.

Hof AL, Van den Berg J. EMG to force processing I: an electrical analogue of the hill muscle model. J Biomech 1981;14:747–58.

Hogan N, Mann RW. Myoelectric signal processing: optimal estimation applied to electromyography—Part 1. Derivation of the optimal myoprocessor. IEEE Trans Biomed Eng 1980a;27:382–95.

Hogan N, Mann RW. Myoelectric signal processing: optimal estimation applied to electromyography—Part 11. Experimental demonstration of optimal myoprocessor performance. IEEE Trans Biomed Eng 1980b;27:396–410.

Komi PV, Linnamo V, Silventoinen P, Sillanpaa M. Force and EMG power spectrum during eccentric and concentric actions. Med Sci Sports Exerc 2000;32:1757–62.

Kumar S, Mital A, editors. Electromyography in ergonomics. Briston, PA: Taylor & Francis; 1996.

Lawrence JH, DeLuca CJ. Myoelectric signal versus force relationship in different human muscles. J Appl Physiol 1983;54:1653–9.

Ljung L. System identification: theory for the user. Upper Saddle River (NJ): Prentice-Hall; 1999. 143–6, 444–52, 491–519.

Martin S, MacIsaac D. Innervation zone shift with changes in joint angle in the brachial biceps. J Electromyogr Kinesiol 2006;16:144–8.

Mathiassen SE, Winkel J, Hagg GM. Normalization of surface EMG amplitude from the upper trapezius muscle in ergonomic studies—a review. J Electromyogr Kinesiol 1995;5:197–226.

Messier RH, Duffy J, Litchman HM, Paslay PR, Soechting JF, Stewart PA. The electromyogram as a measure of tension in the human biceps and triceps muscles. Int J Mech Sci 1971;13:585–98.

Miller I, Freund JE. Probability and statistics for engineers. Englewood Cliffs (NJ): Prentice-Hall, Inc.; 1977. p. 272–5.

Parker P, Englehart K, Hudgins B. Myoelectric signal processing for control of powered limb prostheses. J Electromyogr Kinesiol 2006;16:541–8.

Pfeifer S, Vallery H, Hardegger M, Riener R, Perreault EJ. Model-based estimation of knee stiffness. IEEE Trans Biomed Eng 2012;59:2604–12.

Potvin JR, Brown SHM. Less is more: high pass filtering, to remove up to 99% of the surface EMG signal power, improves EMG-based biceps brachii muscle force estimates. J Electromyogr Kinesiol 2004;14:389–99.

Prakash P, Salini CA, Tranquilli JA, Brown DR, Clancy EA. Adaptive whitening in electromyogram amplitude estimation for epoch-based applications. IEEE Trans Biomed Eng 2005;52:331–4.

Rack PMH, Westbury DR. The effects of length and stimulus rate on tension in the isometric cat soleus muscle. J Physiol 1969;204:443–60.

Rainoldi A, Nazzaro M, Merletti R, Farina D, Caruso I, Gaudenti S. Geometrical factors in surface EMG of the vastus medialis and lateralis muscles. J Electromyo Kinesiol 2000;10:327–36.

Rancourt D, Hogan N. Stability in force-production tasks. J Motor Behav 2001;33(2):193–204.

Sanger TD. Bayesian filtering of myoelectric signals. J Neurophysiol 2007;97:1839–45.

Shin D, Kim J, Koike Y. A myokinetic arm model for estimating joint torque and stiffness from EMG signals during maintained posture. J Neurophysiol 2009;101:387–401.

Solomonow M, Guzzi A, Baratta R, Shoji H, D'Ambrosia R. EMG–force model of the elbow's antagonistic muscle pair: the effect of joint position, gravity and recruitment. Am J Phys Med 1986;65:223–44.

Staudenmann D, Kingma I, Daffertshofer A, Stegeman DF, van Dieen JH. Heterogeneity of muscle activation in relation to force direction: a multi-channel surface electromyography study on the triceps surae muscle. J Electromyogr Knnesiol 2009;19:882–95.

Staudenmann D, Roeleveld K, Stegeman DF, van Dieen J. Methodological aspects of SEMG recordings for force estimation—a tutorial and review. J Electromyogr Kinesiol 2010;20:375–87.

Thelen DG, Schultz AB, Fassois SD, Ashton-Miller JA. Identification of dynamic myoelectric signal-to-force models during isometric lumbar muscle contractions. J Biomech 1994;27:907–19.

Vieira TMM, Merletti R, Mesin L. Automatic segmentation of surface EMG images: improving the estimation of neuromuscular activity. J Biomech 2010;43:2149–58.

Vredenbregt J, Rau G. Surface electromyography in relation to force, muscle length and endurance. New Develop Electromyogr Clin Neurophysiol 1973;1:607–22.

Zajac FE. Muscle and tendon: properties, models, scaling, and application to biomechanics and motor control. Crit Rev Biomed Eng 1989;17:359–411.

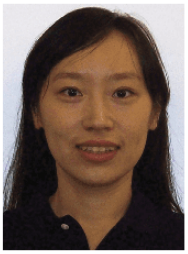

Pu Liu received the B.S. degree from Fudan University, Shanghai, China and the M.S. degree from Worcester Polytechnic Institute (WPI), Worcester, MA, both in Electrical Engineering. She is currently working toward the Ph.D. degree from the Department of Electrical and Computer Engineering, WPI. Her research interests include signal processing, modeling and instrumentation, principally as applied to biomedical engineering.

Lukai Liu graduated in Electrical and Computer Engineering from Illinois Institute of Technology in 2009 with a M.Sc. degree. He is currently a Ph.D. student in the Laboratory for Sensory and Physiologic Signal Processing in the Department of Electrical and Computer Engineering, Worcester Polytechnic Institute (WPI), Massachusetts. His research interests include electromyogram signal processing and machine learning.

François Martel is currently completing a Master's degree in Mechanical Engineering at Sherbrooke University, after graduating in Mechanical Engineering from the same institution in 2010. His various R&D internships and international collaborations reinforced his skills in design, modeling and identification of physical systems. These activities led him to publish several scientific contributions related to his research interests in human performance enhancement and safety.

Denis Rancourt received his Ph.D. from MIT in the department of Mechanical Engineering in 1995, after completing a Master's degree in Mechanical Engineering at École Polytechnique de Montréal in 1989. After ten years as a professor in Mechanical Engineering at Laval University, he was appointed Professor in the division of Bioengineering at Sherbrooke University, QC, Canada, in 2003. His expertise in design, modelling and control of physical systems has led him to conduct several contractual R&D projects with various industries and the community, notably, Alpine and Athletics Canada, for the development of new sports equipment for the Vancouver 2010 and London 2012 Paralympics Games. His research interests are primarily focused on human performance enhancement and the prevention of musculo-skeletal injuries through advanced modelling and design work. He is currently leading the Center for Radical Innovation Research at Sherbrooke University and the Research Group Perseus in human performance and safety.

Edward A. Clancy received the B.S. degree from Worcester Polytechnic Institute (WPI), and the S.M. and Ph.D. degrees from Massachusetts Institute of Technology (MIT), all in Electrical Engineering. He has worked in industry for medical instrumentation and analysis companies interested in EMG, EEG, ECG and blood pressure, and the defense industry (aircraft instruments and radar). He is Associate Professor of Electrical and Computer Engineering, and of Biomedical Engineering at WPI. He is interested in signal processing, stochastic estimation and system identification, particularly as applied to problems in medical engineering and human rehabilitation.

CHAPTER 14

Copy of published journal paper:

Lukai Liu, Pu Liu, Edward A. Clancy, Erik Scheme and Kevin B. Englehart. "Electromyogram Whitening for Improved Classification Accuracy in Upper Limb Prosthesis Control." *IEEE Transactions on Neural Systems and Rehabilitation Engineering*, Vol. 21, No. 5, pp. 767–774, 2013.

Electromyogram Whitening for Improved Classification Accuracy in Upper Limb Prosthesis Control

Lukai Liu, Pu Liu, Edward A. Clancy, *Senior Member, IEEE*, Erik Scheme, *Student Member, IEEE*, and Kevin B. Englehart, *Senior Member, IEEE*

***Abstract*—Time and frequency domain features of the surface electromyogram (EMG) signal acquired from multiple channels have frequently been investigated for use in controlling upper-limb prostheses. A common control method is EMG-based motion classification. We propose the use of EMG signal whitening as a preprocessing step in EMG-based motion classification. Whitening decorrelates the EMG signal and has been shown to be advantageous in other EMG applications including EMG amplitude estimation and EMG-force processing. In a study of ten intact subjects and five amputees with up to 11 motion classes and ten electrode channels, we found that the coefficient of variation of time domain features (mean absolute value, average signal length and normalized zero crossing rate) was significantly reduced due to whitening. When using these features along with autoregressive power spectrum coefficients, whitening added approximately five percentage points to classification accuracy when small window lengths (< 100 ms) were considered.**

***Index Terms*—Coefficient of variation, electromyography, EMG, myoelectric, prosthesis, whitening.**

I. Introduction

APPROXIMATELY 1.5 million people in the U.S. are living with upper or lower limb loss, with 230 000 new cases occurring each year [1], [2]. Surface electromyogram (EMG) controlled powered hand/wrist/elbow prostheses are used by some of these amputees to return partial upper-limb function. Conventional transradial prostheses, for example, can use surface EMG amplitudes from the residual forearm flexors and extensors to control hand opening and closing. Additional degrees of freedom (e.g., wrist rotation) cannot currently be controlled simultaneously in commercial systems. Rather, prostheses apply EMG-based or mechanical mode switching, so that the same EMG sites sequentially control the additional function(s) [3], [4]. It is reported that control of more degrees of freedom is the greatest desired prosthetic improvement for below-elbow amputees [5]. Accordingly, a pattern recognition approach has been emerging over the past several years in which EMG signals in the forearm are used to discern desired movements of the hand and wrist [3], [6]–[11]. Continuous control of multiple degrees of freedom is achieved by applying the pattern recognition algorithm in a continuous manner along the EMG signal stream. The approach consists of four sequential steps: EMG signal conditioning and preprocessing, feature extraction, dimension reduction and pattern classification.

Common time-domain features that are extracted include the EMG mean absolute value (MAV), signal length and zero crossing rate [6]. Frequency-domain features have also been used, e.g., the coefficients of autoregressive power spectral modeling of the EMG [10]. In both cases, features are extracted from an epoch/window of the EMG signal stream for classification. The extent to which these features—or their dimensionally reduced representations—distinguish the different motion classes directly relates to the accuracy of the classifier. Limitations in class separation in the feature space represent a *systematic* error (i.e., bias) in the classifier. Because the EMG signal presents itself as a stochastic process, a distinct *random* error (i.e., variance) also exists. That is, even if amputees produce a repeatable force pattern in their residual limb, the EMG-derived features will vary trial-to-trial due to the inherent variations in the EMG signal.

Errors due to the stochastic component of the EMG signal are also problematic in the related areas of EMG amplitude estimation and EMG-force processing [12]–[15]. In these applications, signal whitening has been used to reduce the random error of the processed EMG, with substantial performance improvements resulting. Whitening temporally decorrelates the EMG signal, increasing the effective number of signal samples (a.k.a., statistical degrees of freedom) and reducing the variance in the amplitude estimate.

Whitening has not previously been applied to the EMG multifunction classification problem. In this paper, we investigate the hypothesis that EMG signal whitening prior to feature extraction will similarly reduce the random error in EMG-based features and lead to improved classification accuracy. This effect should be most prominent at short window durations, since long window durations already experience high classification accuracy (often above 95%, for which little improvement is either available or needed). Shorter window durations are relevant, because they reduce the delay between user command

Manuscript received April 30, 2012; revised January 15, 2013; accepted January 20, 2013. Date of publication March 07, 2013; date of current version September 04, 2013. This work was supported in part by NSERC under Discovery Grant 217354-10.

L. Liu, P. Liu, and E. A. Clancy are with the Electrical and Computer Engineering Department, Worcester Polytechnic Institute, Worcester, MA 01609 USA (e-mail: lliu35@wpi.edu; puliu@wpi.edu; ted@wpi.edu).

E. Scheme and K. B. Englehart are with the Institute of Biomedical Engineering, University of New Brunswick, Fredericton NB E3B 5A3, Canada (e-mail: escheme@unb.ca, kengleha@unb.ca).

Color versions of one or more of the figures in this paper are available online at http://ieeexplore.ieee.org.

Digital Object Identifier 10.1109/TNSRE.2013.2243470

and prosthesis actuation, permitting higher speed (bandwidth) movement and more realistic motion [16]. A preliminary report of this work appeared in [17].

II. Analytic Time-Domain Feature Performance

For purposes of classification analysis, the random variation of an EMG feature can be quantified as the standard deviation of the feature (σ) relative to its mean value (μ), i.e., the feature's coefficient of variation: CoV $= \sigma/\mu$. Lower CoVs should facilitate higher classification accuracy. An analysis of the CoV of common EMG time-domain classification features does not appear to have been previously reported. Thus, we do so here.

A common model of the EMG samples, $m[n]$, from one window, is that of a wide sense stationary, correlation-ergodic, zero-mean, Gaussian random process [13], [14], [18], where n is the sample index and $m[\cdot]$ is measured in millivolts. Without loss of generality, assume that successive model samples are independent [15], [18], [19]. In fact, these samples are correlated due to the limited bandwidth of the EMG signal. However, let window length N_{Eq} represent the equivalent number of independent samples within a window, given by [20]

$$N_{\mathrm{Eq}} = 2B_sT \tag{1}$$

where B_s is the statistical bandwidth of the EMG (Hz) and T is the window length (seconds). Since whitening increases N_{Eq} via an increase in statistical bandwidth [14], [15], the relevant analytic relationship is to determine the CoV versus N_{Eq} for each time-domain feature.

The MAV of an EMG window of N_{Eq} samples is defined as

$$\mathrm{MAV}_{N_{\mathrm{Eq}}} = \frac{1}{N_{\mathrm{Eq}}} \sum_{n=0}^{N_{\mathrm{Eq}}-1} |m[n]|. \tag{2}$$

Its CoV is the inverse of the signal-to-noise ratio (SNR), which has been previously analyzed [21]. Inverting the SNR result gives

$$\mathrm{CoV}_{\mathbf{MAV}}[N_{\mathrm{Eq}}] = \sqrt{\frac{\pi-2}{2N_{\mathrm{Eq}}}} \cong \frac{0.755}{\sqrt{N_{\mathrm{Eq}}}}. \tag{3}$$

The average signal length of N_{Eq} samples, in millivolts per second per sample, is defined as

$$\mathrm{SL}_{N_{\mathrm{Eq}}} = \frac{f_s}{N_{\mathrm{Eq}}-1} \sum_{n=1}^{N_{\mathrm{Eq}}-1} |m[n]-m[n-1]|. \tag{4}$$

The gain factor $f_s/N_{\mathrm{Eq}}-1$, not normally included in the definition of signal length, normalizes its values across sampling rates and window lengths. Since the $m[n]$ are zero-mean Gaussian, so is each difference term in the sum, but with a doubled variance. An analytic form for the sum was not readily apparent due to the correlation between adjacent differences, which share a common EMG sample. Hence, the CoV of average signal length was approximated numerically in MATLAB by creating 10^6 replicates of Gaussian vectors of size N_{Eq} and computing the sample mean and standard deviation of the average signal length, across these replica. Window length N_{Eq} was varied from 2–2000. The resulting CoV values versus N_{Eq} closely fit the model

$$\mathrm{CoV}_{\mathrm{SL}}[N_{\mathrm{Eq}}] \cong \frac{0.911}{\sqrt{N_{\mathrm{Eq}}}}. \tag{5}$$

The normalized zero crossing rate of N_{Eq} samples is defined as the number of adjacent samples with different polarity, normalized by the ratio between sampling rate and the number of samples

$$\mathrm{ZC}_{N_{\mathrm{Eq}}} = \frac{f_s}{(N_{\mathrm{Eq}}-1)} \sum_{n=1}^{N_{\mathrm{Eq}}-1} [1-\mathrm{sgn}(m[n]\ m[n-1])]. \tag{6}$$

The gain factor $f_s/(N_{\mathrm{Eq}}-1)$ normalizes the zero crossing values across sampling rates and window lengths, so that its unit is Hertz, and

$$\mathrm{sgn}(t) = \begin{cases} 1, & t > 0 \\ 0, & t \le 0 \end{cases}$$

For independent identically distributed Gaussian samples, the probability of a sign change between a pair of samples is 0.5. Thus, the number of sign changes in N_{Eq} samples follows a Binomial distribution with $N_{\mathrm{Eq}}-1$ trials, and its coefficient of variation is [22]

$$\mathrm{CoV}_{ZC}[N_{\mathrm{Eq}}] = \frac{\sigma_{ZC}}{\mu_{ZC}} = \frac{\frac{f_s}{N_{\mathrm{Eq}}-1} \cdot \sqrt{\frac{N_{\mathrm{Eq}}-1}{4}}}{\frac{f_s}{N_{\mathrm{Eq}}-1} \cdot \frac{N_{\mathrm{Eq}}-1}{2}} = \frac{1}{\sqrt{N_{\mathrm{Eq}}-1}} \cong \frac{1}{\sqrt{N_{\mathrm{Eq}}}}. \tag{7}$$

We see that the CoV for each time-domain feature is (asymptotically) a univariate function of the number of equivalent independent samples, in the form of a constant divided by $\sqrt{N_{\mathrm{Eq}}}$, where N_{Eq} represents the equivalent number of independent samples. We expect that signal whitening will increase N_{Eq}, thereby reducing CoVs for any given window duration, with better classification accuracy hypothesized to result. An experimental trial evaluated this hypothesis.

III. Methods

A. Experimental Methods

Experimental data from two prior studies were analyzed. The Worcester Polytechnic Institute (WPI) Institutional Review Board (IRB) approved and supervised this analysis. Data from ten intact-limbed subjects, aged 19–32 years, had been collected at the University of New Brunswick [7]. Briefly, ten adhesive Duotrode electrodes (manufactured by 3 M) were applied about the circumference of the forearm of each intact subject. Twelve equally spaced locations were marked along the entire forearm circumference at 1/3 the distance from the elbow to the wrist, beginning at the palmar aspect (see [7] and Fig. 2).

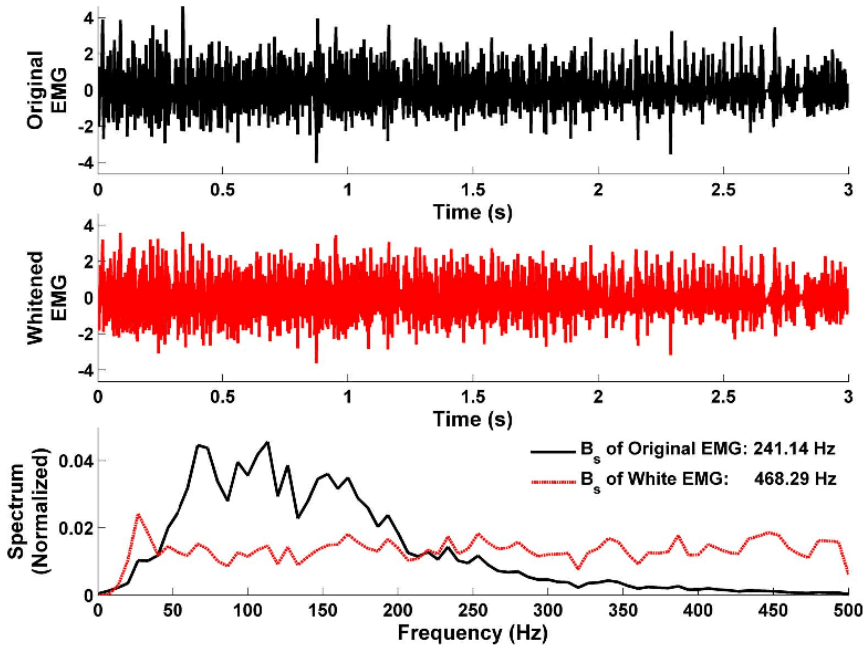

Fig. 1. Sample original EMG epoch (top), same epoch after whitening (middle) and the normalized spectrum of each (bottom). Statistical bandwidth, $\boldsymbol{B_s}$, of each signal is listed. Data from healthy subject 6, channel 3, fine pinch grip motion, epoch 2.

The most medial and lateral locations were omitted(leaving ten locations). Bipolar electrodes had a contact diameter of 1.4 cm and a center-to-center distance of 2 cm. A subject began and ended each trial at rest (fixed posture with no motion attempted, muscle effort minimized) with their elbow supported on an armrest. Each trial consisted of two repetitions of the 11 motion classes: 1) and 2) wrist pronation/supination; 3) and 4) wrist flexion/extension; 5) hand open; 6) key grip; 7) chuck grip; 8) power grip; 9) fine pinch grip; 10) tool grip; and 11) no motion. Each motion class within a trial was maintained for 4 s, and the subject returned to the rest posture for a specified inter-motion delay period prior to producing the next motion class. Trials 1–4 used an inter-motion delay of 3, 2, 1, and 0 s respectively, and trials 5–8 used an inter-motion delay of 2 s. The eight trials were performed twice and a minimum of two minutes inactivity was given between each trial. A general familiarization session was provided prior to data collection, typically lasting approximately 15 minutes in duration. The EMG data were collected using a custom-built pre-amplification system (Liberating Technologies, Inc., Holliston, MA) with a frequency response from 30–350 Hz, and sampled at 1000 Hz using a 16-bit ADC.

The Rehabilitation Institute of Chicago collected EMG data from five subjects aged 28 to 77 years, who had received unilateral transradial amputation three months to 21 years prior [9]. Three subjects were myoelectric prosthesis users, one subject used a body-powered prosthesis and one subject had not yet received a prosthesis. A total of 12 self-adhesive Ag/AgCl snap bipolar electrodes with a 1.25-cm-diameter circular contact and center-to-center distance of 2 cm (Noraxon USA, Inc) were used. Eight of the 12 electrodes were placed around the proximal portion of the forearm over the apex of the muscle bulge and the other four on the distal end [see [9] and Fig. 1(a)]. In this study, we used only the first ten electrodes, to most closely match the electrode placement of the intact-limbed subjects. Only data from the amputated side was used. The experiment protocol was the same as that of the intact subjects, including subject posture, the general familiarization session and the motion trials. Identical motion trial data were available for analysis. The EMG data were transduced using Liberating Technologies preamplifiers, bandpass filtered between 5–400 Hz and sampled at 1000 Hz using a 16-bit ADC.

B. *Methods of Analysis*

1) Feature Computation: The trials were segregated into training and testing data, as described in the following. The inter-trial delay segments were removed from data recordings, resulting in 22 4-s segments per electrode per trial (two repetitions of 11 motion classes). Each segment was zero-phase notch-filtered (0.4 Hz bandwidth) at the power-line frequency and its harmonics. When desired, each four-second segment was also whitened. To do so, each segment was highpass filtered at 15 Hz, then adaptively whitened using an algorithm that was tuned to the power spectrum of each EMG channel [12], [23]. Whitening filters were calibrated from a training trial by manually selecting, subject-by-subject for each electrode, the trial with the largest MAV. A no motion trial was also used to represent resting EMG in the whitening calibration. Prior to feature extraction, 0.5 s of data were truncated from the beginning and end of each segment to account for filter startup transients. Contiguous, nonoverlapping windows were formed from the remaining three-second epochs.

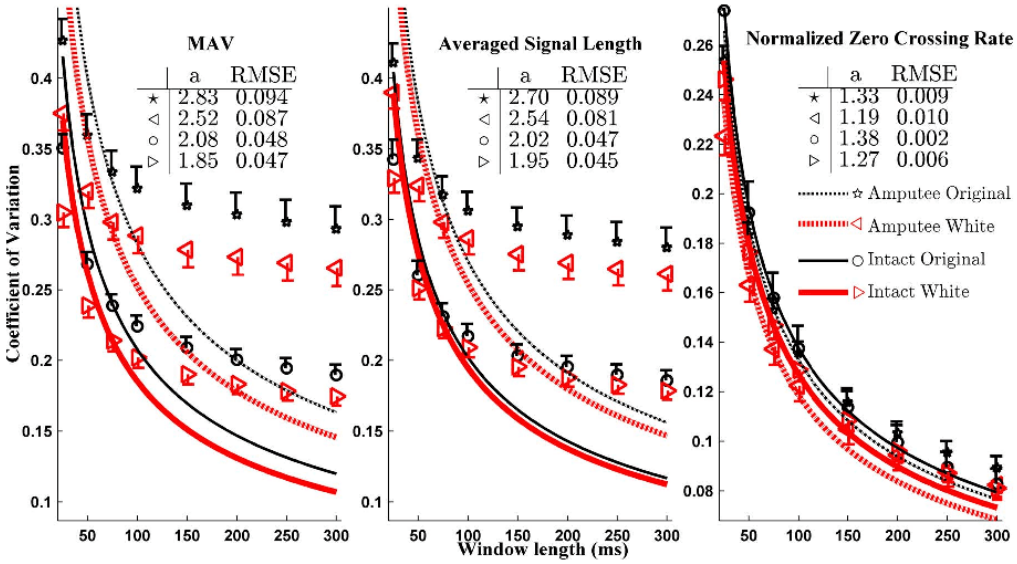

Fig. 2. Average coefficient of variation (plus or minus one standard error) for the time-domain features from ten intact and (separately) five amputee subjects. Two recordings per channel per subject with the largest MAV EMG were used for this analysis. Lines show fit to power decay model: $\mathrm{CoV}[N] = a/\sqrt{N}$. Inset tables show fit parameter "a" and fit rms error (RMSE). Scale of y-axis differs for normalized zero crossing rate. Sample size is 100 for intact subjects, 50 for amputee subjects.

Feature sets were extracted in each window within an epoch. The time-domain feature set consisted of the three featuresdescribed earlier: MAV, average signal length and normalized zero-crossing rate. Hysteresis as described in [6] was applied to normalized zero-crossing rate. Specifically, a zero-crossing was not counted if the absolute difference between the two adjacent samples did not exceed a fixed threshold value. The threshold value was set to approximately 1/6th the average RMS value of the no-motion class of all subjects and all electrodes. A frequency domain feature set consisted of the estimated AR coefficients of a seventh order AR model [10], [24]. A third (combined) feature set concatenated the seven AR coefficients and MAV. It has been shown that linear classification models give different weights to each feature, and the MAV feature alone tends to have a large amount of motion classification power.

2) Coefficient of Variation Analysis: CoV values were computed for each of the three time-domain EMG features. Because CoV is the ratio between standard deviation and the mean of a feature, EMG signals with a small mean value can lead to unstable CoV estimates (due to dividing two small numbers in the presence of noise). Thus CoV was calculated using only two training trials per channel by manually selecting, subject-by-subject for each channel, the two trials with the largest MAV. All motion classes were considered when searching for the maximum MAV. The sample standard deviation divided by the sample mean of the contiguous feature values from a 3-s epoch formed a CoV value. The average CoV from the two trials per channel served as the CoV estimate for that channel. Data from the intact subjects were studied separately from those of the amputee subjects. CoV values that compared unwhitened to whitened signals were computed for the following window durations: 25, 50, 75, 100, 150, 200, 250 and 300 ms. Once the CoV had been determined as a function of sample length N, we fit these results to the power decay model: $\mathrm{CoV}[N] = a/\sqrt{N}$.

We defined N as the number of samples corresponding to the window duration. The number of samples (N) is always greater than the equivalent number of independent samples (N_{Eq}) due to signal correlation. In practice, this correlation cannot be entirely eliminated via whitening. A more direct measure of whitening performance is to assess the statistical bandwidth of the EMG before and after whitening. The same 3-s epochs as previously mentioned were used to do so. The discrete-time power spectrum, $S_{mm}(k)$, of each epoch was estimated using Welch's method (window length of 150 ms, Hamming window, 50% overlap), where k is the frequency index. The statistical bandwidth was then estimated as [20]

$$B_s = \frac{\Delta f \cdot \left(\sum_{k=0}^{K-1} S_{mm}(k)\right)^2}{\sum_{k=0}^{K-1} S_{mm}^2(k)} \tag{8}$$

where K specifies the range of positive-valued frequencies and $\Delta f = 6.67$ Hz is the frequency increment. Values from the two trials per channel were averaged.

3) Classification Analysis: A linear discriminant classifier was employed. Trials 1–4 of the two repetitions were used to train the coefficients of the classifier and trials 5–8 to test classifier performance. The model was trained and tested for each individual subject using all features of a feature set, and only test results are reported. Eight window durations were used: 25, 50, 75, 100, 150, 200, 250 and 300 ms. We repeated the analysis after the EMG signal had been whitened.

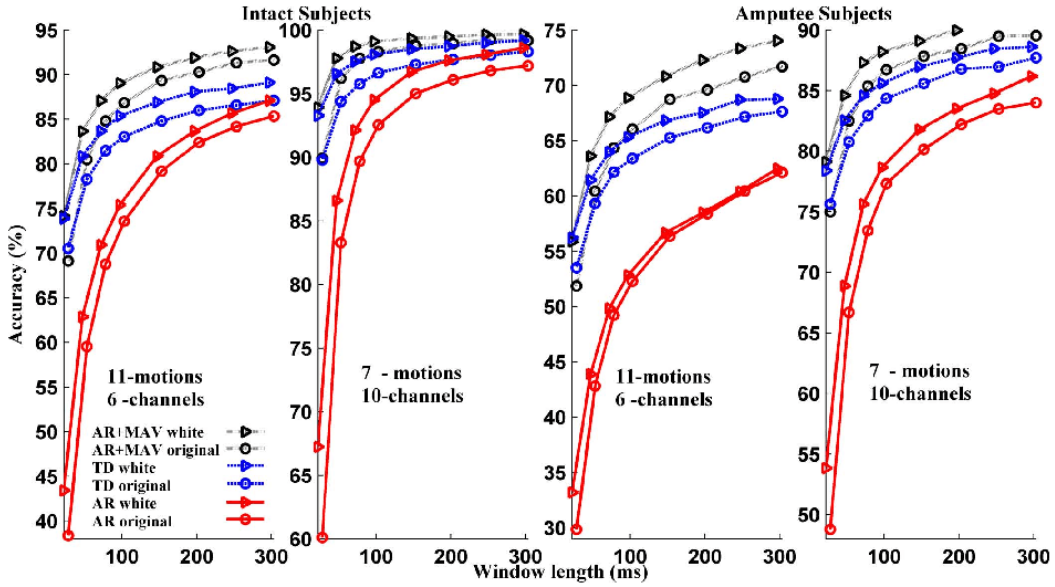

Fig. 3. Average classification accuracies from ten intact (left) and five amputee (right) subjects for each of the three feature sets, with and without whitening. Motion-channel combinations shown represent the lowest accuracies (fewest channels and most motion classes) and highest (most channels and fewest classes). Note the different y-axis scale for each plot.

Two global processing variants were also considered. First, the entire analysis was repeated using only seven preselected motion classes (the classes denoted above as numbers 1–5, 8 and 11), and again using only nine preselected motion classes (1–8 and 11), thereby giving three motion variations. Second, the entire analysis was repeated using a preselected set of six of the electrode channels (channels 1–6, spread around the arm circumference), giving two channel variations.

IV. Results

1) Coefficient of Variation Results: Fig. 1 shows a sample 3-s raw EMG epoch, the same epoch after whitening, and the spectrum of each of these two signals (normalized to the total power in each spectrum). The spectra show how whitening equalizes the contributions across frequency, increasing the statistical bandwidth of the signal. Fig. 2 shows all CoV results, averaged across subjects, for the three time-domain features, together with the standard errors. Lines within the figure show the best fit power decay model and the inset tables list the fit errors. The sample size for calculating the CoV and standard error was 100 for intact subjects (10 subjects × 10 EMG channels/subject) and 50 for amputees (5 subjects × 10 EMG channels/subject). The CoV for each feature improved (i.e., decreased) with window length and due to whitening, although the MAV and SL results were a poor fit to the power decay model. The normalized zero crossing rate exhibited substantially lower CoV values than the other two features and fit well to the power decay model. CoV values for intact subjects were consistently lower than those of amputee subjects. Paired sign tests were conducted between whitened and unwhitened features at each window duration and for each of the intact and amputee data sets. All comparisons were significant for MAV ($p < 10^{-4}$) and for average signal length ($p \leq 0.006$ for intact subjects, $p < 10^{-4}$ for amputees). For normalized zero crossing rate, whitened features only differed from unwhitened features in intact subjects when the window length was ≤ 50 ms ($p < 0.002$), and in amputees when the window length was ≤ 200 ms ($p < 0.008$).

TABLE I
Average ± Standard Deviation Statistical Bandwidths. Sample Size is 100 for Intact Subjects, 50 for Amputee Subjects

Subjects	Condition	
	Unwhitened	Whitened
Intact	238.0 ± 49.8 Hz	413.2 ± 73.0 Hz
Amputee	254.1 ± 53.4 Hz	423.1 ± 52.7 Hz

Table I shows the results of the statistical bandwidth computations. Whitening increased the statistical bandwidth by 65%–75%, on average. Statistically, the ten statistical bandwidth values per subject (one per electrode) were averaged. These values for unwhitened versus whitened processing were compared using a paired t-test. Results were significant for both the intact and amputee subjects ($p < 10^{-4}$).

2) Classifications Results: Complete classification results were produced for six classifier variants (11 or 9 or 7 motion classes versus ten or six electrodes). Higher accuracies were found when fewer motions and/or more electrode channels were included in the classifier. Hence, our presentation of results will be limited to the highest (7-motion, 10-channel) and lowest (11-motion, 6-channel) performing classifiers—all four remaining result variants fell between these two extremes. Fig. 3 shows the average test accuracies for intact and amputee subjects, for window lengths between 25 and 300 ms, for each feature set with and without whitening. The combined AR-MAV feature set gave the highest overall accuracy in each case, and the AR

features the lowest. For all feature sets, accuracy was generally improved by approximately 5% at shorter window durations (< 100 ms) due to whitening. The improvement was smaller as window duration increased further. Accuracy values for intact subject were consistently higher than those of amputee subjects. Because sample sizes were small (DoF $= 9$ for ten intact subjects, DoF $= 4$ for five amputees) paired t-tests compared unwhitened to whitened processors at each window duration. For the AR-MAV feature set and intact subjects, differences were significant for: the 7-motion, 10-channel case when the window length was ≤ 300 ms ($p < 0.009$), and the 11-motion, 6-channel case for all window lengths except 400 ms ($p < 0.005$). For the AR-MAV feature set and amputees, differences were significant for: the 7-motion, 10-channel case when the window length was ≤ 50 ms ($p < 0.006$), and the 11-motion, 6-channel case when the window length was ≤ 100 ms ($p < 0.008$). For the TD feature set, results were only significant for intact subjects with the 7-motion, 10-channel case when the window duration was ≤ 300 ms ($p < 0.01$) and in amputee subjects in the 11-motion, 6-channel case when the window duration was 25 ms ($p = 0.004$). For the AR feature set of amputees, unwhitened versus whitened result differences were significant in all cases when the window length was 25 ms ($p < 0.006$) and in intact subjects with the 7-motion, 10-channel case when the window duration was ≤ 400 ms ($p < 0.003$).

V. Discussion

We studied the use of EMG signal whitening in classification algorithms for prosthesis control. Signal whitening methods have existed for several years [12]–[15], having been shown in the laboratory to improve EMG amplitude estimation [12] as well as EMG-force estimation [25]. They had not previously been applied to the EMG multifunction classification problem. Whitening decorrelates the EMG signal in time—increasing its statistical bandwidth—resulting in a larger number of effective degrees of freedom in the data [20]. Essentially, whitening increases the effective sample size (N_{Eq}) of each individual data epoch, making each epoch more representative of the entire sequence.

Theoretically, the influence of epoch sample size on the MAV feature had been previously studied via the SNR (inverse of the CoV) [19]. The CoV decreases in a square root fashion with sample size. We extended this analysis to the other two time-domain features. The CoV of the average signal length and normalized zero crossing rate also each decrease in a square root relationship with sample size. Our theoretic model for normalized zero crossing rate did not include hysteresis. However, this effect is generally considered small when an appropriate (small) level of hysteresis is applied [6].

In practice, whitening increased statistical bandwidth by 65%–75% (Table I) and CoV was reduced for each of the three time-domain features (Fig. 2). However, the MAV and average signal length features produced CoV values that did not fit the power decay model. Further, our CoV values were consistently much higher than the model predictions, based on the statistical bandwidth. For example, for whitened data from intact subjects

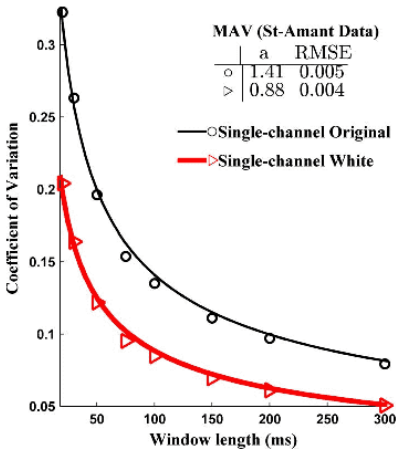

Fig. 4. Inverse of average SNR gives an estimate of average coefficient of variation, with and without whitening for MAV feature, from the data of St-Amant *et al.* [28]. Lines show fit to power decay model CoV$[N] = a/\sqrt{N}$. Inset table shows fit parameter "a" and fit rms error (RMSE).

(average bandwidth of 413 Hz from Table I) using a 300 ms window, (1) and (2) can be used to compute an anticipated CoV_{MAV} of 0.048. Our result of ~ 0.175 shown in Fig. 2 is well above this value. Visual inspection of the calibration data from both intact and amputee subjects found substantial modulations in EMG amplitude *within* each 3-s epoch. For the MAV and average signal length features, such modulations would greatly increase the standard deviation of the contiguous features extracted from an epoch, resulting in the observed CoV increase. Recall that intact subjects were not provided force feedback; amputee subjects cannot be provided such feedback. While such feedback could be provided to the intact subjects, it is generally considered best to train classifiers using the same conditions representative of their use—which would *exclude* feedback. Consistent with these observations, consider the SNR results of St-Amant *et al.* [26], which were produced by intact subjects utilizing force feedback. The inverse of their SNR calculation provides a CoV estimate. Fig. 4 plots the inverse of their average SNR measurements versus window length, as well as fits to our power decay model. The excellent model fits the result. Although the St-Amant *et al.* data are from different muscles using a smaller inter-electrode distance, they are supportive of the role of EMG amplitude modulation in artificially increasing estimated CoV values. Conversely, the zero crossing feature *did* follow a power decay model as a function of window length and had CoV values that followed theoretic expectations. So long as the crossing signal does not have a peak or trough near zero voltage, even a modest amount of amplitude modulation will not alter proper identification of the crossing. Hence, zero crossings would not be substantially affected by amplitude modulations, as observed in our results.

In any case, the experimental CoV for whitened features was consistently better (smaller) than that of unwhitened features for MAV and average signal length, and better at shorter epoch lengths for normalized zero crossing rate. Thus, the variability

of the time-domain features was generally reduced by preprocessing the signal with a whitening filter. Features with less variability would be expected to lead to more accurate classification. However, classification analysis does not solely rely on the CoV of the features. Individual features may be weighted differently in the linear classifier, giving a larger impact to some features than others; and small changes in the classification model space can have varied influence on classification accuracy.

The classification accuracy results consistently showed an improvement due to whitening, when the shorter epoch durations were considered. The shortest epoch durations of 25–100 ms generally experienced the greatest improvement—an approximate 4%–5% increase in accuracy. It is not surprising that the improvement diminishes with increased epoch length, since all accuracies are improving, but cannot exceed 100%. Larger sample sizes might be useful in demonstrating significant improvements due to whitening at these longer epoch lengths. Consistent with prior research [7], [9], our results also found that higher accuracies resulted when fewer motions and/or more electrode channels were included in the classifier.

Because the performance improvements due to whitening are modest, its inclusion in a prosthesis controller should be weighed versus its costs. Disadvantages/challenges of using whitening include its substantial added computation and memory requirements, the need to collect calibration data, and possible robustness issues in the presence of high frequency noise. Advantages include that whitening is implemented as a stand-alone preprocessing step whose output can be fed into all further EMG processing steps, accuracy improvements at the shorter epoch durations may facilitate the use of shorter epochs thereby reducing prosthesis response time, and that modern signal processing hardware is increasingly capable of the required processing demands. A logical next step to all of this work is to evaluate whitening within a myoelectric-controlled prosthesis.

We considered only simple feature vectors and classifiers in this analysis. Many more complex features/classifiers have appeared in the literature [7], [8], although their classification performance is not markedly distinct from those reported herein. Nonetheless, one would expect that EMG signal whitening would similarly improve the performance of those classifiers. Note that the data available to this research was collected from EMG electrodes with bandwidth out to 350–400 Hz. This bandwidth is common. However, whitened signals have been shown to take advantage of a wider bandwidth (out to nearly 2000 Hz in some cases [27], [28]), with additional performance improvement provided. Future work may wish to utilize a wider band EMG data acquisition system. In addition, we calibrated the whitening filters from available functional contractions that contained visible amplitude modulations. It may be better to collect dedicated calibration contractions at 0% and 50% MVC [12], [27].

In conclusion, we have shown that whitening the EMG signal leads to time-domain features with an increased statistical bandwidth and concomitantly smaller CoV, leading to a consistent increase in classification accuracy in both intact and amputee subjects in a laboratory evaluation. Whitening added approximately five percentage points to classification accuracy at the shortest epoch durations ($\sim 25 - 100$ ms). Improvement in classification accuracy at these shortest epoch durations is important, as it may allow prosthesis control systems to use shorter epochs, thereby improving response time.

ACKNOWLEDGMENT

The authors thank G. Li and the Neural Engineering Center for Artificial Limbs, Rehabilitation Institute of Chicago, Chicago, IL 60611 USA, for providing the amputee data for this study.

REFERENCES

[1] P. F. Adams, G. E. Hendershot, and M. A. Marona, "Current estimates from the national health interview survey, 1996," *Nat. Ctr. Health Statistices, Vital Health Stat.*, vol. 10, no. 200, pp. 81–93, 1999.

[2] T. R. Dilingham, L. E. Pezzin, and E. J. MacKenzie, "Limb amputation and limb deficiency: Epidemiology and recent trends in the United States," *South Med. J.*, vol. 95, pp. 875–883, 2002.

[3] P. Parker, K. Englehart, and B. Hudgins, "Myoelectric signal processing for control of powered limb prostheses," *J. Electromyogr. Kinsesiol.*, vol. 16, pp. 541–548, 2006.

[4] H. A. Varol, F. Sup, and M. Goldfarb, "Multiclass real-time intent recognition of a powered lower limb prosthesis," *IEEE Trans. Biomed. Eng.*, vol. 57, no. 3, pp. 542–551, Mar. 2010.

[5] D. Atkins, D. C. Y. Heard, and W. H. Donovan, "Epidemiologic overview of individuals with upper-limb loss and their reported research priorities," *J. Prosthet. Orthot.*, vol. 8, pp. 2–11, 1996.

[6] B. Hudgins, P. Parker, and R. N. Scott, "A new strategy for multifunction myoelectric control," *IEEE Trans. Biomed Eng.*, vol. 40, no. 1, pp. 82–94, Jan. 1993.

[7] L. J. Hargrove, G. Li, K. B. Englehart, and B. S. Hudgins, "Principle component analysis for improved classification accuracies in pattern-recognition-based myoelectric control," *IEEE Trans. Biomed Eng.*, vol. 56, no. 6, pp. 1407–1414, Jun. 2009.

[8] M. R. Ahsan, M. I. Ibrahimy, and O. O. Khalifa, "Advances in electromyogram signal classification to improve the quality of life for the disabled and aged people," *J. Comp. Sci.*, vol. 6, pp. 706–715, 2010.

[9] G. Li, A. E. Schultz, and T. A. Kuiken, "Quantifying pattern recognition-based myoelectric control of multifunctional transradial prosthesis," *IEEE Trans. Neural Sys. Rehab. Eng.*, vol. 18, no. 4, pp. 185–192, Aug. 2010.

[10] D. Graupe and W. K. Cline, "Functional separation of EMG signals via ARMA identification methods for prosthesis control purposes," *IEEE Trans. Sys. Man Cyber.*, vol. 5, no. 2, pp. 252–259, Apr. 1975.

[11] R. Boostani and M. H. Moradi, "Evaluation of forearm EMG signal features for the control of a prosthetic hand," *Physio. Meas.*, vol. 24, pp. 309–319, 2003.

[12] E. A. Clancy and K. A. Farry, "Adaptive whitening of the electromyogram to improve amplitude estimation," *IEEE Trans. Biomed. Eng.*, vol. 47, no. 5, pp. 709–719, May 2000.

[13] E. A. Clancy, E. L. Morin, and R. Merletti, "Sampling, noise-reduction and amplitude estimation issues in surface electromyography," *J. Electromyogr. Kinsesiol.*, vol. 12, pp. 1–16, 2002.

[14] N. Hogan and R. W. Mann, "Myoelectric signal processing: Optimal estimation applied to electromyography—Part I: Deviation of the optimal myoprocessor," *IEEE Trans. Biomed. Eng.*, vol. BME-27, no. 3, pp. 382–395, Mar. 1980.

[15] N. Hogan and R. W. Mann, "Myoelectric signal processing: Optimal estimation applied to electromyography—Part II: Experimental demonstration of optimal myoprocessor performance," *IEEE Trans. Biomed. Eng.*, vol. BME-27, no. 3, pp. 396–410, Mar. 1980.

[16] T. R. Farrell and R. F. Weir, "The optimal controller delay for myoelectric prostheses," *IEEE Trans. Neur. Sys. Rehab. Eng.*, vol. 15, no. 2, pp. 111–118, Apr. 2007.

[17] L. Liu, P. Liu, E. A. Clancy, E. Scheme, and K. B. Englehart, "Signal whitening preprocessing for improved classification accuracies in myoelectric control," in *Proc. IEEE 37th Northeast Bioeng. Conf.*, 2011.

[18] E. Kwatny, D. H. Thomas, and H. G. Kwatny, "An application of signal processing techniques to the study of myoelectric signals," *IEEE Trans. Biomed. Eng.*, vol. 17, no. 2, pp. 303–313, Feb. 1970.
[19] E. A. Clancy and N. Hogan, "Theoretic and experimental comparison of root-mean-square and mean-absolute-value electromyogram amplitude estimation," in *Proc. Annu. Inter. Conf. IEEE Eng. in Med. and Bio. Soc.*, 1997, vol. 19, pp. 1267–1270.
[20] J. S. Bendat and A. G. Piersol, *Random Data: Analysis and Measurement Procedures*. New York, NY, USA: Wiley, 1971.
[21] E. A. Clancy and N. Hogan, "Probability density of the surface electromyogram and its relationship to amplitude detectors," *IEEE Trans. Biomed. Eng.*, vol. 46, no. 4, pp. 730–739, Apr. 1999.
[22] A. W. Drake, *Fundamentals of Applied Probability Theory*. New York, NY, USA: McGraw-Hill, 1967, pp. 272–272.
[23] P. Prakash, C. A. Salini, J. A. Tranquilli, D. R. Brown, and E. A. Clancy, "Adaptive whitening in electromyogram amplitude estimation for epoch-based applications," *IEEE Trans. Biomed. Eng.*, vol. 52, no. 2, pp. 331–334, Feb. 2005.
[24] A. Neumaier and T. Schneider, "Estimation of parameters and eigenmodes of multivariate autoregressive models," *ACM Trans. Math. Software*, vol. 27, pp. 27–57, 2001.
[25] E. A. Clancy, L. Liu, P. Liu, and D. V. Moyer, "Identification of constant-posture EMG-torque relationship about the elbow using nonlinear dynamic models," *IEEE Trans. Biomed. Eng.*, vol. 59, no. 1, pp. 205–212, Jan. 2012.
[26] Y. St-Amant, D. Rancourt, and E. A. Clancy, "Influence of smoothing window length on electromyogram amplitude estimates," *IEEE Trans. Biomed. Eng.*, vol. 45, no. 5, pp. 795–800, May 1998.
[27] E. A. Clancy and N. Hogan, "Single site electromyogram amplitude estimation," *IEEE Trans. Biomed. Eng.*, vol. 41, no. 1, pp. 159–167, Jan. 1994.
[28] P. Liu, L. Liu, F. Martel, D. Rancourt, and E. A. Clancy, "EMG-Torque estimation of constant-posture, quasi-constant torque contractions at varied joint angles," in *Proc. IEEE 37th Northeast Bioeng. Conf.*, 2011.

Lukai Liu received the B.S. degree in electrical engineering from Xian Jiaotong University, in 2003, and M.S. degree in electrical and computer engineering from the Illinois Institute of Technology, Chicago, IL, USA, in 2009. He is currently working toward the Ph.D. degree in electrical and computer engineering at Worcester Polytechnic Institute, Worcester, MA, USA.

His research interests include biomedical signal processing, biomedical imaging and machine learning.

Pu Liu received the B.S. degree from Fudan University, China, and the M.S. degree from Worcester Polytechnic Institute (WPI), Worcester, MA, USA, all in electrical engineering. She is currently working towards the Ph.D. degree in electrical and computer engineering at WPI.

She is interested in signal processing, modeling and instrumentation, principally as applied to biomedical engineering.

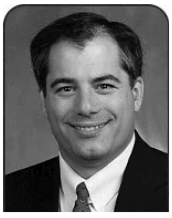

Edward A. Clancy (S'83–M'91–SM'98) received the B.S. degree from Worcester Polytechnic Institute (WPI), Worcester, MA, USA, and the S.M. and Ph.D. degrees from Massachusetts Institute of Technology (MIT), Cambridge, MA, USA, all in electrical engineering.

He has worked in industry for medical instrumentation and analysis companies interested in EMG, EEG, ECG and blood pressure, and the defense industry (aircraft instruments and radar). He is an Associate Professor of Electrical and Computer Engineering, and of Biomedical Engineering at WPI. He is interested in signal processing, stochastic estimation and system identification, particularly as applied to problems in medical engineering and human rehabilitation.

Erik Scheme (S'08) received the B.Sc. degree in electrical engineering and the M.Sc. degree from the University of New Brunswick (UNB), Fredericton, NB, Canada, in 2003 and 2005, respectively. He is working toward the Ph.D. degree at the Institute of Biomedical Engineering, UNB.

He is a Project Engineer and his research interests include biological signal processing and the clinical application of prosthetic control research.

Mr. Scheme is a Registered Professional Engineer and a member of the IEEE Engineering in Medicine and Biology Society.

Kevin B. Englehart (SM'06) received the B.Sc. degree in electrical engineering and the M.Sc. and Ph.D. degrees from the University of New Brunswick (UNB), Fredericton, NB, Canada, in 1989, 1992, and 1998, respectively.

He is currently the acting Director of the Institute of Biomedical Engineering at UNB. His research interests include neuromuscular modeling and biological signal processing using adaptive systems, pattern recognition, and time-frequency analysis.

Dr. Englehart is a Registered Professional Engineer, and a member of the IEEE Engineering in Medicine and Biology Society, the International Society of Electrophysiology and Kinesiology, and the Canadian Medical and Biological Engineering Society.

CHAPTER 15

Copy of published journal paper:

Meera Dasog, Kishor Koirala, Pu Liu and Edward A. Clancy. "Electromyogram Bandwidth Requirements When the Signal is Whitened." *IEEE Transactions on Neural Systems and Rehabilitation Engineering*, in press.

Electromyogram Bandwidth Requirements When the Signal is Whitened

MeeraDasog,KishorKoirala, Pu Liu, andEdward A. Clancy, *Senior Member, IEEE*

***Abstract*—Whitening the surface electromyogram (EMG) improves EMG amplitude (EMGσ) and EMG-torque estimation. Laboratory studies utilizing contraction levels up to maximum voluntary contraction (MVC) show that whitening is useful over a frequency band extending to 1000–2000 Hz. However, EMG electrode systems with such wide bandwidth are uncommon, particularly in real-time applications; and these contraction levels are also not common. Thus, we studied the influence of the frequency band over which whitening was performed vs. the resulting performance. Low-level, torque-varying contractions (average torque level of 18.5% flexion MVC) of the elbow were contrasted with medium-level 50% MVC constant-torque contractions. For each, the maximum whitening bandwidth was varied between 30–2000 Hz. The low-level contractions (which incorporate the contraction range of most daily tasks) showed that performance utilizing frequencies out to 400–500 Hz was not statistically different (p<0.01) than results out to the full available frequency (2000 Hz). For the medium-level (50% MVC) contractions, frequencies out to 800–900 Hz were statistically equivalent to the full bandwidth. These results suggest that conventional electrodes with a typical passband of ~500 Hz are appropriate when whitening data from contraction levels typically experienced in many applications. Wider bandwidths may be advantageous for strenuous activities.**

***Index Terms*— Biological system modeling, biomedical signal processing, electromyography, EMG amplitude estimation, EMG signal processing, whitening.**

I. Introduction

WHITENING of the electromyogram (EMG) signal has been performed for several decades, dating back at least to the work of Kaiser and Petersen in 1974 [1]. Whitening temporally decorrelates EMG samples, reducing the variance of parameters that are extracted from it [2]–[11]. These parameters are used in various applications, including: myoelectric prosthesis control [12], ergonomic assessment [13], [14], clinical biomechanics [15], [16], motor control research [17], control of powered exoskeletons [18]–[22] and the actuation of powered rehabilitation devices [23]–[25]. In laboratory studies, whitened EMG processors have been shown to improve the signal to noise ratio (SNR) by 32–65% in the assessment of constant-torque EMG [2], [3], [8], [9], reduce classification errors by 25–50% in myoelectric multifunction selection [4], [11] and reduce EMG-torque estimation errors by 12–26% [3], [26]–[30].

Referring to Fig. 1, the EMG spectrum peaks (mode frequency) at ~100–150 Hz, then decays as the frequency increases. Accordingly, whitening filters exhibit their minimum gain in the frequency range of 100–150 Hz, with an increase in gain as the frequency increases [8]. At different effort levels, the EMG spectrum maintains the same general shape, but is amplitude modulated [3]. In contrast, EMG background noise is considered constant in spectral shape and amplitude. Hence, Fig. 1 depicts that the relative SNRas a function of frequency varies with the effort level; higher effort levels maintain a higher SNR. Whitening should be limited to those frequencies at which there is significantly more signal power than noise power. At high effort levels, there exists significantly more signal than noise out to higher frequencies. At low effort levels, there exists significantly more signal than noise out to a much lower frequency.

To resolve these contrasting whitening bandwidth needs, Kaiser and Peterson [1] implemented whitening with an adaptive analog filter. Their filter was comprised of a broadband fixed whitening filter, cascaded with an adaptive lowpass filter. At high effort levels, frequencies out to at least 1000 Hz were whitened; while at low effort levels, whitening was only applied at frequencies out to the EMG mode frequency. Filter shapes were a function of the analog components. A similar adaptive concept has since been implemented in discrete-time [31], [32]. This system cascades a fixed broadband digital whitening filter with an adaptive Wiener filter/noise canceller. The Wiener filter assumes a lowpass characteristic. These filters are tuned to the spectrum of each subject via two calibration contractions—one at rest (to estimate the noise spectrum) and another at a modest contraction effort, typically 50% maximum voluntary contraction (MVC). At 100% MVC, these filters whiten out to 2048 Hz (the Nyquist frequency).

In each of the above adaptive filtering methods, the EMG acquisition system incorporated a passbandfrom just above DC out to 1000–2000 Hz. Such a wide passband is not characteristic of many commercially-available electrode systems (particularly when also considering the real-time computational requirements of some applications) and, thus, were custom-built by the respective investigators. Many commercial passbands for surface EMG systems only extend to ~500–600 Hz, limited either by the analog electrodes or by sampling rates/processor computation power (e.g., the standard

Asterisk indicates corresponding author.

M. Dasog, K. Koirala, P. Liu and *E. A. Clancy are with Worcester Polytechnic Institute (WPI), Worcester, MA 01609 USA (e-mail: mgdasog@wpi.edu; kkoirala@wpi.edu; puliu@wpi.edu; ted@wpi.edu).

Delsys Inc. Bagnoli Desktop EMG Systems are limited by their acquisition system to a maximum frequency of 450 Hz). This bandwidth limit is consistent with the frequency band containing most of the EMG signal power (see Fig. 1 and [3]). While the wider passbands appear usefulwhen whitening at high effort contractions, the vast majority of contraction levels in most EMG applications are relatively low (e.g., [33], [34]). Thus, the benefit of the custom passband and increased computation/throughput is unclear in these applications, particularly weighed vs. their cost. In fact, the need for custom wide bandwidth electrode systems can be an impediment to adoption of whitening into these applications.

Thus, this project investigated the role of whitening bandwidth, contrasting low- and medium-intensity contractions from the same data set. The low-intensity contractions consisted of constant-posture, torque-varying contractions of the elbow, limited in effort over the range from 50% MVC extension to 50% MVC flexion. The μ±σ instantaneous contraction level was 18.5 ± 11.1% MVC flexion (MVC_F). EMG was related to joint torque, with the RMS error between actual torque and EMG-estimated torque serving as our performance measure. Medium-intensity contractions consisted of constant-posture, constant-torque contractions at 50% MVC. In this case, the more customary SNR was used as the performance measure. In each case, we characterized performance as a function of the whitening bandwidth. Preliminary results of this work appeared in [35].

II. Methods

A. Experimental Data and Experimental Methods

Experimental data from 54 subjects (30 male, 24 female; aged 37.6±16.5 years) from three prior experimental studies were analyzed. This study was approved and supervised by the WPI IRB. All subjects had previously provided written informed consent. The three studies had nearly identical experimental apparatus and protocols (fully described in [31], [36]). Subjects were seated and secured with their shoulder abducted 90°, forearm oriented in a parasaggital plane, wrist fully supinated and elbow flexed 90°. Their right wrist was tightly cuffed to a load cell (Biodex dynamometer; or Vishay Tedea-Huntleigh Model 1042, 75 kg capacity) at the styloid process. The skin surface above the muscles under investigation was scrubbed with an alcohol wipe. In one study, a small bead of electrode gel was massaged into the skin. Four bipolar electrode-amplifiers were placed transversely across each of the biceps and triceps muscles, midway between the elbow and the midpoint of the upper arm, centered on the muscle midline. Each electrode-amplifier had a pair of 4-mm (or 8-mm) diameter, stainless steel, hemispherical contacts separated by 10 mm edge-to-edge, oriented along the muscle's long axis. The distance between adjacent electrode-amplifiers was ~1.75 cm. A single ground electrode was gelled and secured above the acromion process or on the upper arm. Custom electronics amplified each EMG signal (CMRR of approximately 90 dB at 60 Hz) followed by bandpass filtering (either a second-order, 10–2000 Hz bandpass filter; or 8th-order highpass at 15 Hz followed by a 4th-order lowpass at 1800 Hz). All signals were sampled at 4096 Hz with 16-bit resolution.

After a warm-up period, MVC torque was measured in both elbow extension and flexion. Two repetitions of five-second duration, constant-posture constant-torque contractions at 50% MVC extension, 50% MVC flexion and rest were recorded. A real-time feedback signal consisting of either the load cell voltage or a four-channel whitened EMGσ processor (formed by subtracting the extensor EMGσ from the flexor EMGσ [36]) was provided on a computer screen. Thirty-second duration, constant-posture torque-varying contraction trials were then recorded. The subjects used the feedback signal to track a computer-generated target that moved acrossthe screen as a band-limited (1 Hz) uniform random process, spanning 50% MVC extension to 50% MVC flexion. Three trials were collected. At least three minutes of rest wereprovided between contractions to prevent cumulative fatigue.

B. Methods of Analysis

All analysis was performed offline in MATLAB. For all EMG-torque analyses, afour-channel, whitened (but bandwidth limited) EMG amplitude (EMGσ—the time-varying standard deviation of the EMG signal) processor was used, one processor for the biceps muscles and separately one for the triceps muscles. For a processor, each of the four EMG channels was highpass filtered (15 Hz cutoff, causal, 5th-order, Butterworth filter) and notch filtered at the power-line and each harmonic frequency (2nd-order IIR filter, notch bandwidth ≤ 1.5 Hz). Each channel wasthenadaptively whitened across all frequencies (causal algorithm of Clancy and colleagues [31], [32], [37]). Whitening filters were calibrated from one of the constant-torque contraction sets, comprised of a 50% MVC extension, 50% MVC flexion and a rest recording. To restrict bandwidth, the (full-band) whitened signal was lowpass filtered using a causal, 9th-order, Chebyshev Type I filter whose cutoff frequency was selectable. The cutoff frequencies investigated were: 30–200 Hz in increments of 10 Hz and 300–2000 Hz in increments of 100 Hz. After bandwidth restriction, each channel was first-order demodulated (i.e., absolute value) and the four channels were ensemble averaged.

The torque-varying contractions served as the low-intensity data set. For these data, each EMGσ signal was formed by decimating the ensemble average by a factor of 100 (effective lowpass filter prior to downsampling of 16.4 Hz, causal, 9th-order, ChebyshevType I) to a sampling rate of 40.96 Hz. Thetorque signal was similarly decimated to 40.96 Hz, yielding EMGσ (input) data with bandwidth approximately ten times that of the (output) torque signal [38]. Extension and flexion EMGσs were related to joint torque via the parametric model [29]:

$$T[m]=\sum_{d=1}^{D}\sum_{q=0}^{Q} e_{q,d}\sigma_E^d[m-q]+\sum_{d=1}^{D}\sum_{q=0}^{Q} f_{q,d}\sigma_F^d[m-q], \qquad (1)$$

where T is the decimated torque signal at samples m, σ_E is the extension EMGσ, σ_F is the flexion EMGσ, $e_{q,d}$ are extension fit coefficients and $f_{q,d}$ are flexion fit coefficients. Integer Q sets the number of signal lags. When integer D=1, the model is

linear. When integer D=2, a nonlinear dynamic model is facilitated. Model parameters were fit using the pseudo-inverse technique to regularize a least squares minimization [29], [39]. The tolerance (*Tol*) for removal of singular values was the ratio of the largest singular value to each other singular value in the design matrix. Based on a prior model optimization study utilizing non-causal processing [29], two optimal model forms (30th-order linear,*Tol*=0.0056; 15th-order nonlinear, *Tol*=0.01) were implemented. Models were calibrated (trained) from two of the torque-varying trials [29] and tested on the third trial per subject. This set of three trials utilized the same real-time feedback signal. The RMS error between the measured torque from the load cell and the EMG-estimated torque on the test trial from each subject was expressed as a fraction of twice the torque at 50% MVC flexion (MVC_F) of each subject. The first 2 s of signal were omitted from the RMS error computation to account for filter startup transients. Error was evaluated as a function of the whitening cutoff frequency, with full bandwidth results (2000 Hz) serving as the reference.

The second set of 50% MVCs served as the medium-intensity data set. Extension electrodes from extension contractions and flexion electrodes from flexion contractions were analyzed separately. Initial EMG processing for each *individual* channel, through the demodulation stage, was the same as above. After demodulation, EMGσ was formed for each individual channel by performing a moving average, using a 125 ms smoothing window. For constant-torque contractions, it is customary to compare performance via the EMG SNR [40]. Thus, the SNR of each EMGσ was computed as the sample mean divided by the sample standard deviation. The first 250 ms of the signal was ignored, to account for filter startup transients. The SNR values from the four channels on one muscle were averaged and this value reported. SNR was evaluated as a function of the whitening cutoff frequency. All statistical comparisons were between pairs of data values and were computed using the paired sign test [41].

III. Results

Fig. 2 shows sample EMG waveformsand their power spectral density estimates from both the low-intensity tracking trials and the medium-intensity 50% MVC trials, contrasting unwhitened vs. whitened processing. While the effects of whitening can be subtle to visualize in the time domain (top plots) at this time-scale, the spectra (bottom plots) of the whitened signals are clearly flatter, as desired. Note that the spectra of the tracking trial exhibit noticeabledownward spikes due to power-line notch filtering.Fig. 3 shows typical processed time-series plots—torque estimates for a low-intensity tracking trial and EMGσ estimates for a medium-intensity 50% MVC trial. The plots contrast full whitening bandwidth (cutoff frequency of 2000 Hz) vs.greatly restricted whitening bandwidth (cutoff frequency of 100 Hz).As would be expected, poorer performance was found at the greatly restricted whitening bandwidth.

Fig.4shows μ±σ error results from 54 subjects vs. the whitening cutoff frequency for the two parametric models (linear and nonlinear), corresponding to the low-intensity contractions.Lower errors correspond to superior performance. For both models, the error remained essentially flat for cutoff frequencies extending from 2000 Hz down to ~400–500 Hz. The error rose slowly thereafter as the cutoff frequency was reduced towards zero, until a rapid rise occurred for frequencies below approximately 50 Hz. For the linear model, the minimum error of 6.05 ± 2.24% MVC_Foccurred at a cutoff frequency of 700Hz, but this error did not differ significantly from the error at the maximum cutoff frequency of 2000 Hz (p=0.77).More importantly, however, was to test when error results first significantly departed from the minimum error at the 700 Hz cutoff frequency. Thus, we applied a *backward progressive* paired sign test. Our backward progressive technique began with a paired sign test using data from the cutoff frequency of the error minimum and one backward frequency increment (i.e., 700 Hz and 600 Hz). If this result was non-significant (p>0.01), we widened the frequency span backward to 700 Hz and 500 Hz and recomputed the paired sign test. The frequency span was progressively increased until a significant difference (p<0.01) was achieved. That corresponding cutoff frequency indicated when the increasing error became statistically significant. This statistically significant change occurred at 400 Hz. For the nonlinear model, the minimum error of 5.39 ± 2.20% MVC_Foccurred at a cutoff frequency of 900 Hz, but this error did not differ significantly from the error at the maximum cutoff frequency of 2000 Hz (p=0.93). A backward progressive paired sign test found that the error first significantly deviated from the location of the minimum error (900 Hz) at a cutoff frequency of 500 Hz. Lastly, we contrasted the linear vs. nonlinear model performances, pairing data from the minimum error location of each, respectively. The nonlinear model had a statistically significant lower error (p<10^{-4}). Note that these lowest average error values, as well as the relative errors found when contrasting the linear to nonlinear models, are consistent with past analysis ofa subset of these data [29].

Fig. 5shows μ±σ SNR results from 54 subjects vs. the whitening cutoff frequency for the 50% MVC constant-torque contractions, corresponding to the medium-intensity contractions. Higher SNRs correspond to superior performance.For both models, the error remained somewhat flat for cutoff frequencies extending from 2000 Hz down to ~800–900 Hz. The SNR decayed progressively thereafter as the cutoff frequency was reduced towards zero. For extension contractions, the maximum SNR of 14.74 ± 2.75 occurred at a cutoff frequency of 1100 Hz, but this error did not differ significantly from the error at 2000 Hz (p=0.25). A backward progressive paired sign test found that the error first significantly deviated from the location of the maximum SNR (1100 Hz) at a cutoff frequency of 800 Hz. For flexion contractions, the maximum SNR of 14.81 ± 4.98 occurred at a cutoff frequency of 1300 Hz, but this error did not differ significantly from the error at 2000 Hz (p=0.34). A backward progressive paired sign test found that the error first significantly deviated from the location of the maximum SNR (1300 Hz) at a cutoff frequency of 900 Hz. Lastly, we contrasted the extension vs. flexion performances, pairing data from the maximum SNR location of each, respectively. The

results did not differ (p=0.55).Note that these highest average SNR results are consistent with past results in the literature [8].

IV. Discussion

Signal whitening has been used in *laboratory settings*to reduce the variability of parameters extracted from the EMG signal since at least the work of Kaiser and Petersen in 1974 [1]. Their work implemented a form of adaptive whitening (based on effort level) in an analog filter. Harba and Lynn [4] implemented whitening off-line in software;continuing advances have been reported in the literature over the intervening years(see [40], [42] for reviews). Unfortunately, few of these advances seem to have transitioned far outside of those research groups who have developed the techniques, and none have seemed to transition to commercial devices. One issue has been the historically limited amount of computation performed onmicroprocessor-controlled commercial devices in prosthetics, orthotics and related areas [43], [44], although manufacturer experience and increases in microprocessor performance over time are likely mitigating this issue. Another issue is the complexity of whitening algorithms, particularly time-adaptive processing to attenuate noise [31]. To combat the challenge in algorithm complexity, Potvin and Brown [27] implemented whitening with a fixed, low-order FIR highpass filter. Of interest, their system sampled EMG at 1024 Hz, hence whitening only occurred out to a frequency of 512 Hz (the Nyquist frequency). Their implementation was inherently bandwidth limited.

The issue investigated in this paper was that of the bandwidth (maximum frequency) required when whitening. Wide bandwidths, out to 1000–2000 Hz have been successfully implemented in the laboratory [1], [31]. But, these wide bandwidths can require the development of custom wideband electrodes and necessitate more powerful microprocessors—factors which can impede the transition of whitening into real-time commercial devices. The literature suggested that the primary advantage of the wider bandwidths is at high contraction levels; such levels have been commonly tested in laboratory studies. However, most routine tasks and most applications of EMG processing primarily utilize the low range of muscle contraction force.

Our results in this study from the low-level contractions (Fig. 4) suggest that conventional electrodes with passbandsout to 400–500 Hz and an inter-electrode spacing of 10 mm edge-to-edge capture *all* of the relevant EMG-torque information in our data, at least if EMGσ is the parameter of interest.This electrode passband and spacing is consistent with many common commercial electrode systems. Joint torque estimation is a common usage of EMG/EMGσ. We found that a cutoff frequency as low as 400–500 Hz was the first to exhibit torque estimation errors that were significantly different from that of the full-band signal (at least as defined using a significance level of p<0.01). Although we termed our torque-varying contractions as "low-level," they span 50% MVC extension to 50% MVC flexion, with approximately equal use of each contraction level in between (uniform distribution). The average instantaneous contraction level was 18.5%MVC_F. Hence, these contractions are representative of a wide class of daily muscle usages and, thus, EMG applications.

To contrast these results, we compared to medium-level,static 50% MVC contractions (Fig. 5). Since these contractions were constant-torque and non-fatiguing, SNR was used as the performance measure. This measure assumes that EMGσ is unchanging during the trial, but takes advantage of not having to assume/estimate a relationship between EMGσ and joint torque. At this higher contraction level, somewhat wider bandwidth proved advantageous, out to approximately 800–900 Hz. SNRs at cutoff frequencies of 800–900 Hz were first to differ statistically from the highest SNRs. This result is consistent with the data shown in Fig. 1 in which recorded EMG is closely represented as the sum of an amplitude modulated "true" EMG (i.e., noise-free) and background noise. As the EMG signal strength is increased, the frequency region over which there exists more signal than noise also increases. These regions can be successfully whitened. Many commercial electrodes systems may not facilitate this full bandwidth, thus reducing (but not eliminating) the improvement due to whitening. Of course, when the EMG signal is *not* whitened, this wider bandwidth is not necessary.

Hence, the required bandwidth for whitening seems largely related to the noise power relative to the true EMG power, as a function of frequency. Logically, increased bandwidth could be utilized if noise power can be reduced. However, noise power due to the acquisition electronics is typically only a few μVs RMS [45] or about 1% of the RMS level at MVC [31]. Additional noise sources, including electrode-skin interface noise, only increase the total RMS noise to approximately 3% of the RMS level at MVC [31]. Hence, large reductions in noise are unlikely, at least for conventional surface EMG with standard skin site preparation.

Our inter-electrode spacing of 10 mm edge-to-edge is typical of many commercial electrodes. However, smaller electrode spacing leads to increased statistical bandwidth of the acquired EMG signal [3], which might then permit whitening out to higher frequencies.Additionally, other factors can influence the bandwidth of the EMG signal. For example, localized muscle fatigue tends to compress the spectrum towards lower frequencies [46]. The resulting reduced bandwidth would likely reduce the range over which whitening should be applied. Finally, other contraction profiles/dynamicsmight also influence the average contraction level or the EMG spectrum [47]—each of which influences the whitening bandwidth.

Although we contrasted results from two different contraction levels, the actual comparison measure varied (EMG-torque error and SNR). However, each measure is applicable to the contraction type studied. For constant-torque contractions, use of the SNR avoids the need for a model relating EMGσ to torque. Since torque was largely held constant during these contractions (no dynamics or even any change in torque level occurred), a model serves little purpose other than to set a system gain. SNR is gain invariant, thereby avoiding the issue altogether. For dynamic (torque-varying) trials, a dynamic EMGσ-torque model is required. In either case, we studied *relative* changes in performance, which should be

more robust to variations in the performance measure. Other factors that might influence the interpretation of these results include the use of alternative electrode shapes and inter-electrode distances, and the extraction of other features from the EMG signal (e.g., zero crossing rate and average signal length).In particular, whitening has been shown to reduce classification errors by 25–50% in myoelectric multifunction selection when utilizing EMGσ, zero crossing rate and average signal length [4], [11], but the role of whitening bandwidth was not investigated. Since most EMG-based multifunction classification utilizes lower-effort contractions, we would hypothesize that the bandwidth requirement of 400–500 Hz provided by our lower-level contractions would be applicable. However, direct evaluation of this hypothesis in the future seems appropriate.

In this off-line study, we limited whitening bandwidth via the use of a lowpass filter inserted after EMG had been whitened to the full Nyquist frequency (2048 Hz). This method was convenient for off-line study of performance vs. whitening bandwidth, but would clearly be inefficient in a real-time system. In practice, anti-aliasing lowpass filters would be applied at the desired whitening cutoff frequency and the signal appropriately sampled at a rate that is a least twice this frequency.Presumably, this rate is well below the rate of 4096 Hz used in this study. Whitening would then be performed in its normal manner, over the full Nyquist frequency, without further bandwidth restriction.

Another advantage of reduced-bandwidth whitening is related to power line interference. At high frequencies (e.g., above 500 Hz), power line interference can easily be larger in magnitude than the EMG signal power. Since whitening accentuates the higher frequency range via high gains, our own whitening algorithms now apply notch filters at the power line frequency and eachof its harmonics. For off-line analysis utilizing double precision floating-point arithmetic, very sharp filters are readily achieved. However, many real-time applications are limited to fixed-point arithmetic, in which such narrow notch filters present a challenge. Reduced-bandwidth whitening may eliminate this problem altogether by simply avoiding these troublesome frequency bands.

In summary, we concludethat the torque-varying contractions studied in these experiments only require a frequency bandwidth of 400–500 Hz when whitening is applied, at least when EMGσ-torque is studied. These contractions uniformly occupied the torque range from 50% MVC extension to 50% MVC flexion (average instantaneous contraction level of 18.5% MVC_F)—thus they include contraction levels at or above typical muscular exertions. Medium-level contractions (e.g., constant-torque 50% MVC contractions) benefit from a bandwidth out to approximately 800–900 Hz. Contractions at even higher levels would presumably benefit from an even wider frequency band.

REFERENCES

[1] E. Kaiser and I. Petersen, "Adaptive filter for EMG control signals," in *The Control of Upper-Extremity Prosthesis and Orthoses*, 1974, pp. 54–57.

[2] N. Hogan and R. W. Mann, "Myoelectric signal processing: Optimal estimation applied to electromyography—Part I," *IEEE Trans. Biomed. Eng.*, vol. 27, pp. 382–395, 1980.

[3] N. Hogan and R. W. Mann, "Myoelectric signal processing: Optimal estimation applied to electromyography—Part II," *IEEE Trans. Biomed. Eng.*, vol. 27, pp. 396–410, 1980.

[4] M. I. A. Harba and P. A. Lynn, "Optimizing the acquisition and processing of surface electromyographic signals," *J. Biomed. Eng.*, vol. 3, pp. 100–106, 1981.

[5] T. D'Alessio, "Some results on the optimization of a digital processor for surface EMG signals," *Electromyogr. Clin. Neurophysiol.*, vol. 24, pp. 625–643, 1984.

[6] G. C. Filligoi and P. Mandarini, "Some theoretic results on a digital EMG signal processor," *IEEE Trans. Biomed. Eng.*, vol. 31, pp. 333–341, 1984.

[7] Y. T. Zhang, P. A. Parker and R. N. Scott, "Study of the effects of motor unit recruitment and firing statistics on the signal-to-noise ratio of a myoelectric control channel," *Med. Biol. Eng. Comput.*, vol. 28, pp. 225–231, 1990.

[8] E. A. Clancy and N. Hogan, "Single site electromyograph amplitude estimation," *IEEE Trans. Biomed. Eng.*, vol. 41, pp. 159–167, 1994.

[9] E. A. Clancy and N. Hogan, "Multiple site electromyograph amplitude estimation," *IEEE Trans. Biomed. Eng.*, vol. 42, pp. 203–211, 1995.

[10] D. Farina and R. Merletti, "Comparison of algorithms for estimation of EMG variables during voluntary isometric contractions," *J. Electromyogr. Kinesiol.*, vol. 10, pp. 337–349, 2000.

[11] L. Liu, P. Liu, E. A. Clancy, E. Scheme and K. B. Englehart, "Electromyogram Whitening for Improved Classification Accuracy in Upper Limb Prosthesis Control," *IEEE Trans. Biomed. Eng.*, in press.

[12] P. Parker, K. Englehart, and B. Hudgins, "Myoelectric signal processing for control of powered limb prostheses," *J. Electromyogr. Kinesiol.*, vol. 16, pp. 541–548, 2006.

[13] S. Kumar and A. Mital, Eds., *Electromyography in Ergonomics*. Briston, PA: Taylor & Francis, 1996.

[14] G. M. Hagg, B. Melin, and R. Kadefors, "Applications in Ergonomics," in *Electromyography: Physiology, Engineering, and Noninvasive Applications*, R. Meletti and P. A. Parker, Eds. Hoboken, NJ: Wiley, 2004, pp. 343–363.

[15] M. G. Benedetti, P. Bonato, F. Catani, T. D'Alessio, M. Knaflitz, M. Marcacci and L. Simoncini, "Myoelectric activation pattern during gait in total knee replacement: Relationship with kinematics, kinetics, and clinical outcome," *IEEE Trans. Rehab. Eng.*, vol. 7, pp. 140–149, 1999.

[16] C. Disselhorst-Klug, T. Schmitz-Rode, and G. Rau, "Surface electromyography and muscle force: Limits in sEMG-force relationship and new approaches for applications," *Clin. Biomech.*, vol. 24, pp. 225–235, 2009.

[17] D. J. Ostry and A. G. Feldman, "A critical evaluation of the force control hypothesis in motor control," *Exp. Brain Res.*, vol. 153, pp. 275–288, 2003.

[18] J. Rosen, M. Brand, M. B. Fuchs, and M. Arcan, "A myosignal-based powered exoskeleton system," *IEEE Trans. Syst., Man, Cybern. A, Syst. Humans*, vol. 31, pp. 210–222, 2001.

[19] K. Kiguchi, T. Tanaka and T. Fukuda, "Neuro-fuzzy control of a robotic exoskeleton with EMG signals," *IEEE Trans. Fuzzy Sys.*, vol. 12, pp. 481–490, 2004.

[20] A. M. Dollar and H. Herr, "Lower extremity exoskeletons and active orthoses: Challenges and state-of-the-art," *IEEE Trans. Robotics*, vol. 24, pp. 144–158, 2008.

[21] Z. O. Khokhar, Z. G. Xiao, and C. Menon, "Surface EMG pattern recognition for real-time control of a wrist exoskeleton," *Biomed. Eng. OnLine*, vol. 9, p. 41, 2010.

[22] T. Lenzi, S. M. M. De Rossi, N. Vitiello and M. C. Carrozza, "Intention-based EMG control for powered exoskeletons," *IEEE Trans. Biomed. Eng.*, vol. 59, pp. 2180–2190, 2012.

[23] L. Lucas, M. DiCicco and Y. Matsuoka, "An EMG-controlled hand exoskeleton for natural pinching," *J. Robotics Mech.*, vol. 16, no. 5, 2004.

[24] L. Dipietro, M. Ferraro, J. J. Palazzolo, H. I. Krebs, B. T. Volpe and N. Hogan, "Customized interactive robotic treatment for stroke: EMG-triggered therapy," *IEEE Trans. Neural Sys. Rehab. Eng.*, vol. 13, pp. 325–334, 2005.

[25] J. Stein, K. Narendran, M. Kailas, J. McBean, K. Krebs and R. Hughes, "Electromyography-controlled exoskeletal upper-limb-powered orthosis for exercise training after stroke," *Am. J. Phys. Med. Rehab.*, vol. 86, pp. 255–261, 2007.

[26] E. A. Clancy and N. Hogan, "Relating agonist-antagonist electromyograms to joint torque during isometric, quasi-isotonic,

non-fatiguing contractions," *IEEE Trans. Biomed. Eng.*, vol. 44, pp. 1024–1028, 1997.
[27] J. R. Potvin and S. H. M. Brown, "Less is more: High pass filtering, to remove up to 99% of the surface EMG signal power, improves EMG-based biceps brachii muscle force estimates," *J. Electromyogr. Kinesiol.*, vol. 14, pp. 389–399, 2004.
[28] D. Staudenmann, J. R. Potvin, I. Kingma, D. F. Stegeman and J. H. van Dieen, "Effects of EMG processing on biomechanical models of muscle joint systems: Sensitivity of trunk muscle moments, spinal forces, and stability," *J. Biomech.*, vol. 40, pp. 900–909, 2007.
[29] E. A. Clancy, L. Liu, P. Liu and D.V. Z. Moyer, "Identification of constant-posture EMG-torque relationship about the elbow using nonlinear dynamic models," *IEEE Trans. Biomed. Eng.*, vol. 59, pp. 205-212, 2012.
[30] E. A. Clancy, O. Bida and D. Rancourt, "Influence of advanced electromyogram (EMG) amplitude processors on EMG-to-torque estimation during constant-posture, force-varying contractions," *J. Biomech.*, vol., 39, pp. 2690–2698, 2006.
[31] E. A. Clancy and K. A. Farry, "Adaptive whitening of the electromyogram to improve amplitude estimation," *IEEE Trans. Biomed. Eng.*, vol. 47, pp. 709–719, 2000.
[32] P. Prakash, C. A. Salini, J. A. Tranquilli, D. R. Brown and E. A. Clancy, "Adaptive whitening in electromyogram amplitude estimation for epoch-based applications," *IEEE Trans. Biomed. Eng.*, vol. 52, pp. 331–334, 2005.
[33] D. S. Jevsevar, P. O. Riley, W. A. Hodge and D. E. Krebs, "Knee kinematics and kinetics during locomotor activities of daily living in subjects with knee arthroplasty and in healthy control subjects," *Phys. Ther.*, vol. 73, 229–242, 1993.
[34] J. L. B. Garza et al., "Observed differences in upper extremity forces, muscle efforts, postures, velocities and accelerations across computer activities in a field study of office workers," *Ergonomics*, vol. 55, pp. 670–681, 2012.
[35] M. Dasog, K. Koirala, P. Liu and E. A. Clancy, "EMG bandwidth used in signal whitening," in *39th Ann. Northeast Bioeng. Conf.*, Syracuse, NY, Apr. 5–7, 2013, pp. 189–190.
[36] E. A. Clancy, "Electromyogram amplitude estimation with adaptive smoothing window length," *IEEE Trans. Biomed. Eng.*, vol. 46, pp. 717–729, 1999.
[37] E. A. Clancy. (2010 Aug.). *EMG Amplitude Estimation Toolbox:User's Guide*. Alpha version 0.07, 2010 [Online]. Available: http://www.wpi.edu/~ted/emg_tool.htm.
[38] L. Ljung, *System Identification: Theory for the User*. Upper Saddle River, NJ: Prentice-Hall, 1999, pp. 491–519.
[39] W. H. Press, S. A. Teukolsky, W. T. Vetterling, and B. P. Flannery, *Numerical Recipes in C*, 2nd ed. New York: Cambridge Univ. Press, 1994, pp. 671–681.
[40] E. A. Clancy, E. L. Morin and R. Merletti, "Sampling, Noise-Reduction and Amplitude Estimation Issues in Surface Electromyography," *J. Electromyogr. Kinesiol.*, vol. 12, pp. 1–16, 2002.
[41] I. Miller and J. E. Freund, *Probability and Statistics for Engineers*. Englewood Cliffs, NJ: Prentice-Hall, 1977, pp. 272–275.
[42] D. Staudenmann, K. Roeleveld, D. F. Stegeman and J. H. van Dieen, "Methodological aspects of SEMG recordings for force estimation—A tutorial review," *J. Electromyo. Kinesiol.*, vol. 20, pp. 375–387, 2010.
[43] C. Lake and J. M. Miguelez, "Evolution of microprocessor based control systems in upper extremity prosthetics," *Tech. Disabil.*, vol. 15, pp. 63–71, 2003.
[44] D. Berry, "Microprocessor prosthetic knees," *Phys. Med. Rehabil. Clin. N. Am.*, vol. 17, pp. 91–113, 2006.
[45] A. C. Metting van Rijn, A. Peper and C. A. Grimbergen, "High-quality recording of bioelectric events; Part 2: Low-noise, low-power multichannel amplifier design," *Med. Biol. Eng. Comput.*, vol. 29, pp. 433–440, 1991.
[46] D. B. Chaffin, "Localized muscle fatigue—definition and measurement," *J. Occ. Med.*, vol. 15, pp. 346–354, 1973.
[47] D. Farina, R. Merletti and R. M. Enoka, "The extraction of neural strategies from the surface EMG," *J. Appl. Physiol,* vol. 96, pp. 1486–1495, 2004.

MeeraDasogreceived her B.E. (Bachelor of Engineering) degree in Electrical and Instrumentation Engineering from B.V.B. College of Engineering, Hubli, India, and M.S. degree from Worcester Polytechnic Institute (WPI), Worcester, MA, in Electrical and Computer Engineering.
She has worked briefly in the semiconductor industry which involved verification and modeling of various analog integrated circuits. Her areas of interests include signal processing, biomedical instrumentation and integrated mixed signal circuit design.

KishorKoiralareceived his B.S. degree in Electronics and Communication Engineering from Pokhara University, Nepal, M.B.A. in Finance from University of Findlay, Findlay, Ohio and M.S. degree in Electrical and Computer Engineering from Worcester Polytechnic Institute, Worcester, MA.
He is currently employed with Aware Inc, Bedford, MA. His research interests include bio-electrical signal processing, machine learning and digital audio processing.

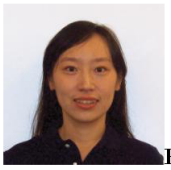

Pu Liureceived the B.S. degree from Fudan University, Shanghai, China and the M.S. degree from Worcester Polytechnic Institute (WPI), Worcester, MA, both in Electrical Engineering.
She is currently working toward the Ph.D. degree from the Department of Electrical and Computer Engineering, WPI. Her research interests include signal processing, modeling and instrumentation, principally as applied to biomedical engineering.

Edward (Ted) A. Clancy (S'83–M'91–SM'98) received the B.S. degree from Worcester Polytechnic Institute (WPI), and the S.M. and Ph.D. degrees from Massachusetts Institute of Technology (MIT), all in Electrical Engineering.

He has worked in industry for medical instrumentation and analysis companies interested in EMG, EEG, ECG and blood pressure, and the defense industry (aircraft instruments and radar). He is Associate Professor of Electrical and Computer Engineering, and of Biomedical Engineering at WPI. He is interested in signal processing, stochastic estimation and system identification, particularly as applied to problems in medical engineering and human rehabilitation.

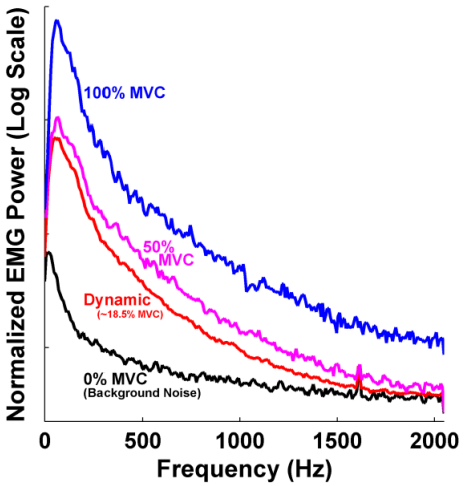

Fig. 1. Power spectra of EMG demonstrating amplitude modulated behavior. All spectra are from constant-posture contractions (see Methods). Top two plots show EMG power spectra at different maximum voluntary contraction (MVC) levels (100% and 50%) during constant-torque contractions.Plot labeled "Dynamic" is from force-varying contractions that averaged 18.5% MVC. Bottom plot is EMG during rest, representing the background noise level. All spectra computed using Welch's method. Subject LB09.

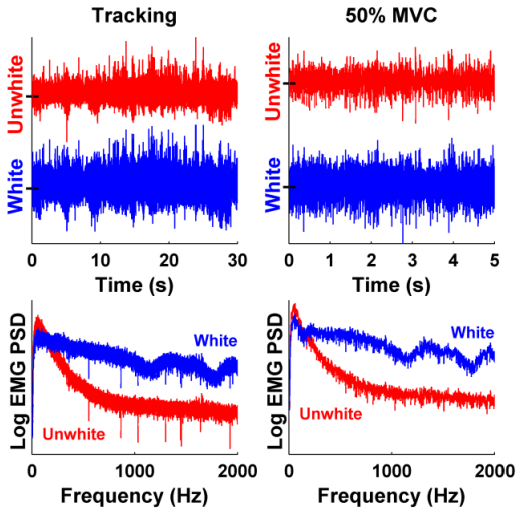

Fig. 2.EMG signals and their spectra, contrasting unwhitened vs. whitened processing. Top left shows unwhite and corresponding whitened EMG signal during a 30 s tracking trial, superimposed on the same axis. Bottom left shows their spectra, each normalized to their respective total signal power. Plots at right show equivalent data from a 5-s duration 50% MVC trial. All spectra computed using Welch's method. Single-channel biceps EMG data from subject LA05.

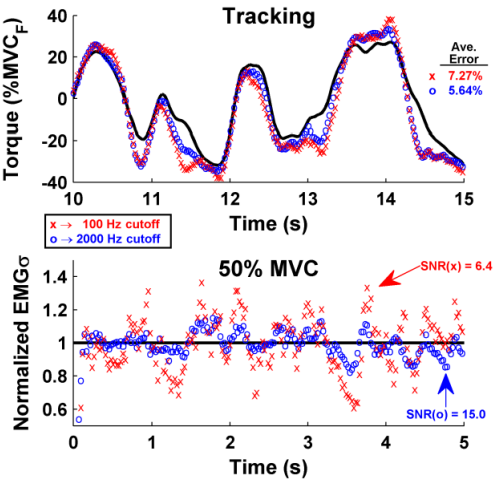

Fig. 3.Typical (low-intensity) torque tracking and (medium-intensity) EMGσ estimates at full bandwidth (2000 Hz cutoff) and restricted bandwidth (100 Hz cutoff). Top shows 10-s portion of the torque estimates from one trial, along with the actual torque (solid line). Trial errors in %MVC$_F$ are listed. Bottom shows normalized EMGσ estimates, along with the ideal EMGσ(solid line). SNRs are listed. Note the EMGσ startup transient during the first 250 ms. Subject wx11 (single-channel biceps data used for 50% MVCs).

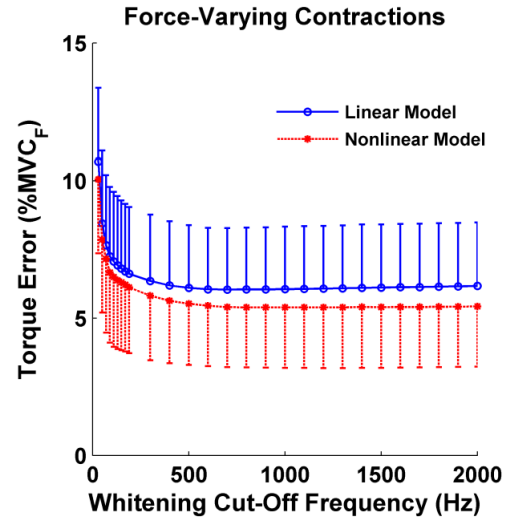

Fig. 4. Low-intensity torque-varying contraction results. Average plus (or minus) one standard deviation error (expressed in percent maximum voluntary flexion contraction—%MVC$_F$) from 54 subjects vs. the whitening cutoff frequency for the linear and non-linear models, each using four EMG channels. Lower error corresponds to better performance.

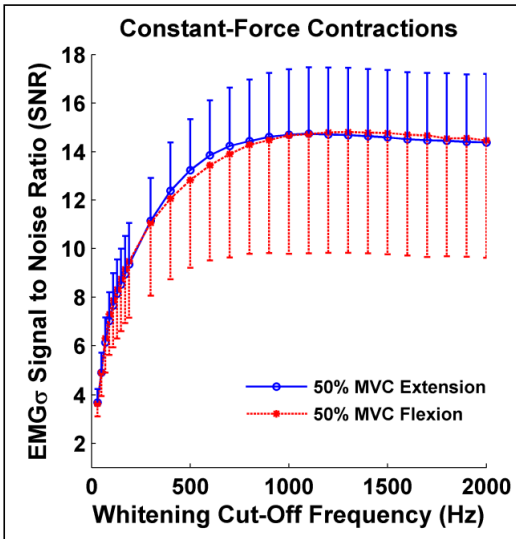

Fig. 5. Medium-intensity contraction results. Average plus (or minus) one standard deviation signal to noise ratio (SNR) from 54 subjects vs. the whitening cutoff frequency for the extension and flexion 50% maximum voluntary contractions. All results are single-channel EMG. Higher SNR corresponds to better performance.

CHAPTER 16

Copy of submitted journal paper:

Kishor Koirala, Meera Dasog, Pu Liu, and Edward A. Clancy. “Using the Electromyogram to Anticipate Torques About the Elbow.” In review.

Using the Electromyogram to Anticipate Torques About the Elbow

Kishor Koirala, Meera Dasog, Pu Liu, and Edward A. Clancy, *Senior Member, IEEE*

***Abstract*—Processed (i.e., rectified, smoothed) electromyogram (EMG) activity from skeletal muscles precedes mechanical tension by 50–100 ms. This property can be exploited to anticipate muscle mechanical activity. Thus, we investigated the ability of surface EMG to estimate joint torque at future times, up to 750 ms. EMG recorded from the biceps and triceps muscles of 54 subjects during constant-posture, force-varying contractions was related to elbow torque. Higher-order FIR models, combined with advanced EMG processing (whitening; four EMG channels per muscle), provided a nearly identical minimum error of 5.48 ± 2.21% MVC_F (flexion maximum voluntary contraction) over the time advance range of 0–60 ms. Error grew for larger time advances. The more common method of filtering EMG amplitude with a Butterworth filter (2nd-order, 1.5 Hz cutoff frequency) produced a statistically inferior ($p<10^{-6}$) minimum torque error of 6.90 ± 2.39% MVC_F, with an error nadir at a time advance of 60 ms. Error was progressively poorer at all other time advances. Lower-order FIR models mimicked the poorer performance of the Butterworth models. The more advanced models provide lower estimation error, require no selection of an electromechanical delay term and maintain their lowest error over a substantial range of advance times.**

***Index Terms*—Biological system modeling, biomedical signal processing, electromyography, EMG amplitude estimation, EMG signal processing, EMG-force.**

I. Introduction

It has long been known that electromyogram (EMG) activity from skeletal muscles precedes the associated mechanical activity [1]. This electromechanical delay may vary with the condition, but is typically measured as a pure delay between peak surface EMG amplitude (e.g., rectified, smoothed EMG) and peak mechanical activity of approximately 50–100 ms [1]–[3]. In many biomechanical models that relate EMG to force/joint torque, it is common to include a model term that accounts for this pure delay [4] [7]. Such models can also account additionally for frequency-dependent delay via a dynamical system model.

A related use of electromechanical delay is to predict muscle forces/joint torques at future times from EMG. Applications that do, or could, benefit from this property include: anticipating head motion in virtual environments to reduce scene vs. sensory alignment errors [8], optimizing controller delay in myoelectric prostheses [9], user control of exoskeleton suits [10]–[12] and the actuation of rehabilitation devices from impaired limbs [13]–[18]. In many of these cases, estimating forces 50–100 ms into the future permits better temporal matching of user motor intent in the presence of computational delays and inherent delays within mechanical actuators.

Since numerous applications might benefit from "anticipatory" EMG-torque estimates, we performed a systematic evaluation of the errors associated with doing so over a broad range of times. No such detailed analysis had been previously identified in the literature. In addition, more advanced EMG-torque models can now incorporate multiple EMG channels per muscle, EMG signal whitening, as well as advanced model identification that is subject-specific [7], [19]–[22]. These techniques have been shown to reduce EMG-torque errors and might influence the realization of electromechanical delay within EMG-torque models. Thus, we have investigated the performance of these advanced EMG-torque algorithms when estimating as much as 750 ms into the future. Preliminary results of this work were presented in [23].

Asterisk indicates corresponding author.

K. Koirala, M. Dasog, P. Liu and *E. A. Clancy are with Worcester Polytechnic Institute (WPI), Worcester, MA 01609 USA (e-mail: kkoirala@wpi.edu; mgdasog@wpi.edu; puliu@wpi.edu; ted@wpi.edu).

II. Methods

A. Experimental Data and Methods

Experimental data from 54 subjects (30 male, 24 female; aged 37.6 ± 16.5 years) from three prior experimental studies were utilized. This reanalysis study was approved and supervised by the WPI IRB. All subjects had previously provided written informed consent. The three studies had nearly identical experimental apparatus and protocols with respect to the data reanalyzed (fully described in [19], [24]). As shown in Fig. 1, subjects were seated and secured with their shoulder abducted 90°, forearm oriented in a parasaggital plane, wrist fully supinated and elbow flexed 90°. Their right wrist was rigidly cuffed to a load cell (Biodex dynamometer; or Vishay Tedea-Huntleigh Model 1042, 75 kg capacity) at the styloid process. Skin above the muscles under investigation was scrubbed with an alcohol wipe. In one study, a small bead of electrode gel was also massaged into the skin. Four bipolar electrode-amplifiers were placed transversely across each of the biceps and triceps muscles, midway between the elbow and the midpoint of the upper arm, centered on the muscle midline. Each electrode-amplifier had a pair of 4-mm (or 8-mm) diameter, stainless steel, hemispherical contacts separated by 10 mm (edge to edge), oriented along the muscle's long axis. The distance between adjacent electrode-amplifiers was ~1.75

cm. A single ground electrode was gelled and secured above the acromion process or on the upper arm. Custom electronics amplified each EMG signal (CMRR of approximately 90 dB at 60 Hz) followed by bandpass filtering (either a 2nd-order, 10–2000 Hz bandpass filter; or 8th-order highpass at 15 Hz followed by a 4th-order lowpass at 1800 Hz). All signals were sampled at 4096 Hz with 16-bit resolution.

After a warm-up period, maximum voluntary contraction (MVC) torque was measured in both elbow extension and flexion. Subjects began at rest, then increased contraction gradually over 2–3 s until their maximum was achieved. Verbal encouragement was provided while the maximum was maintained for 2–3 s. The average of the maximum strain gauge voltage level from two such MVC trials was used as the voltage corresponding to MVC. Next, five-second duration, constant-posture constant-force contractions at 50% MVC extension, 50% MVC flexion and rest were recorded for calibration of advanced EMG amplitude (EMGσ) estimation algorithms [19], [25]. Then, a real-time feedback signal consisting of either the load cell voltage or a four-channel whitened EMGσ processor (formed by subtracting the extensor EMGσ from the flexor EMGσ) was provided on a computer screen. Thirty-second duration, constant-posture force-varying contraction trials were then recorded. The subjects used the feedback signal to track a computer-generated target that moved on the screen in the pattern of a band-limited (1 Hz) uniform random process, spanning 50% MVC extension to 50% MVC flexion. Three trials were collected. At least three minutes of rest was provided between contractions to prevent cumulative fatigue.

B. Methods of Analysis

All analysis was performed offline in MATLAB. Two distinct EMGσ processors were used: single-channel unwhitened (using a centrally located electrode) and four-channel whitened [19], [25], [26]. Each processor used a 15 Hz highpass filter (causal, 5th-order, Butterworth filter), notch filters at the power-line and each harmonic frequency (2nd-order IIR filter, notch bandwidth ≤ 1.5 Hz), and first-order (i.e., absolute value) demodulation. The four-channel processor whitened each channel prior to demodulation (causal algorithm of Clancy and colleagues [19], [25], [26]) and then averaged the four channels after demodulation. Finally, the EMGσ signal was formed by decimating this signal by a factor of 100 to a sampling rate of 40.96 Hz. To do so, the signal was decimated twice by a factor of ten (effective lowpass filter prior to downsampling of 16.4 Hz, causal, 9th-order, Chebyshev Type I). The torque signal was similarly decimated, yielding an EMG (input) data set with bandwidth approximately ten times that of the torque signal (output) being estimated [27]. Note that additional lowpass filtering of EMGσ (typically below 1–2 Hz, see Fig. 7 for an example) is implicitly accomplished by the parametric modeling that relates EMGσ to joint torque (described subsequently), with the cutoff frequency optimized to each subject.

Initially, extension and flexion EMGσs were related to joint torque via the parametric model [21]:

$$T[m+i]=\sum_{d=1}^{D}\sum_{q=0}^{Q} e_{q,d}\,\sigma_E^d[m-q]+\sum_{d=1}^{D}\sum_{q=0}^{Q} f_{q,d}\,\sigma_F^d[m-q] \quad (1)$$

where T is the decimated torque signal, m is the current sample, i is the future time advance in samples, σ_E is the extension EMGσ, σ_F is the flexion EMGσ, $e_{q,d}$ are extension fit coefficients and $f_{q,d}$ are flexion fit coefficients. Integer Q sets the number of signal lags. When integer D=1, the model is linear. When integer D=2, a nonlinear dynamic model is facilitated. Model parameters were fit using the pseudo-inverse technique to regularize a least squares minimization [21], [28]. The tolerance (*Tol*) for removal of singular values was the ratio of the largest singular value to each singular value in the design matrix. Based on a prior model optimization study utilizing non-causal processing [21], two optimal model forms (30th-order linear, 15th-order nonlinear) were selected for both EMG processors, with the *Tol* for each as listed in Table 1.

In addition to these optimal models, two groups of other models were examined for comparison. First, many investigators cascade a fixed low-order Butterworth filter after each of the extension and flexion EMGσ signals, setting their difference as the estimated torque. Thus, we utilized 2nd-order Butterworth filters, one for the extension EMG and one for the flexion EMG, with cut-off frequencies at 1.5 Hz. The gains of both filters, representing the fit coefficients for the Butterworth model, were simultaneously calibrated for each subject in the training stage via least squares. These gains were fit separately for each time advance. Both EMG processors were investigated. Second, our linear FIR models, specified in (1), use a large number of lag values compared to what might be commonly found in the literature. Thus, we also investigated the linear model form with lag values of: Q=3, 5, 7, 9, 12 and 15. Only the four-channel whitened processor was investigated. The pseudo-inverse tolerance was 0.0056 for all lag values.

All models estimated torque for 151 future time advances between 0 and 750 ms, at an increment of 5 ms. Models were calibrated (trained) from two of the trials [21] and tested on the third trial per subject. This set of three trials utilized the same real-time feedback signal. The RMS error between the measured torque from the load cell and the EMG-estimated torque on the test trial from each subject was expressed as a fraction of twice the torque at 50% MVC flexion (MVC_F) of each subject. The first 2 s of signal were omitted from the RMS error computation to account for filter startup transients. Mean and standard deviation (μ±σ) errors from the 54 subjects are reported. Statistical comparisons utilized ANOVA when comparing across time advances *within* a particular combination of model and EMG processor. Pair-wise comparison *between* distinct models or EMG processors was performed at the best time advance and utilized paired sign tests [29], each utilizing all 54 subjects.

III. Results

Fig. 2 shows μ±σ error results from 54 subjects vs. future time advance for the two optimal-order (i.e., high-order) FIR models and the two EMG processors. The minimum average

error for each model-EMG processor combination, listed in Table 1, occurred at a time advance of 0 ms. At this optimal time advance, paired sign tests (54 subjects) showed that each model-EMG processor pair was significantly different than the other ($p<10^{-4}$). Thus, the nonlinear model using four channel whitened EMG processing exhibited the lowest error. ANOVAs applied separately to each of the four plots in Fig. 2 each showed a significant change in error vs. time advance over the full 750 ms (54 subjects x 151 advance times, $F(150, 8003)>68$, $p<10^{-6}$ for each). More importantly, however, was to test when error results first significantly departed from the minimum error at zero time advance. Thus, we applied a *forward progressive* ANOVA to the results of each plot condition. Our forward progressive technique began with an ANOVA using data from the time location of the error minimum and one forward time increment (i.e., 0 and 5 ms; 54 subjects x 2 advance times). If this result was non-significant ($p>0.05$), we increased the time range forward to include 0, 5 and 10 ms (54 subjects x 3 advance times) and recomputed the ANOVA. The time range was progressively increased until a significant difference ($p<0.05$) was achieved. That corresponding time advance indicated when the upward trend became statistically significant. For all four plots, the time advance for a statistically significant change was between 140–170 ms, with individual results shown in Table I.

Fig. 3 shows a sample time-series plot of the actual and EMG-estimated torque using the nonlinear model with four channel whitened EMG processing, at three distinct time advances. At time advances of 0 ms and 60 ms, both the shape and phase of the estimated torque closely match that of the actual torque, yielding a low RMS error. At a time advance of 400 ms, the general shape of the estimated torque matches that of the actual torque, but the estimated torque *lags* in phase. In addition, the estimated torque exhibits higher variance. Substantially higher RMS error results.

Fig. 4 shows $\mu\pm\sigma$ error results from the Butterworth models for both EMG processors. With single channel unwhitened EMG processing, the minimum error of $9.16 \pm 4.58\%$ MVC_F occurred at a time advance of 60 ms. This value did not differ significantly (ANOVA $F(1, 106)=1.9$, $p=0.30$) from the results at a time advance of 0 ms. A forward progressive ANOVA starting at the minimum error advance time (60 ms) showed that the upward trend became statistically significant at 160 ms. With four channel whitened EMG processing, the minimum error of $6.90 \pm 2.39\%$ MVC_F also occurred at a time advance of 60 ms. This value did differ significantly (ANOVA $F(1,106)=5.54$, $p=0.02$) from the results at a time advance of 0 ms. A forward progressive ANOVA starting at the minimum error advance time (60 ms) showed that the upward trend became statistically significant at 120 ms. The optimal error locations between Butterworth plots were compared using a paired sign test (54 subjects), and these values differed ($p<10^{-4}$). Finally, the best Butterworth model (four channel whitened EMG processor, 60 ms time advance) was compared to *i)* the best linear model (30th-order, four channel whitened EMG processor, 0 ms time advance) and, separately, *ii)* the best nonlinear model (15th-order, four channel whitened EMG processor, 0 ms time advance) using paired sign tests (54 subjects). Both comparisons were significant ($p<10^{-6}$), thus this best Butterworth model had inferior RMS error performance compared to each.

Fig. 5 shows sample time-series results (actual vs. EMG-estimated torque) using the Butterworth model with four channel whitened EMG processing, for the same time advances as Fig. 3. In all cases, the *shape* of the estimated torque matches that of the actual torque, but at a 0 ms time advance the estimated torque slightly *leads* in phase—this lead is subtle to observe, but consistent throughout the data—while at the 400 ms time advance, the estimated torque *lags* substantially in phase (and exhibits a decreased force range). The RMS error is lowest at the 60 ms time advance, which is properly phase aligned.

Fig. 6 shows mean error results from each of the lower-order linear FIR models using the four channel whitened EMG processor. Model orders 3 and 5 exhibit a substantial nadir in RMS error near 100 ms, whereas model orders above 9 demonstrate no noticeable dip in this error. Each of the low-order models achieves a minimum average error at an advance time above 0 ms, but that time approaches 0 ms as the order increases. Similarly, RMS error decreases as model order increases, although the error decrease slows with increasing order. (At order 30, the error is 6.24 ± 2.21, as shown in Table I and Fig. 2.) Fig. 6 lists the location and value of the minimum average error for each model order. Fig. 6 also lists the ANOVA *p*-value comparing the results at each order's minimum error location to the within-order results at a time advance of 0 ms (54 subjects x 2 advance times, for each order). For model orders 3 and 5, these differences were significant. Next for each adjacent model order pair, a paired sign test (54 subjects) was conducted at the respective location of the minimum error. All five paired comparisons were significant ($p<10^{-6}$). Time-series torque plots for model orders 3 and 5 (not shown) exhibited phase trends similar to the Butterworth models—the estimated phase slightly led at 0 ms, was appropriate at the time advance corresponding to the lowest average error and lagged at 400 ms.

The linear EMGσ-torque models whose results are shown in Fig. 6 can be split into a linear FIR flexion model and a linear FIR extension model, as described in (1). Fig. 7 shows sample normalized magnitude and phase responses of the flexion portion of one subject's EMGσ-torque model, for three different linear model orders (3, 7 and 15) and two time advances (0 and 60 ms). Also shown in each plot is the Butterworth model. Since most of the torque power was below 1 Hz, this frequency span is most important. The magnitude responses are rather similar over the 0–1 Hz span, with more shaping occurring in the FIR models as the order increases. But, there are substantial differences between the phase responses. At model order 3 (high average errors, see Fig. 6), the FIR responses cannot add sufficient phase delay (if we consider the phase of the lower-error 15th-order model as closer to ideal). At model order 15 (low average errors, see Fig. 6), the FIR models are able to adapt their phase responses to the advance time, while the Butterworth phase is fixed. In any case, the phase

responses are all quite linear over the 0–1 Hz span.

IV. Discussion

Our interest in this work was to exploit the electromechanical delay between surface EMG and joint torque, in order to estimate torque in advance of its occurrence. While some literature on this topic has appeared in the past in which a few advance times were studied, we conducted a finely-grained analysis and incorporated more recent EMG-torque processing approaches. Applications that might benefit from torque estimation at advanced times include: anticipatory head motion in virtual environments, myoelectric prosthesis control, control of exoskeleton suits and powered rehabilitation devices. The observed delay between *peak* EMG *amplitude* and *peak* force is typically 50–100 ms [1]–[3]. Many biomechanical models, particularly those based on 1st- or 2nd-order Butterworth filter dynamics, include a pure delay term of this time duration. We systematically studied time advances ranging from 0–750 ms, using high-order linear (30th-order) and nonlinear (15th-order) models with and without advanced EMG processing (whitening and multiple channel combination). The selection of these model orders, and the pseudo-inverse tolerance used in the associated least squares training, was optimized based on a prior study of a subset of these data [21]. We also studied Butterworth models and lower-order FIR models, as these forms are commonly found in the literature.

For the high-order optimal models, Fig. 2 shows that torque could be estimated for time advances of ~0–60 ms with no discernible change in minimum error, and out to 140–170 ms before a statistically significant change in error occurred (at the p=0.05 level of significance). Thus, these EMG-torque models would not benefit from the use of a pure delay term, which simply time-shifts the x-axis in this plot. At very large time advances, the error consistently approached an average error of ~18.5% MVC_F. This error is comparable to the error that would be achieved if the input EMG were ignored and a constant torque, set in the mid-range of all experimental torques, was used; implying that EMG is no longer providing any useful predictive information at these advance times. The errors for all of the models display this same maximum average error. Consistent with prior research [7], [19]–[22], the high-order models also showed that the nonlinear models produced lower error than the linear models and that advanced EMG processing (multiple-channel, whitened) produced lower error than standard EMG processing.

The Butterworth models (Fig. 4) and the low-order FIR models (Fig. 6) exhibited error that contained a single nadir as a function of advance time. This error nadir occurred at a time advance of 60 ms for the Butterworth models and 115 ms for the 3rd-order FIR model. The error at each of these locations was significantly lower (statistically) than the respective error at a time advance of 0 ms. Figs. 3 and 5 suggest that a primary reason for an increasing error as the advance time moved away from the nadir was improper phase alignment of the EMG-based estimated torque. The sample magnitude and phase responses in Fig. 7 further support this contention—the magnitude responses of this linear model do not differ much across the 0–1 Hz range, but the phase responses do at the higher-order (thus, more accurate) models. The Butterworth model has a fixed phase response that cannot adjust to the subject or time advance. The low-order FIR models do not seem to have a sufficient number of degrees of freedom/filter lags in order to accommodate the necessary phase response. For each, the result is an estimated torque that *leads* the actual torque (albeit slightly) for short time advances but *lags* the actual torque for long time advances. Additionally, the existence of an error nadir explains why these models can benefit from a pure delay term; the delay term attempts to time shift the torque to the advance time corresponding to the error nadir. As the FIR model order increased, the nadir in the models disappeared and was replaced with a plateau region—concomitant with an overall decrease in error.

At the physiologic level, an electromechanical delay of 50–100 ms [1], [2] is measured as the time between some *processed* reference EMG activity (e.g., rectified and lowpass filtered) and the resulting *peak* force. Physiologically, this delay includes the delay in excitation-contraction coupling, any delay due to slack in the muscle, and delay due to force development (i.e., the rise time from force initiation to force peak) [30]. The excitation-contraction delay is quite small, approximately 5 ms [31].

However, delay is incurred by the filters which process the EMG and force signals, and must also be considered. The exact delay is specific to the filtering utilized and force profiles utilized (i.e., input excitation frequencies). Thelen et al. [4] avoided these signal processing delays by computing EMG amplitude offline with zero-phase (two-pass) filters, then cascading a pure delay in their EMGσ-torque model. Their optimal pure delay ranged between 111–218 ms. This technique is not available for real-time systems. The classic work of Inman et al. [1] computed their EMG amplitude via a full-wave rectifier (no delay) and a passive RC lowpass filter. As with most filters, their RC filter has rather linear phase over the frequency range from 0–1 Hz (the frequency range relevant to most physiologic contractions, including those used in this study). Their RC time constant (R = 50 kΩ, C = 2 μF) of 100 ms corresponds to a pure delay of ~90.0 ms (over the 0–1 Hz range). They cite a delay from *processed* EMG peak to force peak of ~80 ms. Hence, their overall delay averaged 170 ms, well within the range found by Thelen et al. [4]. In this study, our pre-processing filters impart a combined delay of ~7 ms, primarily due to the whitening filters. (We need not account for the ~76 ms delay due to the lowpass filters in the decimation operation, since the torque signal was similarly decimated.) As shown in Fig. 7, this sample 15th-order flexion filter imparts an input-output delay of 150 ms at a time advance of 0 ms (the phase is approximately linear between 0–1 Hz, with a value of –54° at 1 Hz). Hence, our overall filtering delay is ~157 ms, also well within the range found by Thelen et al. [4]. Further, as the time advance increases, the time delay required by our EMGσ-torque model decreases. This change is shown in Fig. 7, with the phase of the 60 ms time advance models exhibiting a lower-valued negative slope.

Note that our constrained (constant-posture) contractions

and limited bandwidth (1 Hz) will not be representative of all possible contraction profiles. Certainly, ballistic motions can exhibit frequencies that easily exceed 1 Hz and may have implications for the desired phase response in an EMG-torque model. Unconstrained motions will necessarily add complexity to the models to account for changes in joint angle.

Most applications which could benefit from anticipatory EMGσ-torque estimates employ real-time processing, usually on a microprocessor. Many modern microprocessors inherently incorporate floating point processing (required for most of these algorithms) and have sufficient computational power for even the most intensive of these algorithms (e.g., multiple-channel EMG whitening combined with the nonlinear EMGσ-torque model). Hence, the processing delay, itself, may only account for a few ms. However, intensive computation is typically achieved at the cost of higher electrical power consumption, which can impact the battery life (and size) in real-time systems.

Overall, our results show that the higher-order optimized models are clearly superior to the second-order Butterworth models and the low-order FIR models. First, the best error in the higher-order models is significantly lower than that of the other model forms, with the nonlinear 15th-order model exhibiting the lowest error of all. Second, a range of times spanning at least 60 ms (and, statistically, up to 140–170 ms) is available in which the error maintains this minimum, whereas the other models only exhibit their minimum average error at one specific time advance. Third, no delay term need be determined; the complete model is calibrated through the least squares fit of the model parameters. And, fourth, most Butterworth models are not calibrated to dynamic contraction trials as we have done here. If constant-force trials are used to calibrate the Butterworth filter gains, then significantly higher errors result (approaching 20% MVC_F), as demonstrated previously on a subset of these data [21]. If force-varying data are available for calibration, researchers might as well choose the higher-order models which can be calibrated from these same data. Our 15th-order nonlinear model, using four channel whitened EMG, provided the lowest error of 5.48 ± 2.21% MVC_F over the time advance range from approximately 0–60 ms. Errors increased as the time advance was increased further.

REFERENCES

[1] V. T. Inman, H. J. Ralston, J. B. de C. M. Saunders, B. Feinstein and E. W. Wright, "Relation of human electromyogram to muscular tension," *Electroencephalo. Clin. Neurophysiol.*, vol. 4, pp. 187–194, 1952.

[2] L. Li and B. S. Baum, "Electromechanical delay estimated by using electromyography during cycling at different pedaling frequencies," *J. Electromyo. Kinesiol.*, vol. 14, pp. 647–652, 2004.

[3] G. Howatson, "The impact of damaging exercise on electromechanical delay in biceps brachii," *J. Electromyo. Kinesiol.*, vol. 20, pp. 477–481, 2010.

[4] D. G. Thelen, A. B. Schultz and J. A. Ashton-Miller, "Quantitative interpretation of lumbar muscle myoelectric signals during rapid cyclic attempted trunk flexions and extensions," *J. Biomech.*, vol. 27, pp. 157 167, 1994.

[5] R. A. Bogey, J. Perry and A. J. Gitter, "An EMG-to-force processing approach for determining ankle muscle forces during normal human gait," *IEEE Trans. Neural Sys. Rehab. Eng.*, vol. 13, pp. 302–310, 2005.

[6] D. Staudenmann, I. Kingma, D. F. Stegeman and J. H. van Dieen, "Towards optimal multi-channel EMG electrode configurations in muscle force estimation: A high density EMG study," *J. Electromyo. Kinesiol.*, vol. 15, pp. 1–11, 2005.

[7] D. Staudenmann, K. Roeleveld, D. F. Stegeman and J. H. van Dieen, "Methodological aspects of SEMG recordings for force estimation—A tutorial and review," *J. Electromyo. Kinesiol.*, vol. 20, pp. 375–387, 2010.

[8] Y. Barniv, M. Aguilar and E. Hasanbelliu, "Using EMG to anticipate head motion for virtual-environment applications," *IEEE Trans. Biomed. Eng.*, vol. 52, pp. 1078–1093, 2005.

[9] T. R. Farrell and R. F. Weir, "The optimal controller delay for myoelectric prostheses," *IEEE Trans. Neural Sys. Rehab. Eng.*, vol. 15, pp. 111–118, 2007.

[10] K. Kiguchi, T. Tanaka and T. Fukuda, "Neuro-fuzzy control of a robotic exoskeleton with EMG signals," *IEEE Trans. Fuzzy Sys.*, vol. 12, pp. 481–490, 2004.

[11] A. M. Dollar and H. Herr, "Lower extremity exoskeletons and active orthoses: Challenges and state-of-the-art," *IEEE Trans. Robotics*, vol. 24, pp. 144 158, 2008.

[12] T. Lenzi, S. M. M. De Rossi, N. Vitiello and M. C. Carrozza, "Intention-based EMG control for powered exoskeletons," *IEEE Trans. Biomed. Eng.*, vol. 59, pp. 2180–2190, 2012.

[13] L. Lucas, M. DiCicco and Y. Matsuoka, "An EMG-controlled hand exoskeleton for natural pinching," *J. Robotics Mech.*, vol. 16, no. 5, 2004.

[14] L. Dipietro, M. Ferraro, J. J. Palazzolo, H. I. Krebs, B. T. Volpe and N. Hogan, "Customized interactive robotic treatment for stroke: EMG-triggered therapy," *IEEE Trans. Neural Sys. Rehab. Eng.*, vol. 13, pp. 325 334, 2005.

[15] M. Mulas, M. Folgheraiter and G. Gini, "An EMG-controlled exoskeleton for hand rehabilitation," *IEEE Conf. Rehab. Robots*, 2005.

[16] J. Stein, K. Narendran, M. Kailas, J. McBean, K. Krebs and R. Hughes, "Electromyography-controlled exoskeletal upper-limb-powered orthosis for exercise training after stroke," *Am. J. Phys. Med. Rehab.*, vol. 86, pp. 255–261, 2007.

[17] Z. O. Khokhar, Z. G. Xiao and C. Menon, "Surface EMG pattern recognition for real-time control of a wrist exoskeleton," *BioMed. Eng. OnLine*, vol. 9:41, 2010.

[18] M. A. Delph, S. A. Fischer, P. W. Gauthier, C. H. Martinez Luna, E. A. Clancy and G. S. Fischer, "Development of a cable driven flexible robotic rehabilitation glove," in *Biomed. Eng. Soc. 2012 Ann. Meet.*, Atlanta, GA, Oct. 24–27, 2012.

[19] E. A. Clancy and K. A. Farry, "Adaptive whitening of the electromyogram to improve amplitude estimation," *IEEE Trans. Biomed. Eng.*, vol. 47, pp. 709–719, 2000.

[20] J. R. Potvin and S. H. M. Brown, "Less is more: High pass filtering, to remove up to 99% of the surface EMG signal power, improves EMG-based biceps brachii muscle force estimates," *J. Electromyogr. Kinesiol.*, vol. 14, pp. 389–399, 2004.

[21] E. A. Clancy, L. Liu, P. Liu and D.V. Z. Moyer, "Identification of constant-posture EMG-torque relationship about the elbow using nonlinear dynamic models," *IEEE Trans. Biomed. Eng.*, vol. 59, pp. 205-212, 2012.

[22] J. Hashemi, E. Morin, P. Mousavi, K. Mountjoy and K. Hashtrudi-Zaad, "EMG-force modeling using parallel cascade identification," *J. Electromyo. Kinesiol.*, vol. 22, pp. 469 477, 2012.

[23] K. Koirala, M. Dasog, P. Liu and E. A. Clancy, "EMG-torque estimation at future times," in *39th Ann. Northeast Bioeng. Conf.*, Syracuse, NY, Apr. 5–7, 2013, pp. 59–60.

[24] E. A. Clancy, "Electromyogram amplitude estimation with adaptive smoothing window length," *IEEE Trans. Biomed. Eng.*, vol. 46, pp. 717–729, 1999.

[25] P. Prakash, C. A. Salini, J. A. Tranquilli, D. R. Brown and E. A. Clancy, "Adaptive whitening in electromyogram amplitude estimation for epoch-based applications," *IEEE Trans. Biomed. Eng.*, vol. 52, pp. 331 334, 2005.

[26] E. A. Clancy, (2010 Aug.). *EMG Amplitude Estimation Toolbox: User's Guide*. Alpha version 0.07, 2010 [Online]. Available: http://www.wpi.edu/~ted/emg_tool.htm.

[27] L. Ljung, *System Identification: Theory for the User*. Upper Saddle River, NJ: Prentice-Hall, 1999, pp. 491–519.

[28] W. H. Press, S. A. Teukolsky, W. T. Vetterling, and B. P. Flannery, *Numerical Recipes in C*, 2nd ed. New York: Cambridge Univ. Press, 1994, pp. 671 681.

[29] I. Miller and J. E. Freund, *Probability and Statistics for Engineers*. Englewood Cliffs, NJ: Prentice-Hall, 1977, pp. 272 275.

[30] P. R. Cavanagh and P. V. Komi, "Electromechanical delay in human skeletal muscle under concentric and eccentric contractions," *Eur. J. Appl. Physiol.*, vol. 42, pp. 159–163, 1979.
[31] T. Moritani, D. Stegeman and R. Merletti, "Basic Physiology and Biophysics of EMG Signal Generation," in *Electromyography: Physiology, Engineering, and Noninvasive Applications*. Hoboken, NJ: John Wiley & Sons, Inc., 2004, pp. 1–25.

Meera Dasog received her B.E. (Bachelor of Engineering) degree in Electrical and Instrumentation Engineering from B.V.B. College of Engineering, Hubli, India, and M.S. degree from Worcester Polytechnic Institute (WPI), Worcester, MA, in Electrical and Computer Engineering.

She has worked briefly in the semiconductor industry which involved verification and modeling of various analog integrated circuits. Her areas of interests include signal processing, biomedical instrumentation and integrated mixed signal circuit design.

Kishor Koirala received his B.S. degree in Electronics and Communication Engineering from Pokhara University, Nepal, M.B.A. in Finance from University of Findlay, Findlay, Ohio and M.S. degree in Electrical and Computer Engineering from Worcester Polytechnic Institute, Worcester, MA.

He is currently employed with Aware Inc., Bedford, MA. His research interests include bio-electrical signal processing, machine learning and digital audio processing.

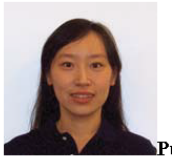

Pu Liu received the B.S. degree from Fudan University, Shanghai, China and the M.S. degree from Worcester Polytechnic Institute (WPI), Worcester, MA, both in Electrical Engineering.

She is currently working toward the Ph.D. degree from the Department of Electrical and Computer Engineering, WPI. Her research interests include signal processing, modeling and instrumentation, principally as applied to biomedical engineering.

Edward (Ted) A. Clancy (S'83–M'91–SM'98) received the B.S. degree from Worcester Polytechnic Institute (WPI), and the S.M. and Ph.D. degrees from Massachusetts Institute of Technology (MIT), all in Electrical Engineering.

He has worked in industry for medical instrumentation and analysis companies interested in EMG, EEG, ECG and blood pressure, and the defense industry (aircraft instruments and radar). He is Associate Professor of Electrical and Computer Engineering, and of Biomedical Engineering at WPI. He is interested in signal processing, stochastic estimation and system identification, particularly as applied to problems in medical engineering and human rehabilitation.

TABLE I
PARAMETERS VALUES AND SUMMARY RESULTS OF THE FULL LINEAR/NONLINEAR FIR MODELS. MINIMUM ERROR VALUES ALL OCCURRED AT A FUTURE TIME ADVANCE OF 0 MS. *Q*: NUMBER OF LAGS. *TOL*: PSEUDO-INVERSE TOLERANCE. ADVANCE: FORWARD TIME ADVANCE TO FIRST CHANGE FROM MINIMUM ERROR (ANOVA $P<0.05$).

Model Linearity	EMG Processor	*Q*	*Tol*	Min. $\mu \pm \sigma$ Error (% MVC_F)	*Advance* (ms)
Linear	1 Channel, Unwhitened	30	0.00032	8.62 ± 3.08	170
Nonlinear	1 Channel, Unwhitened	15	0.0056	7.65 ± 2.73	160
Linear	4 Channels, Whitened	30	0.0056	6.24 ± 2.33	145
Nonlinear	4 Channels, Whitened	15	0.01	5.48 ± 2.21	140

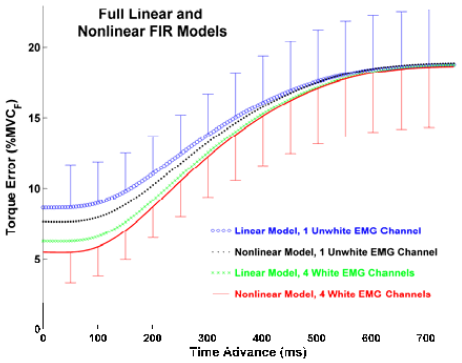

Fig. 2. Mean errors (one-sided standard deviations shown for two of the models) from 54 subjects vs. future time advance for the two optimal-order models and two EMG processors. Mean values computed every 5 ms, std. dev. values only shown every 50 ms.

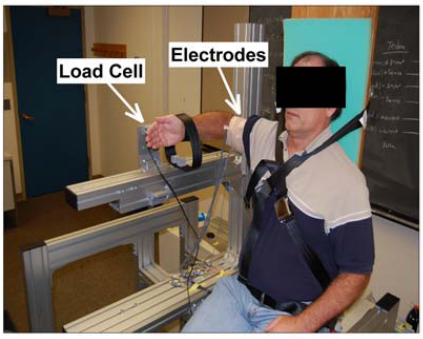

Fig. 1. Experimental apparatus from experiment WX. A subject's right arm is oriented in a plane parallel to the floor, the upper arm is directed laterally outward from the shoulder, the wrist is fully supinated and the angle between the upper arm and the forearm is 90°. Four EMG electrodes are mounted over the biceps and triceps muscles. The wrist is tightly cuffed to a load cell at the level of the styloid process.

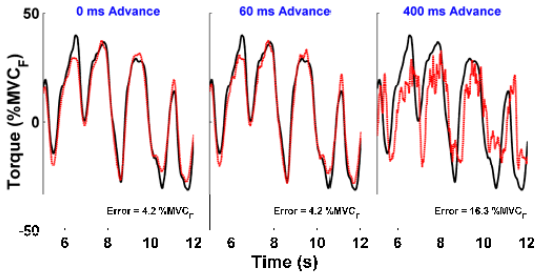

Fig. 3. Sample time-series plots of the actual (solid) and EMG-estimated (dashed) torque using 15th-order order nonlinear model with four channel whitened EMG processing, at three distinct time advances. Seven second segments shown in each plot. Subject WX15.

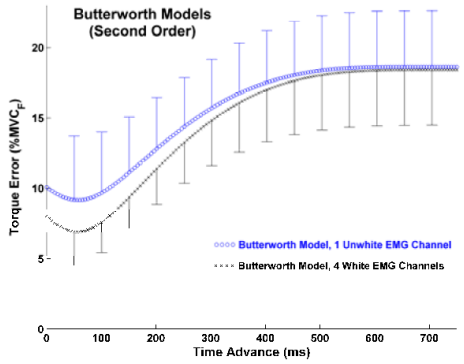

Fig. 4. Mean and one-sided standard deviation errors from 54 subjects vs. future time advance for the Butterworth filter model. Separate plot for each EMG processor. Mean values computed every 5 ms, std. dev. values only shown every 50 ms.

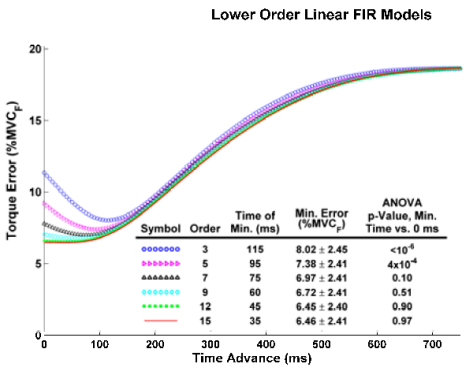

Fig. 6. Mean errors from 54 subjects vs. future time advance for the lower-order linear FIR models. EMG processing used four whitened channels in each case. Inset table shows the advance time value and error value ($\mu \pm \sigma$) corresponding to the minimum location of each plot; as well as the ANOVA *p*-value comparing the results at each minimum location to the results at an advance time of 0 ms, within each plot.

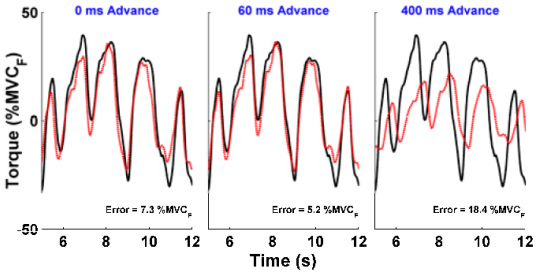

Fig. 5. Sample time-series plots of the actual (solid) and EMG-estimated (dashed) torque using the Butterworth model with four channel whitened EMG processing, at three distinct time advances. Seven second segments shown in each plot. Subject WX15.

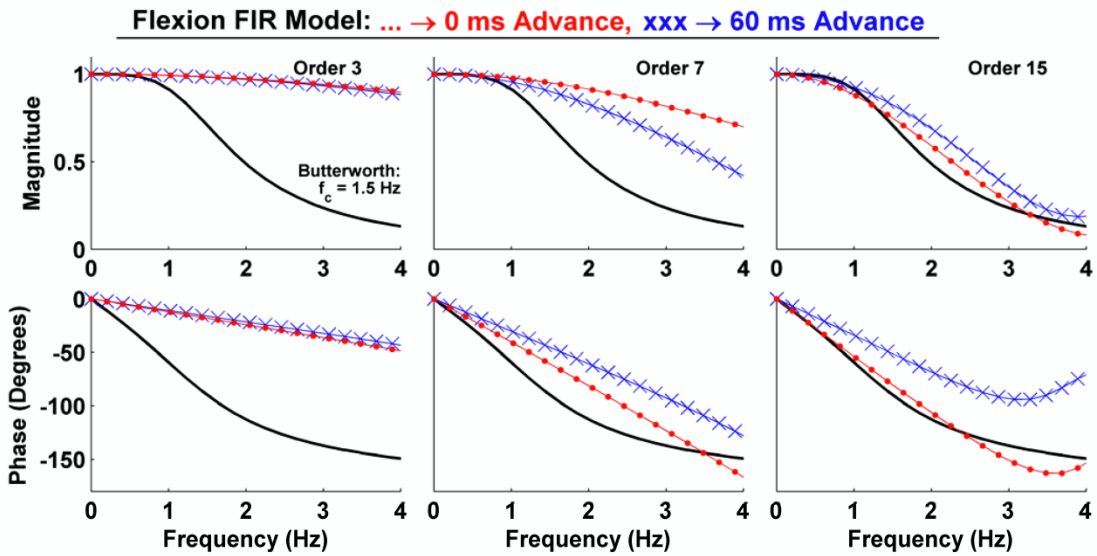

Fig. 7. Sample magnitude and phase responses of the flexion portions of linear FIR EMGσ-torque models at different model orders, plotted along with a second-order Butterworth filter (f_c = 1.5 Hz). All magnitude responses normalized to the DC gain. EMG processing used four whitened channels in each case. Subject WX15.

CHAPTER 17

Copy of drafted journal paper:

Pu Liu, Lukai Liu and Edward A. Clancy. “Influence of Joint Angle on EMG-Torque Model During Constant-Posture, Torque-Varying Contractions.” In preparation.

Influence of Joint Angle on EMG-Torque Model During Constant-Posture, Torque-Varying Contractions

Pu Liu[a], Lukai Liu[a] and Edward A. Clancy[a]

[a]Worcester Polytechnic Institute, Worcester, MA 01609 USA

Keywords—Biological system modeling, electromyography, EMG amplitude estimation, EMG signal processing, joint angle influence

Correspondence to:
Edward (Ted) A. Clancy
Department of Electrical and Computer Engineering
Worcester Polytechnic Institute
100 Institute Road, Worcester, MA 01609
Tel. +1 (508) 831-5778
Fax. +1 (508) 831-5491
Email: ted@wpi.edu

ABSTRACT:

Relating the electromyogram (EMG) to joint torque is useful in various application areas, including prosthesis control, ergonomics and clinical biomechanics. Limited study has related EMG to torque across varied joint angles. We related the biceps-triceps surface EMG of 22 subjects to elbow torque at six joint angles (spanning 60° to 135°) during constant-posture, torque-varying contractions. Three nonlinear EMGσ-torque models, advanced EMG amplitude (EMGσ) estimation processors (i.e., whitened, multiple-channel) and the duration of data used to train models were investigated. When EMG-torque models were formed separately for each of the six distinct joint angles, a minimum "gold standard" error of 4.01 ± 1.2% MVC_{F90} resulted (i.e., error relative to maximum voluntary contraction at 90° flexion). This model structure, however, did not directly facilitate interpolation across angles. The best model which did so, achieved a statistically equivalent error of 4.06 ± 1.2% MVC_{F90}. Results demonstrated that advanced EMGσ processors lead to improved joint torque estimation as do longer model training durations.

1. Introduction

For several decades, the surface electromyogram (EMG) has seen extensive investigation as a non-invasive measure that can be used to estimate muscle tension and/or joint torque [see Staudenmann et al. (2010) for a recent review] (An et al., 1983; Clancy et al., 2006; Clancy and Hogan, 1997; Clancy et al., 2012; Doheny et al., 2008; Gottlieb and Agarwal, 1971; Hasan and Enoka, 1985; Hashemi et al., 2012, 2013; Heckathorne and Childress, 1981; Hof and Van den Berg, 1981; Hogan and Mann, 1980b; Inman et al., 1952; Lawrence and DeLuca, 1983; Liu et al., 2013b; Messier et al., 1971; Potvin and Brown, 2004; Sanger, 2007; Shin et al., 2009; Solomonow et al., 1986; Staudenmann et al., 2009; Thelen et al., 1994; Vredenbregt and Rau, 1973). A common approach is to estimate the EMG standard deviation (EMGσ, a.k.a. EMG amplitude) from one or more sites on muscles about a joint, and then use system identification techniques to model an EMGσ-torque relationship. These non-invasive estimates are used in prosthesis control (Parker et al., 2006), clinical biomechanics (Disselhorst-Klug et al., 2009; Doorenbosch and Harlaar, 2003) and ergonomics analysis (Hagg et al., 2004; Kumar and Mital, 1996; Mathissen et al., 1995). Numerous system identification approaches have been successfully applied, with most studies now accounting for agonist-antagonist co-activation (Solomonow et al., 1986) and individual subject differences in the EMG-torque relationship (Hansan and Enoka, 1985). Because EMG is a stochastic signal, methods which lower the variance of EMGσ estimates—e.g., whitening and multiple-channel combination—have been shown to lower EMG-torque errors, as have improved system identification methods (Clancy et al., 2002, 2006, 2012; Clancy and Farry, 2000; Clancy and Hogan, 1995, 1997; Hashemi et al., 2012, 2013; Hogan and Mann, 1980a, 1980b; Potvin and Brown, 2004; Sanger, 2007; Staudenmann et al., 2010; Thelen et al., 1994).

A topic with more limited investigation is the role of joint angle. The EMG-torque relationship changes with angle, at least due to the length-tension relationship (Rack and Westbury, 1969; Zajac 1989), changes in muscle moment arms (Messier et al., 1971) and the movement of electrodes with respect to underlying muscle tissue and the innervation zone (Martin and MacIsaac, 2006; Rainoldi et al., 2000). Vredenbregt and Rau (1973), as well as more recent studies (Doheny et al., 2008; Hashemi et al., 2013; Liu et al., 2013b), found evidence of a multiplicative influence of angle on EMG-torque, at least during constant-torque contractions at various torque levels. That is, the EMG-torque curve has the same shape at each angle, but is scaled by a gain factor that is distinct for each angle.

In this study, we report on continued improvements to EMG-torque processing, with an emphasis on the influence of joint angle. We extended the experimental conditions to force-varying contractions conducted over a range of fixed joint angles. We specifically investigated the appropriateness of the multiplicative model vs. joint angle. With these force-varying contractions, we also compared standard EMGσ processing to advanced processors that include signal whitening and multiple channel combination. Finally, two areas of system identification were contrasted. First, we contrasted linear dynamic models to nonlinear dynamic models. Second, the duration of data available for model training has seen limited evaluation (Clancy et al., 2012). Hence, we also evaluated this modeling variant.

2. Methods

2.1 Experimental Data and Methods

Experiments were approved and supervised by the WPI IRB. Experimental data were acquired from 22 healthy subjects (12 male, 10 female; aged 18–56 years), each of whom provided written informed consent. Subjects were seated and strapped into a custom-built straight-back chair (see Fig. 1 of Liu et al., 2013b) with their right shoulder abducted 90°, their forearm oriented in a parasaggital plane, and their supinated wrist (palm perpendicular to the floor) tightly cuffed to a load cell (Vishay Tedea-Huntleigh Model 1042, 75 kg full scale). The angle between the upper arm and the forearm was fixed, but selectable. Skin above the biceps and triceps muscles was cleaned with an alcohol wipe and a bead of electrode gel was massaged into the overlying skin. Six bipolar EMG electrode-amplifiers were applied in a row, transversely across each of the biceps and triceps muscle groups, midway between the elbow and the midpoint of the upper arm (to avoid the innervation zone proximally and the tendon distally). Only the middle four of each set of six were analyzed. Subjects were instructed to tense their muscles at both angular extremes (60°, 135°) to aid in visualizing the distal tendon and the muscle midpoint locations. EMG recording over the tendon is discouraged because the tissue is not electrically active and prone to motion artifacts. Recording over the innervation zone (typically located near the muscle mid-point) can lead to large variations in EMGσ values with small changes in location (Rainoldi et al., 2000). The center of the row of electrodes was aligned with the muscle midline, to best avoid crosstalk from adjacent muscles. Each electrode-amplifier had a pair of 8 mm diameter, stainless steel, hemispherical contacts separated by 1 cm edge-to-edge, oriented along the muscle's long axis. The distance between adjacent electrode-amplifiers was ~1.75 cm. A ground electrode was gelled and secured on the upper arm. Custom electronics amplified and filtered each EMG signal (CMRR > 90 dB at 60 Hz; 8th-order Butterworth highpass at 15 Hz; 4th-order Butterworth lowpass at 1800 Hz) before being sampled at 4096 Hz with 16-bit resolution.

All contractions were constant-posture, with the elbow angle selectable. Subjects were provided a warm-up period, then rested three minutes. Separate extension and flexion MVCs were then measured at a joint angle of 90°. Subjects took 2–3 seconds to slowly ramp up to MVC and maintained that force for two seconds. The average load cell value during the contraction plateau was taken as the MVC. Five second duration, constant-force contractions at 50% MVC extension, 50% MVC flexion and at rest (arm removed from the wrist cuff) were next recorded at 90°. These contractions were used to calibrate advanced EMGσ estimation algorithms (Clancy and Farry, 2000; Prakash et al., 2005). Then, a sequence of constant-posture, torque-varying contractions was conducted at randomized elbow angles (the included angle between the forearm and upper arm) of 60°, 75°, 90°, 105°, 120° and 135°. At each angle (other than 90°). MVC torque was measured in both elbow extension and flexion. Then, four tracking trials of 30 s duration were recorded during which the subjects used the load cell as a feedback signal to track a computer-generated torque target. The target moved on the screen in the pattern of a bandlimited (1 Hz) uniform random process, spanning 50% MVC extension to 50% MVC flexion. Two minutes of rest were provided between trials to avoid cumulative fatigue. A total of 24 tracking trials were recorded (four trials for each of six angles).

2.2 Methods of Analysis

Analysis was performed offline in MATLAB. The sampled EMG signals were notch filtered at the power line frequency and its harmonics (2^{nd}-order IIR comb filter, notch bandwidth $\leq$ 0.5 Hz each, dual-pass filtered—filter applied in the forward, then reverse time directions to achieve zero phase), since whitening at high frequencies is particularly susceptible to signal interference; and then each signal was highpass filtered (15 Hz cutoff, 5^{th}-order Butterworth, duel-pass filtered). Next, two distinct EMGσ variations were created for each of the extension and flexion muscle groups for each 30 s trial. Estimators were either single-channel, unwhitened (using a centrally located electrode) or four-channel whitened (using the four centrally located electrodes). Whitened channels used the non-causal adaptive whitening algorithm of Clancy and Farry (2000) and Prakash et al. (2005). After optional whitening, each processor utilized a first-order demodulator (rectifier). Thereafter, signals were lowpass filtered at 16 Hz then downsampled by a factor of 100 to 40.96 Hz. The torque signal was similarly decimated, producing an EMG data set with a bandwidth approximately 10 times that of the torque signal being estimated. This decimated sampling rate is best for system identification, being large enough to capture the system dynamics and small enough to avoid noise existing out of the signal band (Clancy et al., 2006; Ljung, 1999). The first and last 2 s of data were excluded from each 30 s trial to account for filter startup and tail transients. The decimated extension

and flexion EMGσ inputs were related to joint torque (output), comparing three dynamic nonlinear polynomial model structures. First, a dynamic model was fit separately at each joint angle, providing the *angle-specific model*:

$$T[m]=\sum_{d=1}^{D}\sum_{q=0}^{Q} f_{d,q,\theta}\,\sigma_F^d[m-q]-\sum_{d=1}^{D}\sum_{q=0}^{Q} e_{d,q,\theta}\,\sigma_E^d[m-q], \qquad (1)$$

where m was the decimated discrete-time sample index; $T[m]$ the measured torque; D the EMGσ polynomial degree (varied from D=1–4, where D=1 produced a linear model); Q the number of time lags (Q=20); θ the elbow joint angle; $f_{d,q,\theta}$ and $e_{d,q,\theta}$ the flexion and extension fit parameters, respectively (which specified the *shape* of the EMGσ-torque relationship); and $\sigma_F[m]$ and $\sigma_E[m]$ the flexion and extension EMGσ estimates, respectively. This model was fit using linear least squares, regularized via the pseudo-inverse; if the ratio of the largest to a given singular value was less than 0.0056, that singular value was omitted (Clancy et al., 2012; Press et al., 1994). This angle-specific model served as the performance "gold standard."

Second, a model which incorporated the hypothesized gain variation in the form of polynomial gain vs. angle functions (one for flexion and another for extension) provided the *polynomial-gain model*:

$$T[m]=\left(\sum_{a=0}^{A} g_{a,F}\,\theta^a[m]\right)\left(\sum_{d=1}^{D}\sum_{q=0}^{Q} f_{d,q}\,\sigma_F^d[m-q]\right)-\left(\sum_{a=0}^{A} g_{a,E}\,\theta^a[m]\right)\left(\sum_{d=1}^{D}\sum_{q=0}^{Q} e_{d,q}\,\sigma_E^d[m-q]\right), \qquad (2)$$

where $g_{a,F}$ and $g_{a,E}$ were the flexion and extension angle fit parameters, respectively (which specified the multiplicative gain vs. joint angle). The angle polynomial degree was varied from A=1–4. Note that the dynamic fit coefficients, $f_{d,q}$ and $e_{d,q}$, were fixed across angle (i.e., *not* a function of angle). This model was fit using nonlinear least squares. The initial dynamic parameters ($f_{d,q}$ and $e_{d,q}$) were those of the angle-specific model at 90°. The initial angle parameters were then found by fixing the dynamic parameters and solving for the $g_{a,F}$ and $g_{a,E}$ parameters via linear least squares (*simultaneously* across all angles). The full nonlinear model was then minimized across all angles. The inclusion of both angle and EMGσ polynomials resulted in one redundant overall scaling parameter. Anecdotally, this additional degree of freedom seemed to aid the least squares minimization, thus was retained. For consistency across models, the angle polynomial was rescaled to a gain of one at 90° after the fit was complete, with a compensatory inverse scaling applied to the EMGσ polynomial. This model immediately interpolates the gain function across all joint angles.

The third model simplified the gain vs. angle relation by utilizing distinct flexion and extension gains at each angle. This *piece-wise-gain model* is:

$$T[m] = g_{\theta,F} \cdot \left(\sum_{d=1}^{D} \sum_{q=0}^{Q} f_{d,q} \, \sigma_F^d[m-q] \right) - g_{\theta,E} \cdot \left(\sum_{d=1}^{D} \sum_{q=0}^{Q} e_{d,q} \, \sigma_E^d[m-q] \right), \qquad (3)$$

where gain parameters $g_{\theta,F}$ and $g_{\theta,E}$ were designated at each of the six angles (total of 12 angle parameters). Again, note that the dynamic fit coefficients were fixed across angle. This model was fit using nonlinear least squares. The initial dynamic parameters ($f_{d,q}$ and $e_{d,q}$) were those of the angle-specific model at 90°. The initial angle parameters could then be found by fixing the dynamic parameters and solving for the $g_{\theta,F}$ and $g_{\theta,E}$ parameters via linear least squares (each pair fit *separately* at each angle). The full nonlinear model (angle parameters and dynamic parameters) was then simultaneously minimized across all angles, and then normalized to a gain of one at 90°. This model did *not* facilitate immediate gain interpolation across angle. However, gain vs. angle interpolations which preserve the exact gain values at the measured angles (e.g., spline functions) can be fit *post hoc* to provide EMG-torque at any angle.

Each subject completed four tracking trials at six distinct angles. Six trials, one per angle, were combined to form an analysis record (four per subject). Initially, one record was used for training and a second record for testing. The mean absolute difference between the test torque and that predicted by the EMG-torque model was computed. This difference excluded the first and last 2 s (due to filter startup and tail transients) as well as an additional 488 ms startup transient due to the Q=20 order dynamic filter. Error values were normalized to twice the torque at 50% flexion MVC at angle 90° (MVC_{F90}). The average test trial error from all 12 possible single-record train-test combinations (full cross-validation) was reported for each subject. Next, two records were used for training and two for testing, with full cross-validation (12 combinations). Finally, three records were used for training and one for testing (4 combinations). For statistical analysis, test error values were subjected to a paired sign test (Miller and Freund, 1977). Twenty two paired values contributed to each sign test (22 subjects).

3. Results

Fig. 1 shows an example of the estimated torque and actual torque vs. time for the six elbow angles using the three different model structures. The best performing parameters, as indicated in the caption, were selected for each model in the figure. The angle-specific model was considered the "gold standard," since it optimized the model coefficients at each particular joint angle. It does not interpolate across angles. Fig. 2 shows example EMG-torque estimation vs. time, comparing training duration and EMGσ processing. Table 1 gives the mean plus/minus standard deviation test error results for the three models when single-channel unwhitened EMGσ processing was used. The analysis dimensions enumerated are:

197 EMGσ-torque model, number of training records used to fit a model, EMGσ polynomial degree (D) and
198 angle polynomial degree (A; applicable to the polynomial gain model, only). Table 2 gives the
199 corresponding results when multiple-channel whitened EMGσ processing was used. The general trends in
200 these results were for lower errors due to multiple-channel whitened EMGσ processing, longer duration
201 training and nonlinear dynamic models (D>1). The lowest errors in the polynomial-gain model always
202 occurred when the angle polynomial equaled A=2.

203 Statistical analysis began by comparing single-channel unwhitened results (Table 1) to multiple-channel
204 whitened results (Table 2). For each combination of EMGσ-torque model and training duration (nine
205 combinations per table), the cell with the lowest average error in Table 1 was compared to the cell with the
206 lowest average error in Table 2. Each of the nine comparisons was statistically different ($p < 10^{-5}$), with
207 multiple-channel whitened results demonstrating lower average errors in each case. Hence, subsequent
208 statistical analysis was limited to the multiple-channel whitened results (Table 2). Next, statistical
209 comparison was made between the number of training records used to fit a model. Within each of the three
210 models, the cell with the lowest average error for one training duration in Table 2 was compared pair-wise
211 to the results from the other two durations (three combinations for each of the three models). Each of the
212 nine comparisons was statistically different ($p < 10^{-5}$), with two training trials always producing lower
213 errors than one training trial and three training trials always producing the lowest error. Hence, subsequent
214 statistical analysis was further limited to the results using three training records in Table 2. Lastly,
215 comparison was made between models. For each model, the cell with the lowest average error in Table 2
216 was compared pair-wise to the similar results from the other two models (three combinations). There was a
217 weak difference when comparing the angle-specific model to the polynomial-gain model (p=0.026) and no
218 difference for the other two model comparisons (p>0.25). Thus, the results from the piece-wise-gain
219 model—which can be interpolated across angle—were not statistically different than results from the "gold
220 standard" angle-specific model. The lowest EMGσ-torque error was 4.01 ± 1.3% MVC_{F90}.
221
222 **4. Discussion**

223 This study evaluated methods for relating EMG to joint torque across a range of angles, during
224 constant-posture force-varying contractions. In general, the processing was conducted in two sequential
225 stages: estimation of extension and flexion EMGσ, followed by system identification of torque from the
226 extension and flexion EMGσ time-series. In the first stage, "standard" EMGσ estimation (single-channel
227 unwhitened) was compared to advanced EMGσ estimation (multiple-channel whitened). As with past
228 experimental studies (Clancy and Hogan, 1995; Clancy and Hogan, 1997; Clancy et al., 2012; Hogan and

229 Mann, 1980b; Liu et al., 2013b; Potvin and Brown, 2004; Prakash et al., 2005), advanced EMGσ
230 estimation resulted in a substantial decrease in torque estimation error. In our study, error was reduced on
231 average by 25% for each of the three EMGσ-torque models studied. This performance improvement is
232 attributed to a reduction in the variance of the EMGσ signal, due to whitening and channel combination
233 (Hogan and Mann, 1980a, b; Liu et al., 2013a). Nonetheless, there may be some drawbacks to the use of
234 multiple-channel EMGσ estimators, including: increased hardware cost: the increased risk of electrode
235 malfunction and its associated precipitous degradation in the EMGσ estimate (Clancy and Hogan, 1995);
236 and the possibility that better models could be formed by including all channels directly in the
237 EMGσ-torque model, rather than combining EMG channels at the amplitude estimation stage
238 (Staudenmann et al., 2009; Vieira et al., 2010).

239 In the second processing stage (relating EMGσ to torque), we studied three model structures. The
240 angle-specific model was considered the "gold standard," since it provided a separate fit at each available
241 angle. The other two models incorporated an angle-invariant EMGσ-relation that was multiplicatively
242 scaled as a function of angle—as suggested by the work of Vredenbregt and Rau (1973). We found that the
243 best angle-invariant models had an error that was not statistically different from the best gold
244 standard/angle-specific model. These EMGσ-torque models account for (and cannot distinguish between)
245 all variations due to changes in angle, including: the muscle length-tension relationship, variation in
246 muscle moment arms and muscle movement under the skin with respect to electrode location. Our results
247 provide further evidence that the constant-posture EMGσ-torque relationship maintains the same *shape*
248 across elbow angles, and need only be scaled to account for different angles. The angle-invariant models
249 are simple and can be easily interpolated over all angles within the range studied.

250 Few studies have rigorously studied the role of training contraction duration on model performance. In a
251 prior study of the elbow with a similar protocol, but limited to only the 90^{o} joint angle, training set
252 durations of 26 s and 52 s were contrasted (Clancy et al., 2012). The longer duration consistently produced
253 better results, particularly as the number of fit parameters increased. The best (lowest error) model formed
254 using 26 s of data had an error of 5.55±4.5% MVC_{F90}, while the best model using 52 s had an error of
255 4.65+3.6% MVC_{F90}. Thus, average error decreased %16 due to the increased training duration. In the
256 present study (across six angles), training durations of 26 s, 52 s and 78 s exhibited best-case average errors
257 of 4.75±1.7% MVC_{F90}, 4.17±1.3% MVC_{F90} and 4.01±1.2% MVC_{F90}, respectively, for the angle-specific
258 model. Hence, increasing from 26 s to 52 s reduced average error by 12%, while increasing from 26 s to 78
259 s reduced average error by 16%. As might be expected, the relative rate of improvement diminishes as the
260 training duration increases.

The optimal EMGσ polynomial degree ranged from D=2–4 when using single-channel unwhitened EMGσ processing and from D=3–4 when using multiple-channel whitened EMGσ processing. The number of dynamic fit parameters (compared to the D=1 linear model, which had 42 dynamic fit parameters) doubles for D=2, triples for D=3 and quadruples for D=4. Thus, the nonlinear dynamic models have a very large number of parameters, which can be a challenge for robust least squares estimation. For this reason, our fit parameter estimates were regularized using the pseudo-inverse approach whenever *linear* least squares fitting was applied (Clancy et al., 2012, Press et al., 1994). In particular, note that regularized *linear* least squares estimation was used to find the initial guess parameters that seeded each of the *nonlinear* least squares estimators. When regularization was not used for the initial guess, several of the nonlinear optimizations failed to converge. More generally, the conditioning of the linear least squares fit (or convergence of the nonlinear least squares minimization) is improved by longer training durations, fewer parameters and data sets that excite all modes of the model (Ljung, 1999); hence our reason for using a broadband torque target in the experimental protocol. Of these factors, it is useful to note that our method of achieving a nonlinear dynamic model (raising EMGσ and its lag values to a power) does not use fit coefficients efficiently. Functions that facilitate a similar model shape, but utilize fewer fit coefficients—such as parallel cascade models (Hashemi et al., 2012)—might be more parsimonious.

For the polynomial-gain model, the best angle polynomial degree was A=2 in all cases. Since only six distinct joint angles were examined, it is likely that overfitting began to occur for degrees above A=2. The piece-wise-gain model avoided this issue entirely by fitting gain only at the available joint angles, facilitating interpolation between angles as a post hoc processing step. Spline functions are an excellent choice for such processing, as they preserve the value of the function at the knots (i.e., at the joint angles at which measurements were made) and provide a smooth fit in between.

The fixed postures imposed during these experiments facilitated study of the system identification methods, and may be representative of conditions experienced by prosthesis users whose remnant musculature may be fixed in orientation. But, fixed postures are not representative of the free movements made during most activities of daily living in non-amputees. Hence, future work should consider conditions during which the joint is dynamically changing angle. In doing so, models may need to consider differences in the EMGσ-torque relationship as a function of concentric vs. eccentric contraction (Komi et al., 2000). While three distinct models were studied in this work, we did not extensively study all possible model parameters (e.g., the number of dynamic model lags was fixed at Q=20, the pseudo-inverse tolerance was set at Tol = 0.0056), instead fixing these values based on a prior study (Clancy et al., 2012). Slight

292 tuning of these values might provide some additional reduction in torque error estimation, albeit rather
293 limited.

294 In summary, models were formed during constant-posture, torque-varying contractions ranging in joint
295 angle from 60^{o} to 135^{o}, using advanced EMGσ estimation techniques and multiple training trials. With
296 EMG-torque models formed separately at each of the six distinct joint angles, a minimum "gold standard"
297 error of 4.01 ± 1.2% MVC_{F90} resulted [EMGσ polynomial degree of D=3, three training records (78 s) and
298 multiple-channel whitened EMGσ processing]. The piece-wise-gain model, which facilitates interpolation
299 across angles, achieved a statistically equivalent error of 4.06 ± 1.2% MVC_{F90}. Compared to single-channel
300 unwhitened EMGσ processing, multiple-channel whitened EMGσ processing reduced torque error by 25%
301 on average. Increasing the training trial duration from 26 s to 52 s reduced average error by 12%, while
302 increasing it from 26 s to 78 s reduced average error by 16%. These results further support the experimental
303 observation that the shape of the EMGσ-torque relationship is the same at each joint angle, but is scaled by
304 a gain factor that is distinct at each angle.
305
306 **Conflict of Interest**
307 None declared.
308
309 **Acknowledgements**
310 Supported by the U.S. Army under ASAMRAA Grant WX81XWH-11-1-0631.
311
312 **References**
313
314 An KN, Cooney WP, Chao EY, Askew LJ, Daube JR. Determination of forces in extensor pollicis longus
315 and flexor pollicis longus of the thumb. J Applied Physiol: Resp Env Exer Physiol 1983; 54: 714–719.
316 Clancy EA, Bida O, Rancourt D. Influence of advanced electromyogram (EMG) amplitude processors on
317 EMG-to-torque estimation during constant-posture, force-varying contractions. J Biomech 2006; 39:
318 2690–2698.
319 Clancy EA, Farry KA. Adaptive whitening of the electromyogram to improve amplitude estimation. IEEE
320 Trans Biomed Eng 2000; 47: 709 719.
321 Clancy EA, Hogan N. Multiple site electromyograph amplitude estimation. IEEE Trans Biomed Eng 1995;
322 42: 203–211.

323 Clancy EA, Hogan N. Relating agonist-antagonist electromyograms to joint torque during isometric,
324 quasi-isotonic, non-fatiguing contractions. IEEE Trans Biomed Eng 1997; 44: 1024–1028.
325 Clancy EA, Liu L, Liu P, Moyer DV, Identification of constant-posture EMG-torque relationships about
326 the elbow using nonlinear dynamic models. IEEE Trans Biomed Eng 2012; 59: 205–212.
327 Clancy EA, Morin EL, Merletti R. Sampling, noise-reduction and amplitude estimation issues in surface
328 electromyography. J Electromyo Kinesiol 2002; 12: 1 16.
329 Disselhorst-Klug C, Schmitz-Rode T, Rau G. Surface electromyography and muscle force: Limits in
330 sEMG-force relationship and new approaches for applications. Clin Biomech 2009; 24: 225-235.
331 Doheny EP, Lowery MM, FitzPatrick DP, O'Malley MJ. Effect of elbow joint angle on force-EMG
332 relationships in human elbow flexor and extensor muscles. J Electromyogr Kinesiol 2008; 18:
333 760–770.
334 Doorenbosch CMA, Harlaar J. A clinically applicable EMG-force model to quantify active stabilization of
335 the knee after a lesion of the anterior cruciate ligament. Clin Biomech 2003; 18: 142–149.
336 Gottlieb GL and Agarwal GC. Dynamic relationship between isometric muscle tension and the
337 electromyogram in man. J Applied Physiol 1971; 30: 345–351.
338 Hagg GM, Melin B, Kadefors R. Applications in Ergonomics. In: Merletti R, Parker PA, editors.
339 Electromyography: Physiology, Engineering, and Noninvasive Applications. Hoboken, NJ: John Wiley
340 & Sons, Inc., 2004: 343–363.
341 Hasan Z, Enoka RM. Isometric torque-angle relationship and movement-related activity of human elbow
342 flexors: Implications for the equilibrium-point hypothesis. Exp Brain Res 1985; 59: 441–450.
343 Hashemi J, Morin E, Mousavi P, Mountjoy K, Hashtrudi-Zaad K. EMG-force modeling using parallel
344 cascade identification. J Electromyogr Kinesiol 2012; 22: 469–477.
345 Hashemi J, Morin E, Mousavi P, Hashtrudi-Zaad K. Surface EMG force modeling with joint angle based
346 calibration. J Electromyogr Kinesiol 2013; 23: 416–424.
347 Heckathorne CW, Childress DS. Relationships of the surface electromyogram to the force, length, velocity,
348 and contraction rate of the cineplastic human biceps. Am J Phys Med 1981; 60: 1–19.
349 Hof AL, Van den Berg J. EMG to force processing I: An electrical analogue of the hill muscle model. J
350 Biomech 1981; 14: 747–758.
351 Hogan N, Mann RW. Myoelectric signal processing: Optimal estimation applied to
352 electromyography—Part 1. Derivation of the optimal myoprocessor. IEEE Trans Biomed Eng 1980a;
353 27: 382–395.

354 Hogan N, Mann RW. Myoelectric signal processing: Optimal estimation applied to
355 electromyography—Part 11. Experimental demonstration of optimal myoprocessor performance. IEEE
356 Trans Biomed Eng 1980b; 27: 396–410.
357 Inman VT, Ralston HJ, Saunders JB, Feinstein B, Wright EW. Relation of human electromyogram to
358 muscular tension. Electroencephalogr Clin Neurophysiol 1952; 4: 187–194.
359 Komi PV, Linnamo V, Silventoinen P, Sillanpaa M. Force and EMG power spectrum during eccentric and
360 concentric actions. Med Sci Sports Exerc 2000;32: 1757–1762.
361 Kumar S, Mital A, editors. Electromyography in Ergonomics. Briston, PA: Taylor & Francis, 1996.
362 Lawrence JH, DeLuca CJ. Myoelectric signal versus force relationship in different human muscles. J Appl
363 Physiol 1983; 54: 1653–1659.
364 Liu L, Liu P, Clancy EA, Scheme E, Englehart KB. Electromyogram whitening for improved classification
365 accuracy in upper limb prosthesis control. IEEE Trans Neural Sys Rehabil Eng 2013a; 21: 767–774.
366 Liu P, Liu L, Martel F, Rancourt D, Clancy EA. Influence of joint angle on EMG-torque model during
367 constant-posture quasi-constant-torque contractions. J Electromyogr Kinesiol 2013b; 23: 1020–1028.
368 Ljung L. System Identification: Theory for the User. Upper Saddle River, NJ: Prentice-Hall, 1999:
369 143–146, 444–452, 491–519.
370 Martin S, MacIsaac D. Innervation zone shift with changes in joint angle in the brachial biceps. J
371 Electromyogr Kinesiol 2006; 16: 144–148.
372 Mathiassen SE, Winkel J, Hagg GM. Normalization of surface EMG amplitude from the upper trapezius
373 muscle in ergonomic studies—A review. J Electromyogr Kinesiol 1995; 5: 197–226.
374 Messier RH, Duffy J, Litchman HM, Paslay PR, Soechting JF, Stewart PA. The electromyogram as a
375 measure of tension in the human biceps and triceps muscles. Int J Mech Sci 1971; 13: 585–598.
376 Miller I, Freund JE. Probability and Statistics for Engineers. Englewood Cliffs, NJ: Prentice-Hall, Inc.,
377 1977: 272–275.
378 Parker P, Englehart K, Hudgins B. Myoelectric signal processing for control of powered limb prostheses. J
379 Electromyogr Kinesiol 2006; 16: 541–548.
380 Potvin JR, Brown SHM. Less is more: High pass filtering, to remove up to 99% of the surface EMG signal
381 power, improves EMG-based biceps brachii muscle force estimates. J Electromyogr Kinesiol 2004; 14:
382 389 399.
383 Prakash P, Salini CA, Tranquilli JA, Brown DR, Clancy EA. Adaptive whitening in electromyogram
384 amplitude estimation for epoch-based applications. IEEE Trans Biomed Eng 2005; 52: 331–334.

385 Press WH, Teukolsky SA, Vetterling WT, Flannery BP. Numerical recipes in C. New York: Cambridge
386 Univ. Press; 2nd ed., 1994, 671–681.
387 Rack PMH, Westbury DR. The effects of length and stimulus rate on tension in the isometric cat soleus
388 muscle. J Physiol 1969; 204: 443–460.
389 Rainoldi A, Nazzaro M, Merletti R, Farina D, Caruso I, Gaudenti S. Geometrical factors in surface EMG of
390 the vastus medialis and lateralis muscles. J Electromyo Kinesiol 2000;10: 327 336.
391 Sanger TD. Bayesian filtering of myoelectric signals. J Neurophysiol 2007; 97: 1839–1845.
392 Shin D, Kim J, Koike Y. A Myokinetic Arm Model for Estimating Joint Torque and Stiffness from EMG
393 Signals during Maintained Posture. J Neurophysiol 2009; 101: 387–401.
394 Solomonow M, Guzzi A, Baratta R, Shoji H, D'Ambrosia R. EMG-force model of the elbow's antagonistic
395 muscle pair: the effect of joint position, gravity and recruitment. Am J Phys Med 1986; 65: 223–244.
396 Staudenmann D, Kingma I, Daffertshofer A, Stegeman DF, van Dieen JH. Heterogeneity of muscle
397 activation in relation to force direction: A multi-channel surface electromyography study on the triceps
398 surae muscle. J Electromyogr Knnesiol 2009; 19: 882-895.
399 Staudenmann D, Roeleveld K, Stegeman DF, van Dieen J. Methodological aspects of SEMG recordings
400 for force estimation—A tutorial and review. J Electromyogr Kinesiol 2010; 20: 375–387.
401 Thelen DG, Schultz AB, Fassois SD, Ashton-Miller JA. Identification of dynamic myoelectric
402 signal-to-force models during isometric lumbar muscle contractions. J Biomech 1994; 27: 907–919.
403 Vieira TMM, Merletti R, Mesin L. Automatic segmentation of surface EMG images: Improving the
404 estimation of neuromuscular activity. J Biomech 2010; 43: 2149–2158.
405 Vredenbregt J, Rau G. Surface electromyography in relation to force, muscle length and endurance. New
406 Developments in Electromyogr, Clin Neurophysiol 1973; 1: 607–622.
407 Zajac FE. Muscle and tendon: properties, models, scaling, and application to biomechanics and motor
408 control. Crit Rev Biomed Eng 1989; 17: 359–411.
409
410
411 Conflict of Interest Statement: None of the authors is aware of any conflict of interest associated with this
412 work or its submission to the Journal of Electromyography and Kinesiology.
413
414
415

Table 1

Mean ± std. dev. EMG-torque test error results from all three models, for *single-channel unwhitened* EMG processing (errors expressed in % mean absolute MVC flexion at 90° from 22 subjects). Each training record was 26 s in duration.

Training records	Angle polynomial degree (A)	EMGσ polynomial degree (D) $D = 1$	$D = 2$	$D = 3$	$D = 4$
Angle-Specific Model:					
One	N/A	6.36 ± 2.3	5.90 ± 2.0	6.17 ± 2.3	6.56 ± 2.6
Two	N/A	6.00 ± 2.1	5.44 ± 1.9	5.54 ± 2.0	5.71 ± 2.2
Three	N/A	5.87 ± 2.0	**5.28 ± 1.8**	5.30 ± 1.7	5.37 ± 1.7
Polynomial-Gain Model:					
One	1	6.59 ± 2.2	5.95 ± 2.1	5.92 ± 2.1	6.25 ± 2.2
	2	6.45 ± 2.4	5.86 ± 2.2	**5.81 ± 2.1**	6.06 ± 2.1
	3	6.48 ± 2.3	6.08 ± 2.3	6.13 ± 2.3	6.74 ± 3.1
	4	7.16 ± 2.4	6.50 ± 2.2	6.48 ± 2.2	6.64 ± 2.5
Two	1	6.48 ± 2.2	5.85 ± 2.1	5.75 ± 2.0	5.78 ± 2.0
	2	6.30 ± 2.2	5.71 ± 2.1	**5.62 ± 2.0**	5.68 ± 2.0
	3	6.30 ± 2.2	5.83 ± 2.1	6.16 ± 2.3	6.30 ± 2.4
	4	8.35 + 5.2	6.88 + 3.1	6.53 + 2.5	6.35 + 2.5
Three	1	6.44 ± 2.2	5.80 ± 2.1	5.72 ± 2.1	5.69 ± 1.9
	2	6.24 ± 2.2	5.66 ± 2.1	**5.61 ± 2.2**	**5.61 ± 2.0**
	3	6.22 + 2.2	5.81 + 2.1	5.91 + 2.2	6.54 + 2.8
	4	8.08 ± 3.5	6.20 ±2.2	7.06 ± 2.8	6.80 ± 3.0
Piece-Wise-Gain Model:					
One	N/A	6.41 ± 2.3	5.87 ± 2.2	6.12 ± 2.3	11.3 ± 20
Two	N/A	6.09 ± 2.1	5.53 ± 1.9	5.59 ± 1.9	5.74 ± 1.9
Three	N/A	5.95 ± 2.0	**5.41 ± 1.8**	5.44 ± 1.9	5.54 ± 1.9

424 **Table 2**
425 Mean ± std. dev. EMG-torque test error results from all three models, for *multiple-channel whitened* EMG
426 processing (errors expressed in % mean absolute MVC flexion at 90° from 22 subjects). Each training
427 record was 26 s in duration.
428

Training records	Angle polynomial degree (A)	EMGσ polynomial degree (D) $D-1$	$D-2$	$D-3$	$D-4$
Angle-Specific Model:					
One	N/A	4.91 ± 1.8	4.66 ± 1.7	4.75 ± 1.7	5.01 ± 2.1
Two	N/A	4.60 ± 1.6	4.17 ± 1.3	4.17 ± 1.3	4.25 ± 1.4
Three	N/A	4.49 ± 1.5	4.04 ± 1.2	**4.01 ± 1.2**	4.05 ± 1.2
Polynomial-Gain Model:					
One	1	5.21 ± 1.6	4.74 ± 1.5	4.70 ± 1.4	4.80 ± 1.4
	2	4.90 ± 1.7	4.46 ± 1.5	**4.41 ± 1.3**	4.47 ± 1.3
	3	4.94 ± 1.7	4.57 ± 1.5	4.68 ± 1.4	4.77 ± 1.4
	4	6.28 ± 2.4	5.03 ± 1.6	5.03 ± 1.5	5.08 ± 1.7
Two	1	5.12 ± 1.6	4.65 ± 1.4	4.57 ± 1.3	4.56 ± 1.3
	2	4.77 ± 1.6	4.33 ± 1.4	4.25 ± 1.3	**4.23 ± 1.2**
	3	4.86 ± 1.6	4.39 ± 1.5	4.49 ± 1.4	4.47 ± 1.4
	4	6.22 ± 2.0	5.56 ± 3.2	5.11 ± 1.7	4.73 ± 1.5
Three	1	5.09 ± 1.6	4.61 ± 1.4	4.53 ± 1.3	4.47 ± 1.2
	2	4.73 ± 1.6	4.28 ± 1.4	4.19 ± 1.2	**4.16 ± 1.2**
	3	4.89 ± 1.6	4.35 ± 1.4	4.37 ± 1.3	4.52 ± 1.4
	4	5.84 ± 1.7	4.92 ± 1.8	4.94 ± 1.6	4.84 ± 1.5
Piece-Wise-Gain Model:					
One	N/A	4.96 ± 1.8	4.50 ± 1.5	4.53 ± 1.4	4.78 ± 1.7
Two	N/A	4.67 + 1.6	4.23 + 1.4	4.16 + 1.2	4.23 + 1.2
Three	N/A	4.57 ± 1.5	4.14 ± 1.3	**4.06 ± 1.2**	4.19 ± 1.3

429
430

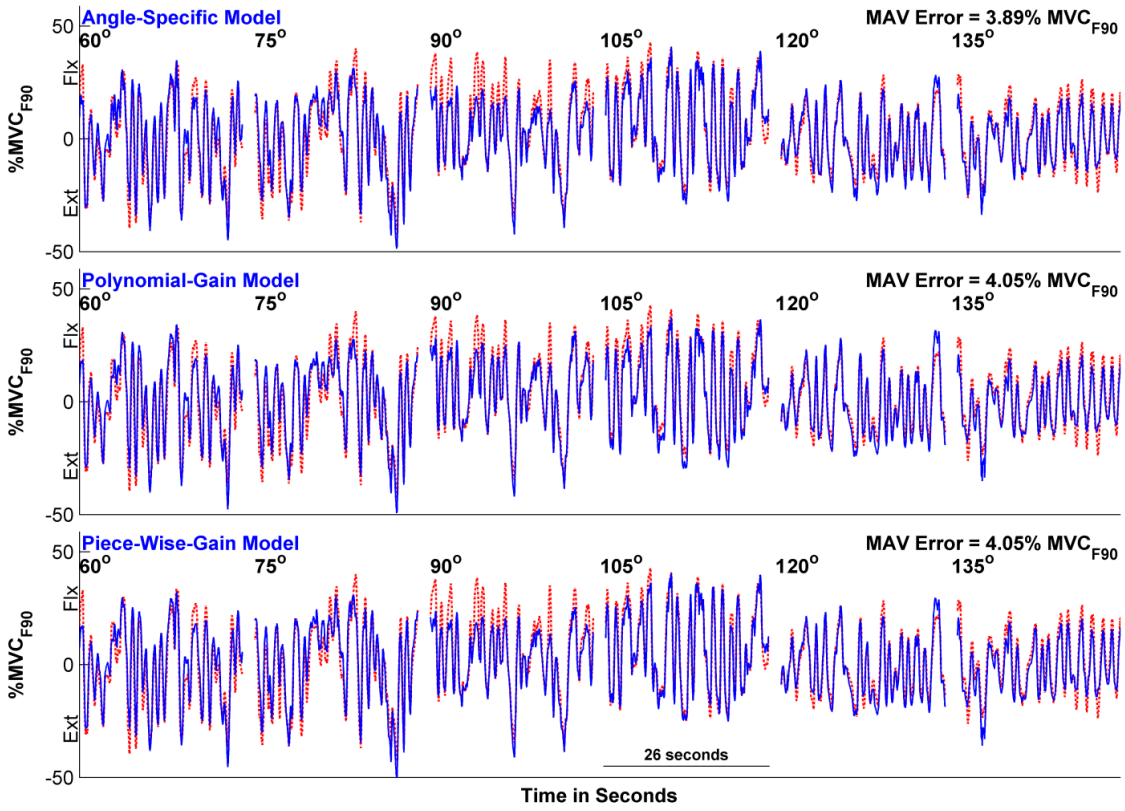

Fig. 1. Sample EMGσ-torque estimation results for the three models. Estimated torque (solid line) and actual torque (dotted line) vs. time. Data for each angle (26 s in duration, after exclusion of transients) were collected during distinct trials, then concatenated in the figure.

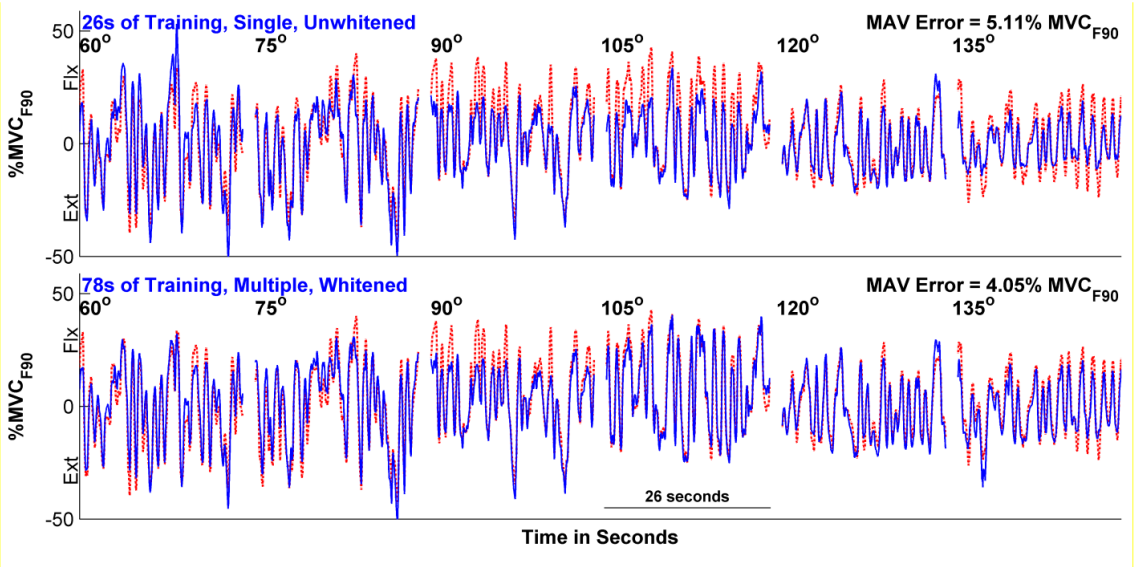

Fig. 2. Top: Sample EMGσ-torque results for the shortest (26 s) training duration, piece-wise gain model, using single-channel unwhitened EMGσ processing and a D=2 nonlinear dynamic model (20th order). Bottom: Sample EMGσ-torque results for the longest (78 s) training duration, piece-wise gain model, using multiple-channel whitened EMGσ processing and a D=3 nonlinear dynamic model (20th order). In each plot, estimate torque shown in solid line, actual torque shown in dotted line.

APPENDIX A

Design and Construction of the Experimental Finger Restraint Apparatus

Overview

The experimental finger restraint was custom-built at WPI, based on a design developed by Francois Martel and Denis Rancourt (Sherbrooke University, Sherbrooke, Quebec, Canada). Apparatus construction was based around the use of the modular aluminum framing system [10 Series Profiles, 80/20 Inc., Columbia City, IN, U.S.A.]. These modular aluminum profiles allow for easy cutting to a specified length and then manual assembly using various hardware accessories (angle brackets, screws, plates, leveling pads, etc.). Modular framing is a particularly strong choice when most/all of the structural pieces of the apparatus are attached at right angles. Attachment for the force sensor was then assembled to the framing. A back and side view of the completed experimental finger restraint apparatus is shown below.

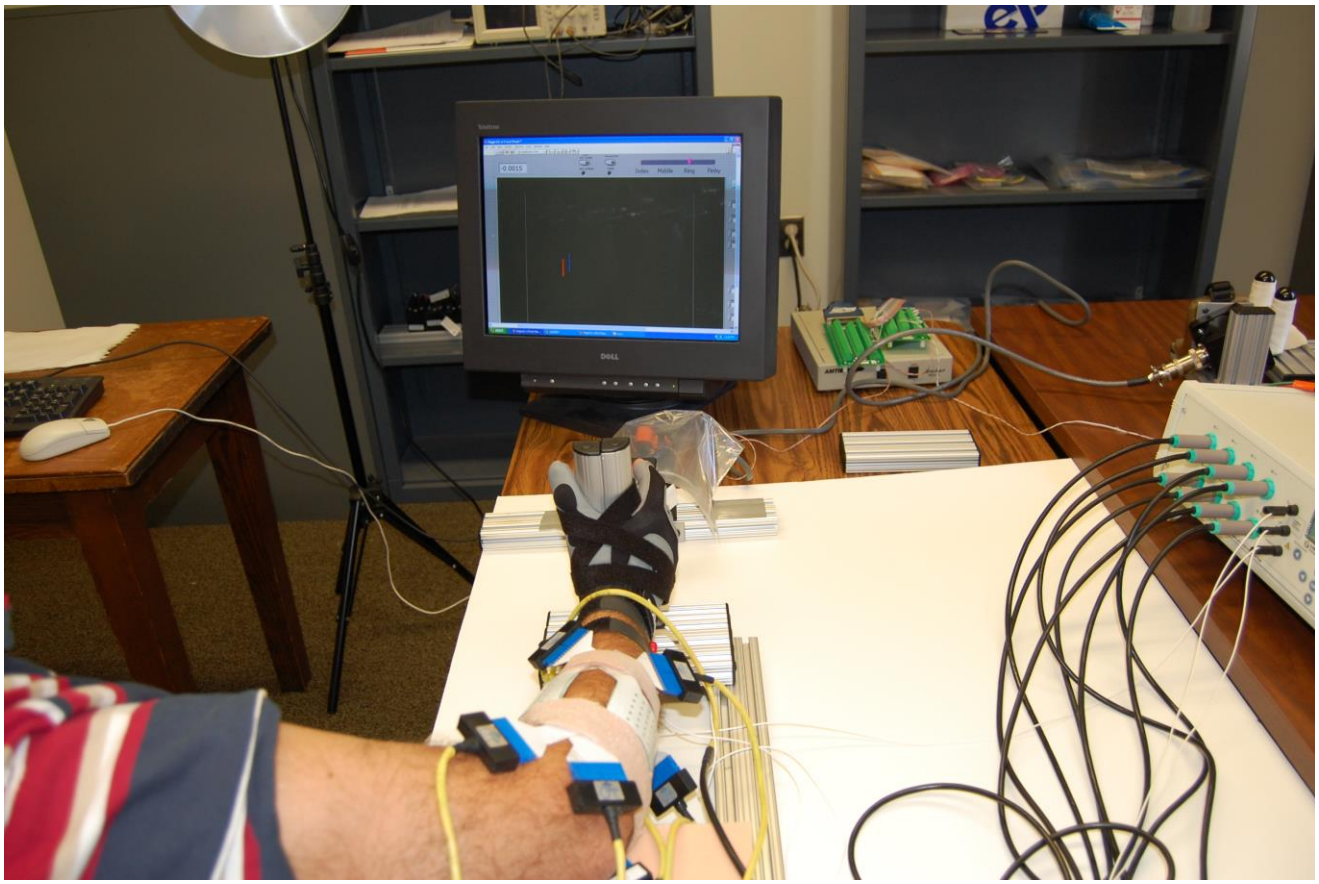

Fig. 1: Back view with hand/arm secured into the experimental finger restraint apparatus.

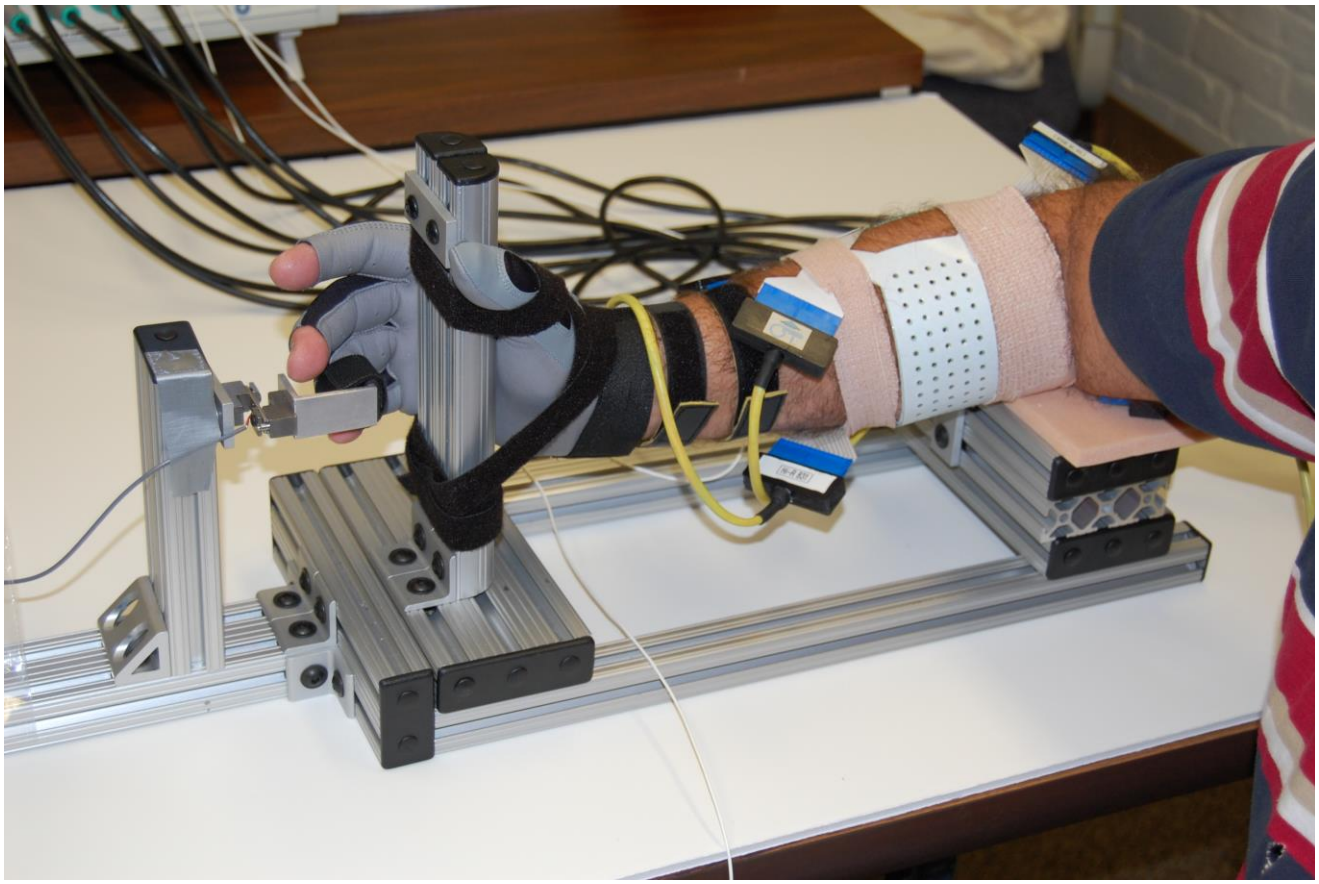

Fig. 2: Side view with hand/arm secured into the experimental finger restraint apparatus.

Parts List

Label	Quantity	80/20 Inc. Aluminum Framing Systems Part Name [Part Number]
A	2	Restraint Upright: T-slotted Profile (curved), length 8.25 inch [1012]
B	1	Support Beam: T-slotted Profile (rectangle with aspect ratio of 2), length 6 inch [1020]
C*	1	Support Beam: T-slotted Profile (rectangle with aspect ratio of 2), length 14 inch [1020]
D	1	Cross Beam: T-slotted Profile (rectangle with aspect ratio of 2), length 8 inch [1020]
E	1	Base: T-slotted Profile (rectangle with aspect ratio of 2), length 7 inch [1020]
F	4	Base: T-slotted Profile (rectangle with aspect ratio of 3), length 7 inch [1030]
G1*	1	Base: T-slotted Profile (rectangle with aspect ratio of 2), length 23 inch [1020]
G2	1	Base: T-slotted Profile (square), length 17 inch [1010]
	18	2 Hole 1/8” Inside Corner Bracket [4108]
	1	4 Hole Inside Gusset Corner Bracket [4134]
	4	2 Hole Joining Strip [4107]
	1	Plain End Caps for 1010 [2015-PI]
	2	Plain End Caps for 1012 [2022-PI]
	~6	Plain End Caps for 1020 [2025-PI]
	~8	Plain End Caps for 1030 [2026-PI]
	~22	1/4-20 x3/8 Flanged BHSCS Screw & Economy T-Nut [3386]
	~7	1/4-20 x1/2 BHSCS Screw & Economy T-Nut [3393]

Table of 80/20 Inc. Aluminum Framing System Parts. Profile parts are cut from stock Series 10 profiles.

* The length of these parts is not critical.

Label	Quantity	Omega Engineering, Inc. Load Cell and Amplifier [Part Number]
H	1	Thin Beam Load Cell with 40 Pound Capacity [LCL-040]
J	1	Strain Gage Amplifier with Voltage Output and 110 Vac Power [DMD-465WB]

Some Notes on Assembling Modular Aluminum Framing Systems

- The primary method for securing parts together in a modular framing system involves screwing a bracket/plate/etc. (which is a part ordered with the framing system) to a nut that is placed within the embedded track of the protrusion framing part. The nut must be placed into the framing from an open end of the part—it *cannot* be inserted throughout the length of the part. If both ends of the part have already been obstructed (e.g., as the part is incorporated into the apparatus), then the nut cannot be inserted. Instead, the apparatus must be partially de-constructed to insert the nut. Therefore, it is advantageous to pre-place the nuts within the appropriate track for each such piece of the system. In some cases, pre-placement of the nuts is not sufficient; rather, it is best to loosely secure one side of the attachment bracket/plate, etc.

- It is best to install end caps only after the complete apparatus is assembled. Once end caps are installed, nuts cannot be inserted using that end of the protrusion.

- It is best to only secure nuts to a modest torque until the entire apparatus is completed. Doing so may help the structure maintain its proper shape and is useful if portions of the structure need rework or access (e.g., to insert a nut).

Assembly of the Primary Frame

As shown in Fig. 3, the restraint contained a rectangular base (part “E”, part “F1”, parts “G1-2”), a cushioned elbow rest plate (parts “F2-3”), a restraint upright (parts “A1-2”), and beams to secure the load cell and amplifier (parts “B”, “C” and “D”).

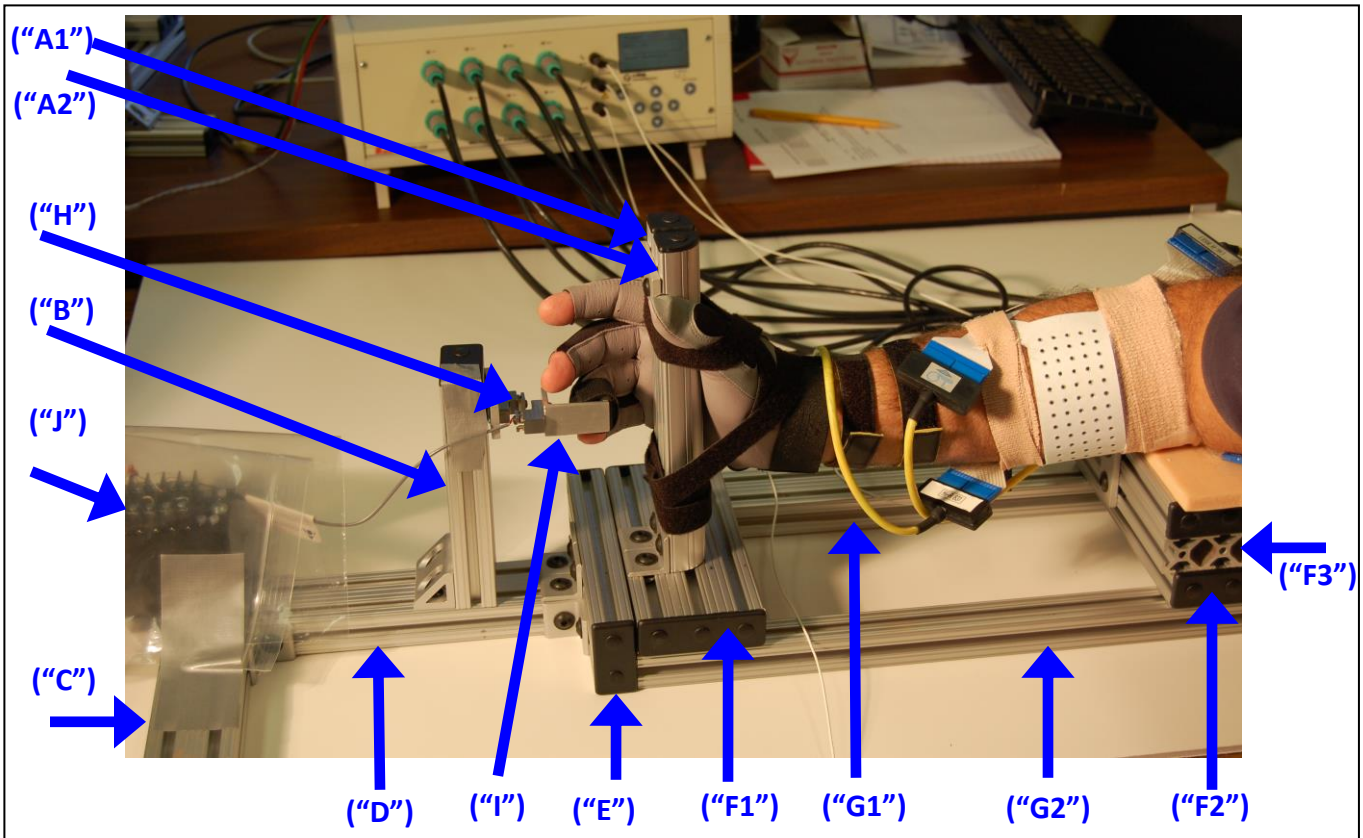

Fig. 3: Side view of the experimental apparatus labeling parts A - J of the assembly.

Two-hole joining strips and the 1/4-20 x1/2 BHSCS screws & economy T-nuts are used to tie parts "A1" and "A2" together and secure the load cell (part "H") to the support beam (part "B"). Two strips are used in total, as marked in Fig. 4.

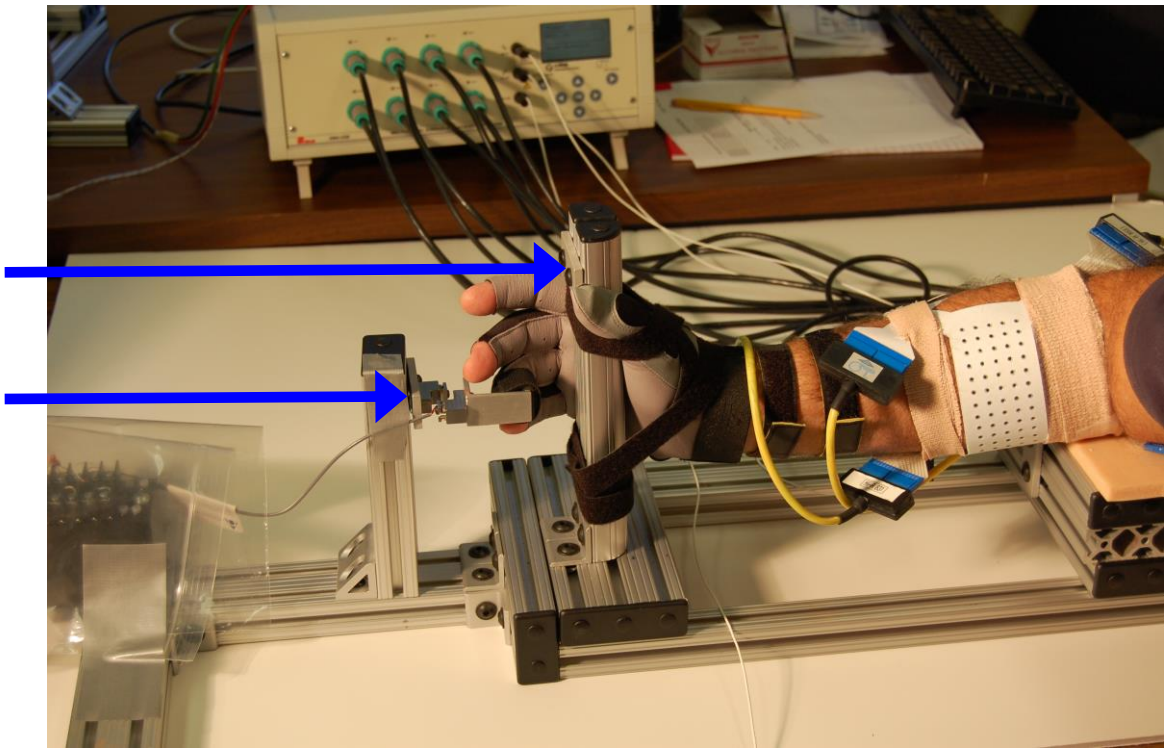

Fig. 4: Side view of the experimental apparatus labeling locations of the 2 Hole Joining strips and 1/4-20 x1/2 BHSCS screws & Economy T-nuts used to tie parts “A1” and “A2” together and secure the load cell (part “H”) to the support beam (part “B”).

The support beam (part “B”) is secured to the cross beam (part “D”) using the 4 hole inside gusset corner bracket and 1/4-20 X 1/2 BHSCS screws & economy T-nuts. One corner bracket of this kind is used, as marked in Fig. 5.

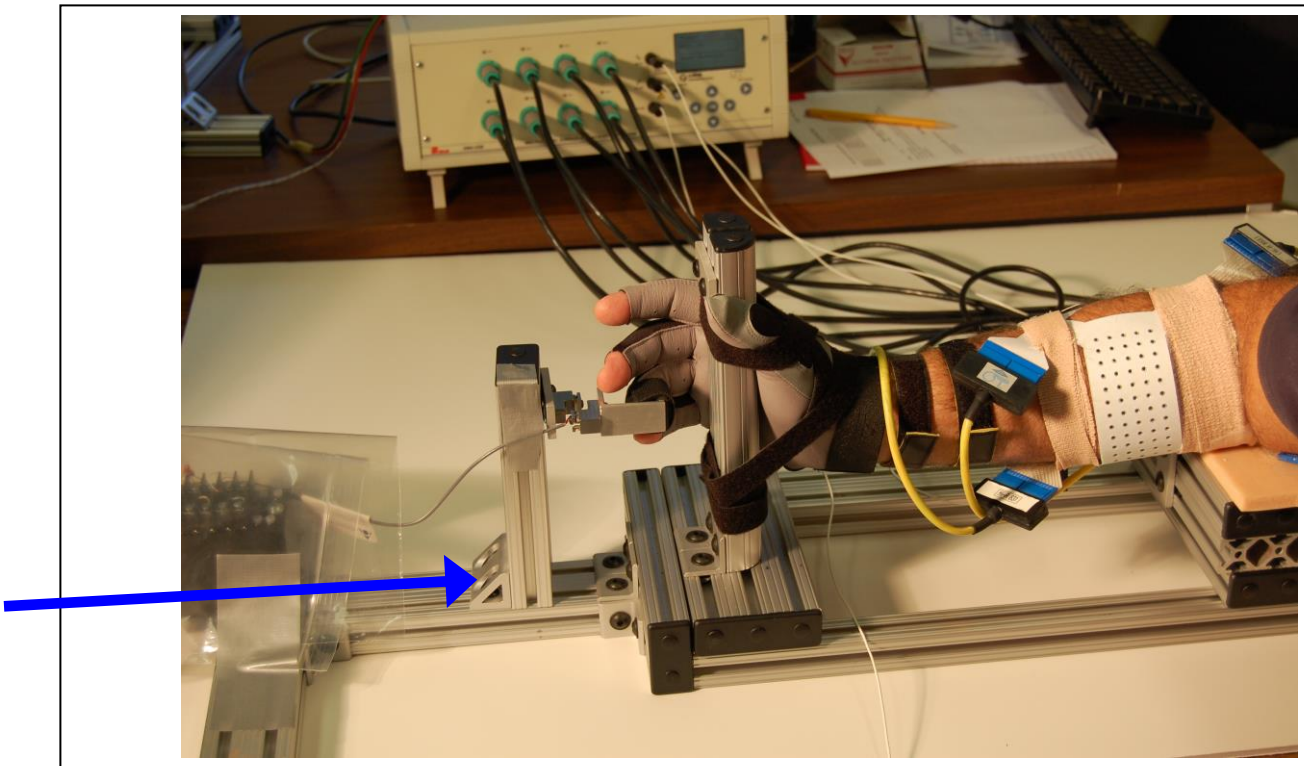

Fig. 5: Side view of the experimental apparatus labeling locations of the 4 Hole Inside Gusset Corner bracket and 1/4-20 X 1/2 BHSCS screws & Economy T-nuts used to secure the support beam (part "B") to the cross beam (part "D").

Parts C, D, E, F1, G1, G2, and F2 are secured to each other using the 2 hole 1/8" inside corner brackets and 1/4-20 x3/8 flanged BHSCS screws & economy T-nuts. 18 corner bracket of this kind are used in total, as marked in Fig.6.

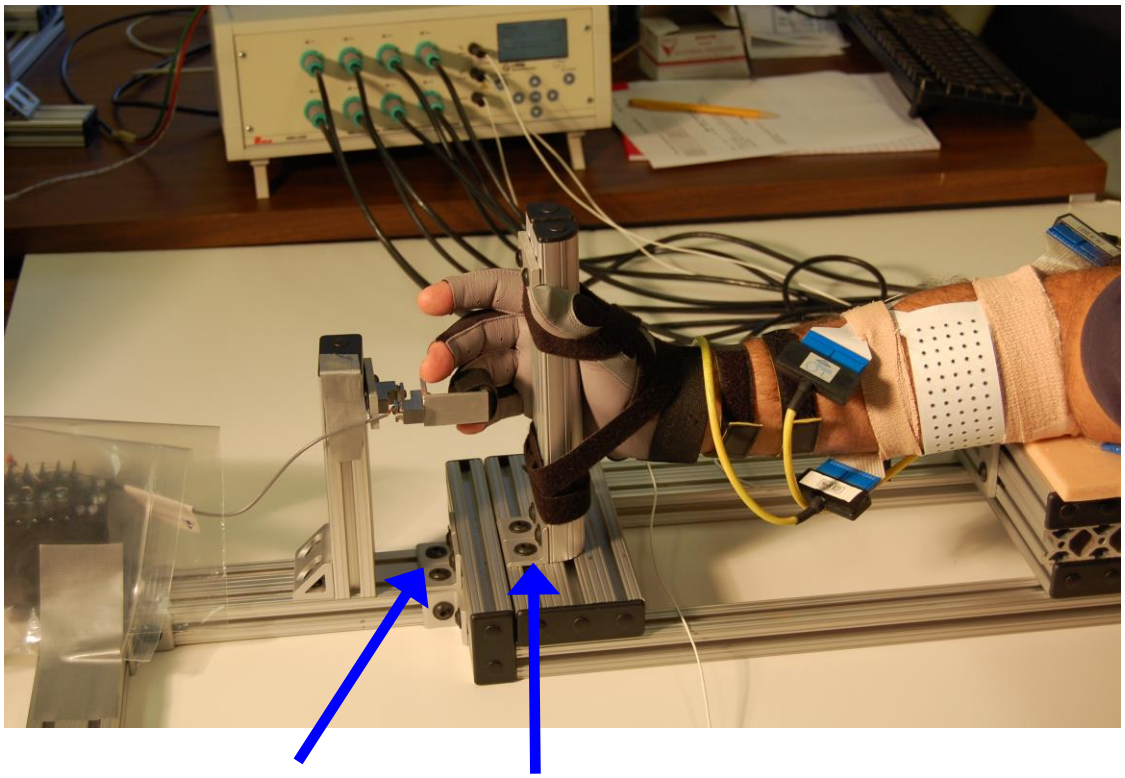

(a)

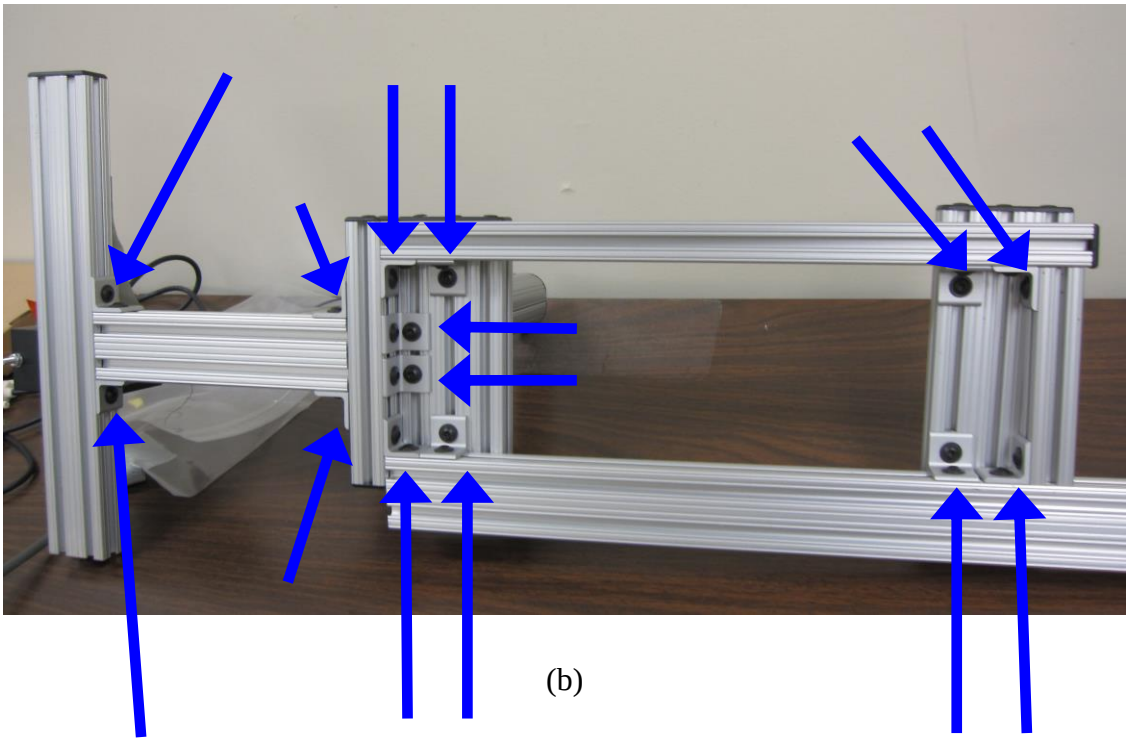

(b)

Fig. 6: Side view (a) and bottom view (b) of the experimental apparatus labeling locations of the 2 Hole 1/8" Inside Corner brackets and 1/4-20 x3/8 Flanged BHSCS screws & Economy T-nuts used to secure the base (Parts C, D, E, F1-2, and G1-2).

A custom piece (part “I”) is attached to the load cell (part “H”) used a regular screw, and the amplifier (part “J”) is secured to part “C” using a long regular screw and a 1/4-20 Economy T-Nut, as marked in Fig. 7.

Part “F3” is not secured to the apparatus. It can be put on or taken away from part “F2” to adjust the height of the elbow. Part “F3” is made of two pieces of the same size of part “F1”or “F2”. Two 2-hole joining strips and 1/4-20 x3/8 flanged BHSCS screws & economy T-nuts are used to tie the two pieces together, as marked in Fig. 8.

When appropriate, end caps are inserted into the end of each aluminum beam.

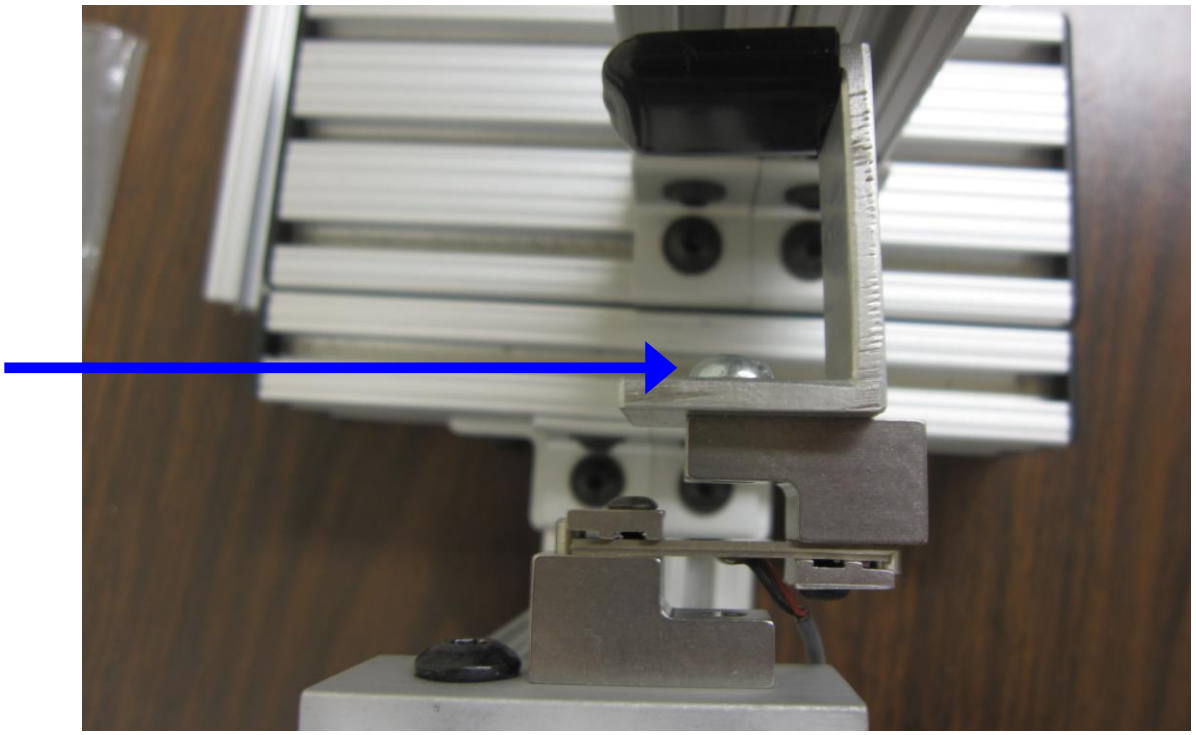

(a)

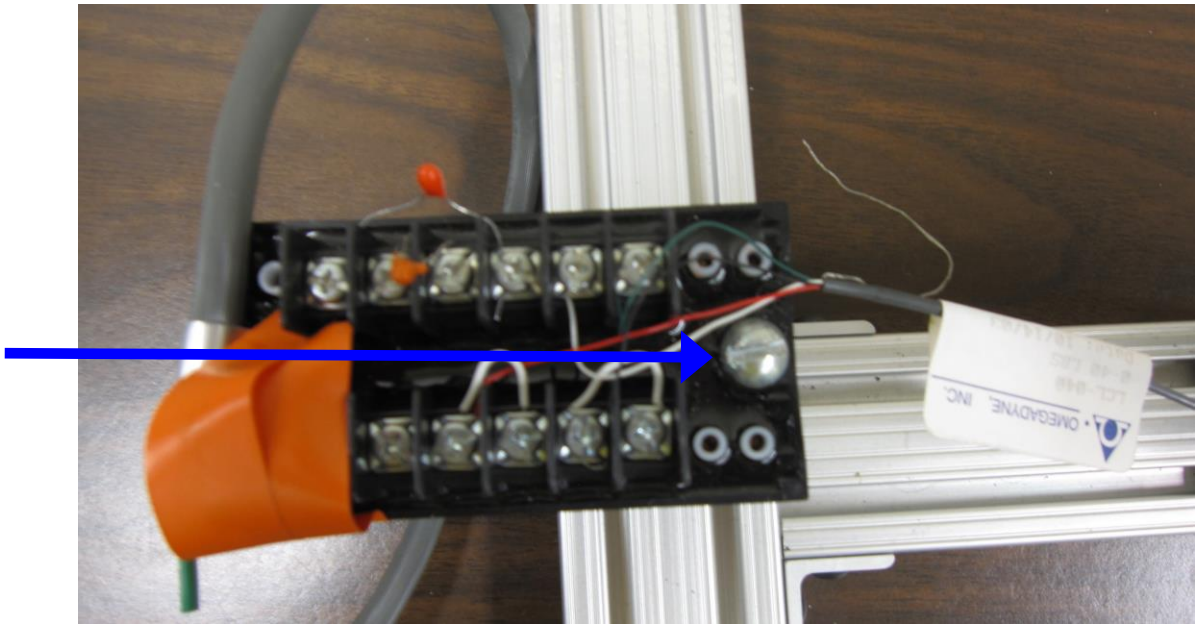

(b)

Fig. 7: (a) Aerial view of the custom piece (part "I") and load cell (part "H") labeling locations of the regular screw. (b) Aerial view of the amplifier (part "J") labeling locations of the long regular screw and 1/4-20 Economy T-Nut.

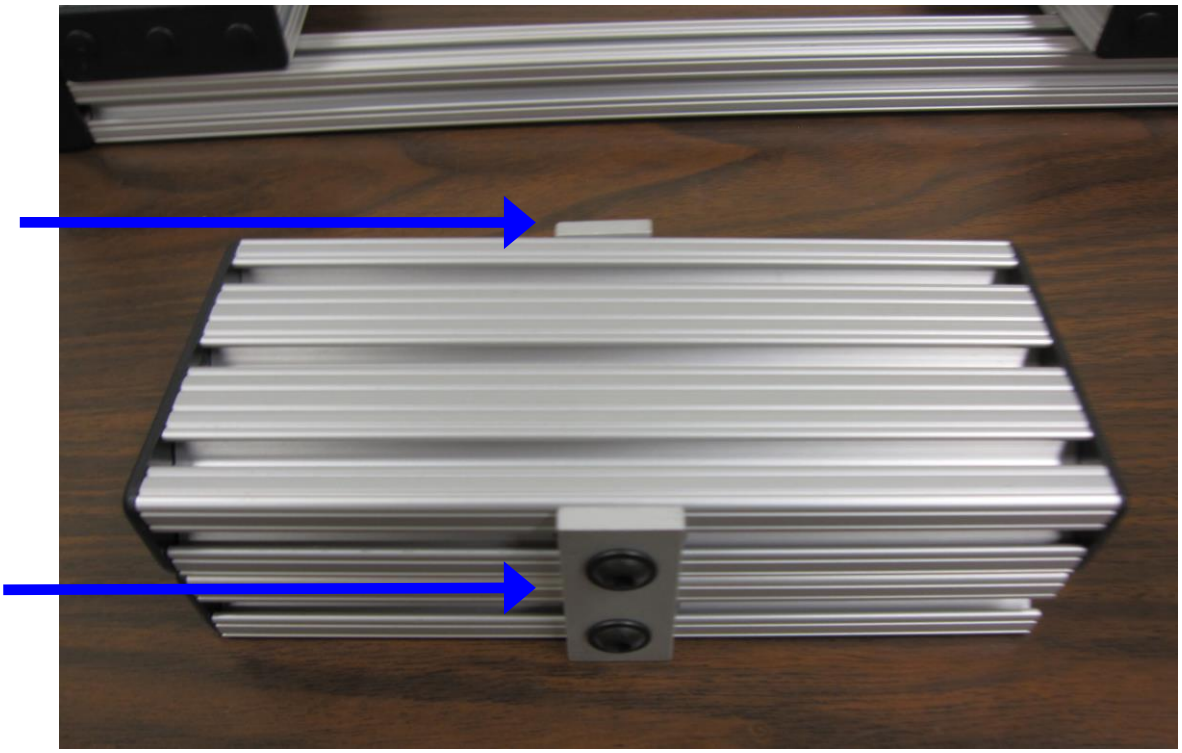

Fig. 8: Aerial view of part “F3” labeling locations of the 2 Hole Joining strips and 1/4-20 x3/8 Flanged BHSCS screws & Economy T-nuts.

APPENDIX B

Design and Construction of the Experimental Wrist Restraint Apparatus

Overview

The experimental wrist restraint device was used for simultaneous measurement of constant-posture wrist flexion-extension, ulnar-radial deviation and pronation-supination. The wrist restraint device was custom-built at WPI, based on a design developed by Francois Martel and Denis Rancourt (Sherbrooke University, Sherbrooke, Quebec, Canada). Apparatus construction was based around the use of the modular aluminum framing system [10 Series Profiles, 80/20 Inc., Columbia City, IN, U.S.A.]. These modular aluminum profiles allow for easy cutting to a specified length and then manual assembly using various hardware accessories (angle brackets, screws, plates, leveling pads, etc.). Modular framing is a particularly strong choice when most/all of the structural pieces of the apparatus are attached at right angles. Attachment for the load cell was then assembled to the framing. A back and a side view of the completed experimental wrist restraint apparatus is shown in Fig.1 and Fig.2.

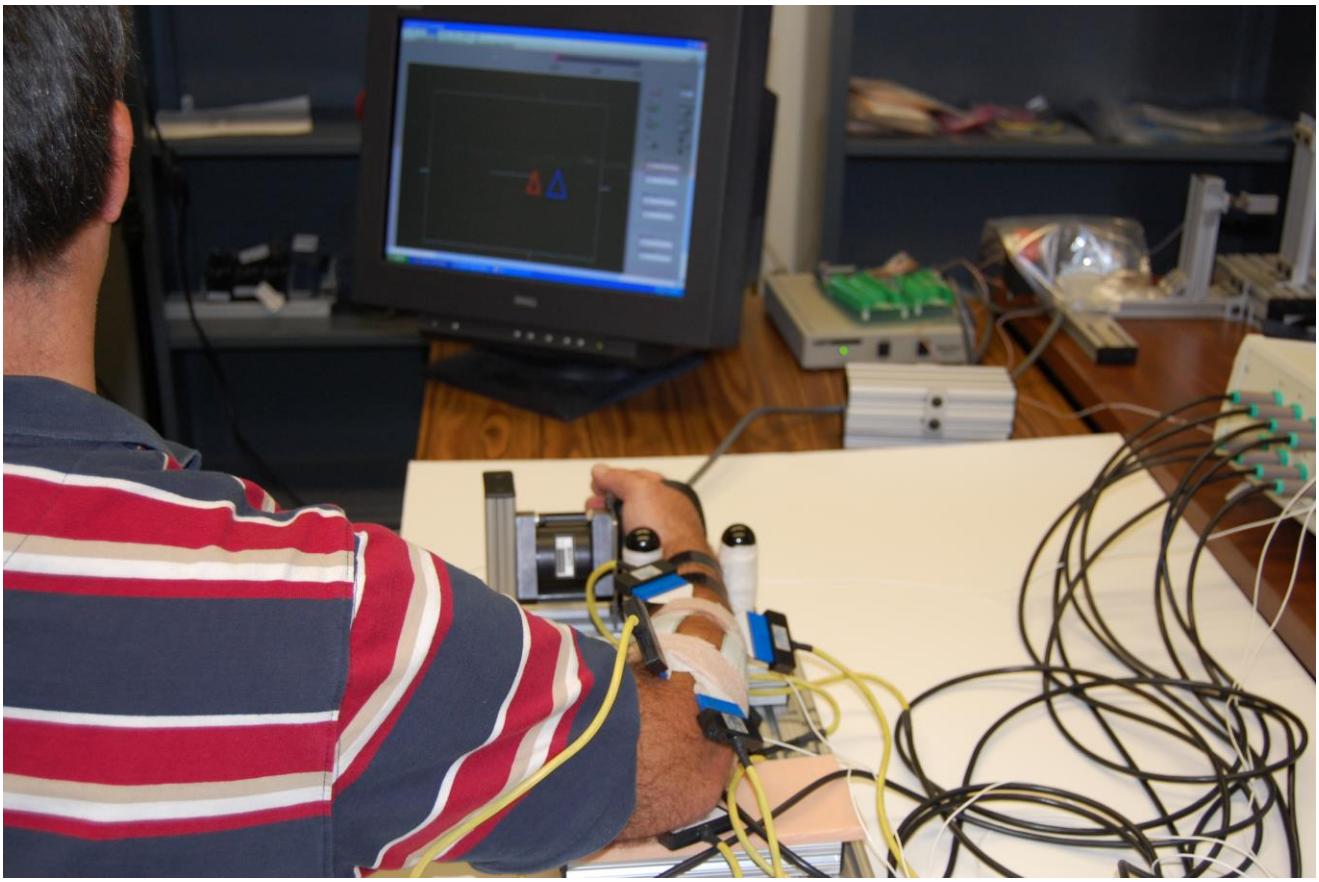

Fig. 1: Back view with hand/arm secured into the experimental wrist restraint apparatus.

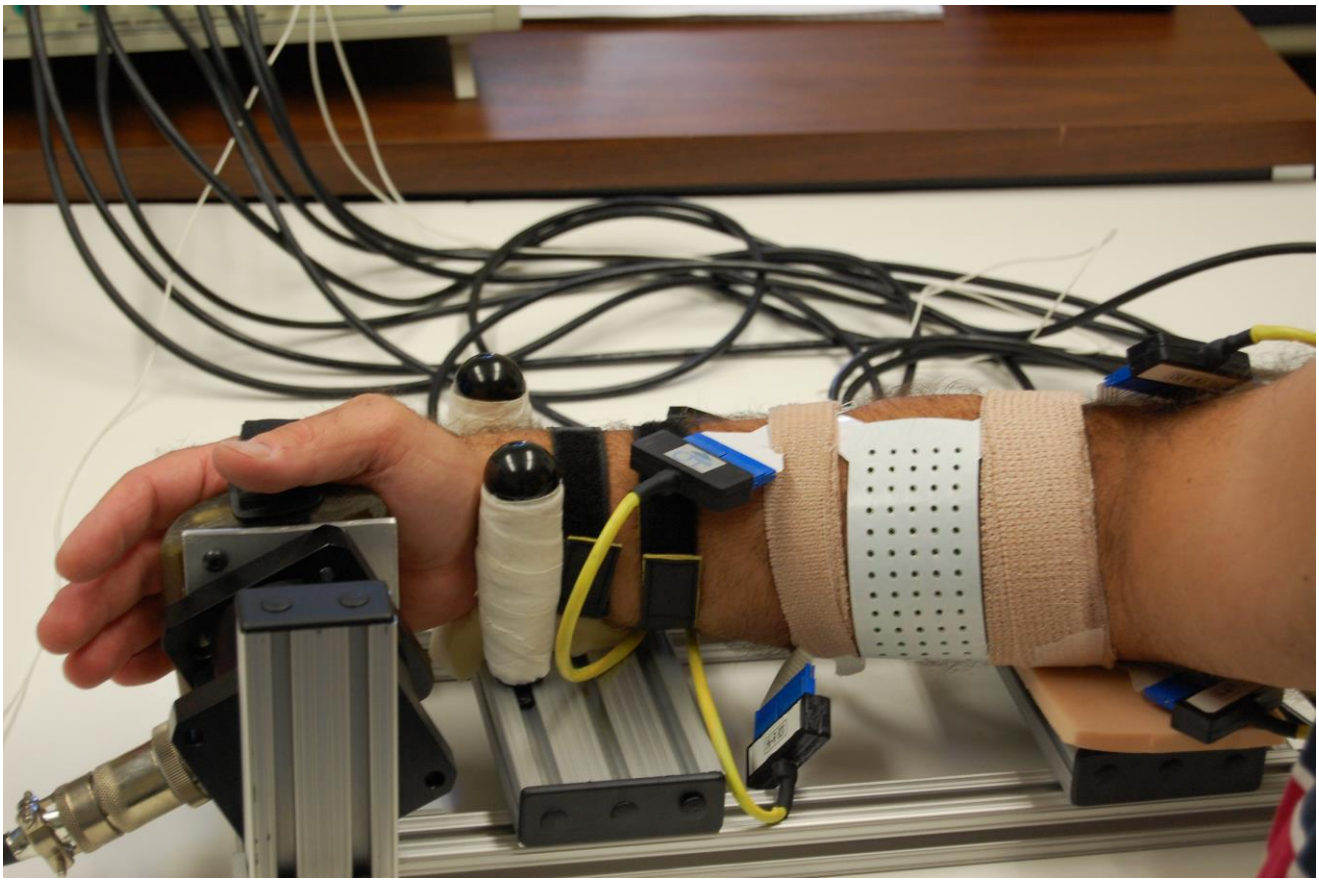

Fig. 2: Side view with hand/arm secured into the experimental wrist restraint apparatus.

Parts List

Label	Quantity	80/20 Inc. Aluminum Framing Systems Part Name [Part Number]
A	1	Support Beam: T-slotted Profile (rectangle with aspect ratio of 2), length 5 inch [1020]
B	1	Base: T-slotted Profile (rectangle with aspect ratio of 2), length 12 inch [1020]
C	2	Base: T-slotted Profile (rectangle with aspect ratio of 3), length 7 inch [1030]
D	1	Base: T-slotted Profile (square), length 14 inch [1010]
E	1	Base: T-slotted Profile (rectangle with aspect ratio of 2), length 20 inch [1020]
J	1	Base: T-slotted Profile (square), length 5 inch [1010]
	8	2 Hole 1/8” Inside Corner Bracket [4108]
	1	4 Hole Inside Gusset Corner Bracket [4134]
	1	2 Hole Joining Strip [4107]
	1	Plain End Caps for 1010 [2015-PI]
	4	Plain End Caps for 1020 [2025-PI]
	4	Plain End Caps for 1030 [2026-PI]
	18	1/4-20 x3/8 Flanged BHSCS Screw & Economy T-Nut [3386]
	4	1/4-20 x1/2 BHSCS Screw & Economy T-Nut [3393]

Table of 80/20 Inc. Aluminum Framing System Parts. Profile parts are cut from stock Series 10 profiles.

Label	Quantity	AMTI Load Cell and Amplifier [Part Number]
F	1	Multi-Component Force Transducer [MC3A-6-250]
*	1	MiniAmp Strain Gauge Amplifier [MSA-6]

* Shown in Fig. 4, it is attached to part “F”.

Label	Quantity	Handle [McMaster-Carr Part Number]
G	2	Phenolic Tapered Handles: Fluted, 1/4”-20 x 3/8” threaded stud, 1-1/8” diameter [62385K32]

Some Notes on Assembling Modular Aluminum Framing Systems

- The primary method for securing parts together in a modular framing system involves screwing a bracket/plate/etc. (which is a part ordered with the framing system) to a nut that is placed within the embedded track of the protrusion framing part. The nut must be placed into the framing from an open end of the part—it *cannot* be inserted throughout the length of the part. If both ends of the part have already been obstructed (e.g., as the part is incorporated into the apparatus), then the nut cannot be inserted. Instead, the apparatus must be partially de-constructed to insert the nut. Therefore, it is advantageous to pre-place the nuts within the appropriate track for each such piece of the system. In some cases, pre-placement of the nuts is not sufficient; rather, it is best to loosely secure one side of the attachment bracket/plate, etc.

- It is best to install end caps only after the complete apparatus is assembled. Once end caps are installed, nuts cannot be inserted using that end of the protrusion.

- It is best to only secure nuts to a modest torque until the entire apparatus is completed. Doing so may help the structure maintain its proper shape and is useful if portions of the structure need rework or access (e.g., to insert a nut).

Assembly of the Primary Frame

As shown in Fig. 3, the apparatus contained a rectangular base (parts “B”, “C1”, “D”, “E” and “J”), an elbow rest plate (part “C2”), and beam to secure the load cell and amplifier (part “A”). In the experiment, a cushion will be put on part “C2”, as shown in Fig. 2.

Parts “G1-2” are used to restrain the wrist. They are secured to part “C1” using Economy T-Nut from 80/20 Inc. Aluminum Framing Systems. The position of part “G2” can be adjusted for each individual subject.

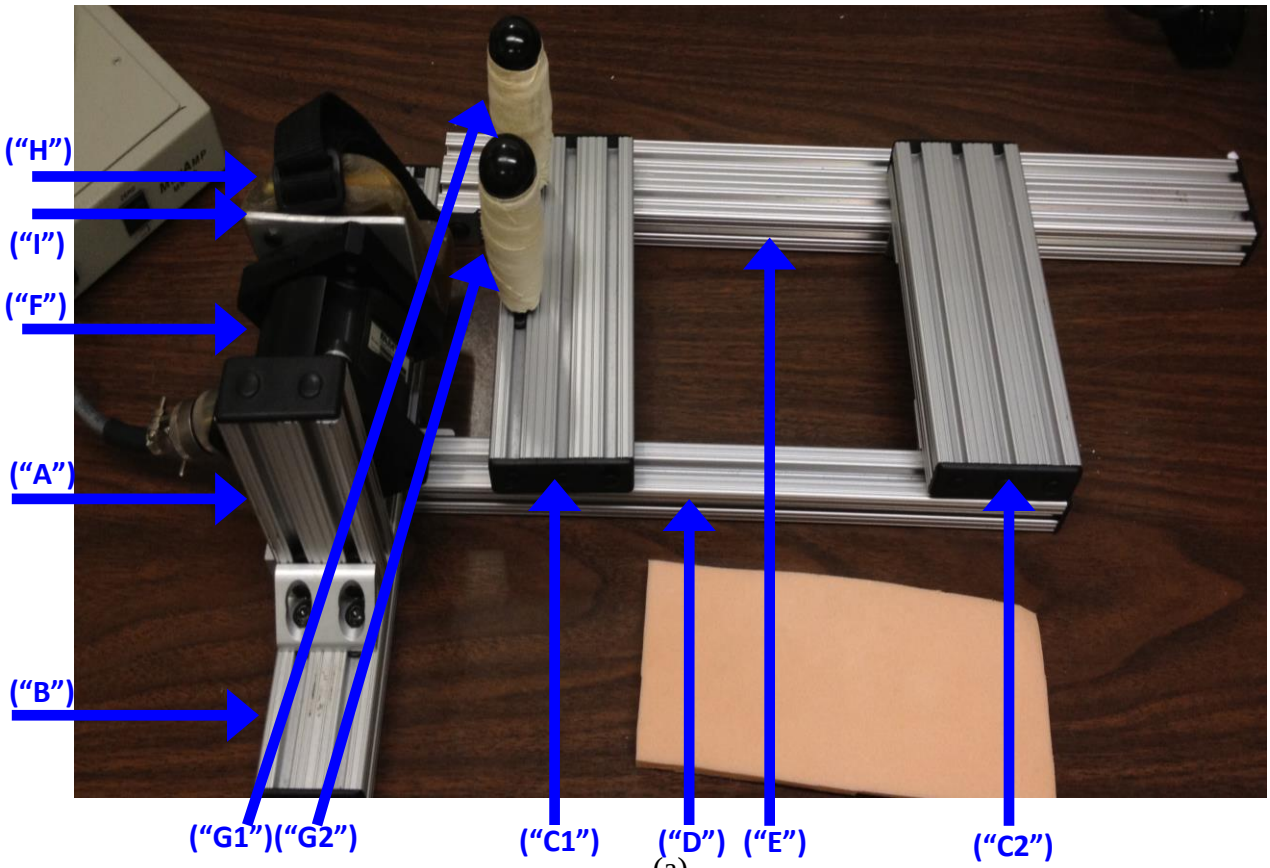

(a)

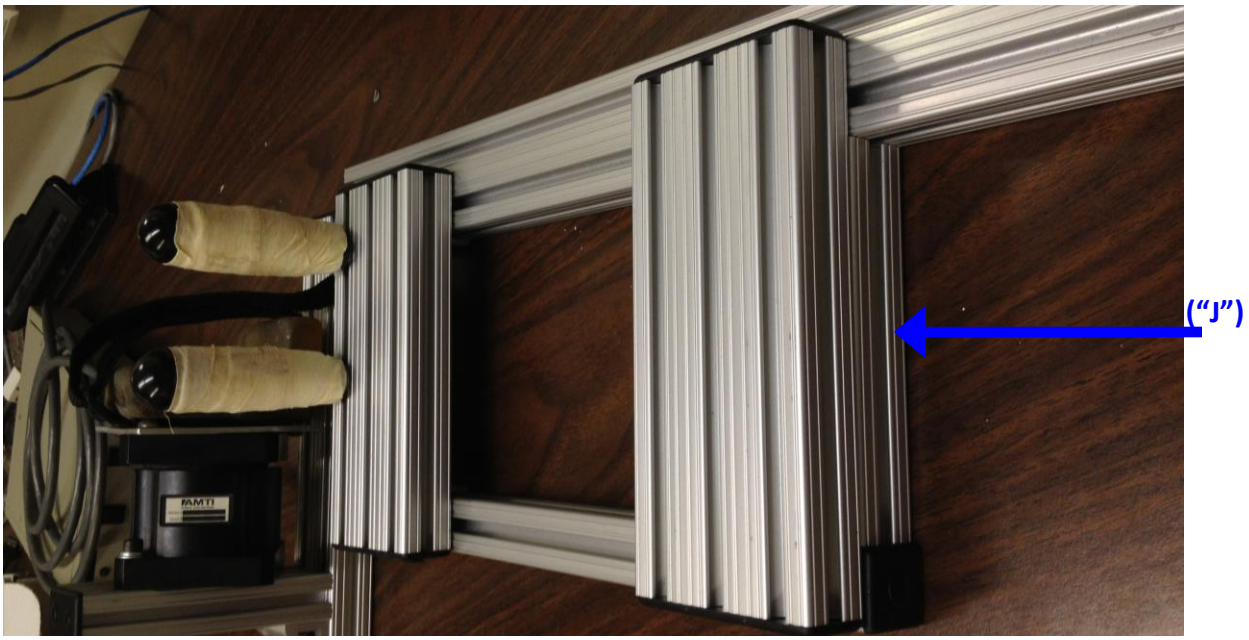

(b)

Fig. 3: Side (a) and end (b) views of the experimental apparatus labeling parts A - J of the assembly.

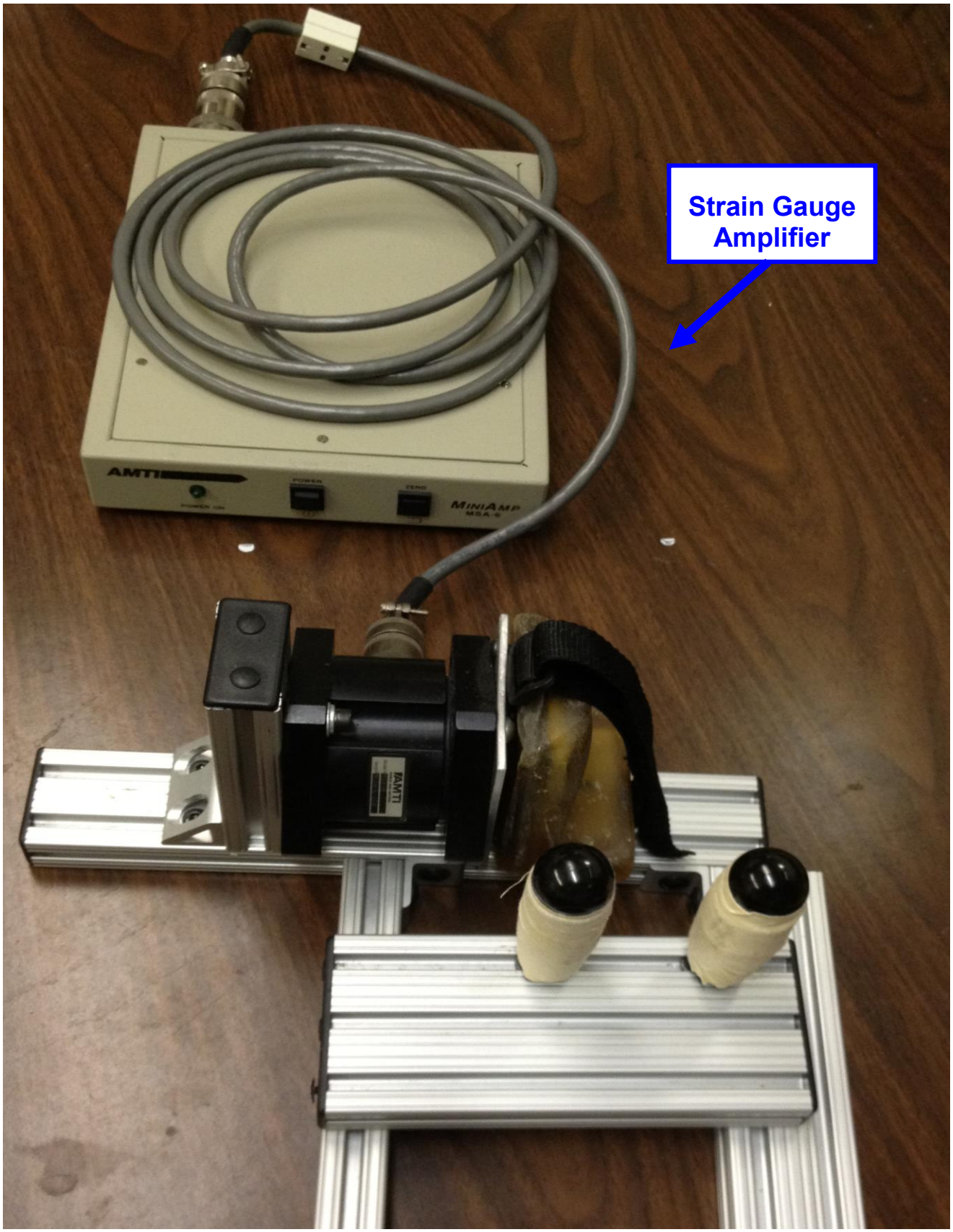

Fig. 4: Top view of the experimental apparatus with strain gauge amplifier attached.

Parts “A” and “B” are tied together using one 2-hole joining strip with the 1/4-20 x3/8 Flanged BHSCS screws & economy T-nuts and one 4-hole inside gusset corner bracket with 1/4-20 x1/2 BHSCS screws & economy T-nuts, as marked in Fig. 5.

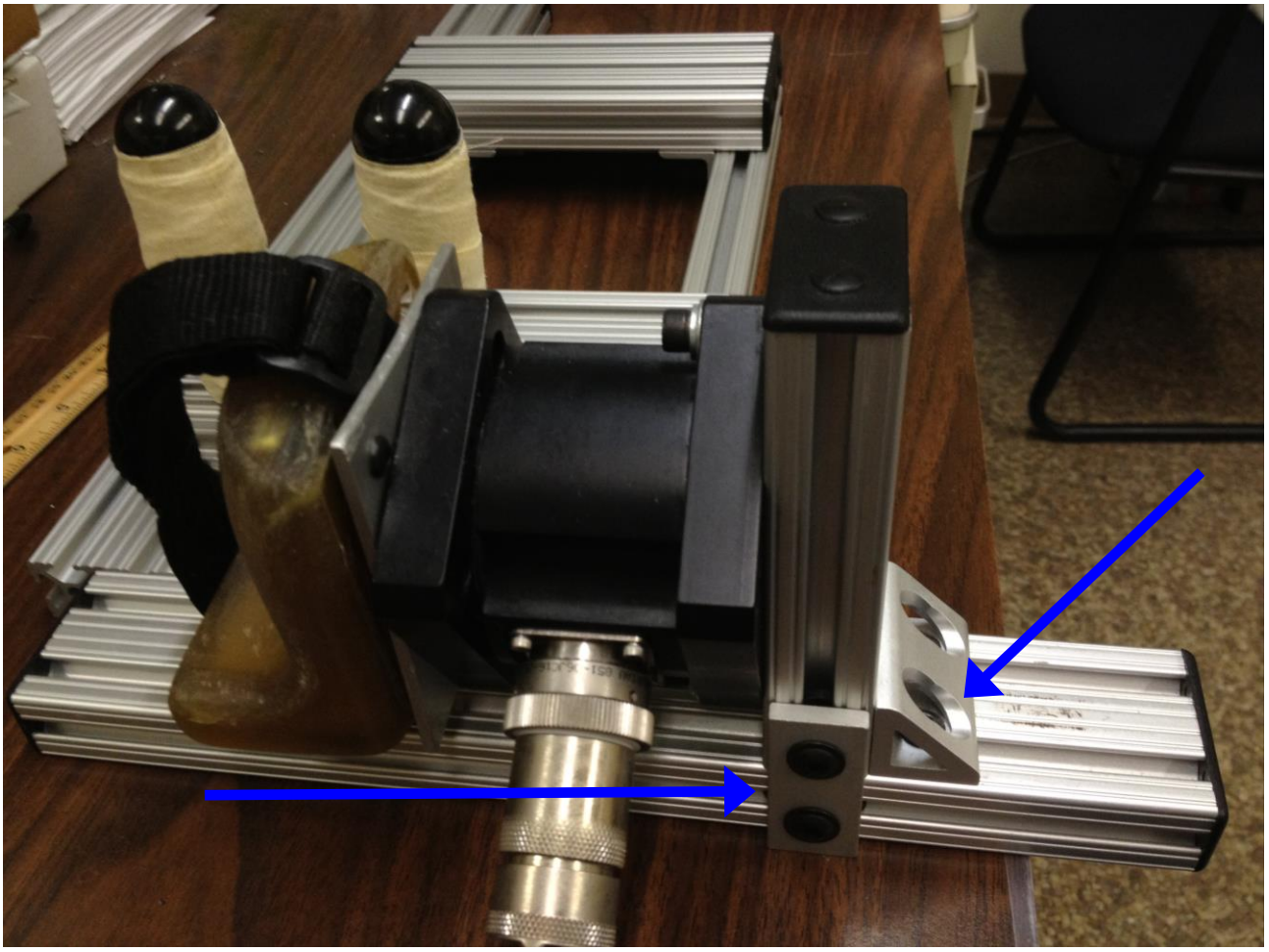

Fig. 5: Front view of the experimental apparatus labeling locations of the 2 Hole Joining strip with 1/4-20 x3/8 Flanged BHSCS screws & Economy T-nuts and the 4 Hole Inside Gusset Corner Bracket with 1/4-20 x1/2 BHSCS screws & Economy T-nuts used to tie part “A” and part “B” together.

Parts B, C1-2, D, E and J are secured to each other using the 2-hole 1/8” inside corner brackets and 1/4-20 x3/8 flanged BHSCS screws & economy T-nuts. Eight corner brackets of this kind are used in total, as marked in Fig. 6.

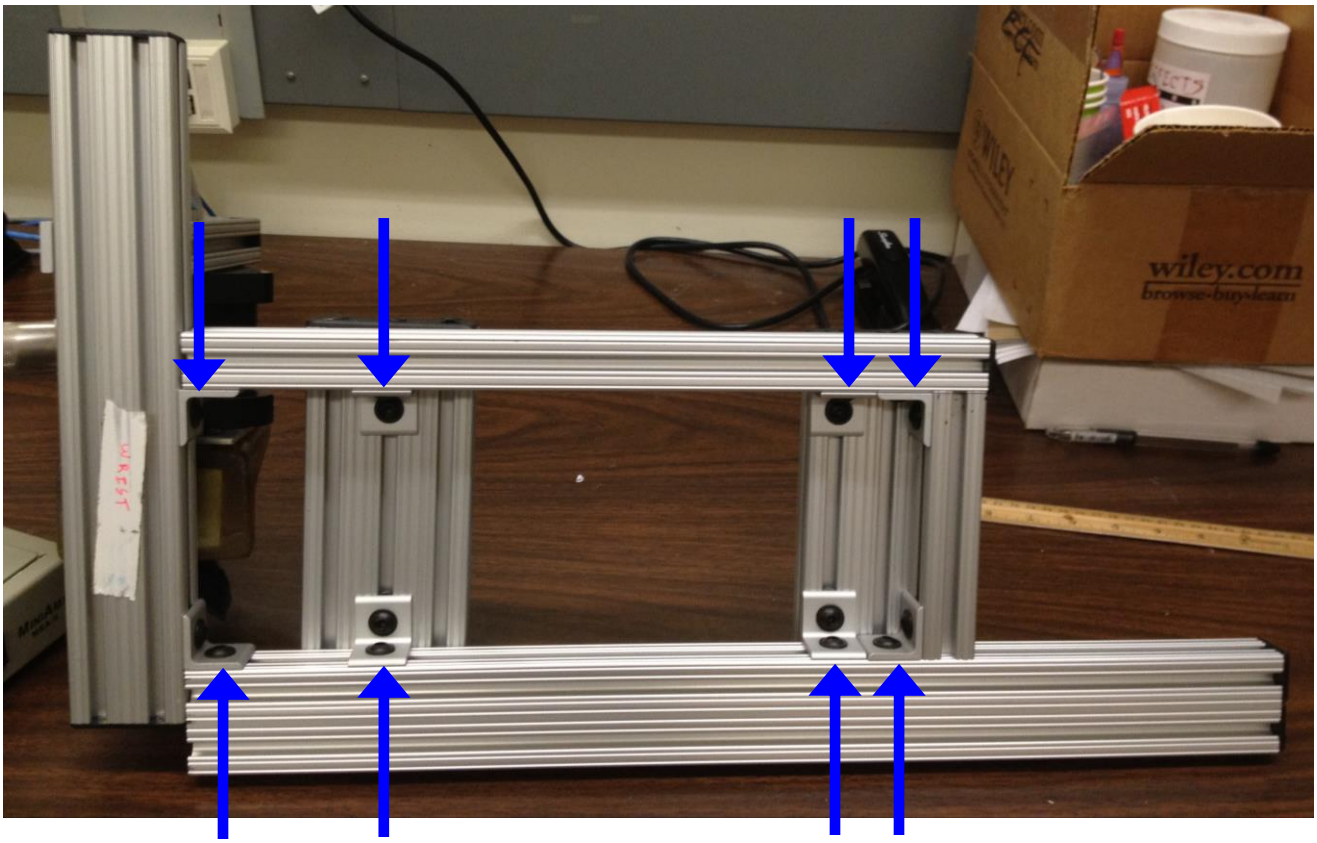

Fig. 6: Bottom view of the experimental apparatus labeling locations of the 2 Hole 1/8" Inside Corner brackets and 1/4-20 x3/8 Flanged BHSCS screws & Economy T-nuts used to secure the base (Parts B, C1-2, D, E and J).

The load cell (part "F") is secured to support beam (part "A") using two screws coming with the load cell. In Fig. 7(a), only the top screw is shown. The other screw is on the bottom.

A custom-built epoxy grip (part "H") is attached to a custom-built metal piece (part "I") using two regular screws. In the left side of Fig. 7(b), only the top screw is shown. The other screw is on the bottom.

Part "I" is secured to the load cell (part "F") using two regular screws. In the right side of Fig. 7(b), only the top screw is shown. The other screw is on the bottom.

A thin Velcro strap is tightly attached to the epoxy grip (part "H") using screws not shown in Fig. 7. In the experiment, the Velcro strap should be tightly wrapped around the posterior of the hand, just proximal to the knuckles, to secure the hand to the epoxy grip.

When appropriate, end caps are inserted into the end of each aluminum beam.

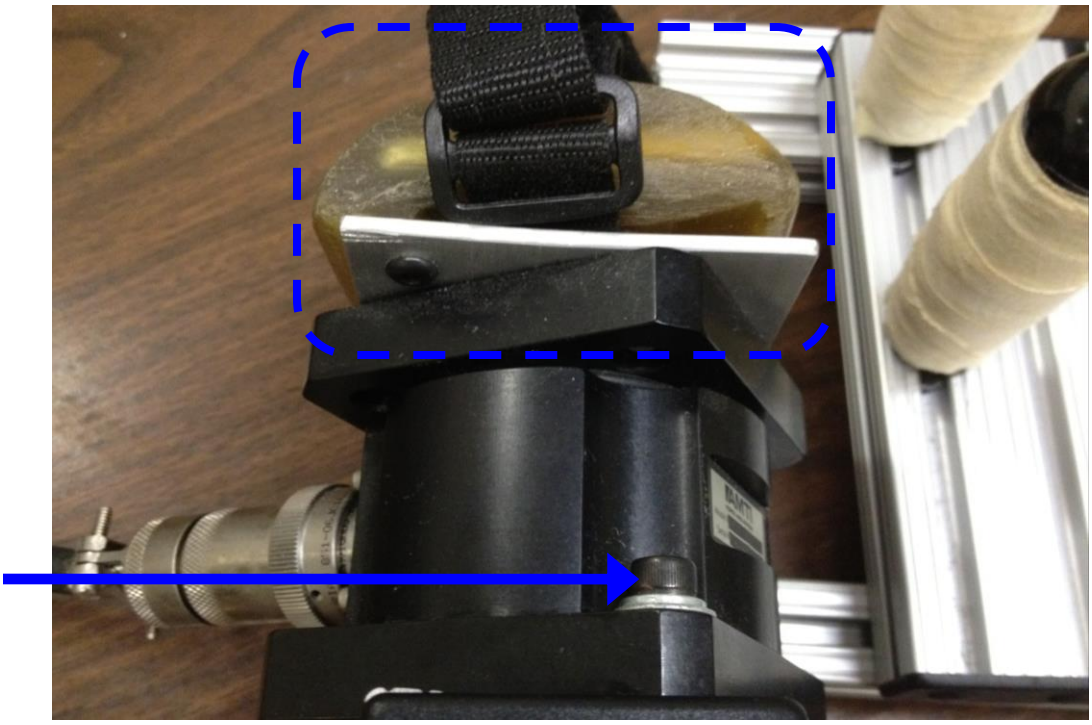

(a)

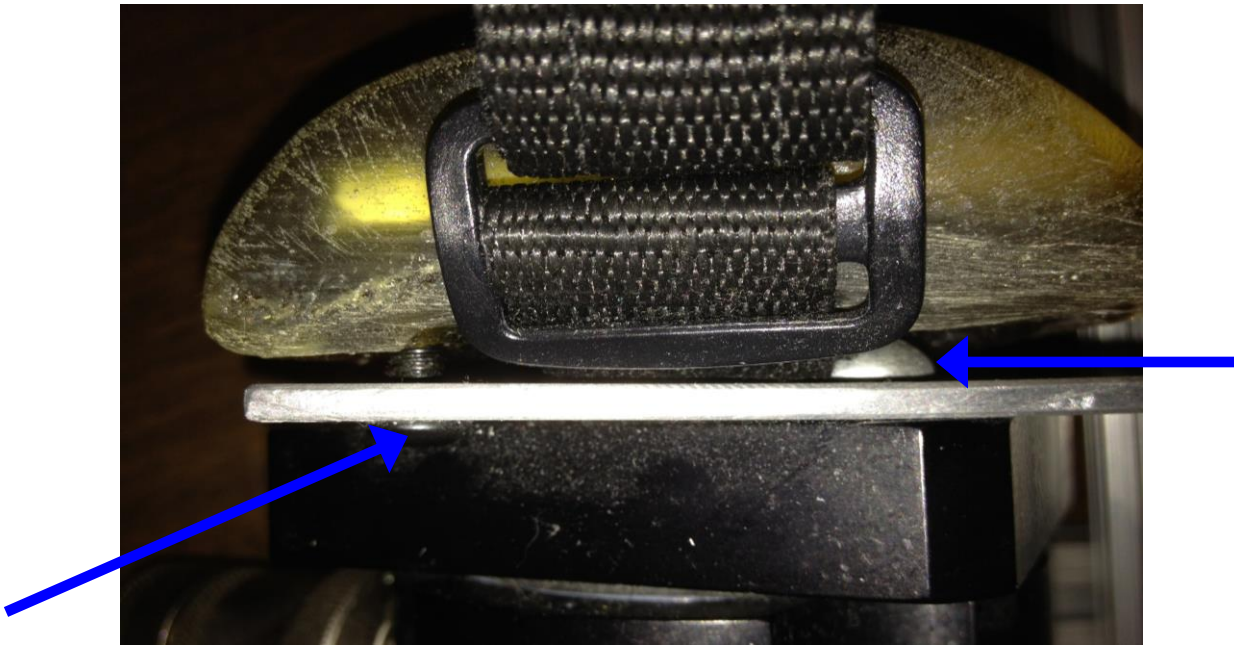

(b)

Fig. 7: (a) Top view of the custom pieces (part “I” and “H”) and load cell (part “F”) labeling locations of screws. (b) Zoomed-in view of the dash-boxed part in (a).